THE MIOCENE TO RECENT TECTONIC EVOLUTION OF AN ACTIVE TRANSFORM FAULT AT THE JUNCTION OF HELLENIC AND CYPRUS ARCS, EASTERN MEDITERRANEAN: THE LINKAGE BETWEEN THE WESTERN ANTALYA BASIN, FINIKE BASIN AND ANAXIMANDER MOUNTAINS

by

Ezgi Çınar

A Thesis, submitted to the

School of Graduate Studies

in partial fulfillment of the requirements for the degree of

Master of Science

Department of Earth Sciences

Memorial University of Newfoundland

January, 2014

St. John s Newfoundland and Labrador

ABSTRACT

The interpretation of 3,500 km of high-resolution seismic reflection profiles revealed that the tectonic evolution of the Finike Basin and its immediate surroundings involves three phases of deformation since the Miocene. A protracted contractional phase dominated by southwest-northeast trending fold-thrust structures ocurred during the Early-Middle Miocene. This phase culminated during the Messinian, and was replaced by an interval of relative tectonic quiescence. The transition from the latest Miocene to Pliocene-Quaternary was marked by a reactivated tectonism. This phase was dominated by partitioned strain, including: (i) reactivation and northwest-southeast directed contraction in the Finike Basin extending into the southern Turkish continental margin, (ii) extension and transtension along the westernmost Antalya Basin and the adjacent continental margin, and (iii) contraction and transpression across the The Sırrı Erinç Plateau and the northern slopes of the Anaxagoras Mountain.

A tectonic model is proposed where the development of these diverse tectonic regions can be explained by the development and temporal evolution of the intra-continental Beydağları Block, which experienced a 20 counterclockwise rotation during the Late Miocene and earliest Pliocene. Here it is proposed that the western and eastern boundaries of the block are delineated by the Burdur-Fethiye Fault Zone and the dextral Antalya Fault, whereas the southern boundary is defined by the northern margin of the Sirri Erinc Plateau and/or the southern margin of the Anaximenes and Anaxagoras Mountains.

ACKNOWLEDGEMENTS

First I would like to thank my supervisors Ali Aksu and Jeremy Hall for giving me the opportunity to be a part of this big family, the eastern Mediterranean Research group. In the past three years I have learned a lot, not just about Earth Science but also about life. It would not be possible to finish this thesis without your help.

Second, I would like to thank my team members, colleagues and friends. Thank you for being there for me whenever I needed you. An extra special thank you goes to Sharon Deemer, Peter Bruce and Dawna Greene for their invaluable advice and technical support. Thank you to all the staff, crew of the Koca Piri Reis R/V and the students at Dokuz Eylul University in Izmir, Turkey for their help for data collection.

Thank you to NSERC for providing the funds for this project through Discovery Grants to A. Aksu and J.Hall. Thank you, also, to Landmark Graphics for kindly providing the processing software used in for thesis.

Last, but certainly not least, I would like to thank my Mom and Dad for their contunious support. My niece, Kardelen, borned during the last year of my study bringing joy, fun and hope to life of our family, I am devoting this thesis to her.

"BeIirIi bir noktadan sonra geri dönüş yoktur. Bu noktaya erişmek de gerekir."

Franz Kafka

Table of Contetnts

List of Tables

List of Figures

List of Plates

Chapter One: Introduction

1.1 Background

The eastern Mediterranean Sea is one of the best natural geological laboratories because it displays the results of numerous tectonic processes, such as (a) rifting and passive margin development, (b) ophiolite emplacement and orogenesis, (c) contraction and associated subduction and (d) collision (Aksu et al., 2005a,b). The region also draws worldwide attention because of extensive salt deposition and deformation. The omnipresence of this thick evaporite succession along the eastern Mediterranean is well-documented by a number of authors (e.g., Hsü et al., 1973; Cita et al., 1978; Hall et al., 2005a,b; Işler et al., 2005). The evaporite sequence was deposited during the desiccation of the Mediterranean associated with the Messinian Salinity Crisis (e.g., Hsü et al., 1973; Cita et al., 1978). On the other hand, the absence of the evaporite succession in the Finike and Rhodes Basins and the adjacent Anaximander Mountains is still not well understood.

This complex region developed during the Late Triassic as a small ocean basin and reached its maximum width during the mid-Cretaceous. The present day eastern Mediterranean Sea (Fig. 1.1) is the remnant of the Neo-Tethyan Ocean which separated the Eurasian Plate from African and Arabian Plates (Moores et al., 1984; Robertson, 1998). The Neogene tectonics of the eastern Mediterranean Sea evolved in association with the collision of the Arabian and African Plates with the Eurasian Plate. This

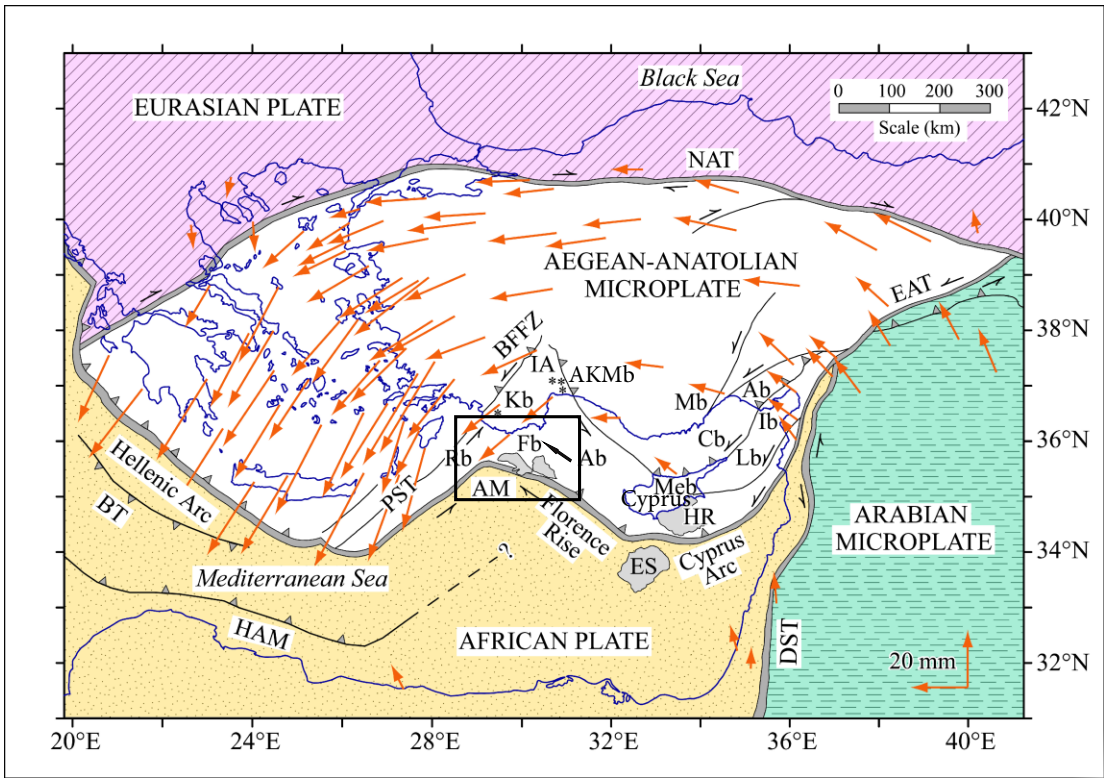

Fig. 1.1 Tectonic map of the eastern Mediterranean Sea and surrounding regions, with the study area highlighted by the black box. Ab = Antalya Basin, AKMb = Aksu, Köprü, Manavgat Basins, AM = Anaximander Mountains (*sensu lato*), BFFZ = Burdur–Fethiye Fault zone, BT = backstop thrust, DST = Dead Sea Transform Fault, EAT = East Anatolian Transform Fault, ES = Eratosthenes Seamount, HAM = Hellenic active margin, HR = Hecateus Ridge, IA = Isparta Angle, Kb = Kasaba Basin, Mb = Mesaoria Basin, NAT = North Anatolian Transform Fault, PST = Pliny–Strabo Trenches, Rb = Rhodes Basin. Large arrows indicate the rate of plate movement and the sense of plate motion relative to a fixed Eurasian plate; half arrows indicate transform/strike-slip faults (modified from Aksu et al., 2009)

collision in the Late Miocene initiated the westward tectonic escape of the Aegean-Anatolian Microplate. During the Pliocene the western portion of the microplate experienced a counter clockwise rotation (Fig. 1.1, Şengör and Y lmaz., 1981).

The displacement of the Arabian and Aegean-Anatolian Microplates and the collision between the African and Eurasian Plates are the events that control the present tectonic framework of the eastern Mediterranean (Aksu et al., 2005a). The Hellenic Arc and the Pliny-Strabo Trenches in the west and the Florence Rise, Cyprus Arc in the east delineate the boundary between the African Plate and Aegean-Anatolian Microplate (Fig. 1.1). A 100 km wide transform fault zone separates the Hellenic and Cyprus Arcs at this convergent plate boundary due to the rollback of subduction below the Hellenic Arc (Govers and Wortel, 2005, Woodside et al., 2002). There is ongoing discussion concerning the Miocene-Recent kinematic evolution of the area, particularly the timing and style of deformation, and the temporal and spatial distribution of displacements, as well as the nature and thickness of the crust across the floor of the eastern Mediterranean Sea (Aksu et al., 2009).

The eastern Mediterranean Project was launched in 1991 by Drs. Ali E. Aksu and Jeremy Hall at the Memorial University of Newfoundland. Marine research cruises took place in the years of 1991, 1992, 2001, 2007, 2008 and 2010 with an international team of researchers who are actively investigating the tectonic evolution of the eastern Mediterranean Sea. Approximately 20,000 km of high resolution multichannel seismic reflection data has been collected in total and the author assisted .. collection of ~5,000

km of data by participating in the cruises during the summer-fall 2008 and 2010. The lines used in this thesis were collected in the summer-fall 2007/2008/2010 cruises and are highlighted in purple with previously collected data highlighted in black (Fig. 1.2).

1.2 Location and geological setting

The study area extends along the Finike Basin, the northern margin of the Sırrı Erinç Plateau and Anaxagoras Mountain, the western and south-western margin of the Antalya Basin and the Turkish continental shelf in the eastern Mediterranean Sea (Fig. 1.3).

The Finike Basin is an approximately 3000 m-deep E-W trending trough situated between the Sırrı Erinç Plateau in the south and the steep Anatolian continental slope in the north. It is bounded by the Antalya Basin in the east and merges with the northern slopes of the Anaxagoras Mountains (sensu lato) in the southeast. To the southwest, it extends into a broadly north-south trending narrow and deep trough referred to as the Anaximander Basin (Aksu et al., 2009; Fig. 1.3). Woodside et al. (2000) suggested that the evolution of the basin took place in post-Messinian time as a result of the westward tectonic escape of the Aegean-Anatolian Microplate in Middle to Late Miocene, as a transtensional phase which also controlled the Hellenic Arc. They further speculated that the evolution of the basin may have occurred as a pull-apart basin as a result of the continuation of the Pliny-Strabo Trenches towards east. On the other hand, Aksu et al. (2009) suggested that the rapid subsidence of the Finike Basin during Pliocene-Quaternary occurred as a flexural response to the loading of the thrust sheets that carry

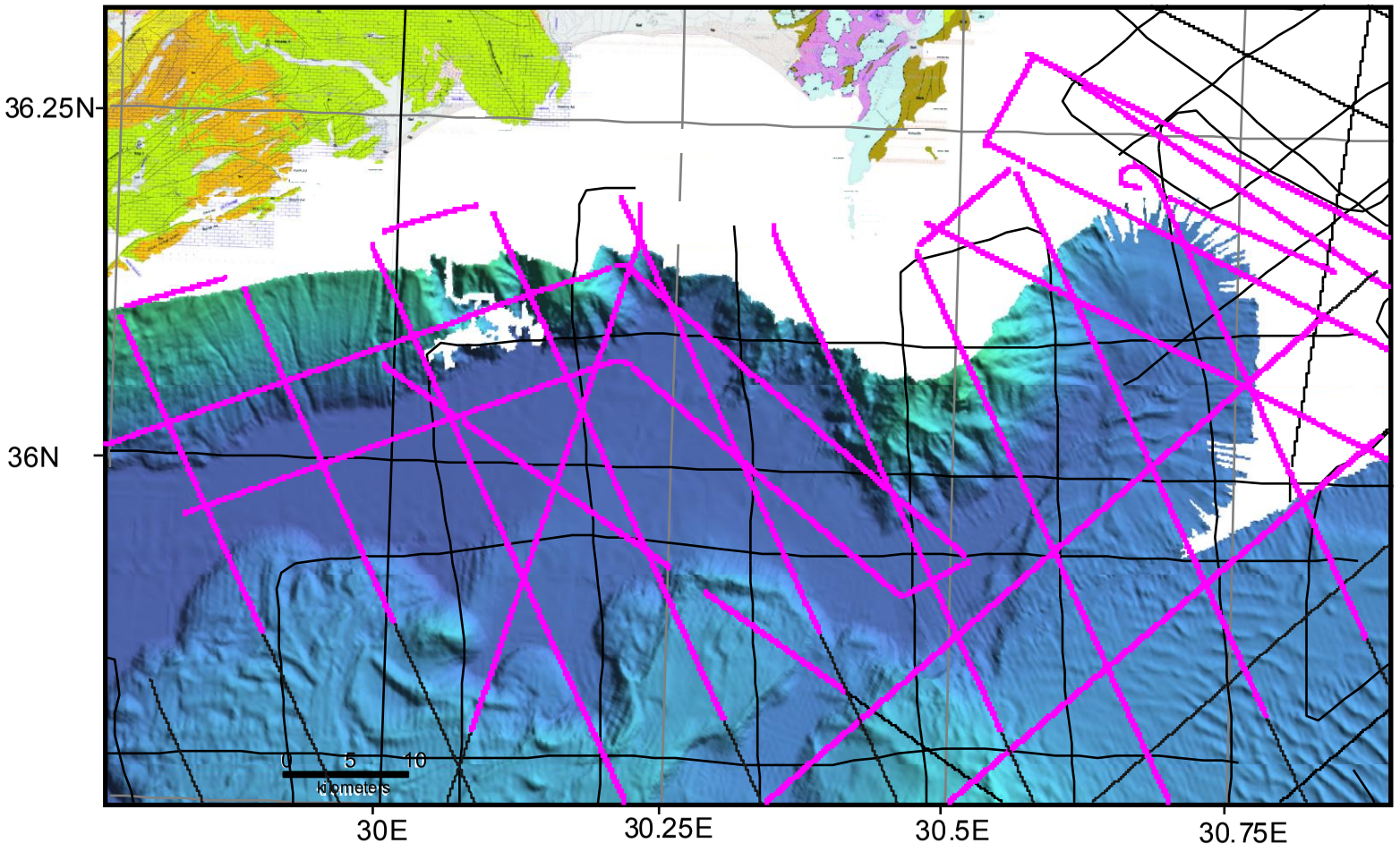

Figure 1.2 Detailed multi-beam bathymetry map of the eastern Mediterranean Sea. The line processes for this thesis are marked with magenta.

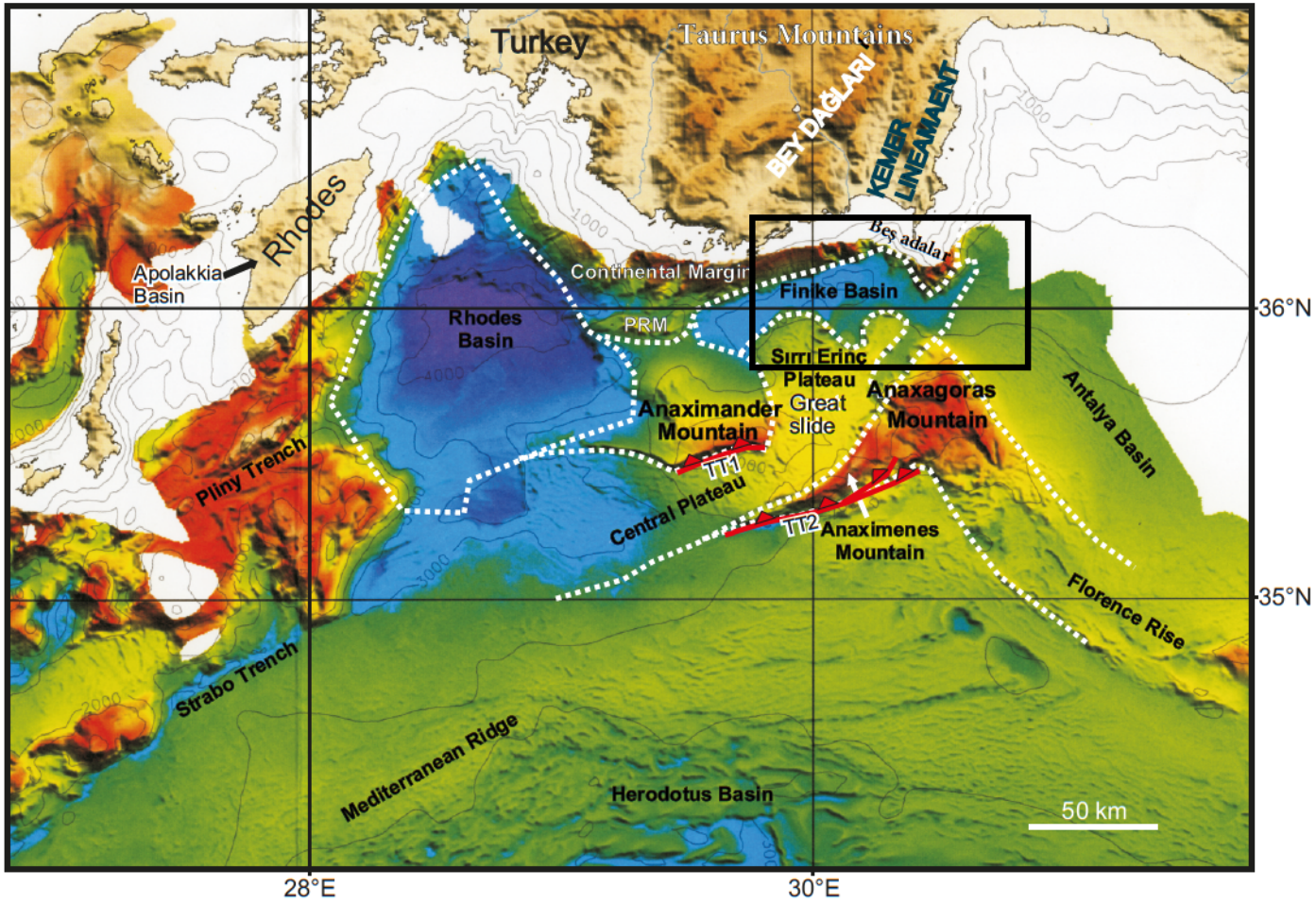

Figure 1.3 Map showing the location of the Anaxagoras Mountain, Anaximander mountain, Anaximenes Maountain, Antalya Basin, Apolakkia Basin,Turkish Continental Margin, Florence Rise, Rhodes Basin, Rhodes Island, Sırrı Erinç Plateau, Taurides Mountain, Beydağları, Kemer Lineament, Beşadalar, TT1 and TT2 thrusts and the study area outlined with black box (see Fig. 1.2, Modified from Hall et al., 2009).

Tauride Mountains to the north. The absence of Messinian evaporites in the Finike Basin is noted in numerous studies and it is suggested that this results from the region being situated above the depositional level during the Messinian Crisis (Woodside et al., 2000, 2002; Aksu et al., 2009).

The Antalya Basin is a NW-SE trending depocentre situated in a forearc setting behind the Florence Rise and Cyprus Arc and on the northeast fringes of the Anaxagoras Mountain (Figs. 1,1, 1.3). In the west it is bounded by the Beydağları Mountains and theirsubmarine extensions, the Anaxagoras and Anaximenes Mountains (Glover and, Robertson, 1998a,b; Işler et al., 2005) and the Finike Basin. The study area includes the western and southwestern segments of the Antalya Basin. Glover and Robertson (1998a) suggested that the Antalya Basin is a 2.5 km-deep actively northward-subsiding basin which is bounded in the NE and NW by high-angle extensional faults. Recent studies in the Antalya Basin suggest that the Miocene to Recent evolution of the basin involves two tectonic phases. Phase one deformation was compressional and took place during Late-Middle Miocene dominating the whole basin and resulted in the creation of a northwest-southeast trending fold-thrust belt (Sage and Letouzey, 1990; Işler et al., 2005). During the Messinian Crisis, a thick evaporite succession was deposited in the basin. The region has been exposed to extensional/transtensional tectonics during the Pliocene to Recent, particularly affecting the northeast segment of the region, whereas transpressional deformation marked by a prominent belt of positive flower structures are observed in the southwest portion of the basin (Işler et al., 2005). This mixed phase deformation style is

associated with the westward tectonic escape of the Aegean-Anatolian Microplate, involving the displacement of the eastern Tauride Mountains (Işler et al., 2005).

The Florence Rise is situated on the southern margin of the Antalya Basin and the eastern flank of the Anaximander Mountains (Figs. 1.1, 1.3). It constitutes the northwestern segment of the Cyprus Arc and extends towards Cyprus in the southeast. Papazachos and Papaioannou (1999) suggested the existence of a NNE trendisg dextral transform fault (i.e., Paphos Transform Fault) situated on the western margin of Cyprus that links the Florence Rise in the west with the Cyprus Arc in the east, creating a continuous boundary between he African and Eurasian plates (Fig. 1.1). Recent studies also suggested that the Florence Rise is a surviving remnant of a former subduction zone separating the passively-subsiding Antalya Basin from the southern and southwestern collisional tectonics which caused the development of a broad dextral wrench zone extending across the Florence Rise toward the Anaximander Mountains (Woodside et al., 2002; Zitter et al., 2003). The tectonic deformation along the Florence Rise is suggested to be the consequence of the westward movement of Cyprus and the northeast movement of the African Plate along the Florence Rise, so that the result of the progressive adjustment of the collisional/compressional plate interaction (Papazachos and Papaioannou 1999; Woodside et al., 2002). The positive flower structures observed along the Florence Rise (Güneş, 2010) further support the transpressional character of the tectonics along the Florence Rise. The present-day deformation along the Florence Rise is related to the presence of the Eratosthenes continental block (Fig. 1.1) choking the subduction zone

along the Cyprus Arc, as well as to the geometry of the possibly stretched and detached African slab beneath the Florence Rise (Woodside et al., 2002).

The Anaxagoras Mountain, which is one of three prominent morphological elements of the underwater mountains (i.e., Anaximander, Anaximenes and Anaxagoras Mountains), is a NW-SE trending broad high which is morphologically connected to the Florence Rise. An arcuate NW-dipping escarpment bounds the northwestern margin of the Anaxagoras Mountain, where the seafloor is elevated approximately 700 m above the Sırrı Erinç Plateau. The northeastern margin of the Anaxagoras Mountain shows two to three small escarpments, leading into the outer Antalya Basin. Through the southwest, the Anaxagoras Mountain is linked to the Anaximenes Mountain, and together they form a NW-facing concave structure (Aksu et al., 2009). Woodside et al. (1997, 1998) suggested that the lithology of the Anaximander Mountain is similar to that onshore, where the Beydağları and Antalya complexes are juxtaposed on the western margin of the Isparta Angle.

Woodside et al. (1997, 1998) and Zitter et al., (2003) suggested that most of the deformation along hıs regıon is the result of strike-slip faulting and that there is only a small amount of crustal shortening across the eastern portion of the Anaximander Mountains (sensu lato). They further suggested that this tectonic phase did not develop new faults, but utilized the existing zones of weakness by reactivating existing faults (e.g., former thrusts of the Florence Rise and normal faults, such as the Kemer lineaments extending from the Isparta Angle south into the northeastern part of Anaxagoras Mountain as major strike-slip faults.

The Sırrı Erinç Plateau is situated on the south-southwest portion of the study area. It is bounded by the southern margin of the Finike Basin in the north and the western portion of the transition from the Antalya Basin to the Anaxagoras Mountain. Woodside et al. (1998) interpreted the plateau as a massive gravitational slide in the region between the Anaximander Mountain and Anaximenes/Anaxagoras Mountains, and referred it as the Great Slide (Fig. 1.3). They speculated that the sliding occurred during the Late Pliocene or Pleistocene as a gravitational flow to the north and south initiated b the presence of gas hydrates in poorly consolidated sediments with higher than normal water content. On the other hand, Aksu et al. (2009) interpreted the Sırrı Erinç Plateau as a major Pliocene-Quaternary transpressional fault system.

The Turkish continental margin is situated north of the Finike Basin and west of the southwestern Antalya Basin (Fig. 1.3). It is bounded in the north onland by the Western Taurus Mountains and the Beydağları Complex. On the northern fringes of the Finike Basin, the i extends from west to east and on the western edge of the Antalya Basin it exhibits a southwest-northeast trend, with a prominent continental shelf extending from the Beşadalar (Fig. 1.3). The margin is a steep slope (about 15 degrees), cut by canyons, separating the shelf from the deep water (~ 3000 m) of the Finike Basin. The origin of the slope is enigmatic and one of the issues addressed in this thesis.

1.3 Scientific Objectives

The study area is situated at the critical junctions of the above-mentioned morphological and structural elements. Thus, this dissertation aims to provide much needed information regarding the tectonic relationships between these morphological and structural elements, and their relationship with the larger-scale tectonism north of the Hellenic and Cyprus arcs. This project is a part of a group effort; King is working on the NW corner of the Antalya Basin; Cranshaw (2010) worked on Anaximander Mountain. My project provides a geographical and geological link among these. Together the projects address the nature and history of the eastern margin of the transform zone joining Hellenic Arc to Florence Rise/Cyprus Arc.

Imaging and mapping the structures associated with the Miocene to Recent tectonic and sedimentary evolution of the Finike Basin and southern margin of SW Anatolia, western Antalya Basin, and northern margins of the Sırrı Erinç Plateau and Anaxagoras Mountainin in the eastern Mediterranean Sea are the principal objectives of this thesis. This will be accomplished by completing the following geophysical and geological objectives;

1.3.1 Geophysical Objectives

The geophysical objectives of this thesis can be summarized as follows:

1. to determine the parameters required to process 1100 km of high resolution multi-channel reflection data from the Finike Basin, Sırrı Erinç Plateau

Anaxagoras Mountains and Antalya Basin (Figure 1.2),

2. to establish the optimal processing flow for this data set by testing the various steps of the flow, and
3. to process the data from the shot-domain to the final migration, while attempting to produce the best possible image of the sub-surface geology.

1.3.2 Geological Objectives

The geological objectives of this thesis can be summarized as follows:

1. to determine the structural and tectonic linkages between the Anaxagoras Mountain, Sırrı Erinç Plateau and the Finike Basin through the western Antalya Basin,
2. to determine the continuation of the active convergence zone, which joins Hellenic and Cyprus Arcs, through the Finike and Antalya Basins,
3. to delineate the detailed structural architecture of the Finike Basin, the southern margin of SW Anatolia, the northern margin of Sırrı Erinç Plateau Anaxagoras Mountain and the western Antalya Basin,
4. to produce detailed maps of the structures to compare structural styles and delineate possible linkages across this complicated region.
5. to understand why the Messinian evaporite succession is omnipresent in the Antalya Basin, but it is absent in the Finike Basin.
6. and finally to clarify the causes of rapid apparent subsidence of Finike Basin during the Pliocene-Quaternary by a critical analysis of whether salt is

truly absent in everywhere within .the Finike Basin.

Chapter Two: Methods and Applications

2.1 Reflection Seismology

The seismic reflection method is used to provide pictures of subsurface geological structures and to detect the physical properties of buried rock volumes (Dobrin, M, 1976, Yılmaz, 2001). This method uses elastic waves generated by a controlled source (vibroseis, dynamite, airgun, sparker, etc.) that are detected by receivers (e.g., hydrophone array, geophone array, etc.) after reflecting from subsurface interfaces. A seismograph is used to record the echoes which correspond to the time that the wave travels from source to reflector and back to the receiver (Fig. 2.1). In order to determine the seismic velocities needed to convert travel times to depth, the usual arrangement is to record reflections from a series of detectors at a range of offsets from the source. The resulting seismogram (Fig. 2.2) shows that the reflection time increases with offset (see Normal Moveout (NMO) correction , later in this chapter) and it is this information that allows for the calculation of velocities.

The downgoing wave from the source reflects from a subsurface boundary when there is a difference in the acoustic impedance (Z, the product of velocity (υ) and density (ρ) across it (Equation 2.1; Yılmaz, 2001).

$$Z = (\upsilon)(\rho) \qquad (2.1)$$

The relative strength of the reflected wave to the incident wave is given by the reflection coefficient, R12, which is also a function of the acoustic impedance (ρυ).

At normal incidence:

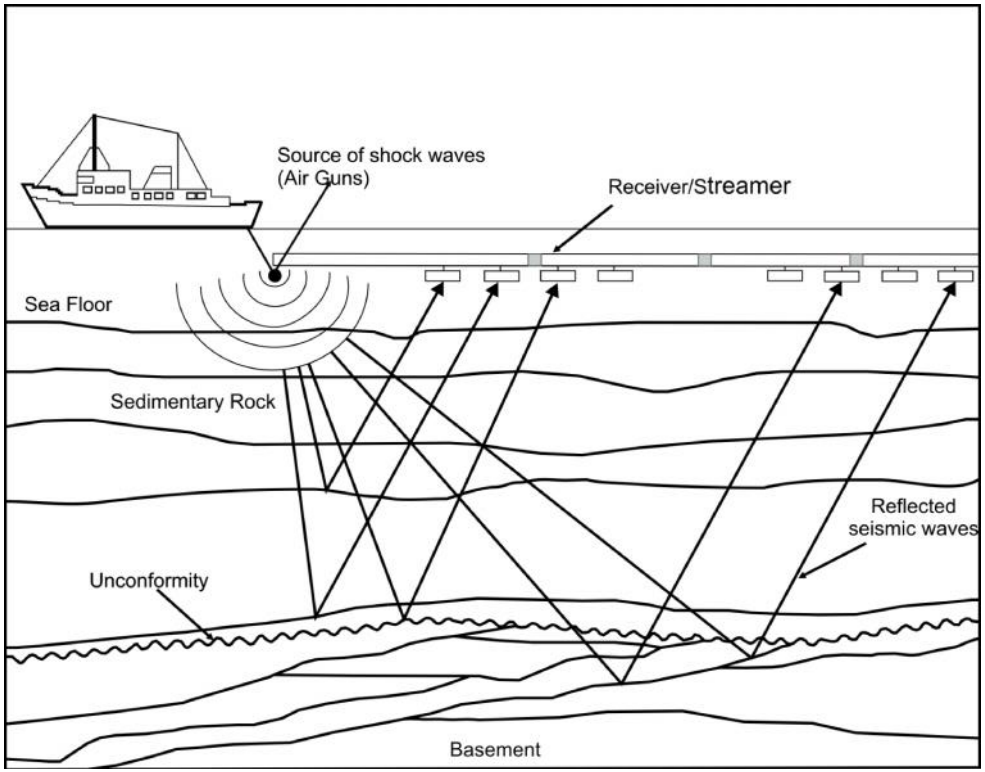

Figure 2.1 General configuration of a seismic reflection survey showing the location of the source (air gun) and receiver/streamer (hydrophones). The seismograph is located onboard ship (Modified from Cranshaw 2010).

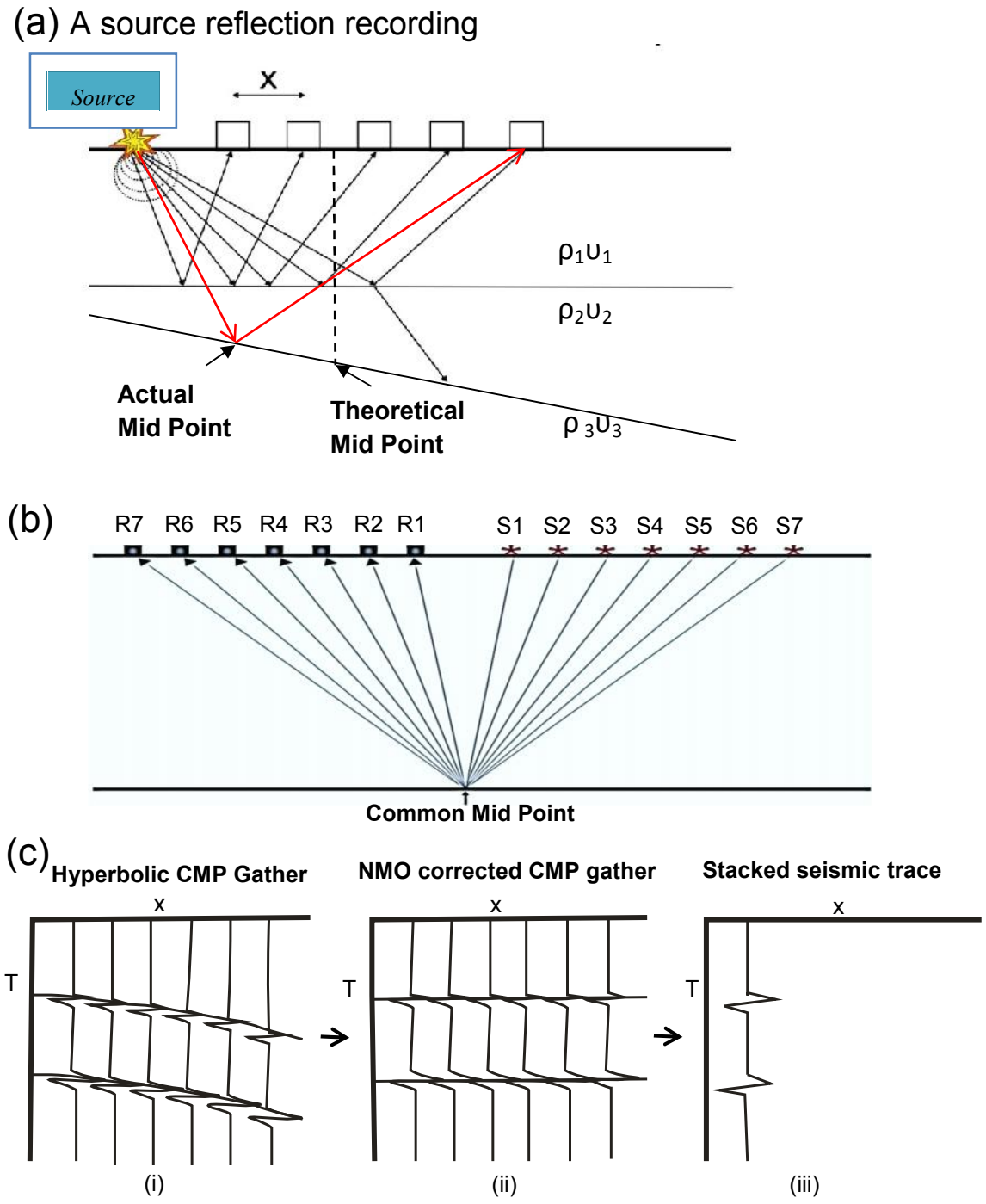

Figure 2.2 Seismic reflection experiment using a) a single source and a number of evenly spaced receivers (x), ρ=density and υ= velocity, b) CMP from multiple shots and receivers, c) the time-distance seismograms for a CMP showing,(i) a hyperbolic function, (ii) then corrected for NMO and (iii) finally stacked trace.

$$R12 = (\rho 2 \upsilon 2 - \rho 1 \upsilon 1) / (\rho 2 \upsilon 2 + \rho 1 \upsilon 1) \quad (2.2)$$

where ρρ1= density of layer 1; υυ1= velocity of layer 1; ρ2= density of layer 2; υυ2= velocity of layer 2.

In the seismic reflection method, it is commonly assumed that seismic waves travel through homogeneous, isotropic media (Krebes, 1985; Krebes 1989; Yılmaz, 2001). A seismic wave loses energy with increasing depth due to spherical divergence, absorption, scattering and anelastic attenuation of higher frequencies. This energy loss dictates the choice of the source bandwidth appropriate for a particular target depth (Yılmaz, 2001), typically 20-200 Hz.

Because the reflection coefficients from within a sedimentary sequence may be quite small (~1%), the subsurface coverage (Figs. 2.2b, 2.2c) from one shot is made to overlap with that of the next so that the subsurface is covered many times. .The resultant data are then sorted into common mıdpoint (CMP) groups and stacked to produce a final image with much greater signal-to-noise ratio than that from single coverage.

2.2 Data Acquisition

2.2.1 Profile Locations

During several eastern Mediterranean cruises (1992, 2001, 2007, 2008 and 2010), ~3500 km of high resolution marine seismic reflection data were obtained over the Finike Basin and vicinity (Fig. 2.3). The highlighted seismic reflection profiles in Figure 2.3 illustrate the data processed by the author. Due to the complicated 3D geology of the

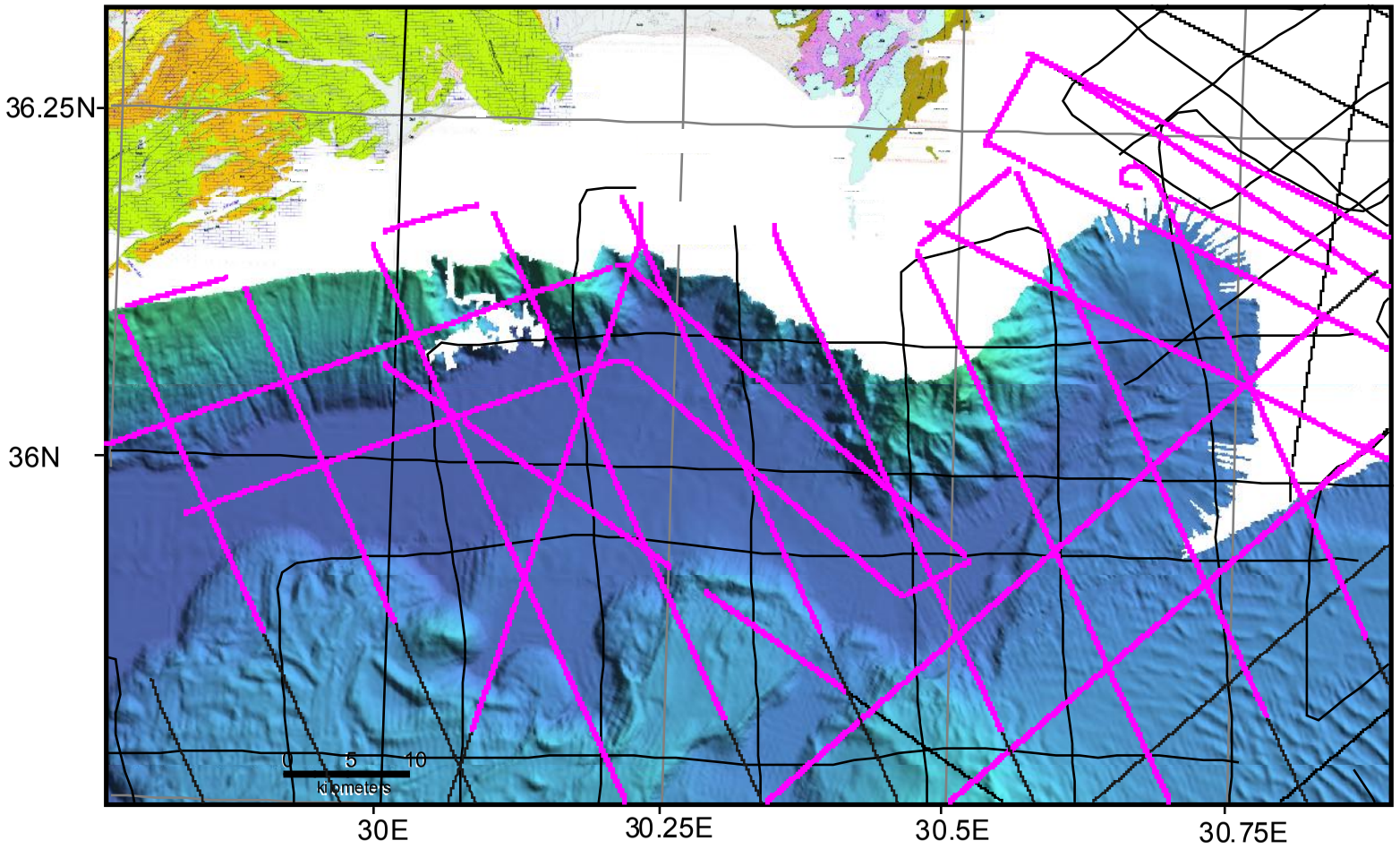

Fig. 2.3 Detailed multi-beam bathymetry map of the eastern Mediterranean Sea. The lines processed for this thesis are marked with magenta. Black lines are previously processed and used

study area, seismic reflection profiles were surveyed in different directions to allow mapping of the variably oriented structures. Accompanying the ~1500 km of seismic profiles which were acquired and processed for this particular study from surveys in 2007, 2008 and 2010, ~2000 km of seismic reflection profiles that were collected during the 1992 and 2001 cruises, were also incorporated in the interpretation.

2.2.2 Scientific Equipment

The seismic profiles were recorded with the seismic equipment supplied by Memorial University of Newfoundland and Dokuz Eylül University by using the research vessel, RV *Koca Piri Reis*, of Dokuz Eylül University. The location of the research vessel was determined by Global Positioning System (GPS); in addition, a logbook was kept with entries every 10 minutes indicating the location and the speed of the vessel, depth of the source as well as the navigation fixes, shot numbers, and notes on any equipment problems.

During the 2007, 2008 and 2010 cruises, seismic reflection data were recorded from shots fired at intervals of about 9-10 seconds, every 25 metres in distance. GPS location of the ship was used to create shot trigger pulses (Fig. 2.4). Position and orientation data were sent to the Nav/Pac by gyro and the navigation system (GPS) of the vessel. The Nav/Pac sent a TTL (transistor-transistor logic) signal to the trigger box every 25 metres travelled. Then, the trigger box sent a signal to the delay box that was followed with a signal sent from the delay box to the gun controller (i.e., Macha) and a user defined delayed TTL to the SeaMUX NTRS-2 seismograph (Fig. 2.4).

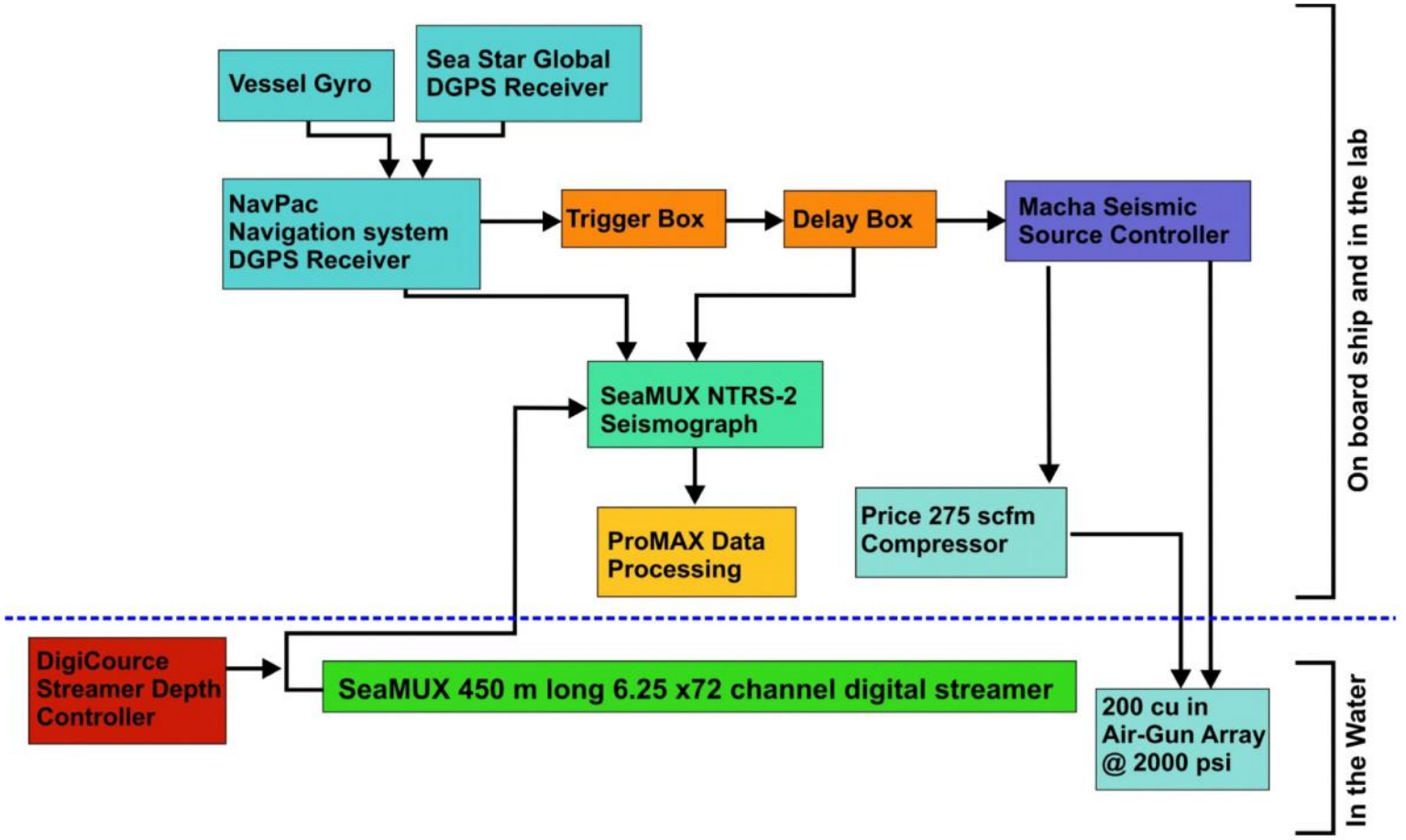

Figure 2.4 Flow chart illustrating the recording equipment as set up for the 2007 eastern Mediterranean seismic survey (Cranshaw 2010)

Ultimately, the guns were fired when a 5V TTL signal, sent from the Macha, was received by the airguns. The delay box was used in 2007 (but not later) so that time required for recording the data could be reduced to avoid recording most of the water layer. This was important for that cruise because of the slow speed of the recording devices. In later surveys, faster processing allowed us to record without using any delay.

During the 2007, 2008 and 2010 cruises, the source was a combination of seven, broad-band, high frequency, sleeve guns belonging to the Memorial University of Newfoundland. The volume of the guns was the same in each survey as follows: 4 x 40 in guns (4 x 655 cm), 1 x 20 in gun (1 x 328 cm), and 2 x 10 in guns (2 x 164 cm), with a total volume of 200 in (3277 cm). In every cruise, two of the 40 cubic inch guns were placed in close proximity to one another, so that when they fired, their bubbles would coalesce to emulate an 80 cubic inch gun (1311 cm^3). Source bandwidth was approximately 20-200 Hz. Seismic reflections were detected with Dokuz Eylül University s high-resolution Hydroscience Technologies Inc. digital streamer, using a different length of streamer and number of channels each year: 450 m-long 72 (x 6.25m) channels in 2007, 600 m-long 96(x 6.25m) channels in 2008 and 1500m-long 240(x 6.25m) channels in 2010. Due to the mechanical issues on the streamer, 2010 data were mostly collected by using 216 channels instead of 240 channels. The streamers were towed at constant depth (3 metres below the surface of the water) in order to improve the data quality and the safety of marine data acquisition, using 8-12 Digi-Course streamer depth controllers (i.e., streamer birds). The data were

recorded in SEG-Y format for 4 seconds with variable delay in 2007, seven seconds with no delay in 2008 and 2010, all at 1 ms sample rate using Dokuz Eylül University s SeaMUX NTRS-2 seismogram. In 2007, the delay depended on water depth. Data were stored on DVDs and the SeaMux hard disk. In addition, a 6-m long single-channel Benthos streamer was used to provide a single-channel display of the seismic reflection data in real time in order to visualize the geology of the subsurface and associated structural trends as well as for data quality control. Detailed acquisition information is given in Table 2.1. The multiple subsurface coverage (known as the fold of the stack) is given by Equation 2.3.

$$\text{Fold} = \text{number of channels} \times (\text{group interval}/\text{shot interval}) \quad (2.3)$$

So in this case,

Fold = 72 x (6.25/25) = 9, for 2007

Fold = 96 x (6.25/25) = 12, for 2008

Fold = 216 x (6.25/25) = 27, for 2010

In 2001 and 1992 cruises, acquisition parameters were close to those used for the following years with a couple of variations such as: the type and the length of the streamer, group interval, recording time and data storage. The data were detected using a Memorial University Teledyne, non-digital, streamer with 600 m-long 48(x12.5) for three seconds below the sea floor with a 1ms sampling rate. Unlike the following surveys, data were stored on DAT (digital audio tapes) tapes or magneto-optical disks using a 48 channel OYO DAS-1 seismograph (2001) or DFSV.

	Data Collected in 2007	Data Collected in 2008	Data Collected in 2010
Number of guns	7	7	7
Volume of guns	4 x 40 in ^{3} guns (4 x 655 cm ^{3}), 1 x 20 in ^{3} gun (1 x 328 cm ^{3}), 2 x 10 in ^{3} guns (2 x 164 cm ^{3})	4 x 40 in ^{3} guns, 1 x 20 in ^{3} guns, 2 x 10 in ^{3} guns	4 x 40 in ^{3} guns, 1 x 20 in ^{3} guns, 2 x 10 in ^{3} guns
Total Volume	200 in ^{3} (3277 cm ^{3})	200 in ^{3} (3277 cm ^{3})	200 in ^{3} (3277 cm ^{3})
Shot interval (m)	25	25	25
Recording Channel Number	72	96	216
Streamer Length(m)	450	600	1500
Group Interval(m)	6.25	6.25	6 .25
Streamer Depth(m)	3	3	3
CDP Interval	3.125	3.125	3.125
Fold	9	12	27
Source-Reciever Offset	70	70	75

Table 2.1. Acquisition parameters above belong to the data processed by the author.

2.3 Data Processing Methods

The aim of data processing is to produce an image of the subsurface geology with minimal noise. Landmark Graphics ProMAX processing software was used. Basic marine seismic processing steps and the processing techniques that are applied are shown in Figure 2.5

2.3.1 SEGY Input

The original recordings in SEG-Y format were loaded into ProMAX , using the SEG-Y Input tool. Where a line consisted of more than 2000 shot files, the data had to be divided into two or three pieces and loaded separately. Using the disk data insert tool, the data were then put together into one file.

2.3.2 Initial Displaying and Processing Techniques

A shot recording contains signal (reflections) and noise. Noise can be both random (e.g. noise from the ship, waves and the recording equipment, etc.) and coherent (e.g. multiple reflections, swell). A display of the raw data for quality control purposes gives an idea about the signal/noise ratio and amplitude levels. It also enables us to detect the bad channels (exceptionally noisy or dead), shot timing errors and selection of initial filters and amplitude correction. A near trace gather, which is a collection of the near-offset trace from each shot gather, gives a valuable first impression of the variation in geology along the line. Figure 2.6 illustrates a delay time error from a near-trace gather that required a recollection of the data for a line of the 2007 survey.

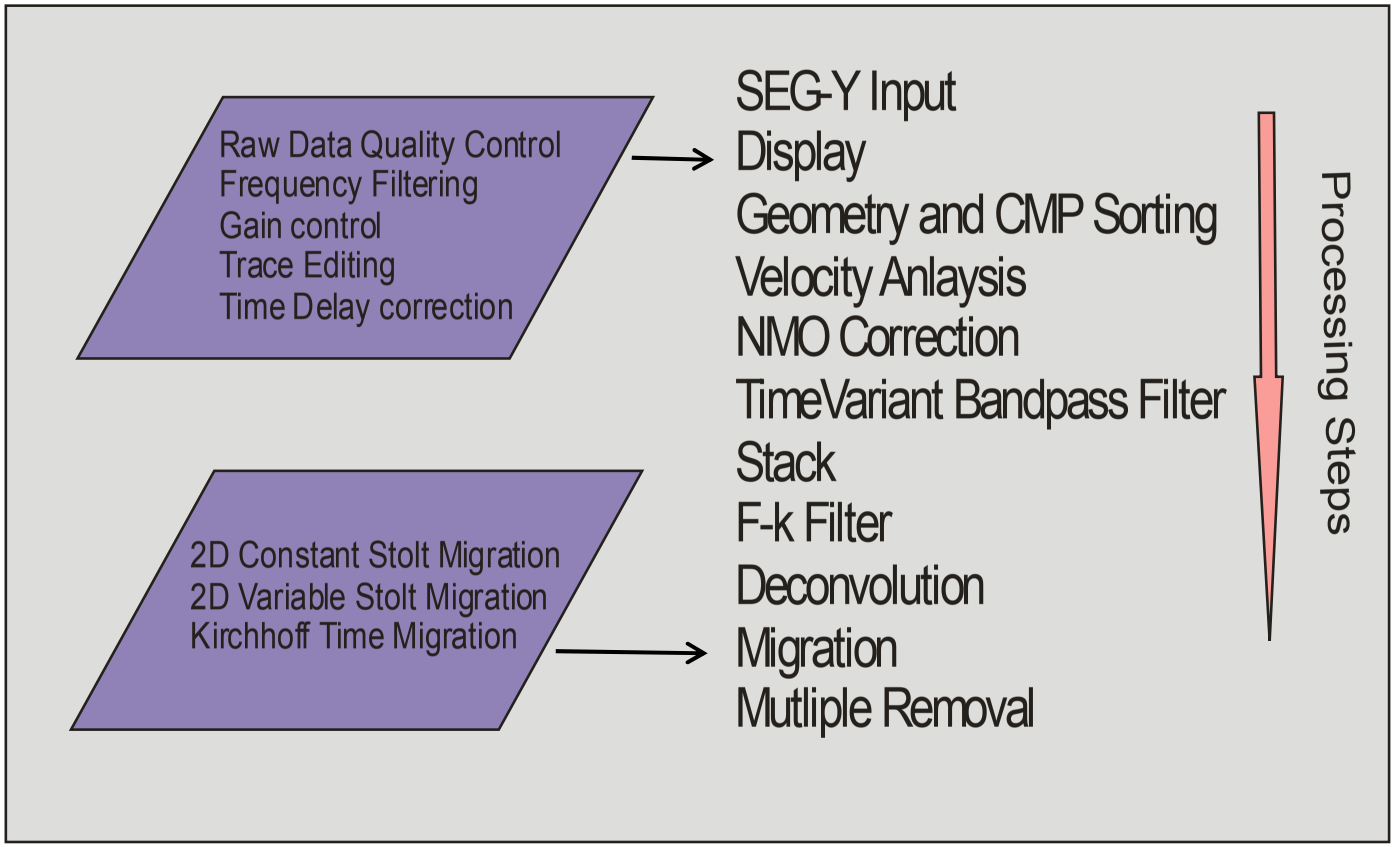

Figure 2.5 Data processing flow of the marine seismic data set used in this thesis. The purple boxes include the side steps that are used as needed.

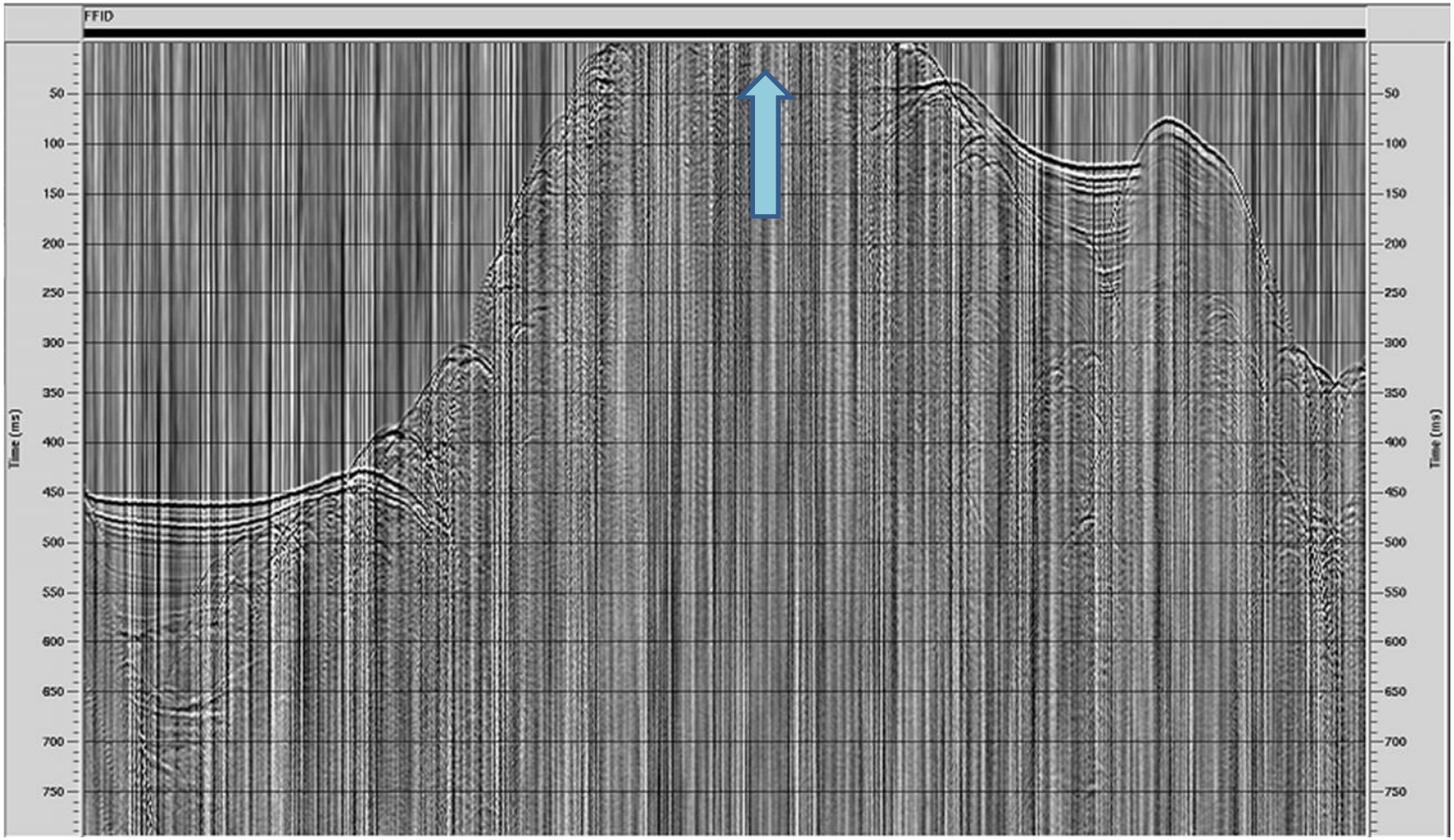

Figure 2.6 Line from 2007 which has a wrong delay time. Blue arrow is delineating the cut-off on the seabed because the recording delay was not reduced as the seabed high was approached.

2.3.2.1 Frequency Filtering

Frequency filtering is applied to the data for noise suppression (especially swell and equipment noise for marine reflection data); hence, the signal/noise ratio is increased. Minimal permanent filtering is applied at this stage, so as to retain as much of the source band width as possible

Spectral analysis was used in order to view the frequency content of the data and a number of Butterworth and Ormsby filters were tested to obtain the optimal signal/noise ratio. The trial and error method yielded slightly different results for each year s data.

Figure 2.7 is an example of a near-trace gather from the 2010 data. The raw data is dominated heavily by very low-frequency noise. A Butterworth bandpass filter was applied with a bandpass of 25-180 Hz with roll-offs of 24 dB/octave and 36 dB/octave at low and high ends, respectively. The low frequency noise was mostly removedwith the choosen parameters (Fig. 2.8). A single bandpass filter was used for display purposes whereas time variant bandpass filter (TVF) was required for use in some of the 2010 lines in order to remove high frequency noise deep in the section. F-K filtering was another type of noise attenuation technique used in some of the 2007 data. These two filters will be discussed later in the chapter, since they were applied later in the processing flow.

2.3.2.2 Gain Control

During the propagation of primary waves into the Earth, energy loss and decay in the seismic amplitudes occurs with time because of the geometrical spreading (spherical

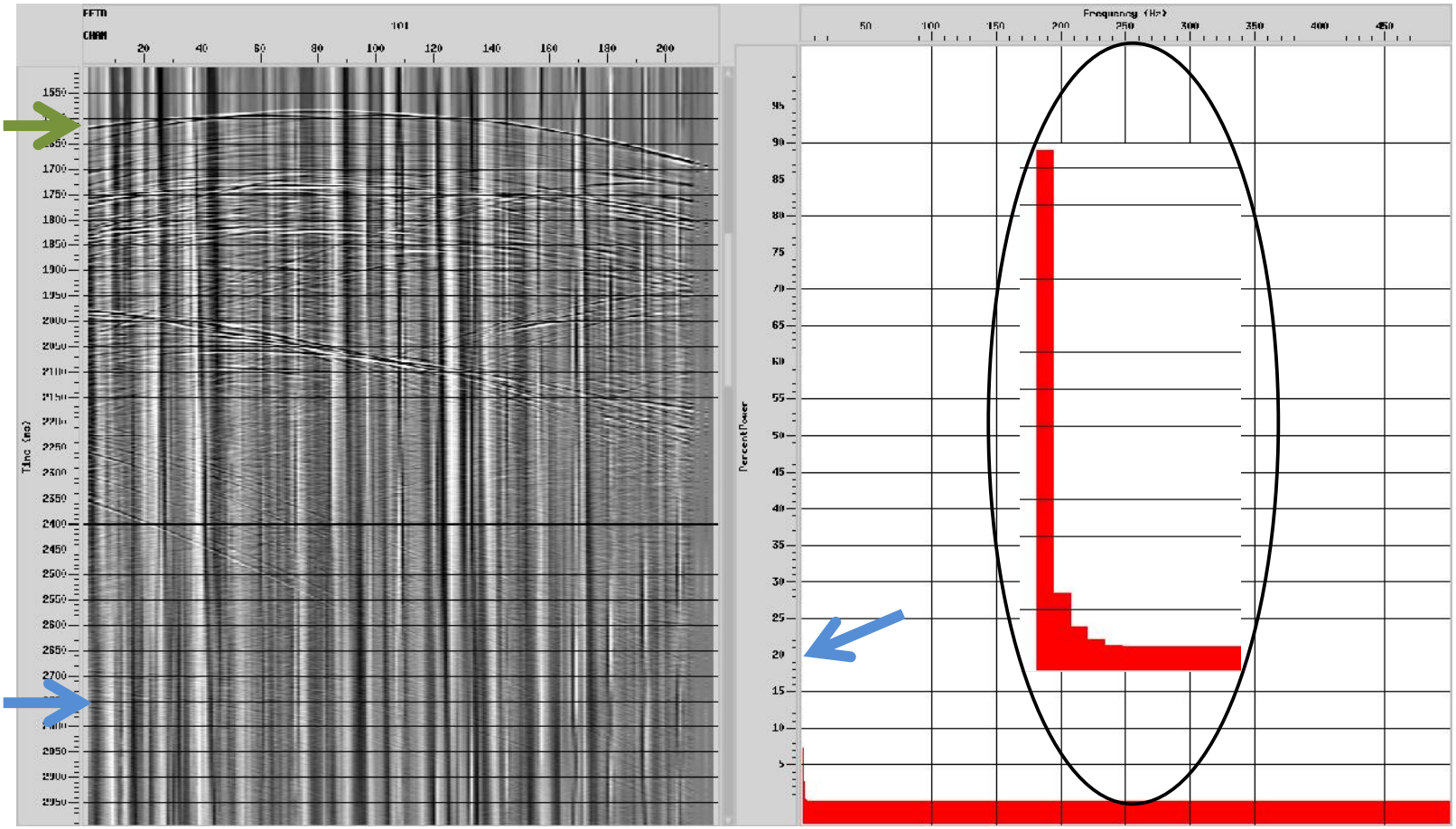

Figure 2.7 Trace display of a raw shot using every channel on the left and its amplitude spectrum on the right. Green arrow shows the seabed reflection and blue arrows point the very low frequency noise dominating the data.

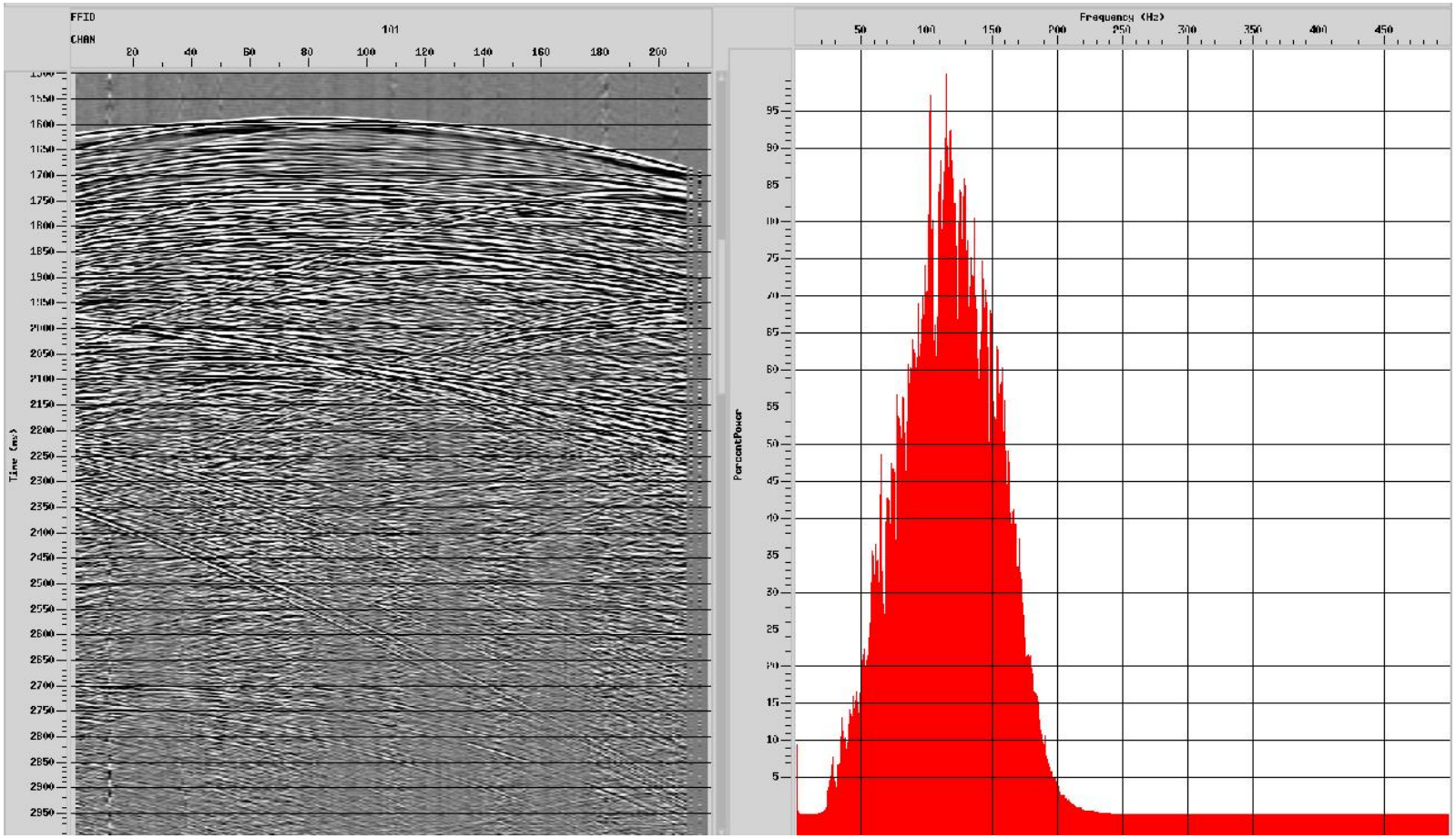

Figure 2.8 The same shot after the application of the single bandpass filter. Notice the suppressed low frequency noise in the data (on the left) and on the amplitude spectrum on the right.

divergence) of the wavefront, inelastic attenuation depending on the elastic properties of the earth and reflection, transmission and conversions of the waves with increasing depth (Yılmaz, 2001). As a consequence, high amplitudes are recorded from shallower depths whereas weak reflections are observed from deep down in the seismic section. In order to compensate for the energy loss and equalize the seismic amplitudes down the seismic section, a spherical divergence gain function, usually proportional to a power of time, is applied as an initial processing step (Yılmaz, 2001).

True Amplitude Recovery (TAR) was used to compensate for spherical divergence (Fig. 2.9). The start time for the correction is chosen to be time zero and a 6 dB/sec correction parameter was used. Automatic Gain Control (AGC) which works by moving down the trace with an overlapping window in order to compute the time-varying scaling factor (e.g., ProMAX User s Manual) was used for display purposes only, with a 500 ms scaling window.

2.3.2.3 Time Delay Corrections

The Finike Basin and vicinity has a complex geology with great variations in seafloor depth from approximately 100 to 4000 ms (Fig. 1.2). Time delays of 500 ms were applied manually to the dathea in t 2007 survey depending on the water depth to allow adequate recording time between shots. Corrections for the manual time delays in the 2007 data were made using the hand-static processor, using the values noted in the log book. Some faulty notes were discovered during QC. In order to confirm the delay times, a near trace gather was displayed and FFID numbers (shot

(a)

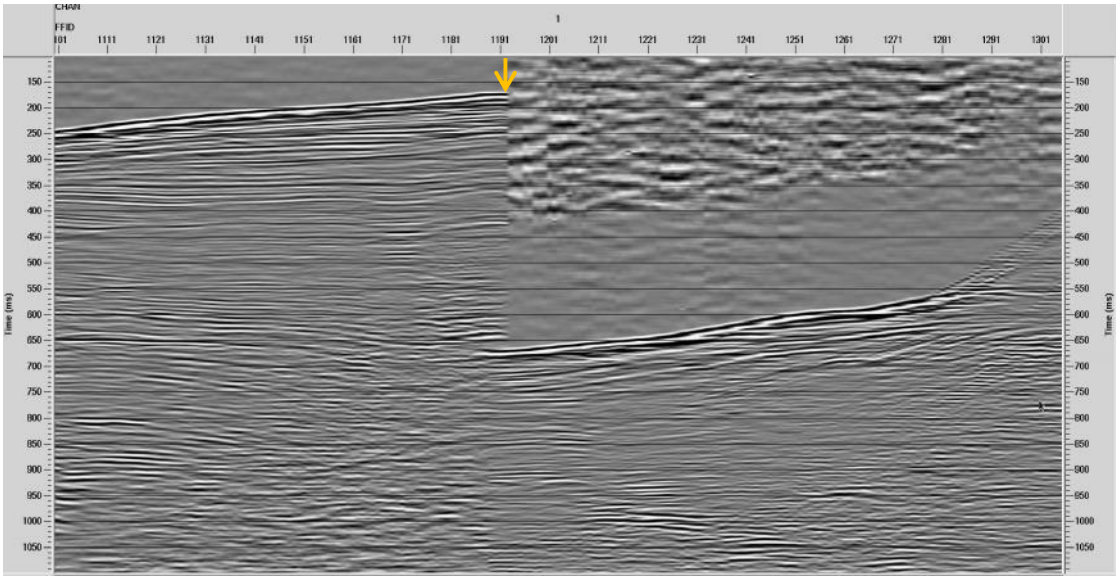

(b)

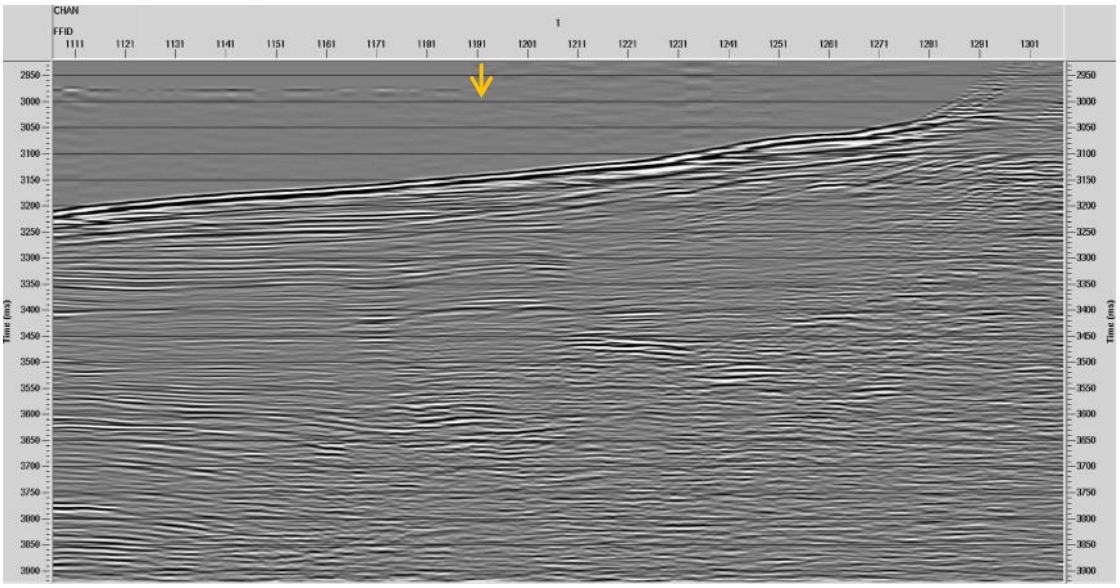

Figure 2.9 Figure showing the geometry loaded near trace gather and the static correction that is needed to be carried out, (a) the static correction for the block on the left is 3000 ms and for the block on the right is 2500 ms. Orange arrow shows the location beyond which the correction is applied, (b) shows the corrected gather

numbers)inspected in detail by zooming (Fig. 2.9a). After noting the exact FFIDs and times required for delays the data was shifted to its real position by using the Hand Statics tool in ProMAX (Fig. 2.9b).

A 30 ms correction had to be applied to the 2008 data to correct for the small delay between the recorder and shot-firing box. The size of this static correction was calculated from the travel time of the direct waves.

2.3.2.4 Trace Editing

It was observed that channel thirteen is dominated by noise in 2007 data (Fig. 2.10). Trace editing was used to kill channel thirteen. The 2008 and 2010 data also had problematic channels. However, since signal quality was good enough, trace killing was not used in order to prevent the loss of primary reflection (Fig. 2.11).

2.3.3 Geometry Load and CMP Sorting

As explained above, the survey ıs desıgned wıth redundant coverage in order to enhance the weak reflections. A Common Mid Point (CMP) is located halfway between a shot and any one receiver. The CMP defines the vertical line along which all reflection points would lie if all the reflectors were horizontal (Figs. 2.2a, 2.2b). Grouping together the reflection traces from separate shot recordings that have the same CMP is called CMP sorting. The addition of all the traces in a CMP gather is called stacking and requires correction for the time variation of variable offset (Yılmaz, 2001) (Fig. 2.2c).

Setting up the geometry is a critical step between initial and further processing. A geometry spreadsheet with acquisition data such as shot/receiver number, spacing and

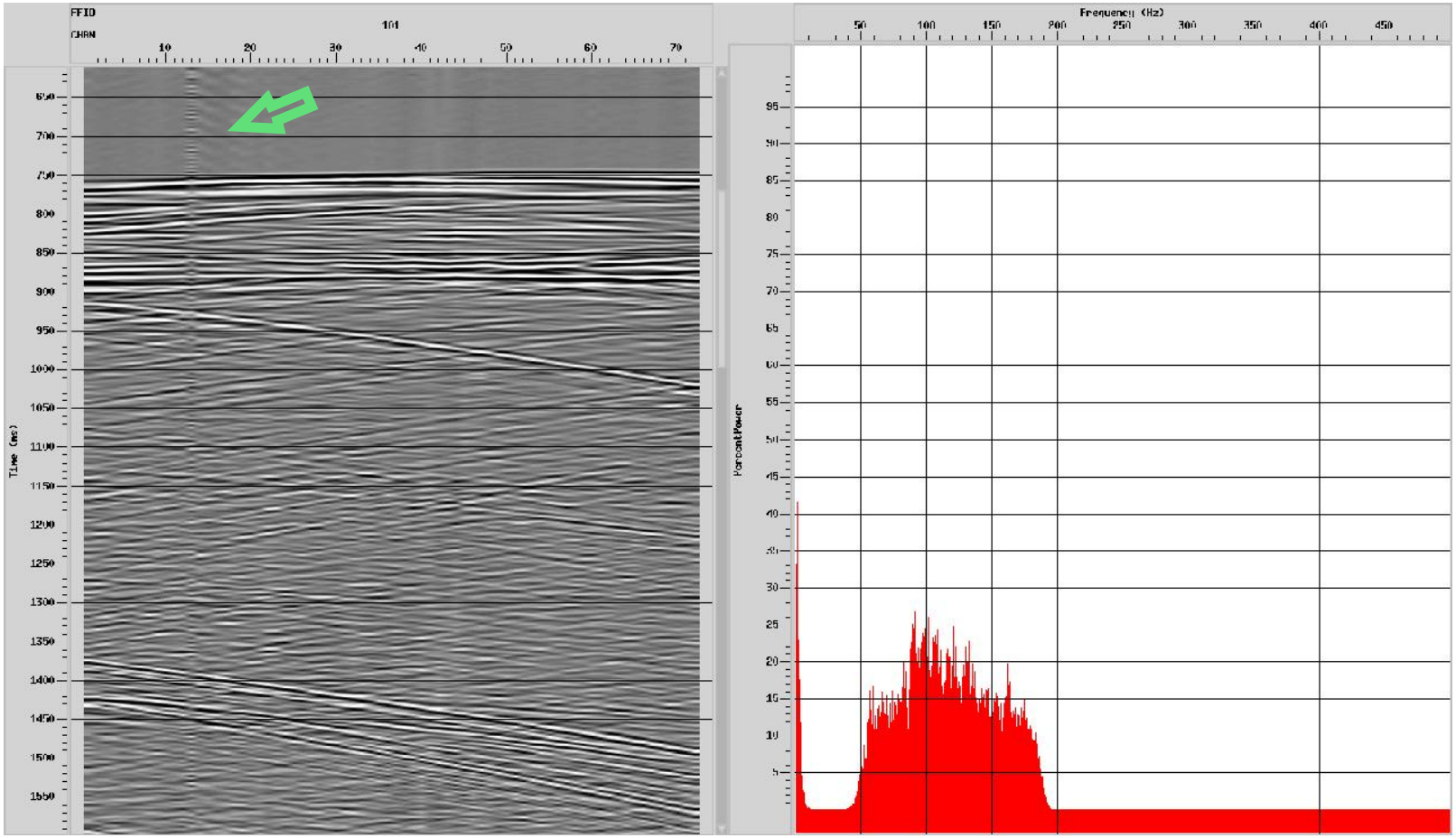

Figure 2.10 A single shot gather displaying the noisy channel thirteen from 2007 survey.

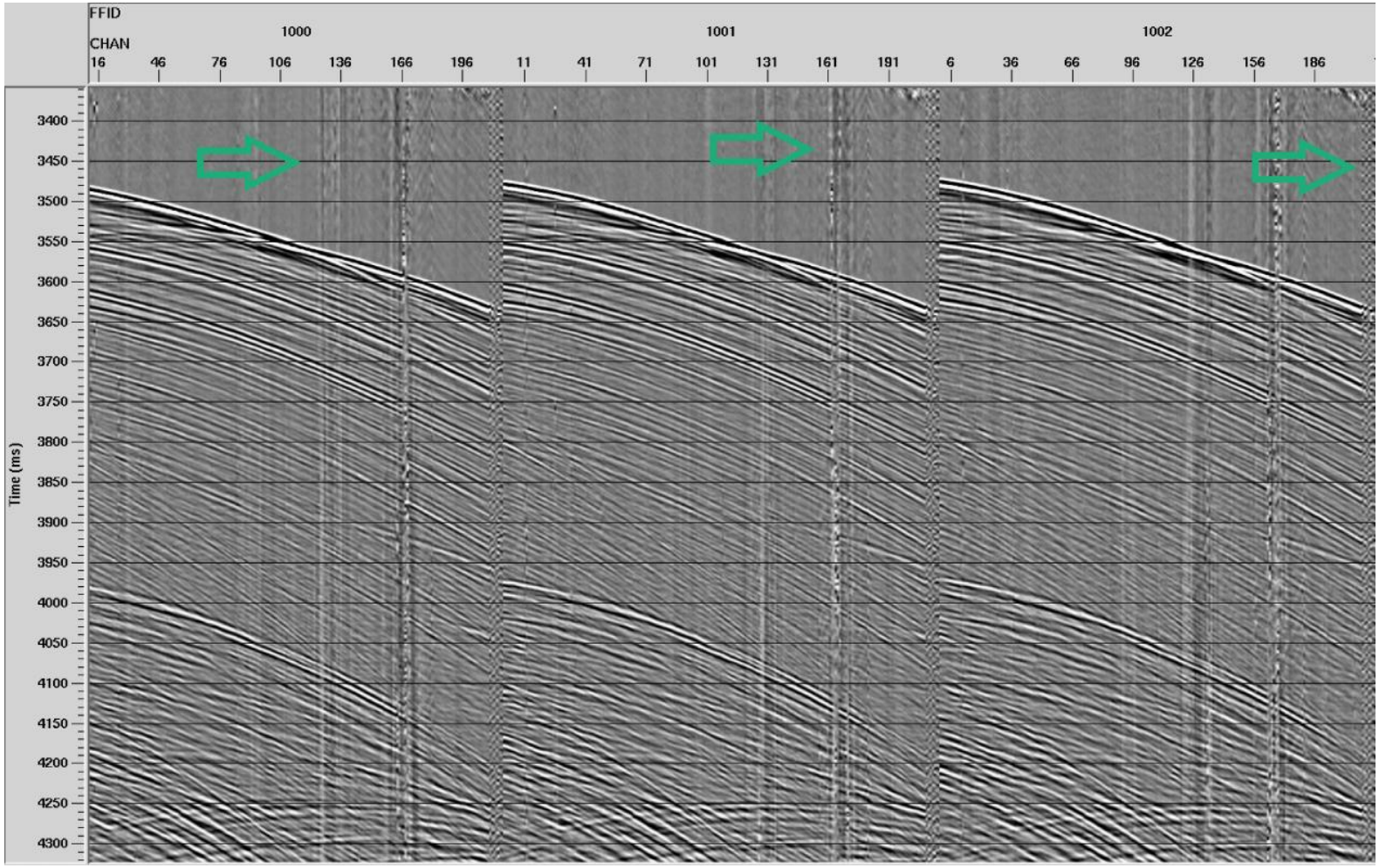

Figure 2.11 Three shot gathers from 2010 survey showing various noisy channels by green arrows

offset etc., was filled manually in the 2D Marine Geometry Spreadsheet After filling the spreadsheets, the coordinates were checked using quality control mapping. Then the last step, binning, was applied by creating a binning spreadsheet that assigns every trace to a CMP.

After CMPs were calculated succesfully for the survey, the geometry data were written to the dataheader of a new file to be used in later processes. TAR was applied to data permanently in this job flow also.

2.3.4 NMO correction, velocity analysis and stacking

The difference in travel time between zero and non-zero offset reflection arrivals (Fig. 2.2c) is called normal moveout (NMO). In the stacking process the NMO has to be removed before the traces are summed. Velocity Analysis is required to determine the NMO corrections. For a single horizontal reflector below a uniform overlying layer, the equation (2.4) relating reflection time (T) to offset (X) is given by (Yilmaz, 2001).

$$V^2T^2 = X^2 + 4D^2 \tag{2.4}$$

From which,

$$T \approx T_0 + \frac{X^2}{2V^2T_o} \tag{2.5}$$

Where,

$$T_0 = '\,normal \text{ incidence travel } time' = \frac{2D}{V} \quad \text{, and } T_N = T - T_o \tag{2.6}$$

Thus,

$$T_N \approx (X^2) / 2V^2 T_o \quad (2.7)$$

- T_N = normal moveout correction
- X = distance between source and receiver
- V = average velocity to the depth corresponding to
- To = normal incidence travel time.

Because the NMO correction is offset dependent, each trace becomes differentially stretched. This leads to a distortion problem, especially prominent at small reflection times and wide offset. A limiting stretch factor (usually around 10 – 20 %) is applied by muting data that would be stretched beyond the limit (Y lmaz, 2001). The stretch mute percentage for this particular data set was chosen between 30 and 50. Although the data set can be considered to be deep water data, there were areas of shallow water on the continental shelf and slope, where this percentage is more important. Large NMO stretch mutes can remove the seabed reflection on the very shallow part of the stacked sections (Fig. 2.12). The combination of changing the stretch mute percentage with velocity editing removed both stretching problem and reverberations (Fig. 2.13).

The aim of velocity analysis is to detect the best possible velocity functions in order to determine NMO corrections. Semblance spectra, CMP gather, dynamic stack and the constant velocity stacks are used in this analysis. A CMP supergather file is formed using the 2D Supergather Formation tool in ProMAX . For each selected supergather, 27 adjacent CMPs were used in 2010 data, 12 in 2008 and 9 in 2007 data.

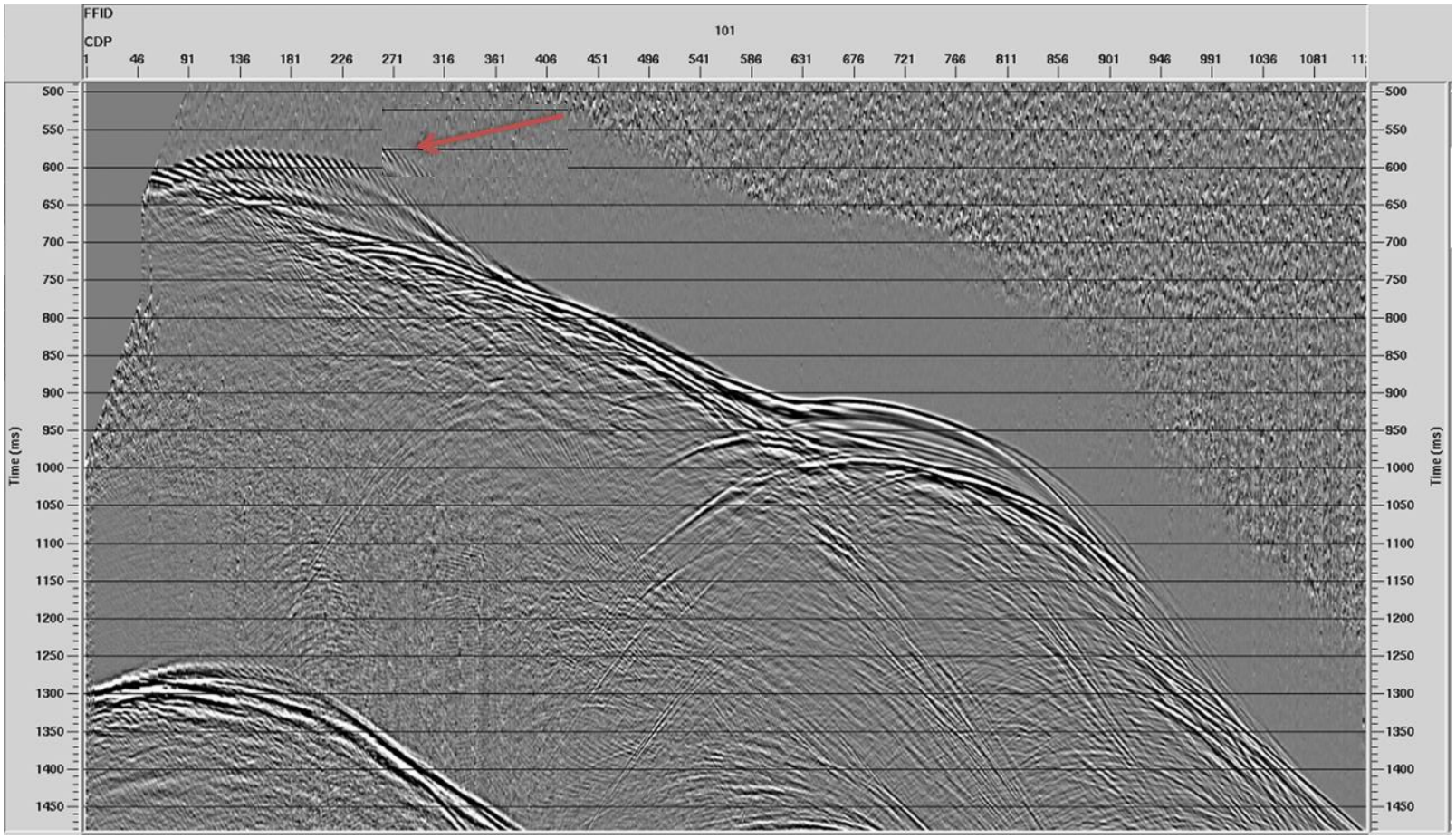

Figure 2.12 Stacked section indicating the reverberation due to the poor velocity control on the shallow part of the seabed with red arrow.

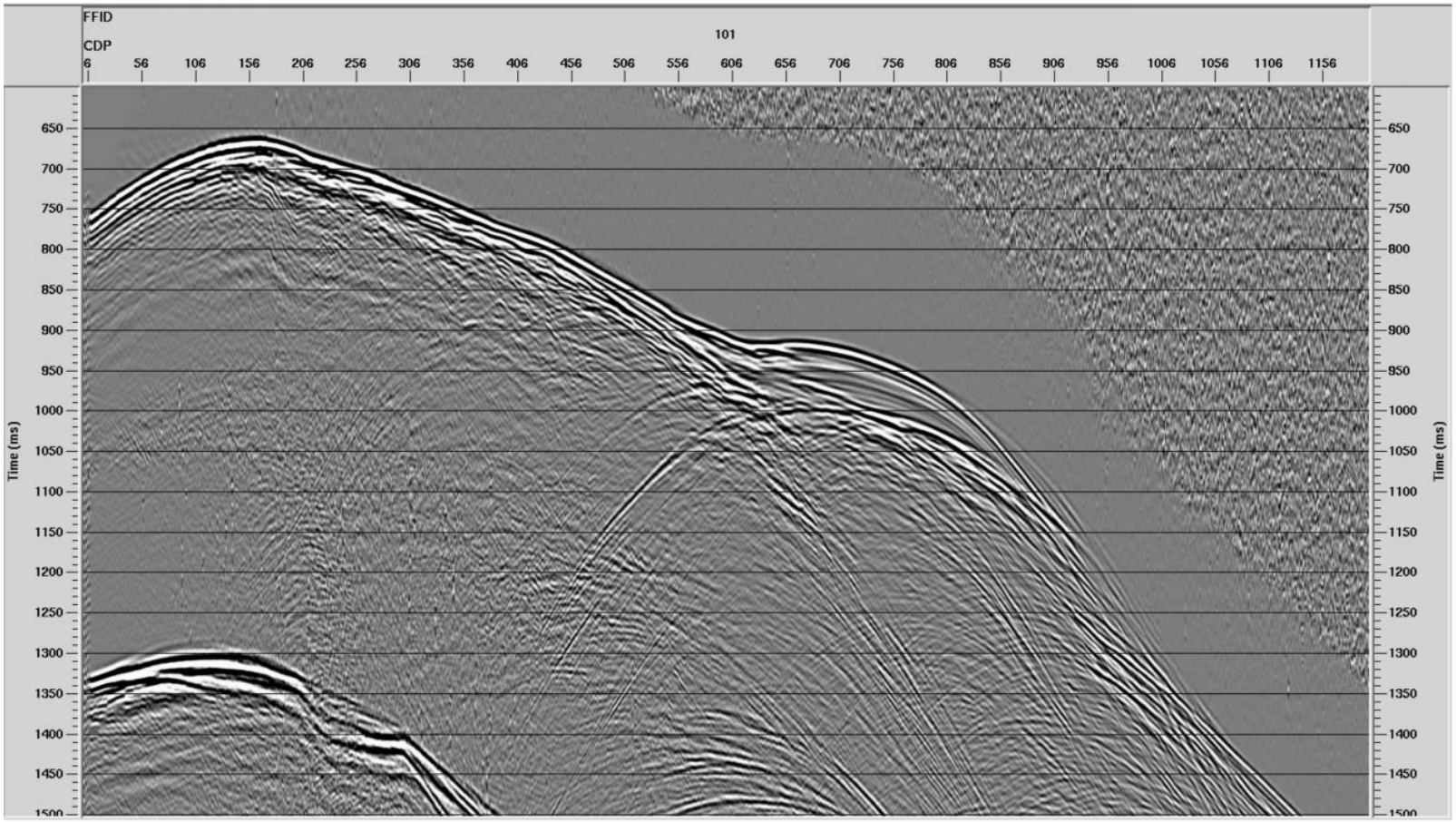

Figure 2.13Illustrates the seabed afterimproved velocity control bythe addition of a number of CDPs for velocity anaylsis and decrease in mute percentage to 30%.

The supergathers enhance signal quality for velocity analysis, provided dip is negligible. Because velocities are linearly interpolated between CMP locations where analyses are made, changes in dip of seabed and subsurface reflectors had a critical role in chooisng specific analysis locations. The semblance spectrum is a function of velocity (horizontal axis) and time (vertical axis) in a contour plot (Fig. 2.14a). The maximum semblance at any time corresponds with the hyperbolic trajectory that provides the maximum coherency. The velocity functions are generated by picking the maximum coherency values (bull s eyes) associated with primary reflections (Y lmaz, 2001, proMAX User s Manual). It is possible to check the accuracy of the picks by applying temporary NMO correction to the CMP gather (Fig. 2.15b). If the NMO applied gathers are curved up, the selected velocity indicates a low value which over-corrects the CMP gather, whereas the gathers will be curved down and under-corrected when the selected velocity is high. The best result would give flat reflectors in time which is discernible in the CMP gather panel and give high amplitudes in the dynamic stack panel (Fig. 2.14c). The best velocities can be determined also by using the constant velocity function stacks which are corrected for NMO (Fig. 2.6d). The function panel was chosen to include twelve constant velocity function stacks varying between 1300-3000 m/s. Figure 2.15 illustrates the same supergather after ta velocity function has been picked. For the supergathers which are located in the deep basin, the velocities varied over a small range (1500-1600 m/ s). The velocity analysis of CMPs associated with complicated geological structures

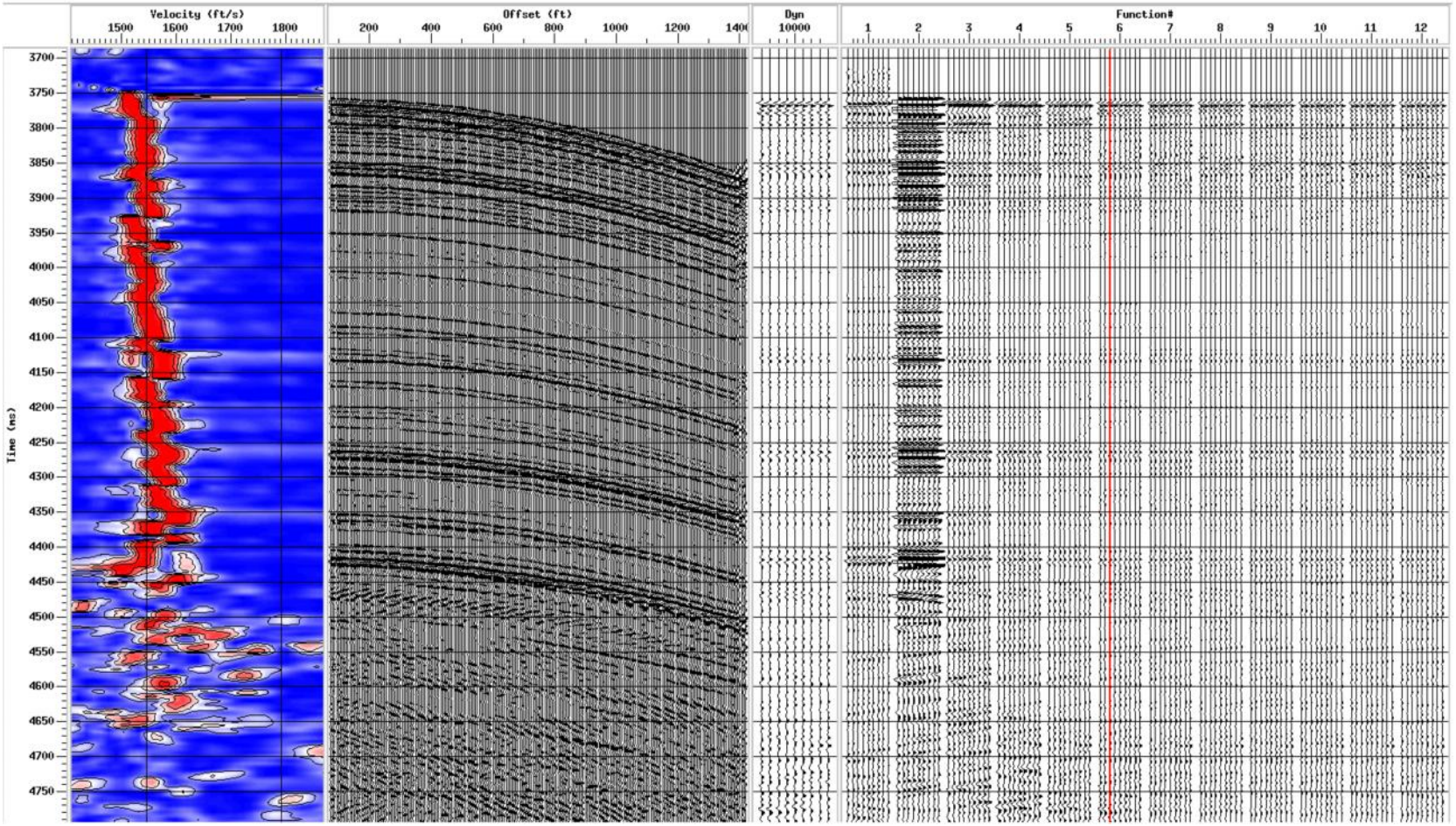

(a) semblance panel (b) gather panel (c) dynamic stack panel (d) velocity function stack panels

Figure 2.14 Illustration of the velocity analysis window including semblance panel, gather panel, dynamic stack panel and velocity function stack panels.

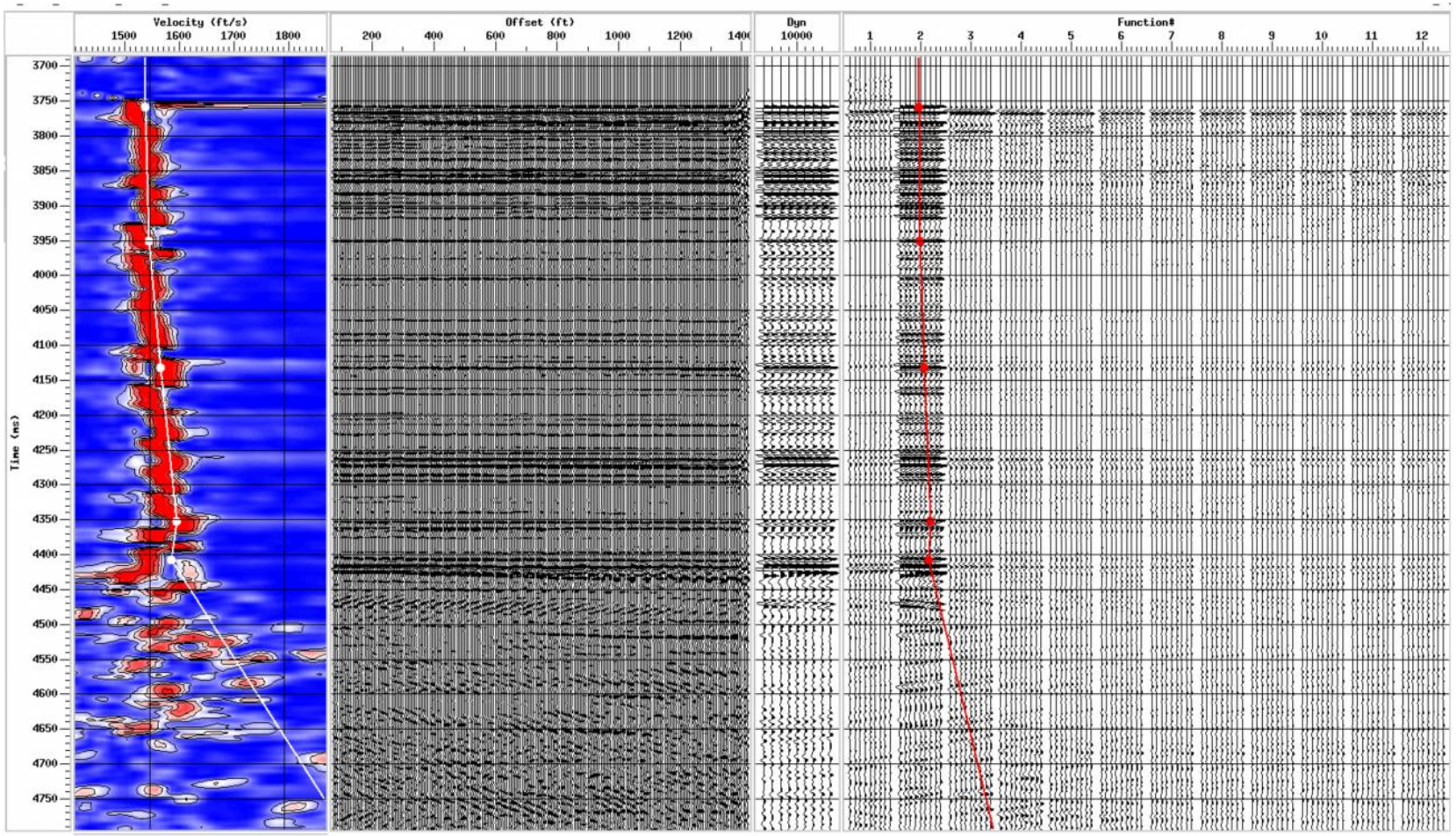

(a) semblance panel (b) gather panel (c) dynamic stack panel (d) velocity function stack panels

Figure 2.15 The same supergather after using apply NMO tool. The resulting gather shows well-corrected flat reflactions. Note that this tool was used for simulation in order to check the accuracy of the rms velocities.

required more careful analysis. Velocity picking of 2010 data was easier because of the greater resolution of the data, provided by the longer streamer, which also affects the accuracy in the semblance (Fig. 2.16-2.18).

After NMO correction, the traces in the corrected CMP gather are added together, and the total normalized by the total number of traces in the gather. This stacking process reduces the traces to a single stacked trace in which reflection time corresponds to a normal incidence travel time (Yılmaz, 2001). The benefit of CMP stacking is to inverse the reflection amplitudes and reduce the effects of noise and multiples (Krebes 1985, 1989). Primary reflections have higher stacking velocities compared to multiple reflections and so accurate NMO corrections reduce the amplitude of multiples.

2.3.5 Time Variant Bandpass Filter before Stack

The 2010 data included unusually high frequency noise deep in the section. In this case using a single band pass filter would not be sufficient because the high frequency response of the shallow sediments would be removed from the data (Fig. 2.19). Therefore, a time variant filter was applied to the data where there was a need and the masking effect of the noise was removed (Fig. 2.20). In practice, three windows were defined by picking four horizons according to their general frequency trends. These selected horizons were the seabed, the two prominent regional reflectors that are later discussed in Chapter 3, and the bottom of the section. In the case of absence of one of the prominent horizons, a minimum 500 ms taper was used in between horizons. It was

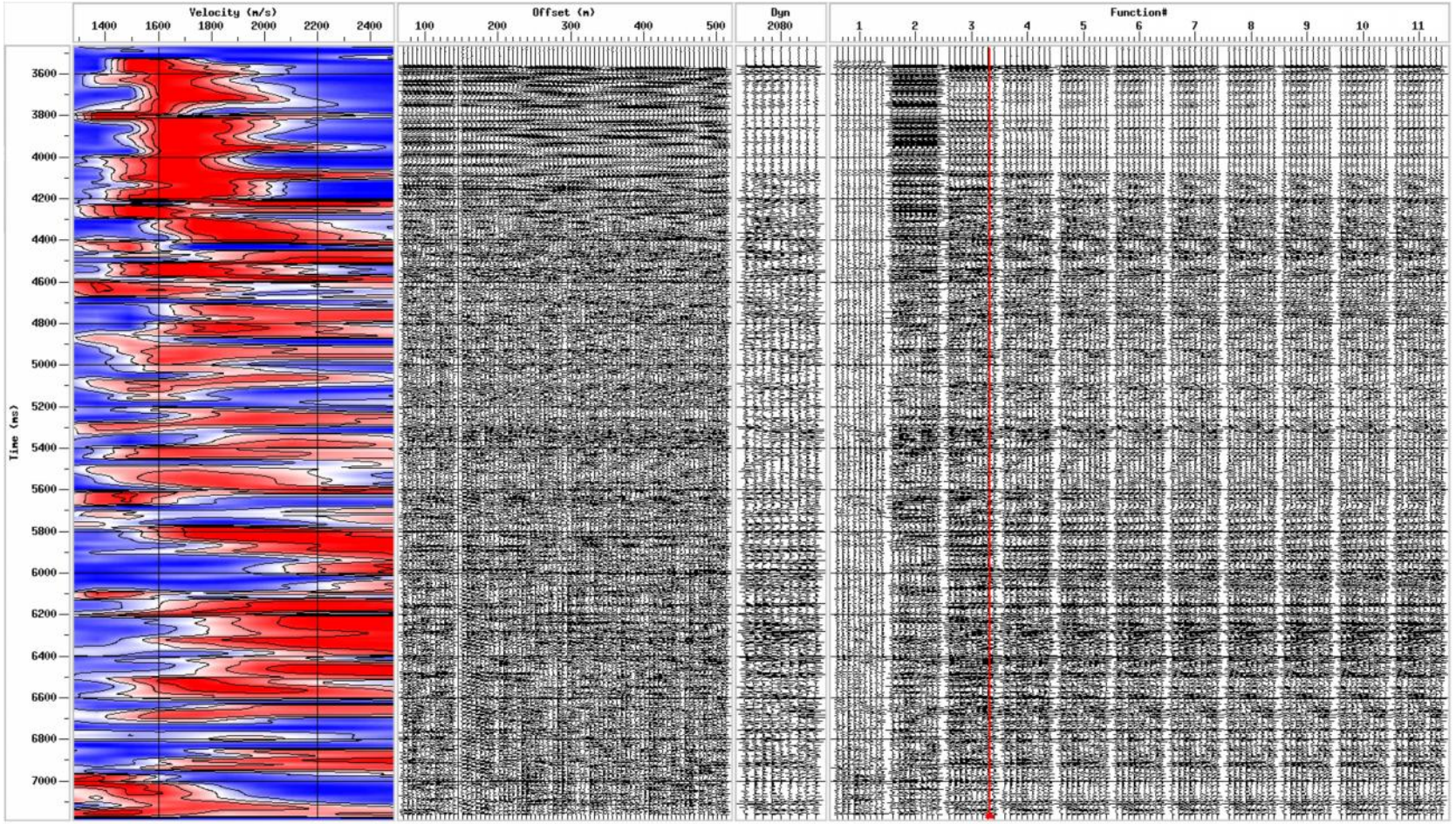

(a) semblance panel (b) gather panel (c) dynamic stack panel (d) velocity function stack panels

Figure.2.16 Velocity analysis window of 2007 data. Notice the wide spread of semblance spectral packs which makes it hard carry out the velocity analysis.

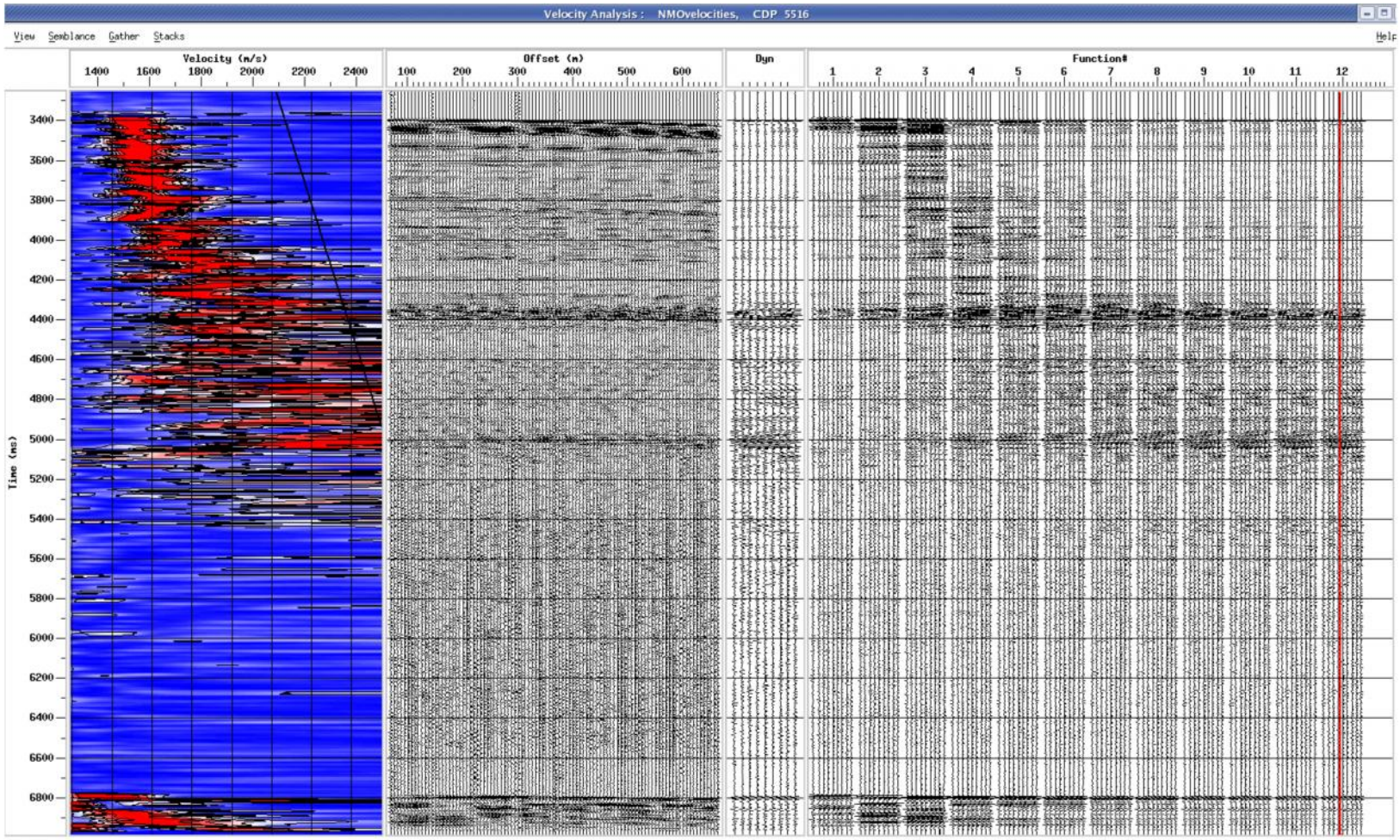

(a) semblance panel (b) gather panel (c) dynamic stack panel (d) velocity function stack panels

Figure 2.17 Velocity analysis window for 2008 data. Note that the semblance spectrum, which displays stack response as a function of time an velocity, is better resolved then the 2007 example (Fig. 2.16) due to the increase in fold.

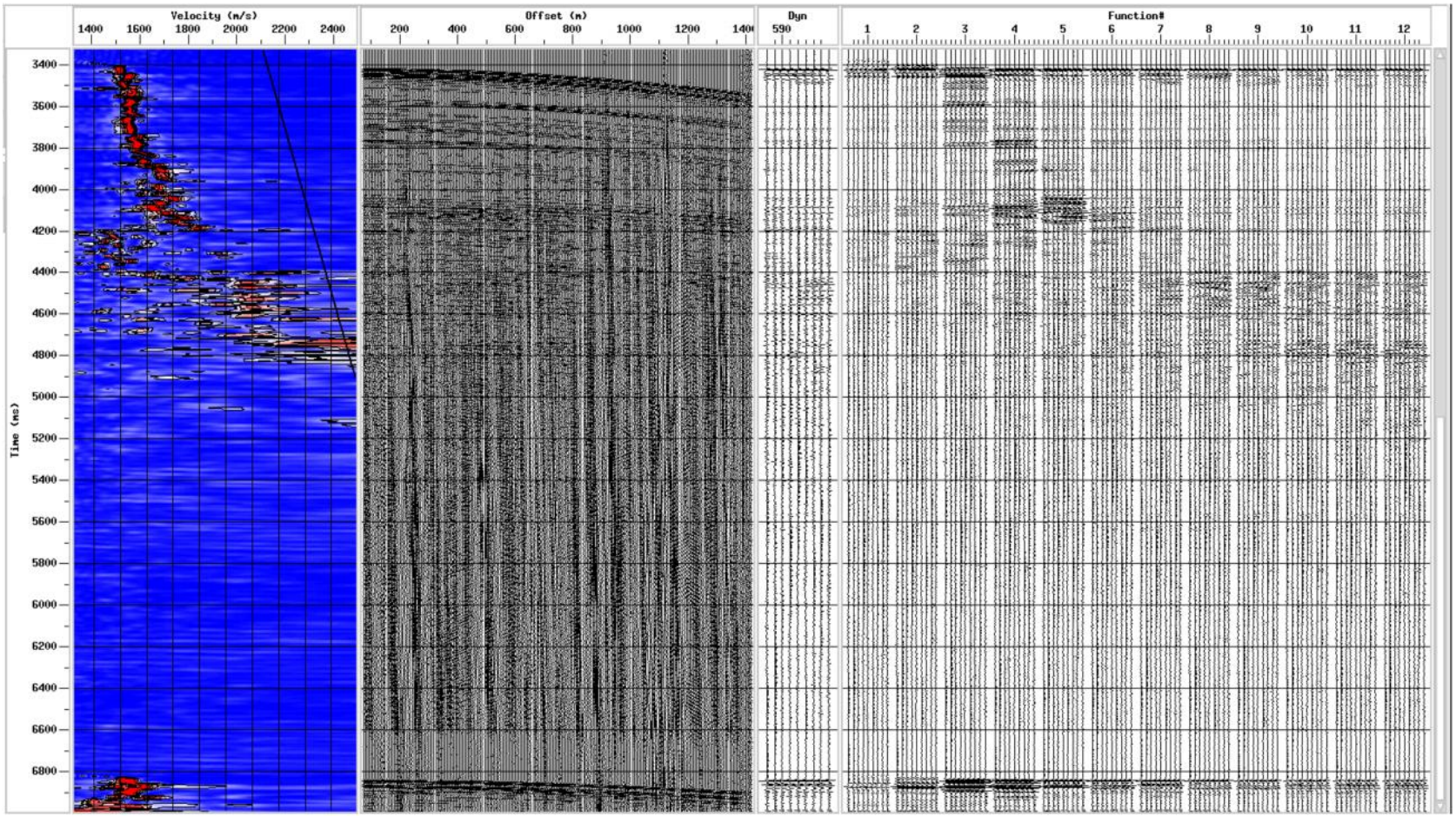

(a) semblance panel (b) gather panel (c) dynamic stack panel (d) velocity function stack panels

Figure 2.18 Velocity analysis window for 2010 data has the best resolved semblance spectrum because of the longer streamer.

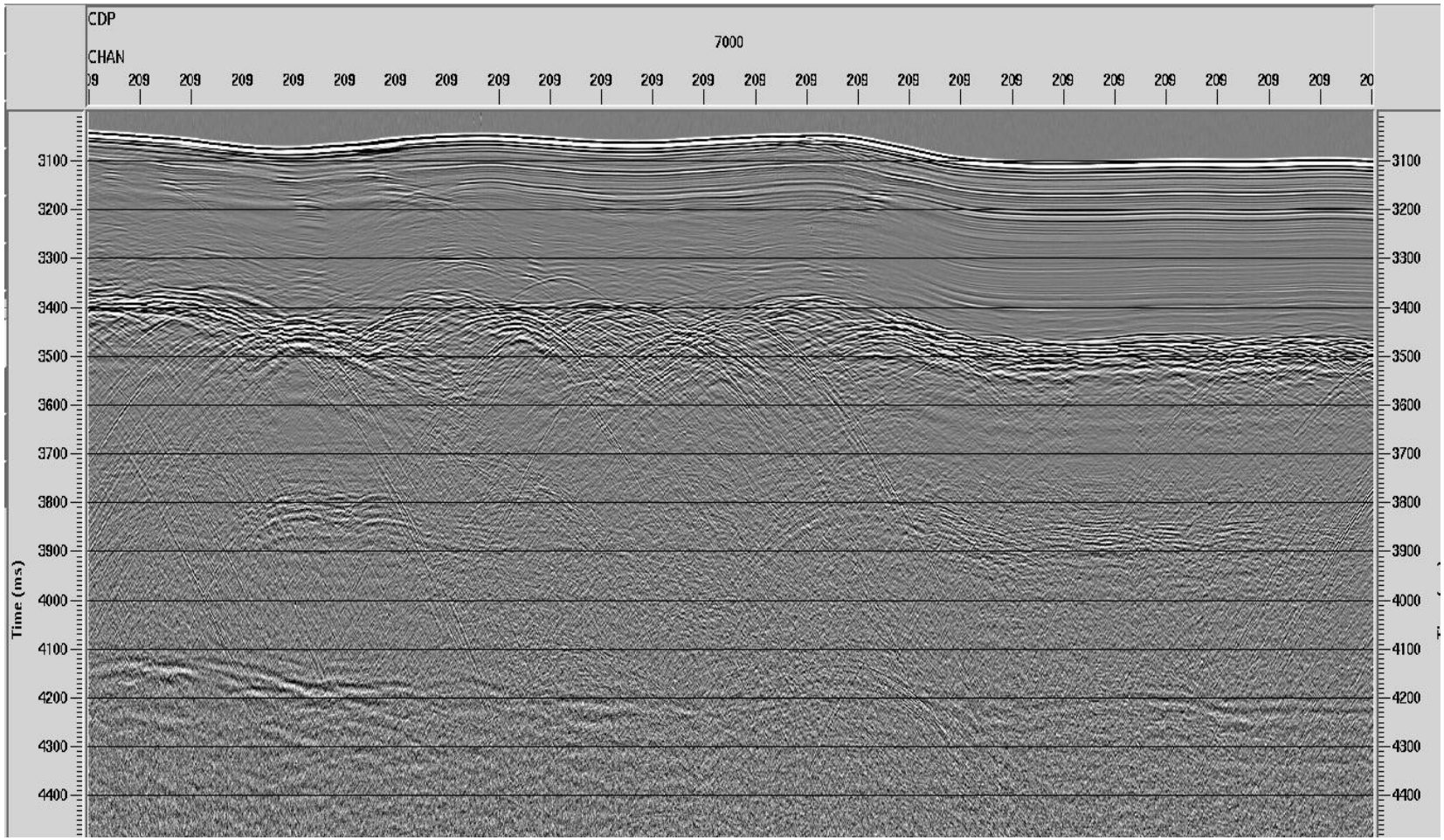

Fig. 2.19 Stacked data without time variant filtering. Notice the high frequency noise which is increasing deeper in the section.

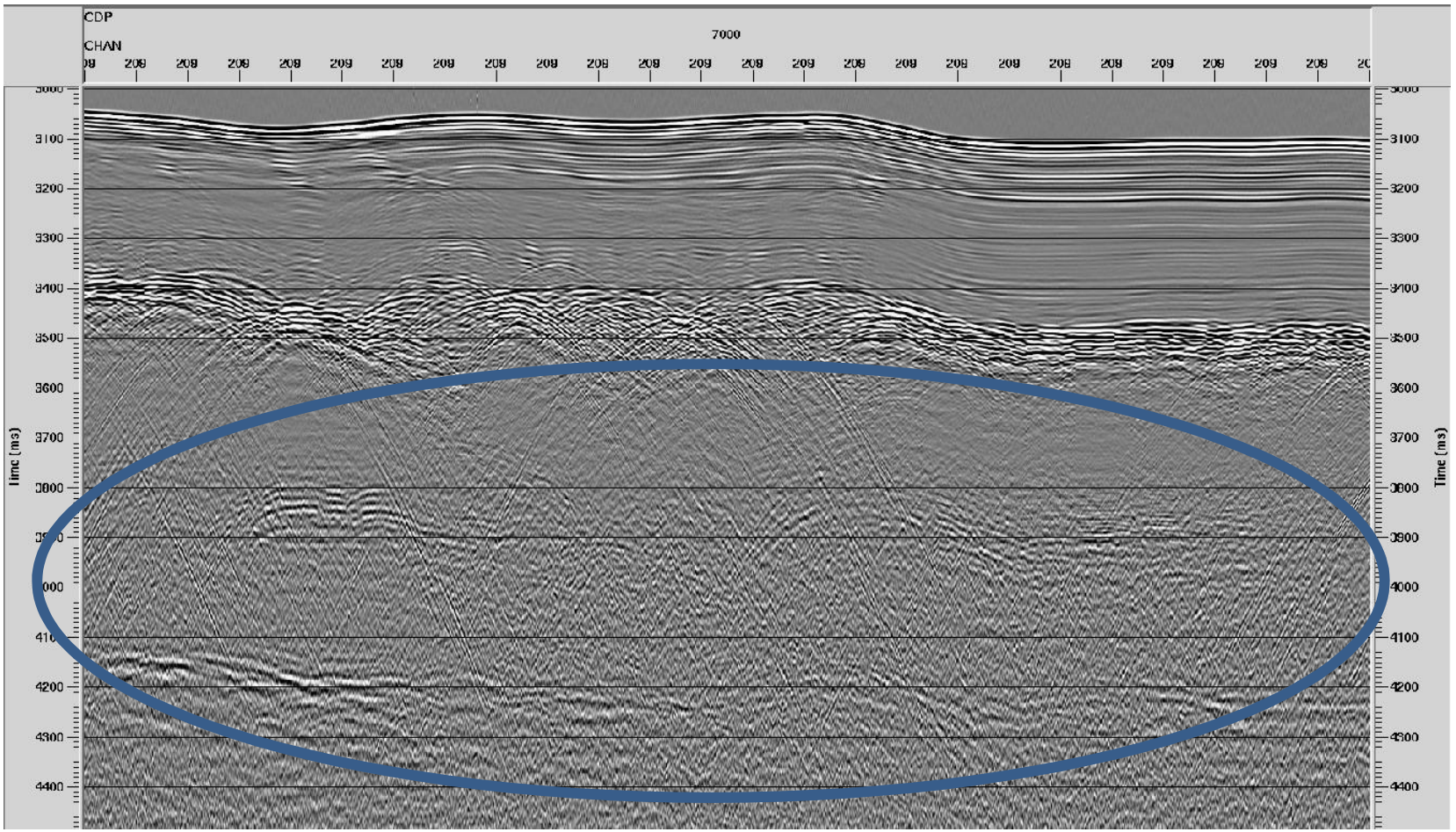

Fig. 2.20 Stacked section after the application of time-variant filtering. Notice the reflections in the circle that were masked before the filer.

important to keep high frequencies in the first window which mostly consisted of Pliocene-Quaternary sediments and the M- reflector.

2.3.6 F-K Filter

F-k filtering was also used on some lines which have coherent low frequency noise that could not be suppressed adequately by time variant filtering. It was only used in a number of 2007 lines before stack which did not yield a satisfactory signal/noise ratio. To carry out the analysis data were displayed both in T-X domain and F-K domain. A pass polygon was defined in F-k space attention to keep the frequency-wavenumber values and velocities of the reflections and other events that are observable in the F-K domain (Fig. 2.21). The colors on the F-K spectrum indicate where the data are concentrated. The aim was to keep signal frequencies in the polygon and leave noisy areas outside of the polygon. It was important not to define a narrow polygon in order to avoid data loss (Fig. 2.21). The F-K analysis tool provided the display of the filter response, which was extremely useful in drawing the optimum polygon (Fig. 2.22). The cross-section on the left in figures 2,21 and 2,22 illustrates a CMP gather with relative offset on horizontal axis and time on vertical axis. The seabed reflection is observed around 3800 ms. The low frequency noise here is concentrated below 10 Hz. Although one polygon can be applied to all data it is possible to apply various polygons in different locations as needed. The way the filter works in this case is to linearly interpolate the polygons between each location (Promax users book). The application generated more noise in

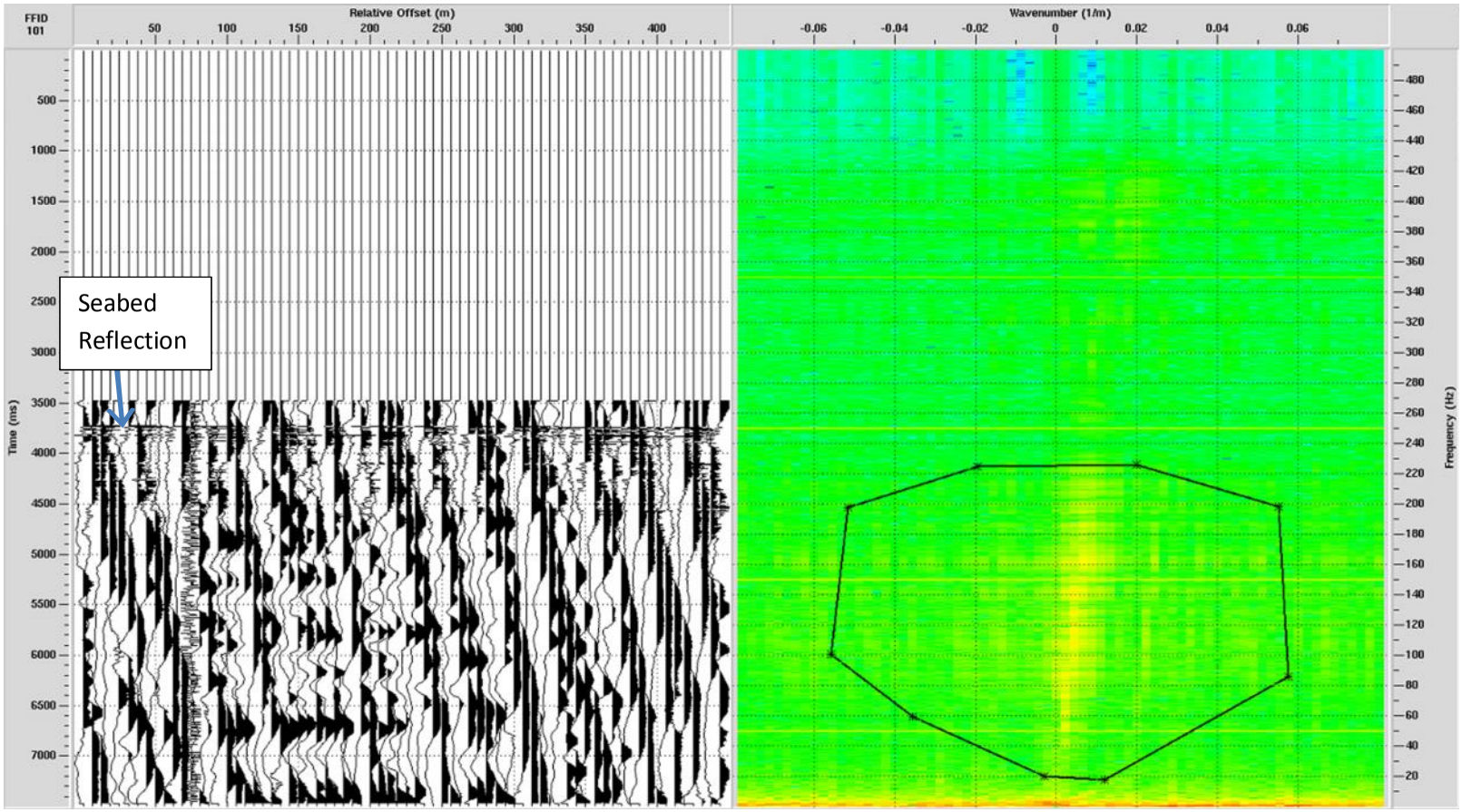

Figure 2.21 Showinga shot gather before the application of the F-k filter on the left and the selected polygon chosen as a pass area on an F-k plo ton the right.Note the high amplitude low frequency noise in the shot gather and the high amplitudes at frequencies less than 10Hz in the spectrum.

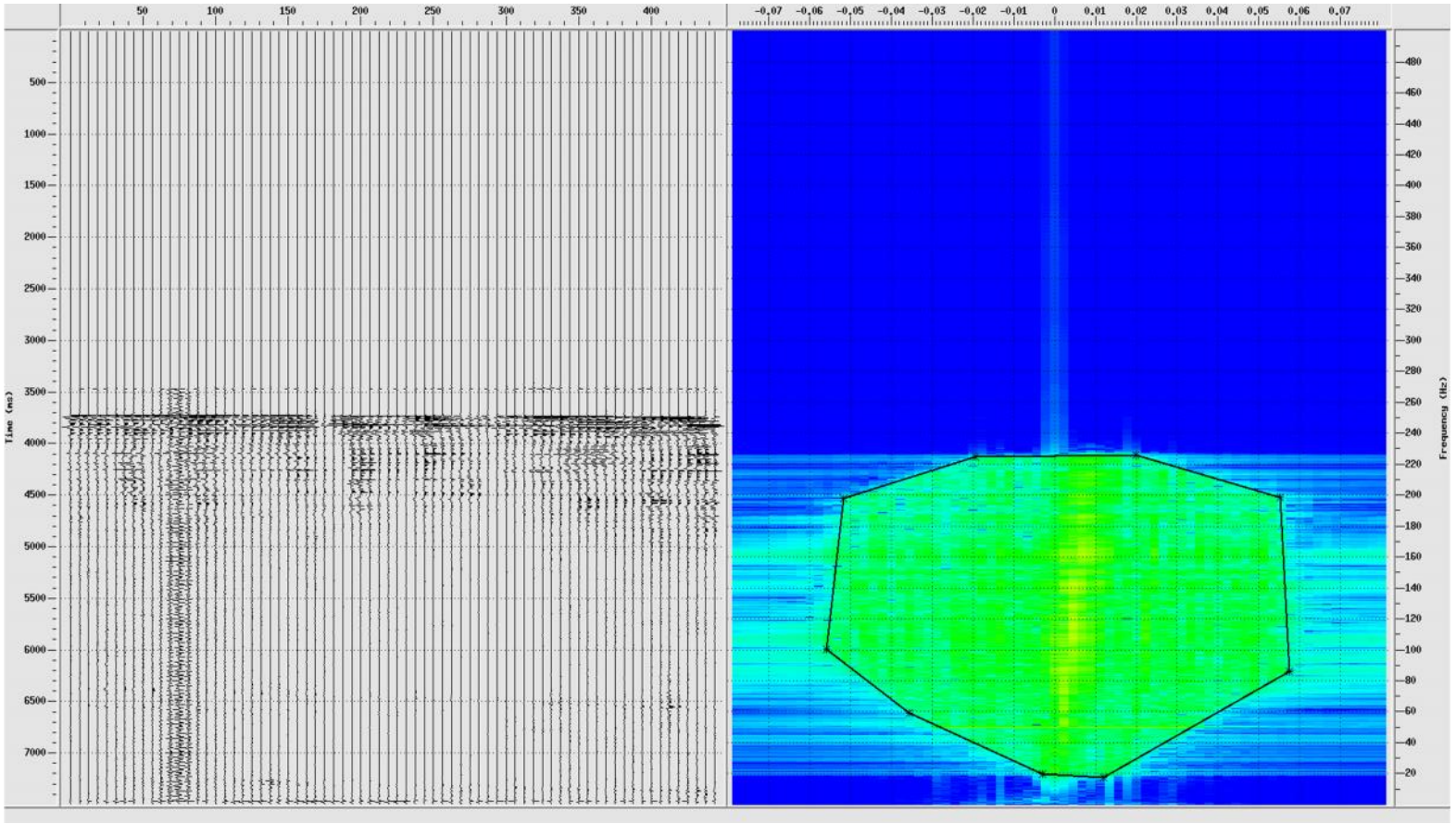

Figure 2.22 Showing the same shot gather as in Fig. 2.21 after the application of the F-k filter on the left and F-k spectrum after filtering on the right. Notice the low frequencies have been removed from both shot gather and the spectrum.

a few lines, therefore, was not preferred but it was efficient on some other lines (Fig. 2.22-2.24)

2.3.7 Deconvolution

The source signature, the receiver response, the instrument response and the geology in the study area, as a combination, form the recorded seismic data (Krebes and Hearn, 1985, Krebes 1989; Yılmaz, 2001). One of the aims of processing is to retrieve the geological information, minus the effects of the source signature, the receiver response and the instrument response. Deconvolution aims to eliminate these extra effects, suppressing the reverberations and short period multiples and improving data resolution.

Deconvolution can be applied both to prestack and to stacked data. Spiking deconvolution is usually applied pre-stack to contract the source wavelet into a spike, hence, enhancing the temporal resolution. In practice, the source wavelet is not independently known so statistical deconvolution is used, which depends on the source wavelet being minimum phase. This means the energy in the wavelet is biased towards the front of the signal. This is only approximately true for marine air-gun sources. The implication of not having a minimum phase wavelet would effect the recovery of the reflectivity. Poststack deconvolution is generally applied to remove the effects of reverberations and multiples.

Deconvolution for this particular data set is not essential since the seabed reflection was acceptably short and, multiples were not an issue because the data were usually collected from deep water. However in some places the resolution was poor and the data were affected by reverberation and ringing which are seismic resonance resulted

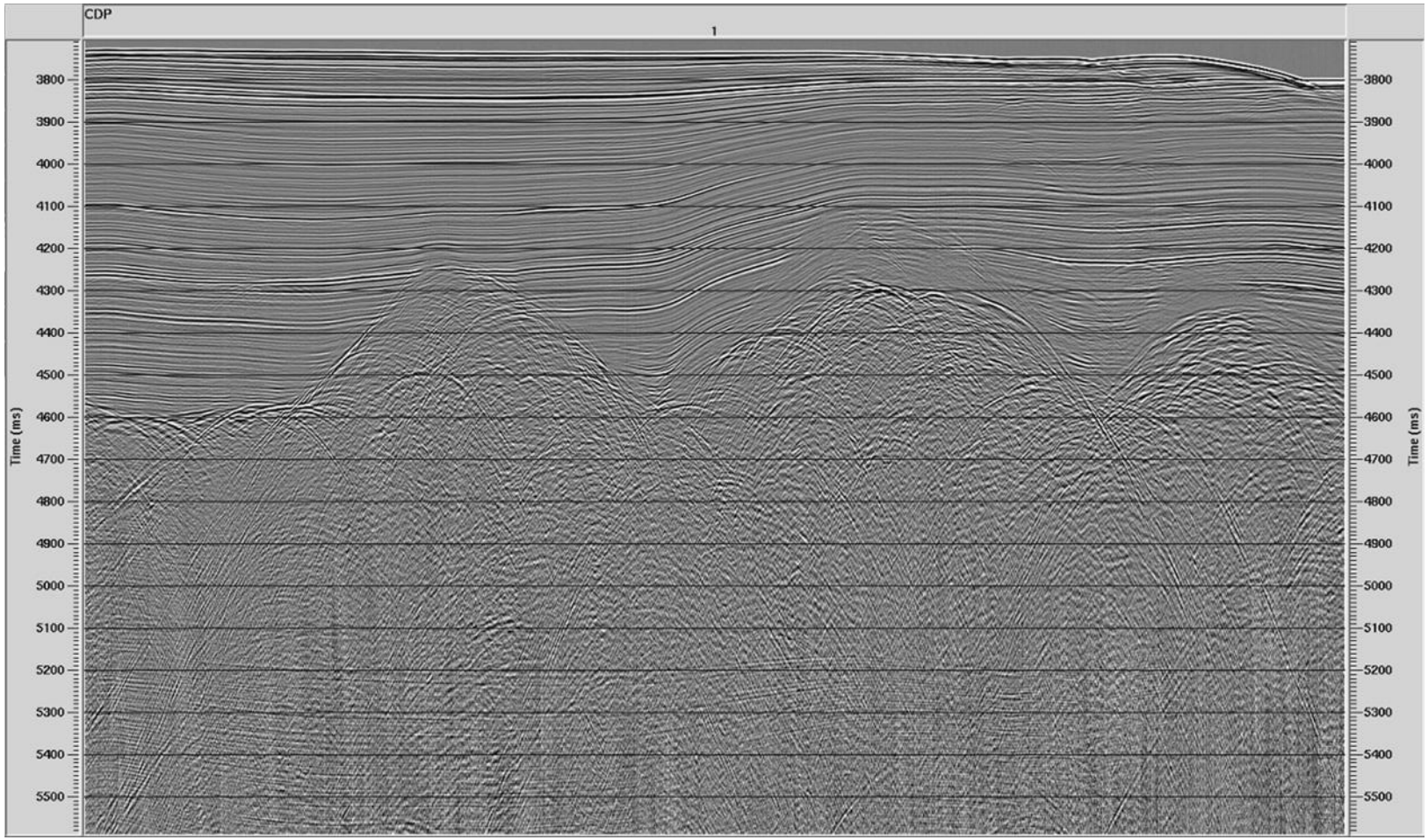

Figure 2.23 Stacked data without F-k filter. The low frequency noise which was observable in the shots is stacked in so that the amplitudes of the noise are higher.

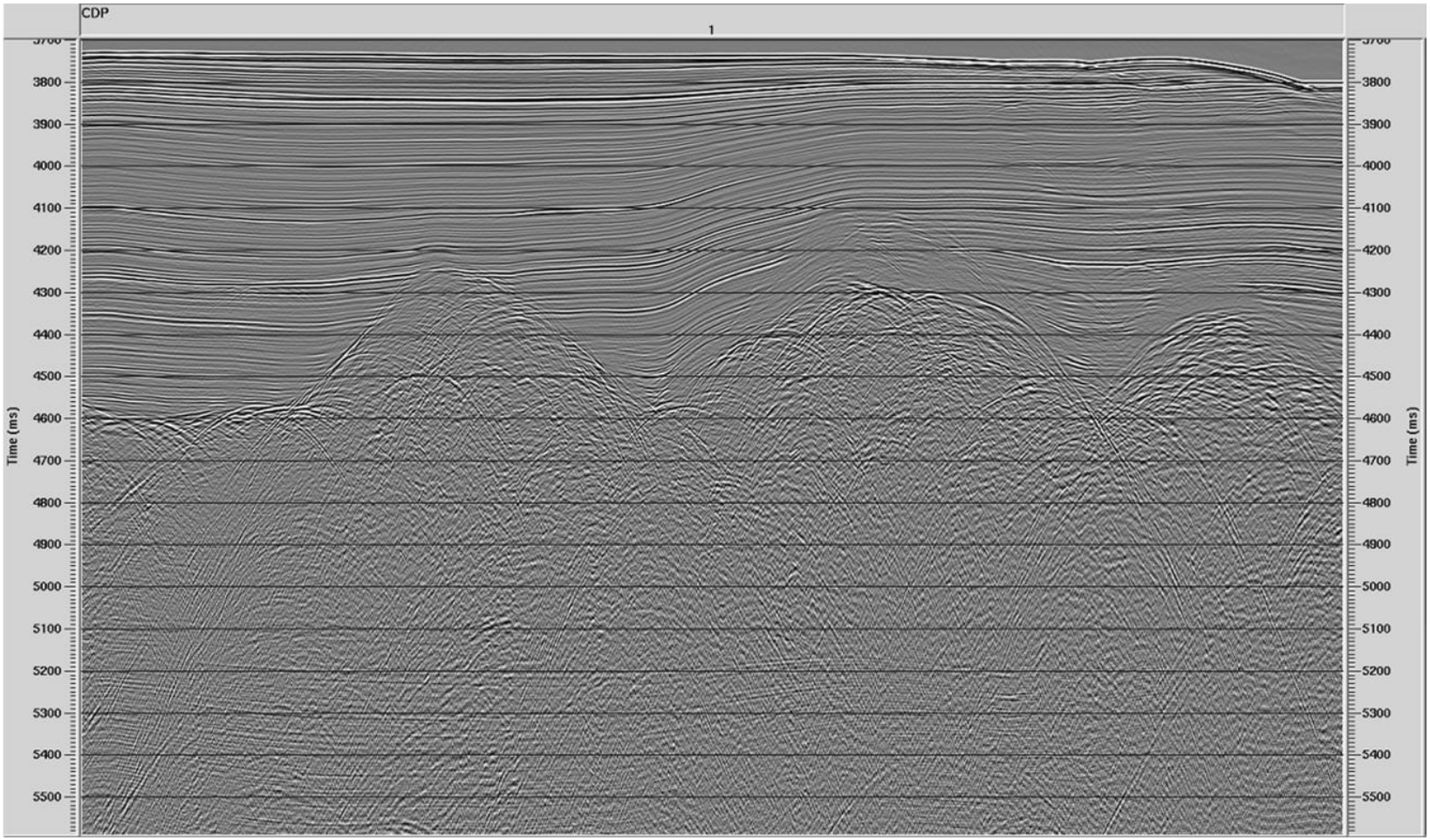

Figure 2.24 Stacked data after F-k filtering. The low frequency noise is abscent in the stack carried with the F-k filtered shots.

from short-path multiples in a water layer. In such cases, spiking deconvolution was tried, but was not useful in increasing the data quality since it generated high frequency noise. It is commonly usable to apply filtering to suppress the resulting noise. Attempts at removing the high frequencies reulting from the spiking deconvolution did not improve the data quality. As a result, a number of trials of short-gap of deconvolution for this particular data set did not improve the image.

2.3.8 Multiple Attenuation

Since much of the data were collected in deep water the seabed multiples were arrived after the most of the primary reflection wavefield. In shallow water, where seabed multiples interfere with reflections, special techniques such as predictive deconvolution, adaptive deconvolution, f-k multiple removal, wave equation multiple removal and radon techniques were tried with negative results. In practice it was possible to stack out the multiples since the velocities suitable for stacking reflections overcorrected multiples. Figure 2.25 depicts an example from 2010 data in which the seabed multiple was reduced by stacking. Further multiple removal was achieved by filtering with a TV bandpass. This was achieved by using the low frequency features of primaries that are temporally deep in the section and distinguishing them from the seabed mutliples which have high frequencies.

2.3.9 Migration

Violation of the assumption that reflectors are horizontal produces artefacts in the images. The problems are that reflection mid-points appear in the wrong place (Fig. 2.26)

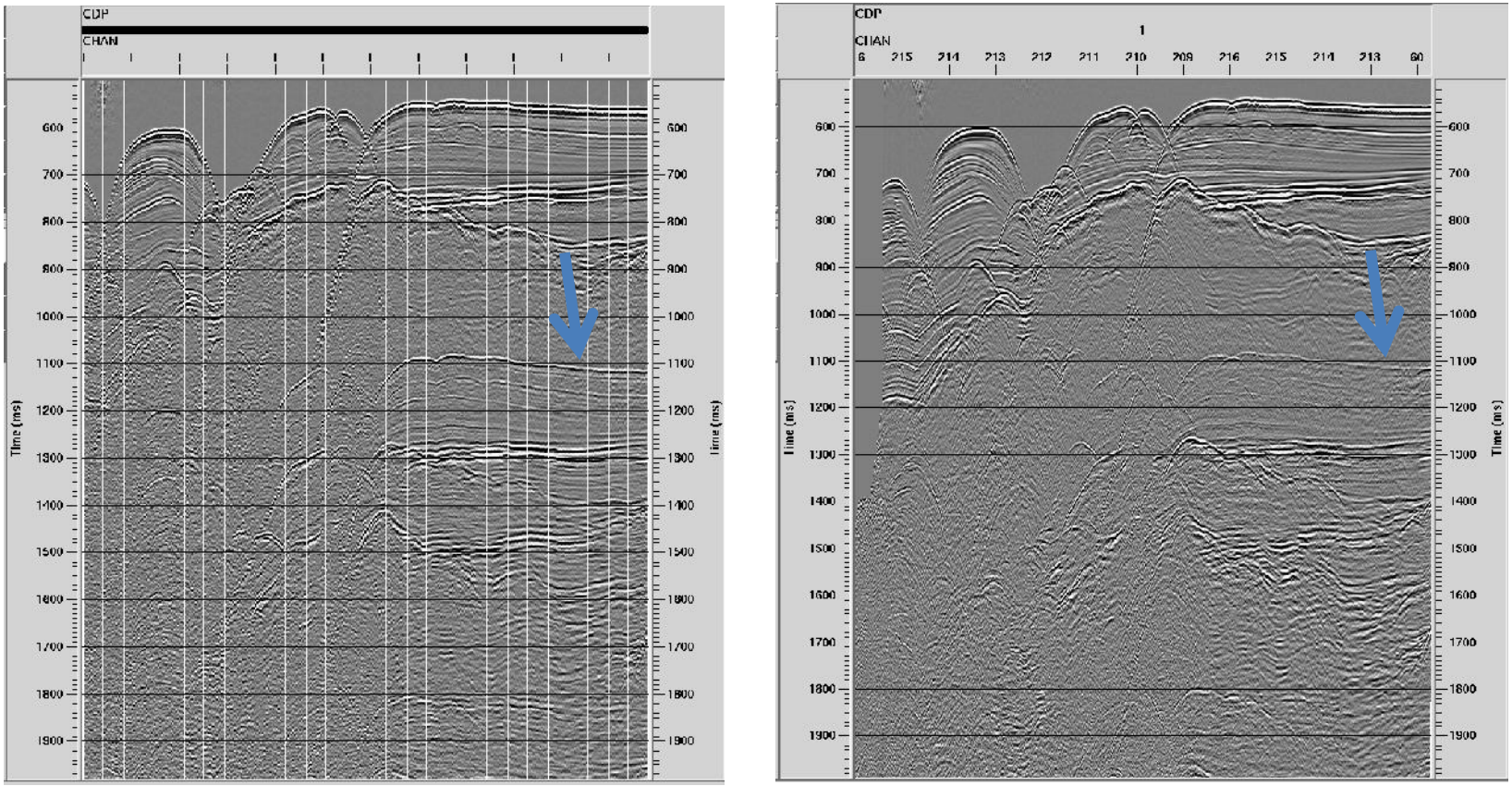

(a) (b)

Figure 2.25(a) Near trace gather and (b) stacked section. The blue arrow on section (a) delineates the first seabed multiple at 2x the time of seabed reflection which was attenuatedto some extent by stacking the multiple out at section (b)

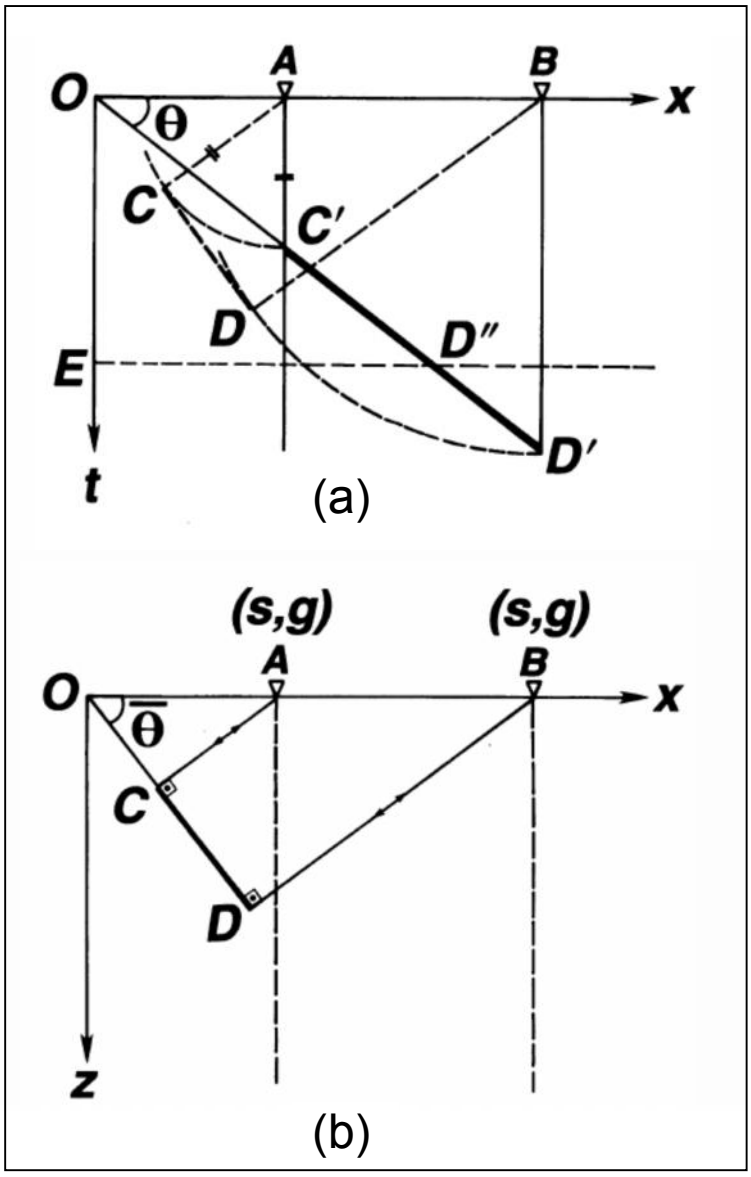

Figure 2.26 Migration principles: The reflection segment C D in the original stacked time section **(a)** is moved up-dip, steepened, shortened, and mapped onto its true subsurface location CD as in **(b)**, when migrated (from Yılmaz, 2001)

and diffractions occur off reflector terminations (e.g., at faults). The aim of the migration process is to correct for this (Fig. 2.26).

A migrated section is generally displayed in time because there is often limited accuracy in the velocity estimation for good depth conversion and it is often useful to compare migrated and unmigrated time sections in interpretation.

Stolt migration and Kirchhoff time migration are the two techniques that were applied to stacked data and used collaboratively. Stolt migration is generally used to find initial velocity function since it uses the fastest algorithm. However, the results are not as effective as Kirchhoff Time Migration, especially on steeply dipping structures. Thus, despite its slower algorithm, Kirchhoff Time Migration is preferred as the final migration techinuque in order to achieve the best imaging.

Migration was extremely challenging depending on the complicated 3D geology of the study area. This step can be considered as the most time-consuming step after velocity analysis for NMO correction.

2.3.9.1 Stolt Migration

Constant velocity Stolt migration was used to start the migration process. A series of constant velocity migrations with velocities between 1500 m/s to 2200 m/s were used to choose the best velocities to image the structures at particular depths (Figs. 2.27-2.29). Velocities were choosen by observing under and over-migrated structures on different constant velocity Stolt plots. Estimation of the optimum velocities, resulted in a variable velocity model by editing the previously created NMO velocity table

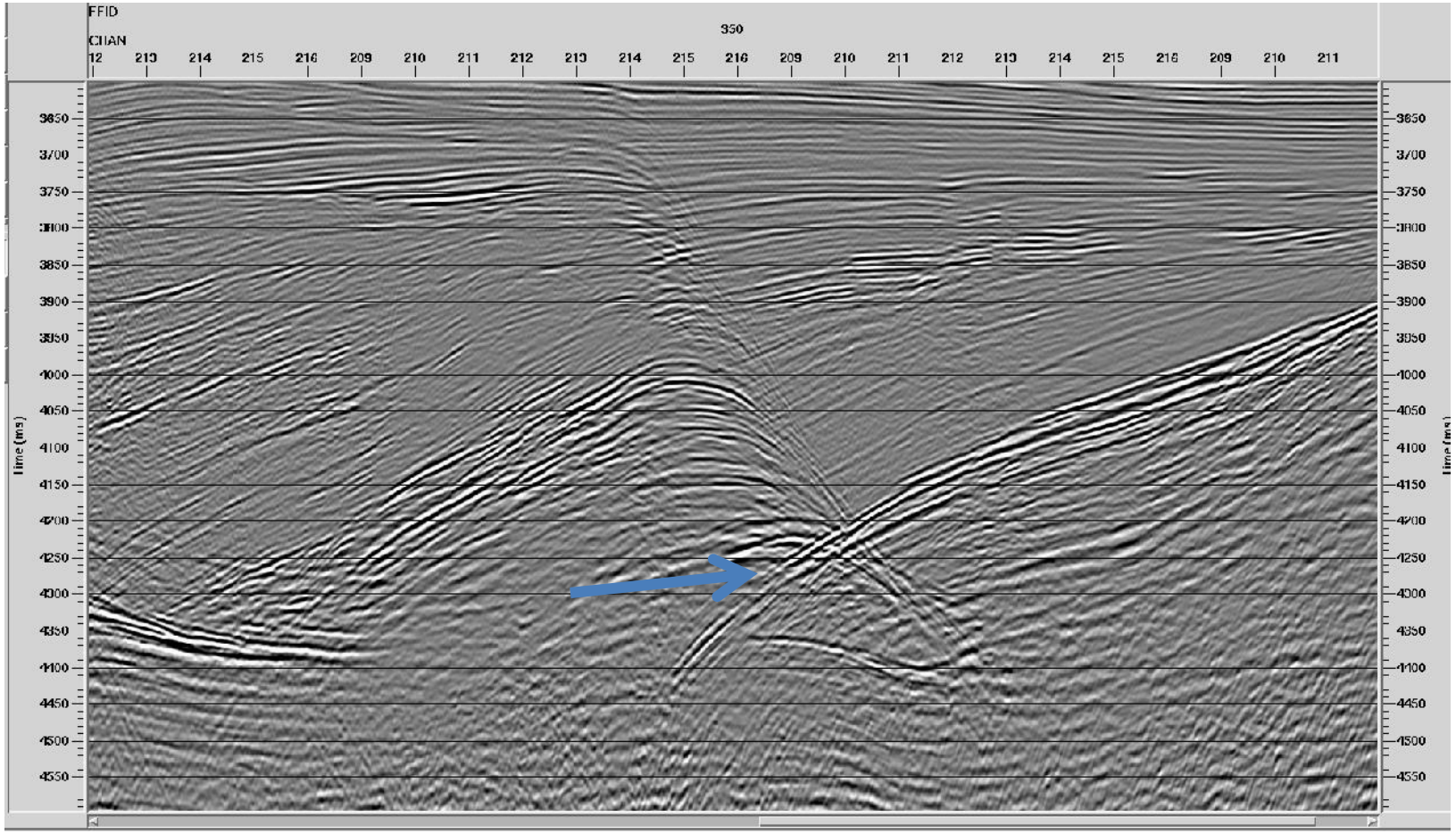

Figure 2.27 Constant velocity Stolt migration with 1500 m/s. Blue arrow shows the diffraction pattern that needs to be migrated with a higher velocity.

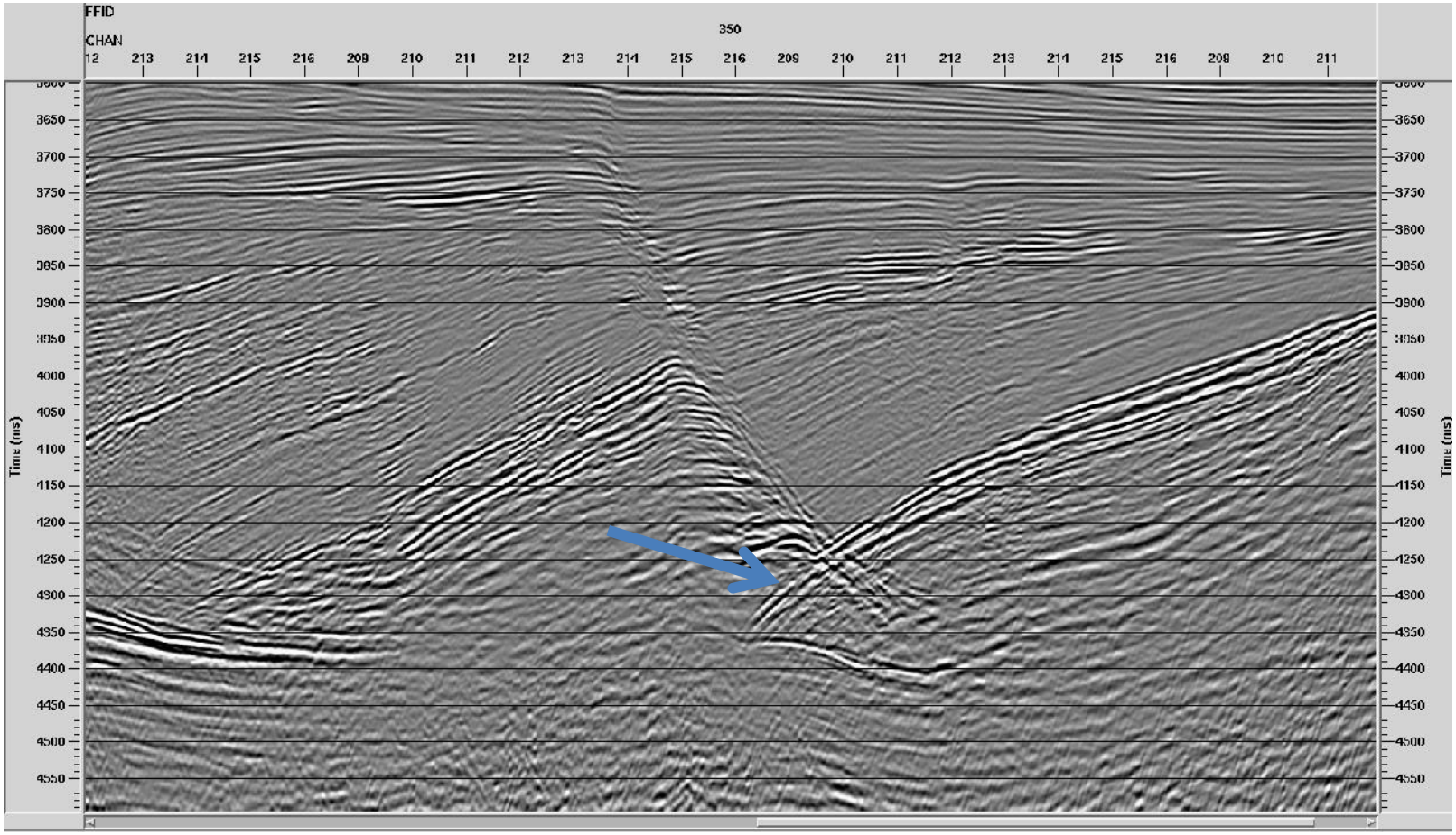

Figure 2.28Constant velocity Stolt migration with 1650 m/s. Blue arrow indicates thatthe diffraction pattern stillneeds to be migrated with a higher velocity.

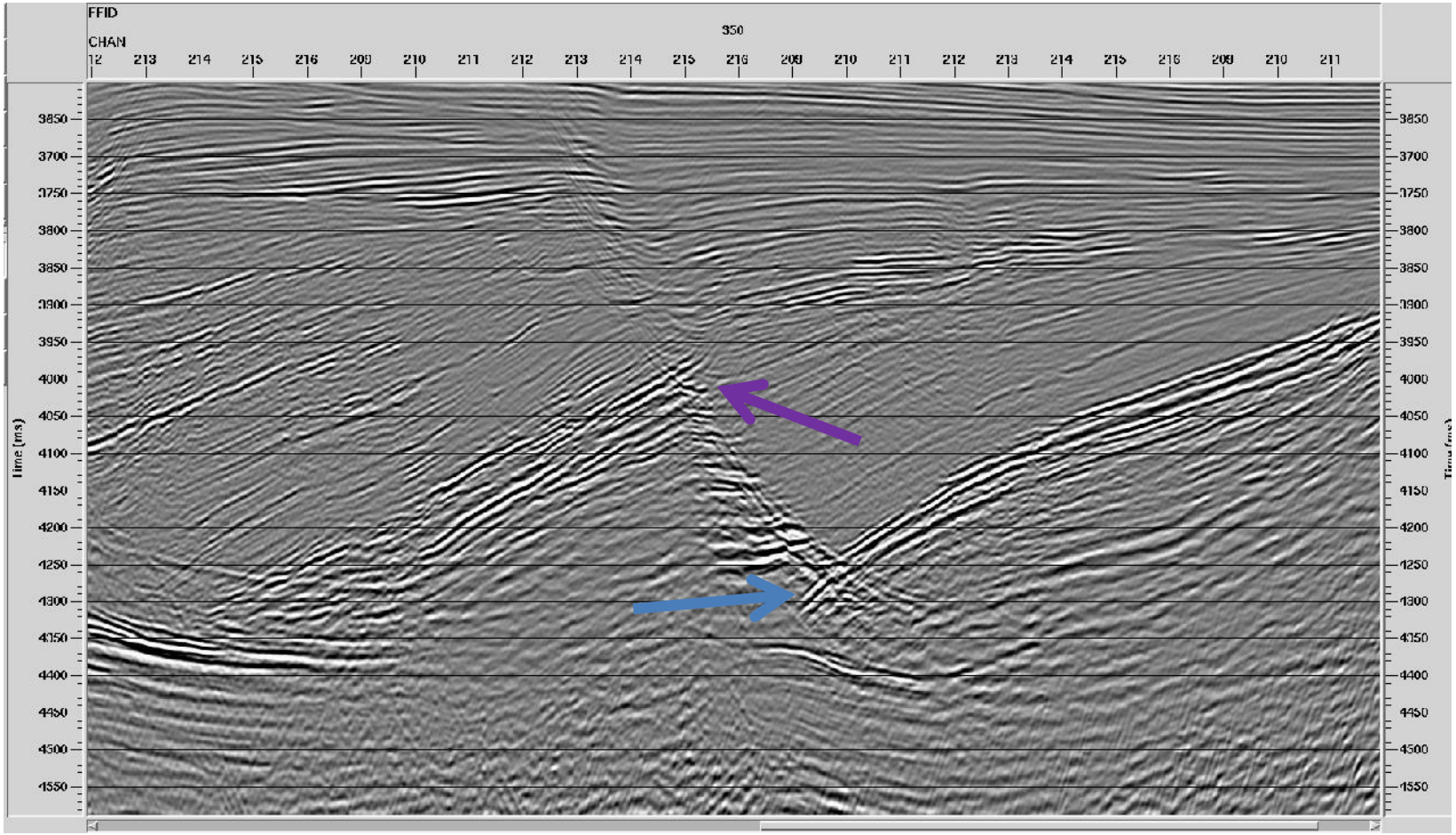

Figure 2.29Constant velocity Stolt migration with 1750 m/s. Blue arrow indicates thatthe diffractionpattern stillneeds to be migrated with a higher velocitywhereas the purple arrow points at the migration smiles indicating a need of lower velocity.

accordingly. The created migration velocity model then improved by the application of variable velocity Stolt migration and Kirchhoff time migration (Figs. 2.30-2.31).

The variable velocity Stolt migration was performed but was not applied to most lines, since it was somewhat unsuccessful in providing consistently good images.

2.3.9.2 Kirchhoff Time Migration

Kirchhoff time migration (KTM) was used as the final step of signal processing. Figure 2.28 illustrates a Stolt migrated section with the constant velocity of 1650 m/s. The diffraction hyperbola is under-migrated. Comparably, Figure 2.32 represents the same section after Kirchhoff migration which was carried out using the same velocity value (1650 m/s) around the diffraction hyperbola. As a result, the diffraction pattern was ~migrated more effectively despite the same velocity value. The experiments showed that the adjustments on the velocity table were critical. It was observed that a proper Stolt migration velocity for a specific structure was high in velocity for Kirchhoff time migration. Figure 2.33 and Figure 2.34 illustrate the effects of high migration velocities (i.e smiles) and low migration velocities (i.e frowns) on structures.

KTM was also good at removing bow-tie effects. Figure 2.35 demonstrates a stacked section and a bow-tie structure. After Kirchhoff time migration, which works efficiently in lateral and vertical velocity changes, the bow-tie effect was removed (Fig. 2.36).

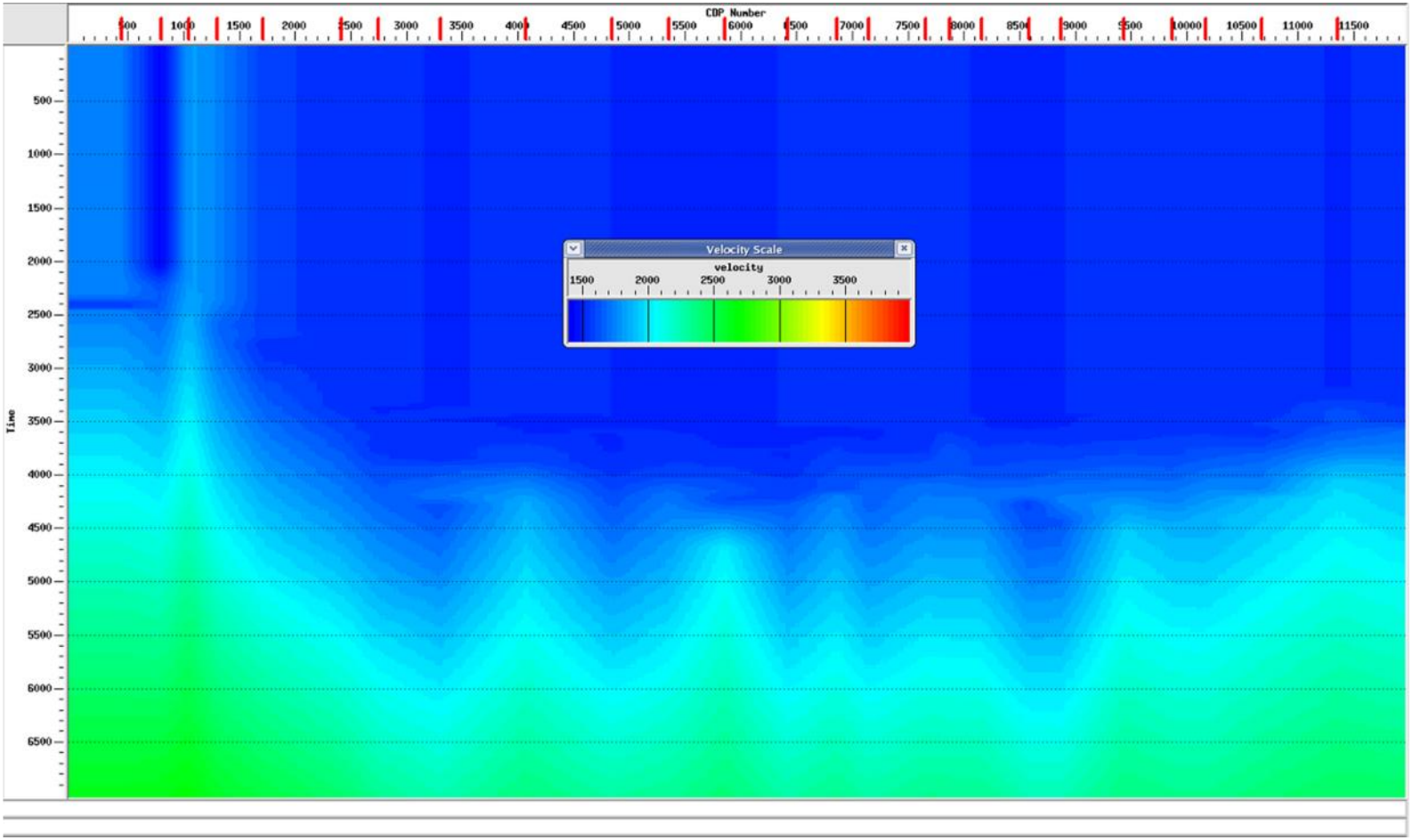

Figure 2.30 NMO velocity spectrum of a seismic profile. The CDP locations where the velocity spectra are determined are shown with red marks on the top and their positions are used as an initial step in the selection procedure of the migration velocity functions.

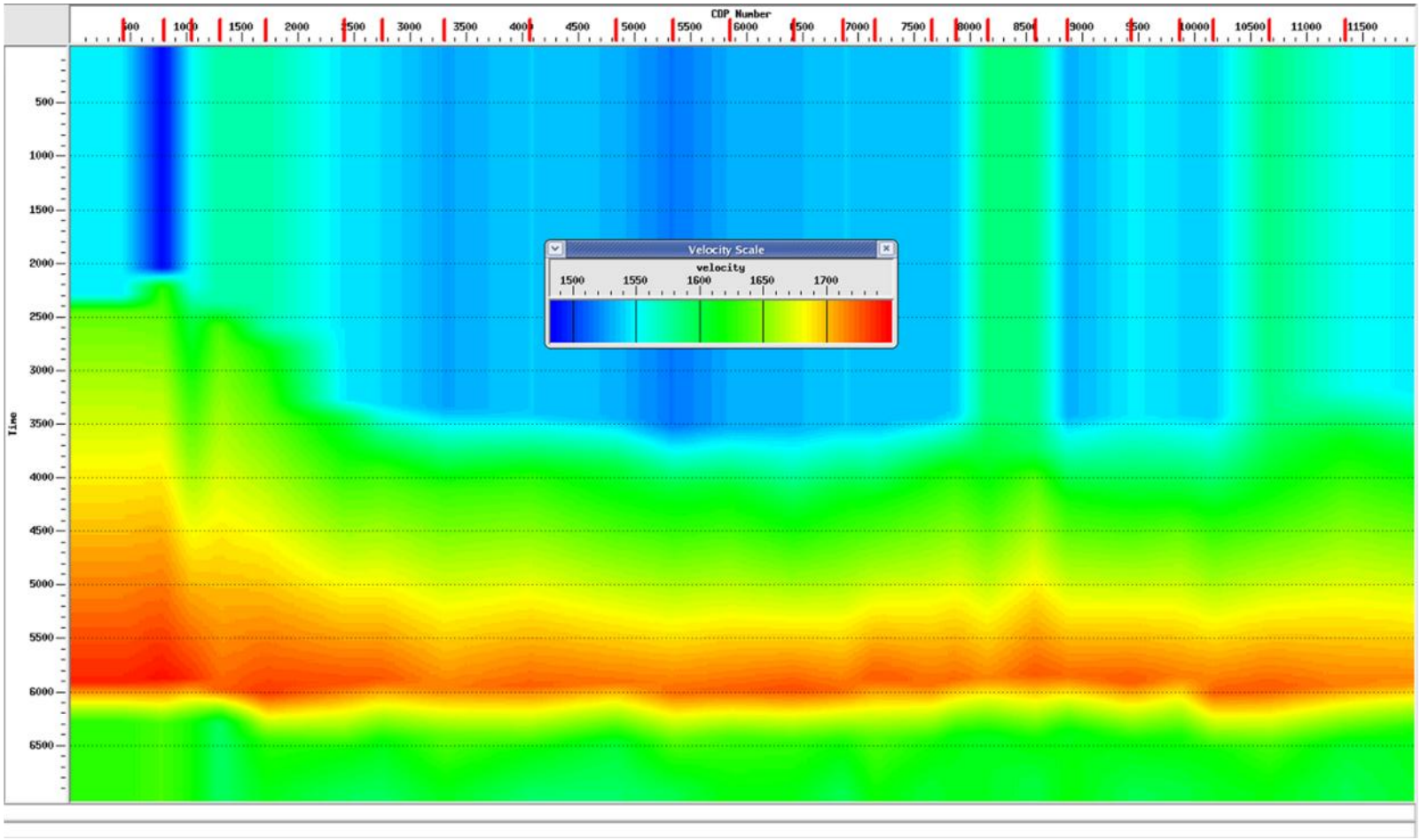

Figure 2.31 Velocity spectrum of the seismic profile in Fig.2.30 that is used for migration. Note the increased number of velocity functions and change in the velocity functions from the NMO velocity function shown in Fig. 2.30.

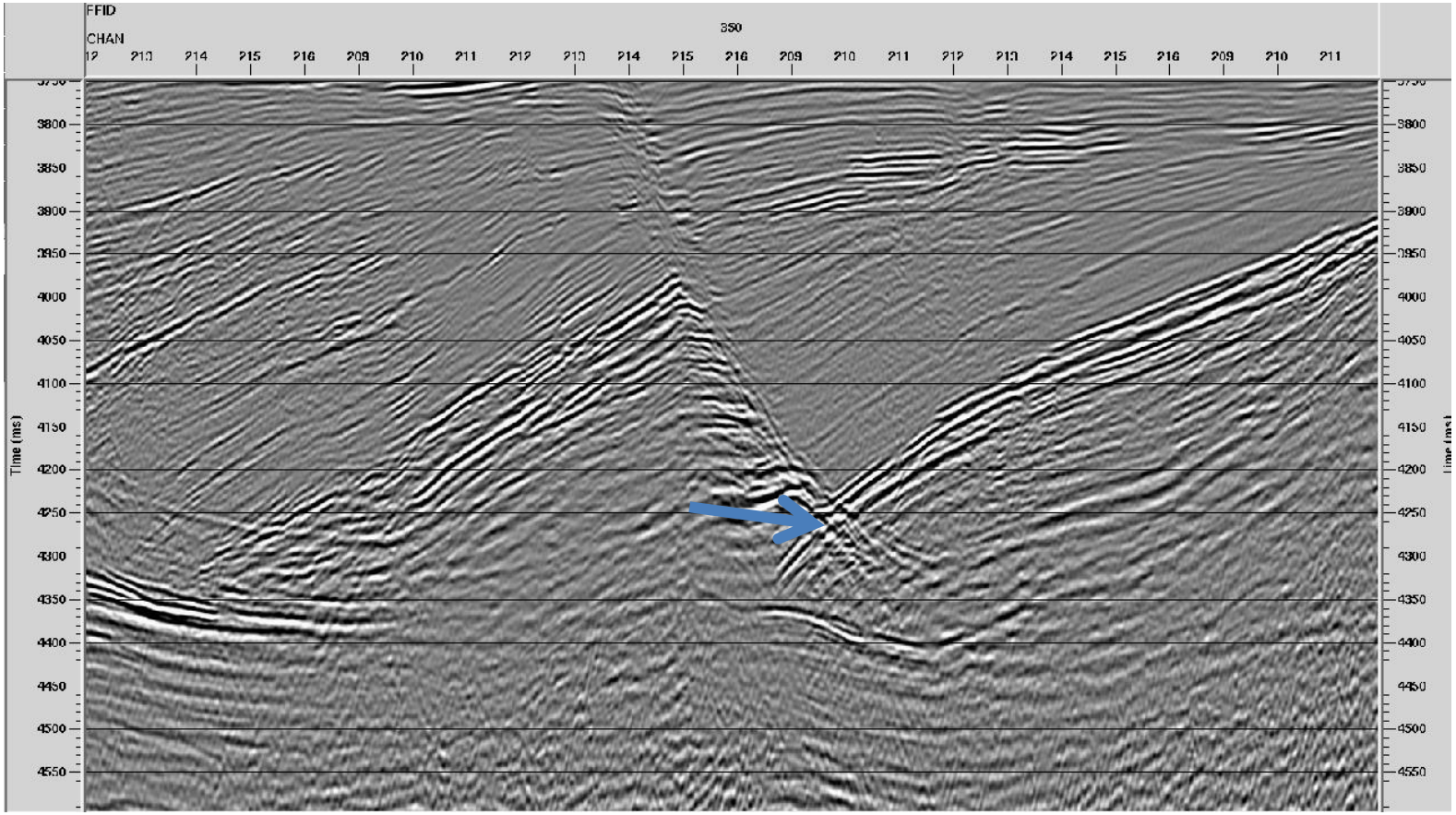

Figure 2.32 Kirchhoff time migration with 1650 m/s around the marked structure. Blue arrow demonstrates the efficiency of Kirchhoff time migration comparing the 1650 m/s constant Stolt migration (Figure 2.28).

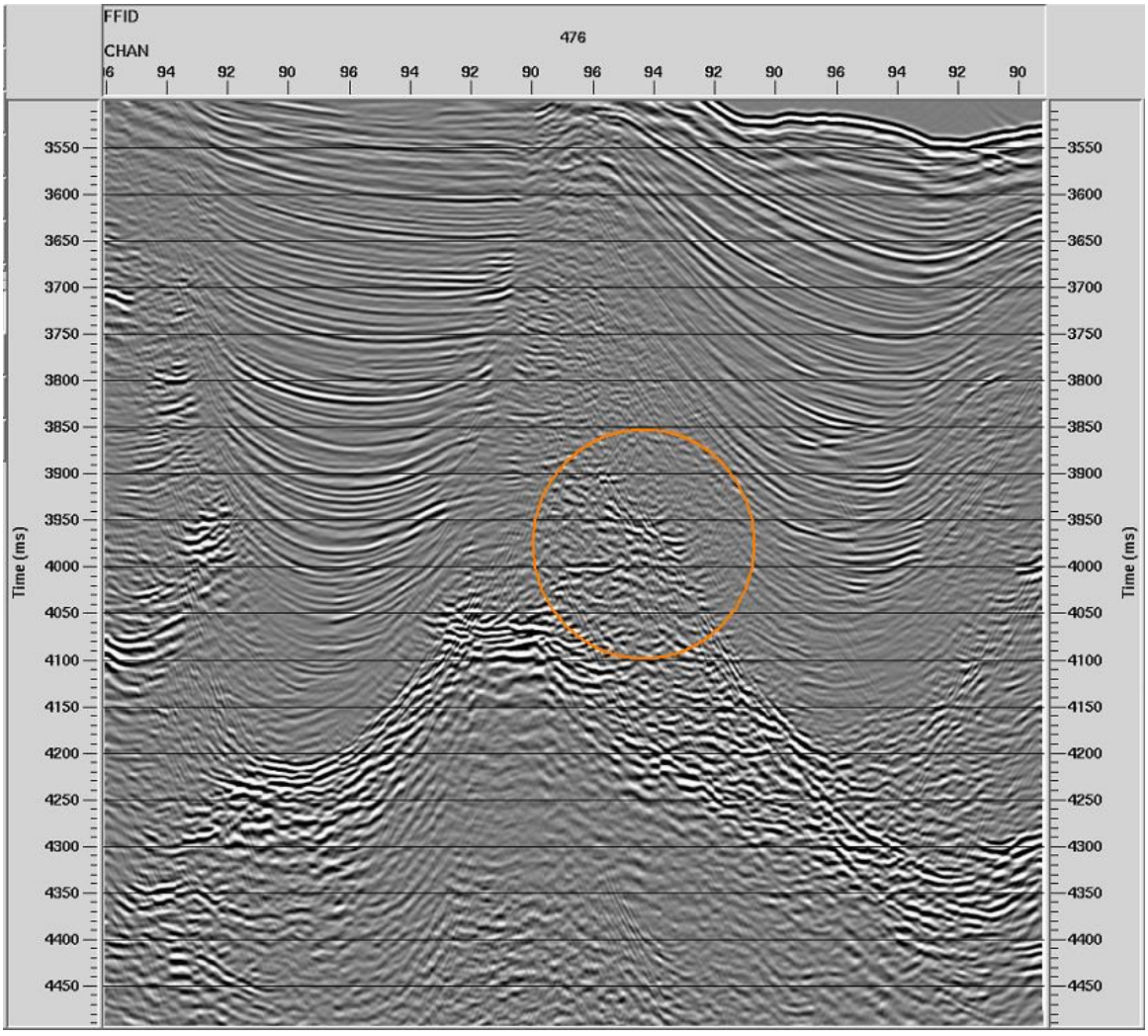

Figure 2.33 A seismic profile in which Kirchhoff Time Migration was applied. The migration smiles resulting from high migration velocities are shown in the orange circle.

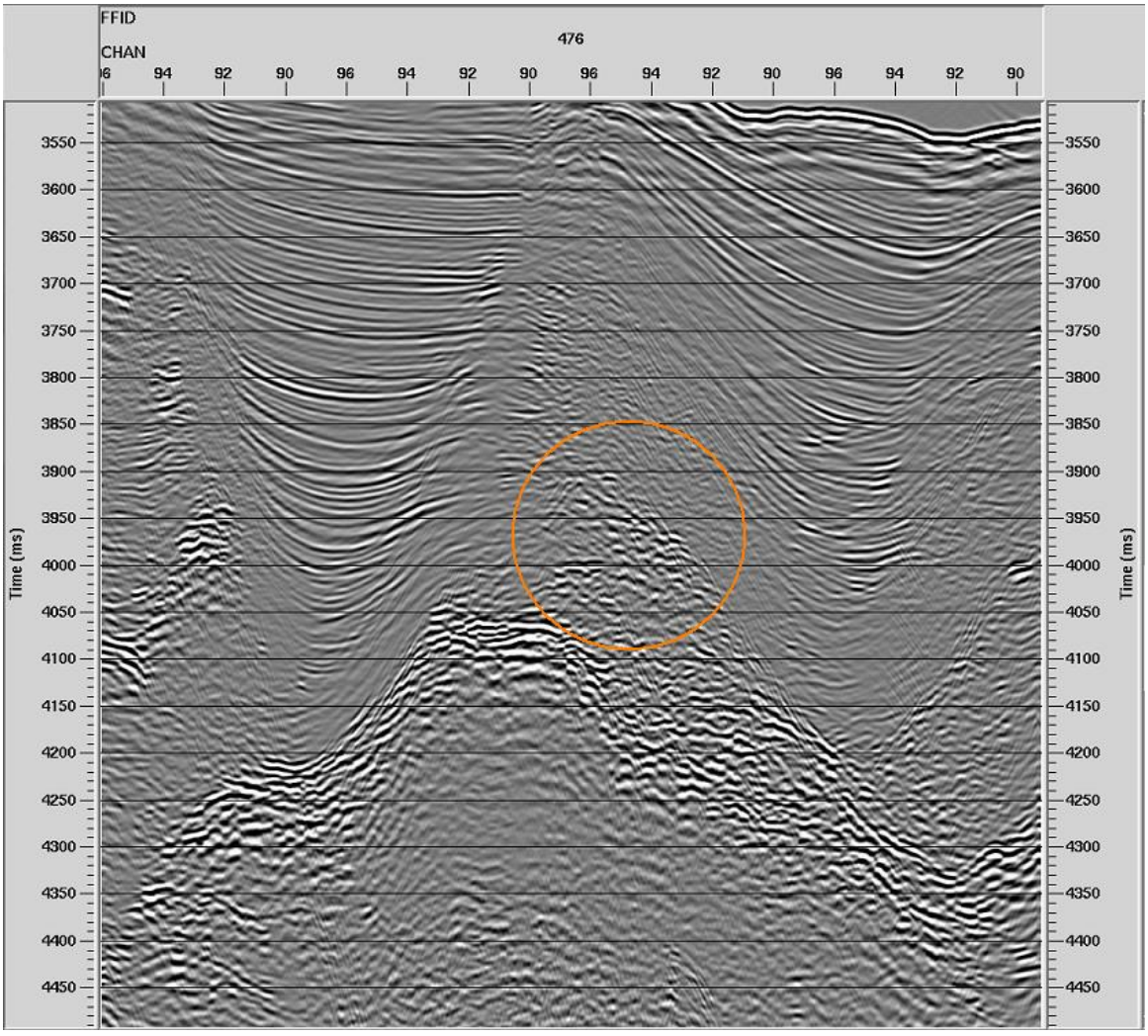

Figure 2.34 A seismic profile in which Kirchhoff Time Migration was applied. The migration frowns resulting from low migration velocities are shown in the orange circle.

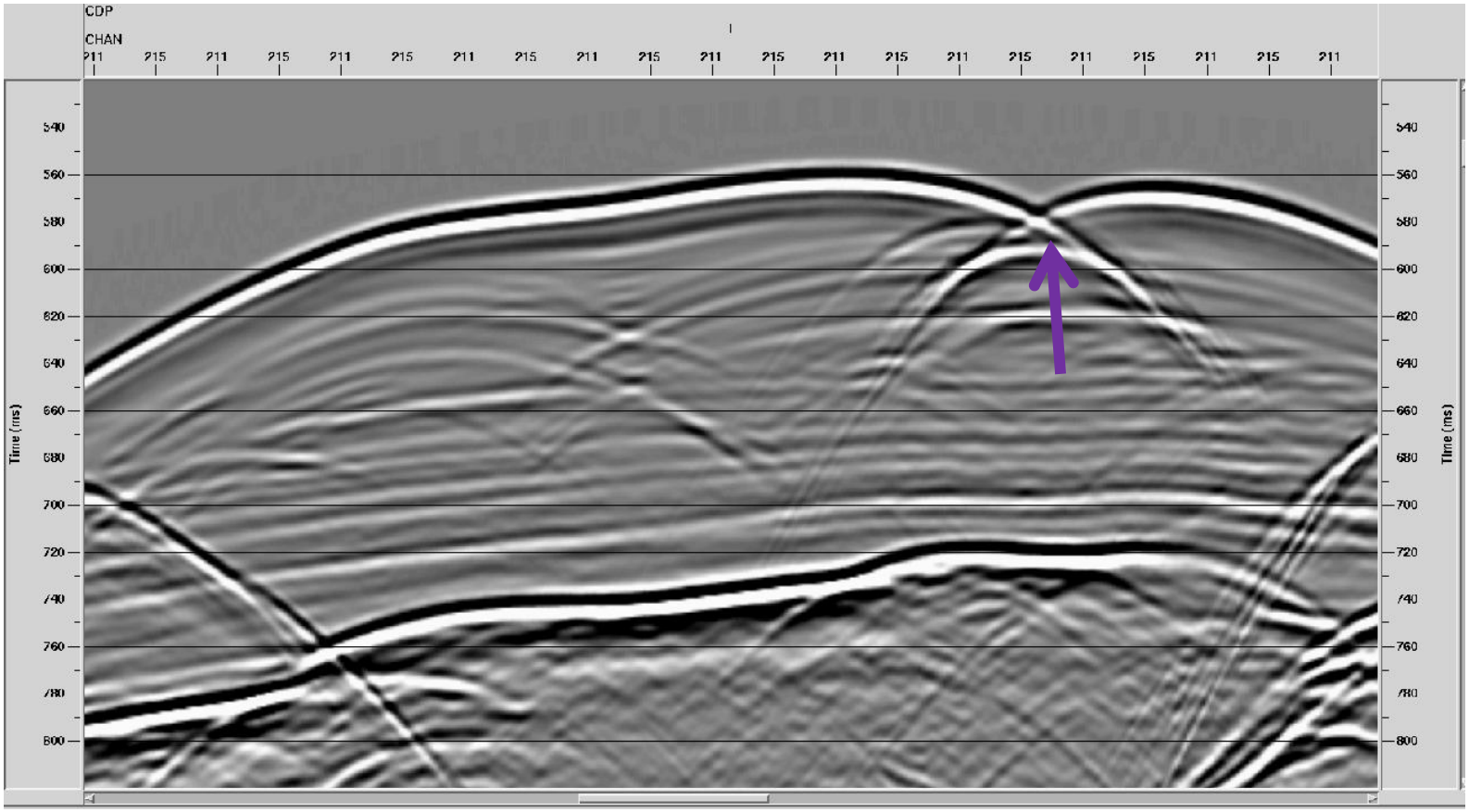

Figure 2.35 Stacked section demonstrating a bow-tie structure by purple arrow.

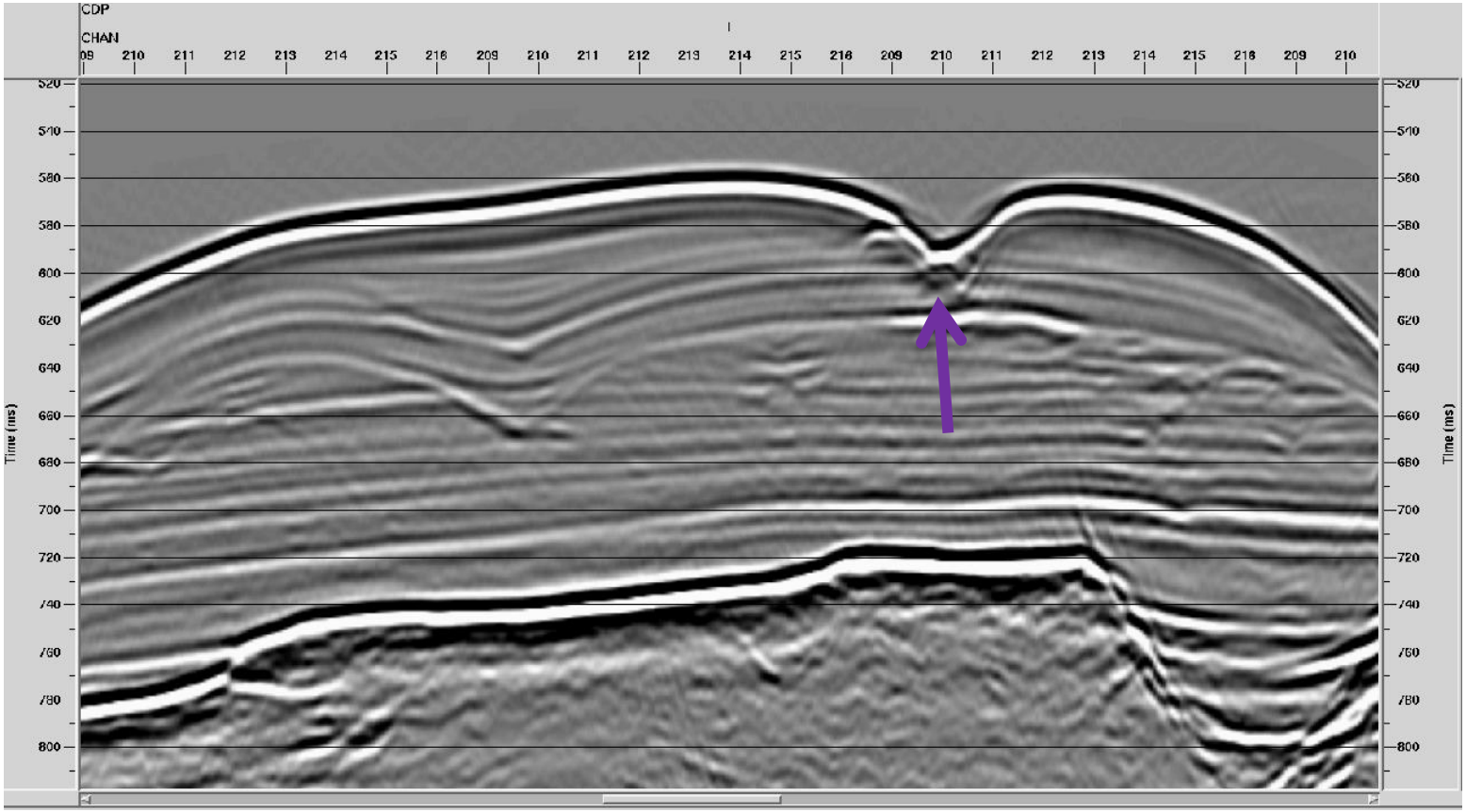

Figure 2.36 Stacked section after Kirchhoff time migration application. Note the bow-tie effect is almost entirely removed.

2.3.10 Time-Depth Conversion

In order to carry out a reasonable time-depth conversion, accurate interval velocities are necessary. The velocity control in the data for time-depth conversion was poor because of the short length of the streamer relative to the depth of the designed image. Thus, the seismic reflection profiles are not depth-converted. However, average interval velocities can be estimated during the velocity analysis step. The average interval velocities for the relatively young sedimentary succession of Unit 1 (see Chapter 4 for detailed explanation) are estimated between 1500-2000 m/s, gradually increasing with depth. Using 2000 m/s as a guide, 1 second of two-way travel time would be 1000 m of Unit 1. Below this variably thick succession, the average interval velocities increase to 4000 (or higher) given a halite composition for Unit 2; thus 1 second of Unit 2 would be a thickness of 2000 m. Finally, 3000 m/s is a reasonable overall average interval velocity for the acoustic basement, Unit 3; hence 1 second of two-way travel time through this unit would be equivalent to 1500 m.

2.3.11 Final Plots

After all the necessary processing is carried out, the data are output as a SEG-Y file and imported to the STARPAK seismic data processing program, where well-controlled tiff plot files are produced. It was important to apply a minimum amount of filtering in the ProMAX software package in order the keep all the data collected for the Eastern Mediterranean Project uniform. For the plot files in STARPAK,

a common Butterworth filter with pass band of 20-200 Hz with cut-off slopes of 24 db/octave and automatic gain control with a 500 ms gain window is applied and location fix numbers were added. Next, the tiff images are imported to CorelDraw program and placed in a standard frame with scales and dip roses added. The final plots are saved in the projects archive at 1200 dpi but can be readily rescaled at 600 (or other) dpi for printing for structural and stratigraphic interpretation. A complete set of 1200 dpi plots of all the profiles processed in this thesis is presented as Plates 1-30.

Chapter Three: Seismic Stratigraphy and Chronology

There are three seismo-stratigraphic units in the Finike Basin and its immediate vicinity (Fig 3.1, Fig. 3.2) Unit 1, Unit 2 and Unit 3, as described below. They show distinctive internal characteristics and are separated from one another by prominent reflections that are explained further in this chapter with the examples from seismic reflection profiles (Fig.3.1). The chronology of the study area is established using (i) two oil exploration wells drilled onland in Kasaba Basin (Şenel and Bölükbaşı, 1977a), (ii) core/dredge samples across the Anaximander Mountains and environs (Woodside et al., 1997), and (iii) a number of boreholes from the Deep Sea Drilling Project Sites 375 and 376 (Fig. 3.23, Shipboard Scientific Party, 1978). Stratigraphic correlation of these units across the area is also aided by seismic data collected during previous years.

3.1 Description of the Stratigraphic Terminations and Interpretation Methods

On the basis of correlation of prominent reflections around a dense grid of seismic reflection profiles, the late Miocene to Recent sedimentary and structural evolution of the Finike Basin is determined by using three main interpretation steps: stratigraphic interpretation, lithological interpretation, and structural interpretation. Once the major unconformities are traced, two-way time thickness maps of the intervening stratigraphic units are made.

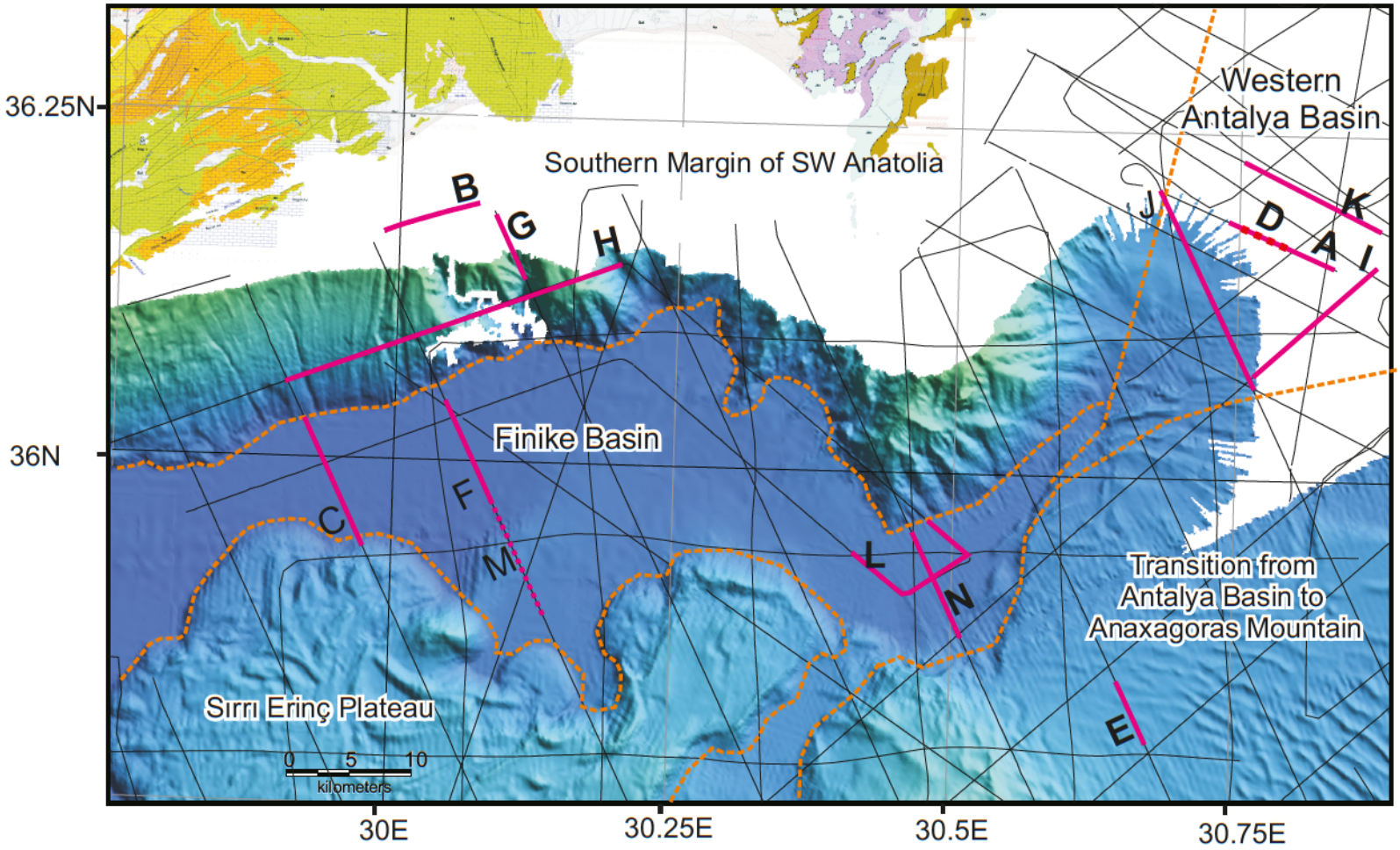

Figure 3.1 Multibeam map showing the morphology of the seafloor, outline of the regional basins and tectonic domains in orange dashed lines, and seismic reflection profiles (A-N) that are used in stratigraphic interpretation in magenta.

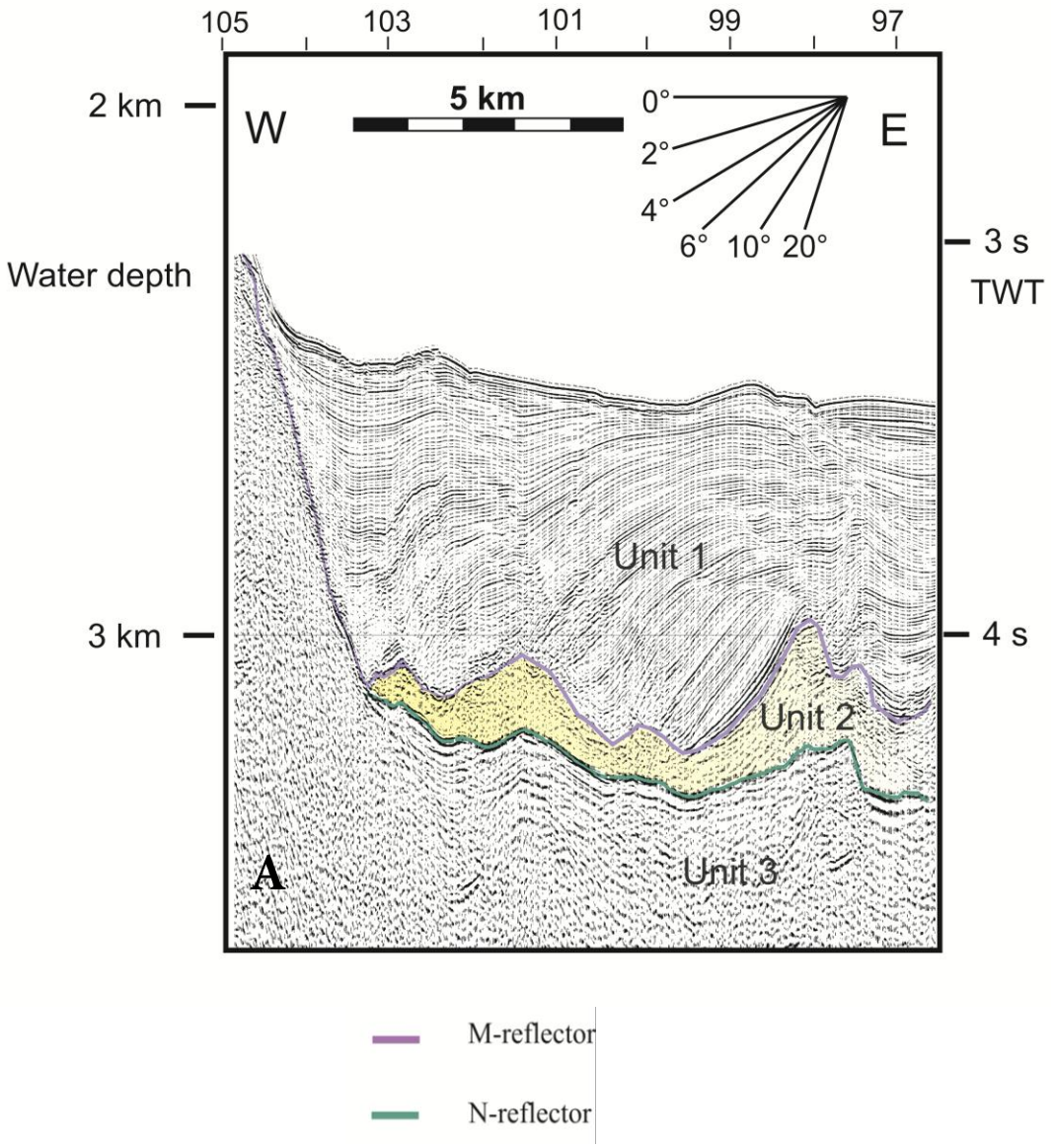

Figure 3.2 Seismic reflection profile A illustrating the major seismic stratigraphic units and prominent reflectors extending across the area (Plate 29, Fixes 105-96).

Sequence stratigraphy is an interpretative, descriptive and theoretical geological approach to the stratigraphic interpretation of seismic data (e.g., Mitchum et al., 1977a,b, Myers and Milton, 1996). A stratigraphic sequence is defined as discrete seismic packages consisting of relatively conformable genetically-related strata-bounded reflections that are delineated at their tops and bases by unconformities or their correlative conformities (e.g., Mitchum et al., 1977a, b, Myers and Milton, 1996). These unconformities are identified in the seismic reflection profiles by distinctive reflection terminations, including truncation, onlap, downlap and toplap (e.g., Fig. 3.3; Mitchum et al., 1977a,b).

The termination of a reflector at a boundary that exhibits clear decapitation of reflections is called truncation. There are two types: fault and erosional truncations (Mitchum et al. 1977a,b). Baselap is the termination of reflections against an underlying seismic surface and involves two different types: downlap and onlap. Downlap occurs where younger surfaces dip more steeply than the underlying strata, whereas onlap occurs when the younger layers dip less steeply than the older surface. The up-dip termination of an inclined reflector against an overlying near horizontal surface in seismic reflection profiles is classified as toplap (Fig. 3.3).

In interpretation of seismic reflection profiles, stratigraphy is usually described first, followed by structure. However the two are not entirely independent from one another. In the eastern Mediterranean, tectonic control of stratigraphy is evident in many

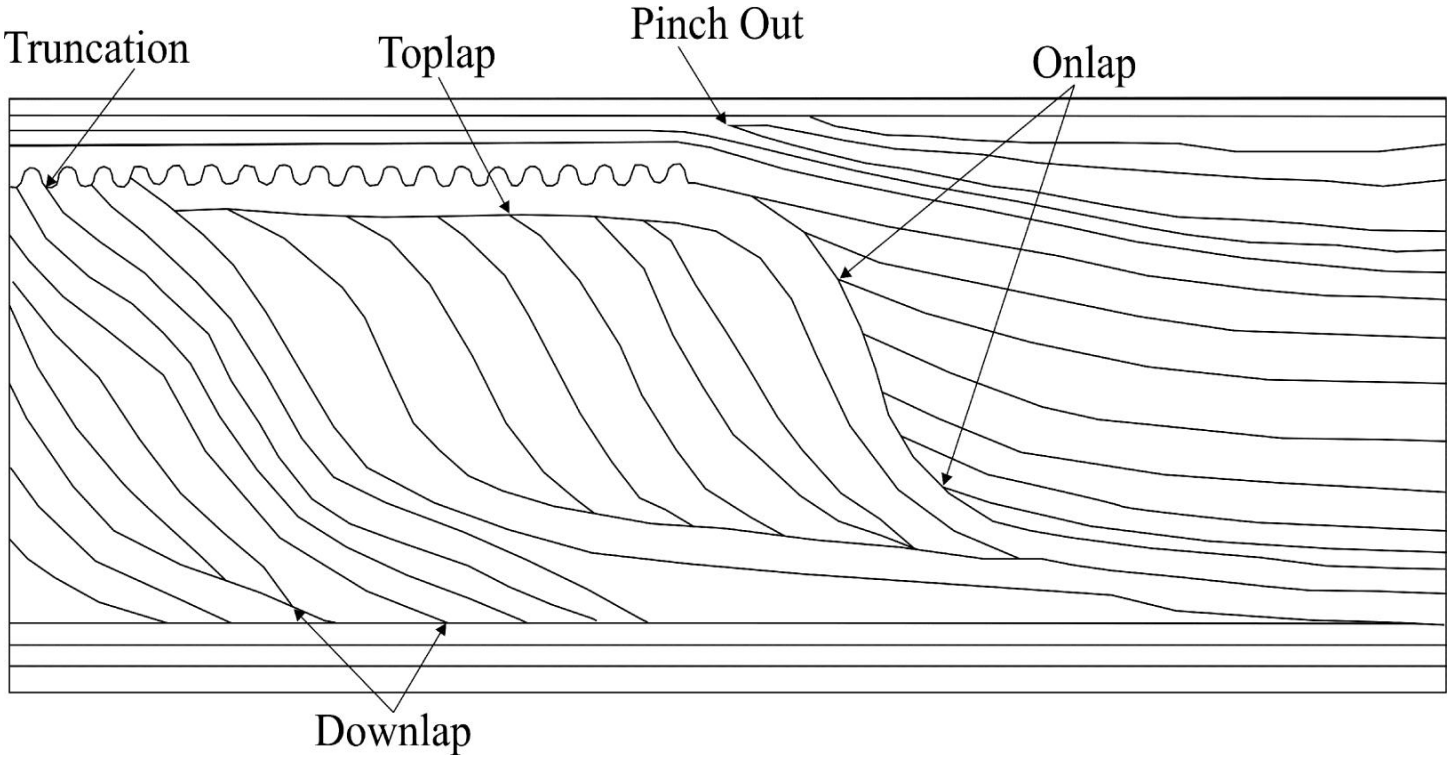

Figure 3.3 Schematic cross section showing onlap, downlap, toplap and truncation reflector terminations observed in seismic reflection profiles (modified from Işler, 2005)

instances where development of growth strata is directly related, if not controlled by, the ensuing tectonism.

All thicknesses and their variations are described in two-way travel time. Isochron maps, which delineate the thickness of the main stratigraphic units, are beneficial in analyzing structural development. Once the seismic profiles are interpreted, the regional geology is summarized graphically by maps of bathymetry, isochrons of the main stratigraphic units, and major structures.

3.2 Description of the Bounding Unconformities

3.2.1 M-reflector

A prominent marker with considerable lateral continuity occurs in the seismic reflection profiles at depths ranging from ~700 ms ~6000 ms (Fig.3.4). This marker, the M-reflector, was first described by Ryan (1969), and subsequently described in nearly all the basinal settings in the eastern Mediterranean Sea from the Rhodes Basin (Hall et al., 2009), to the Anaximansder Mountains (Aksu et al., 2009), and Antalya, Cilicia, Adana, Iskenderun, Latakia, Cyprus and Mesaoria Basins (Aksu et al., 2005b; Burton-Ferguson et al., 2005; Calon et al., 2005 a,b; Hall et al., 2005a,b; Işler et al., 2005). The M-reflector separates the Messinian evaporite successions from the overlying Pliocene-Quaternary deposits in deeper basinal settings where the Messinian evaporites are present, but separates the pre-Messinian Miocene and/or older successions from the Pliocene-Quaternary deposits where the Messinian evaporites are absent (Zitter et al., 2003; ten Veen et al., 2004; Burton-Ferguson et al., 2005; Işler et al., 2005; Aksu et al., 2009). The

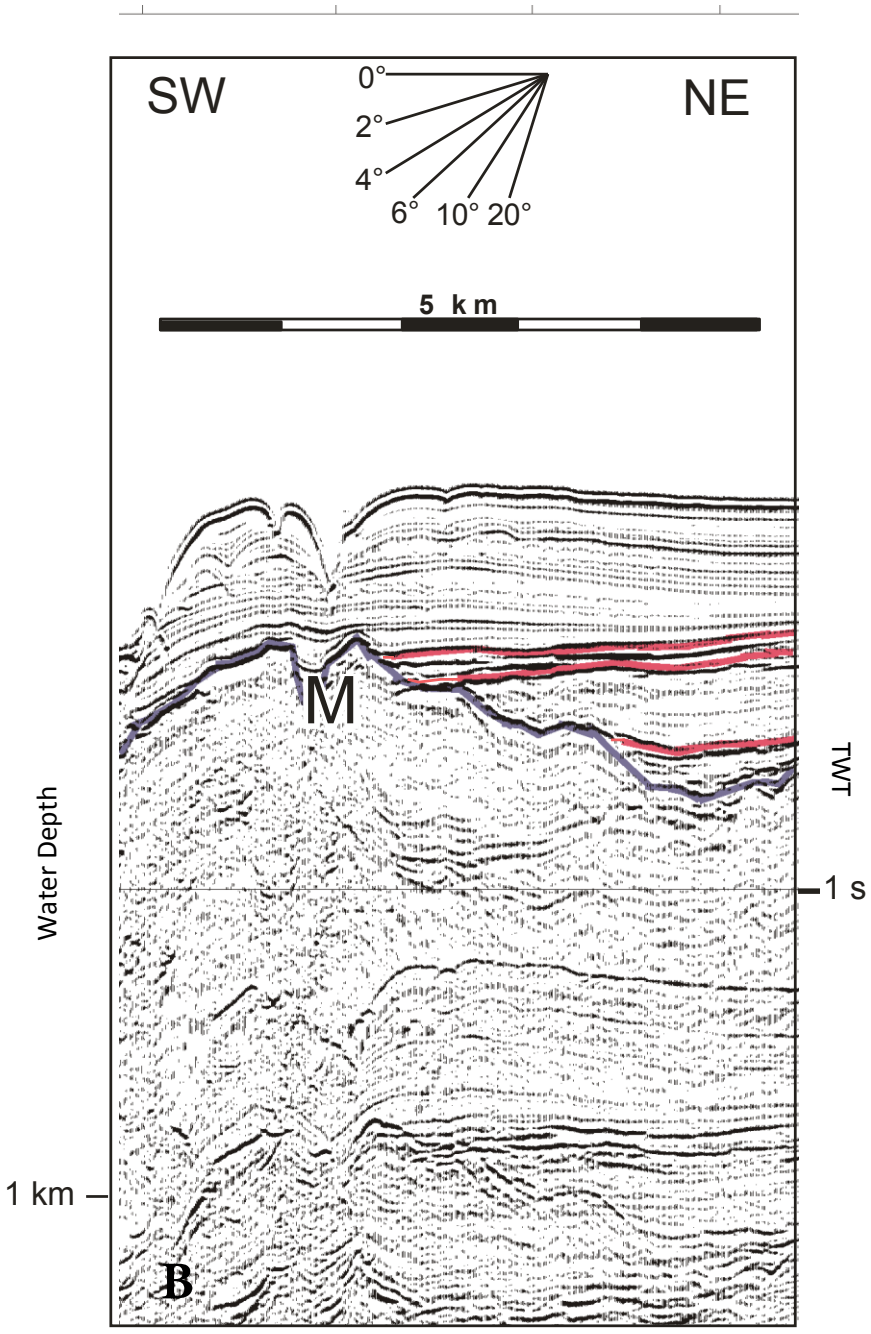

Figure 3.4 Seismic reflection profile B illustrating the minimum depth of M-reflector in the study area at depth ~700ms marked in purple. The lines in pink illustrate the onlap of Pliocene-Quaternary sediments on M-reflector (Plate 20. Fixes 965-970).

M-reflector is usually strong, due to the large contrast in acoustic impedance between the Pliocene-Quaternary siliciclastic sediments and the underlying Messinian evaporites or older rocks.

3.2.2 N-reflector

A second prominent marker is known as the N-reflector. This marker is described by Işler et al. (2005) as an unconformity separating Messinian evaporites from the pre-Messinian successions (Fig 3.2). The N- reflector is present in the westernmost Antalya Basin portion of the study area, where there is a thick succession of Messinian evaporites.

The architecture of the N-reflector can be described as a strong marker, usually showing a low frequency response (western Antalya Basin), but can also be weak (easternmost Finike Basin), probably because of the differing nature of the pre-Messinian succession from place to place.

3.3 Seismic Units

3.3.1 Unit 1: Pliocene-Quaternary

Unit 1 is the youngest sediment package that occurs within the Finike Basin and its vicinity. It is characterised by highly reflectivity package with a frequency response ranging between ~90 Hz -130 Hz (Fig. 3.5). This package shows remarkable lateral continuity where individual reflections can be confidently carried across the Finike Basin for tens of kilometres. It extends from the seabed to the prominent M-reflector at its base (Fig.3.5).

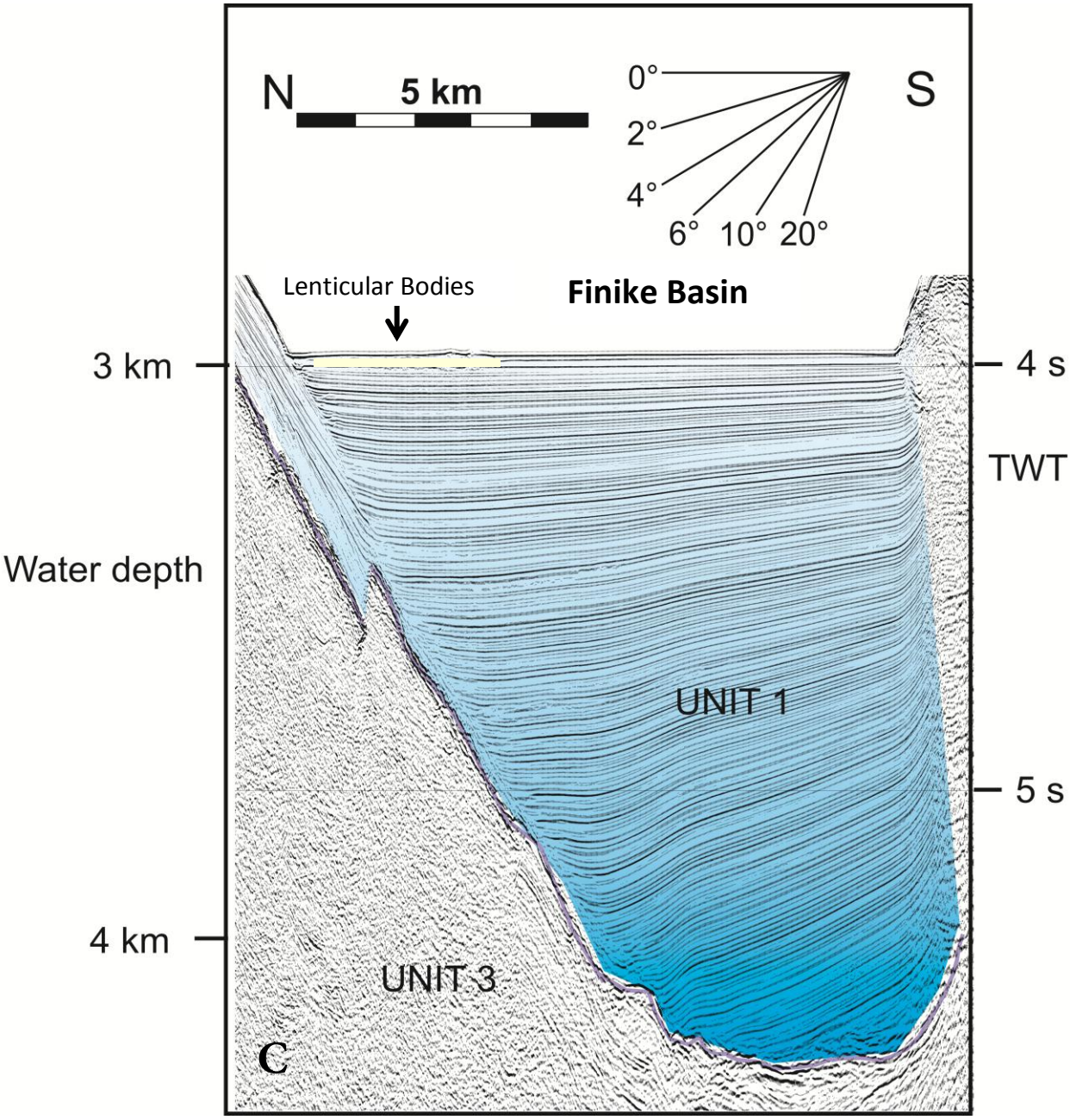

Figure.3.5 Multichannel seismic reflection profile C showing the internal architecture of seismic stratigraphic Unit 1. Note the lenticular body within Unit 1 with lttle internal reflectivity (Plate 18, Fixes 1124-1131).

In the southwestern portion of the westernmost Antalya Basin, Unit 1 includes prominent unconformity surfaces delineated by the erosional truncation of the underlying reflections and the progressive onlap of overlying reflections (e.g., Figs. 3.6, 3.7). Detailed examination of the seismic reflection profiles shows that a number of these local unconformities are associated with local tectonic events: these are further described in Chapter 5. These unconformities are also observed in the Anaximender Mountains (*sensu lato*) and described by Cranshaw (2010). The thickness of Unit 1 in the westernmost Antalya Basin reaches up to 1000ms down into the basin (Fig. 3.2)

In the deep Finike Basin, Unit 1 includes a series of variably thick lenticular deposits which exhibit few coherent internal reflections or chaotic and disordered reflections (Figs. 3.5, 3.8). These deposits often display irregular, corrugated tops and flatter and erosive bases. They are thickest in the northern portion of the Finike Basin and thin toward the south, giving a lens-like cross-sectional view.

In the uppermost portion of the northern Finike Basin slope, immediately south of the Turkish coastline, some seismic profiles show the presence of a number of vertically stacked and seaward prograded successions (Fig. 3.9). Each prograded succession is 120-200ms thick and is composed of seaward-dipping oblique-prograded clinoforms. These prograded packages are separated from one another by prominent local unconformities (Fig. 3.9). At present, they are situated between 800 - 1500 ms water depth. They resemble prograded shelf-edge deltas (Pinous 2001), where the topset to foreset transitions marking the approximate position of the former

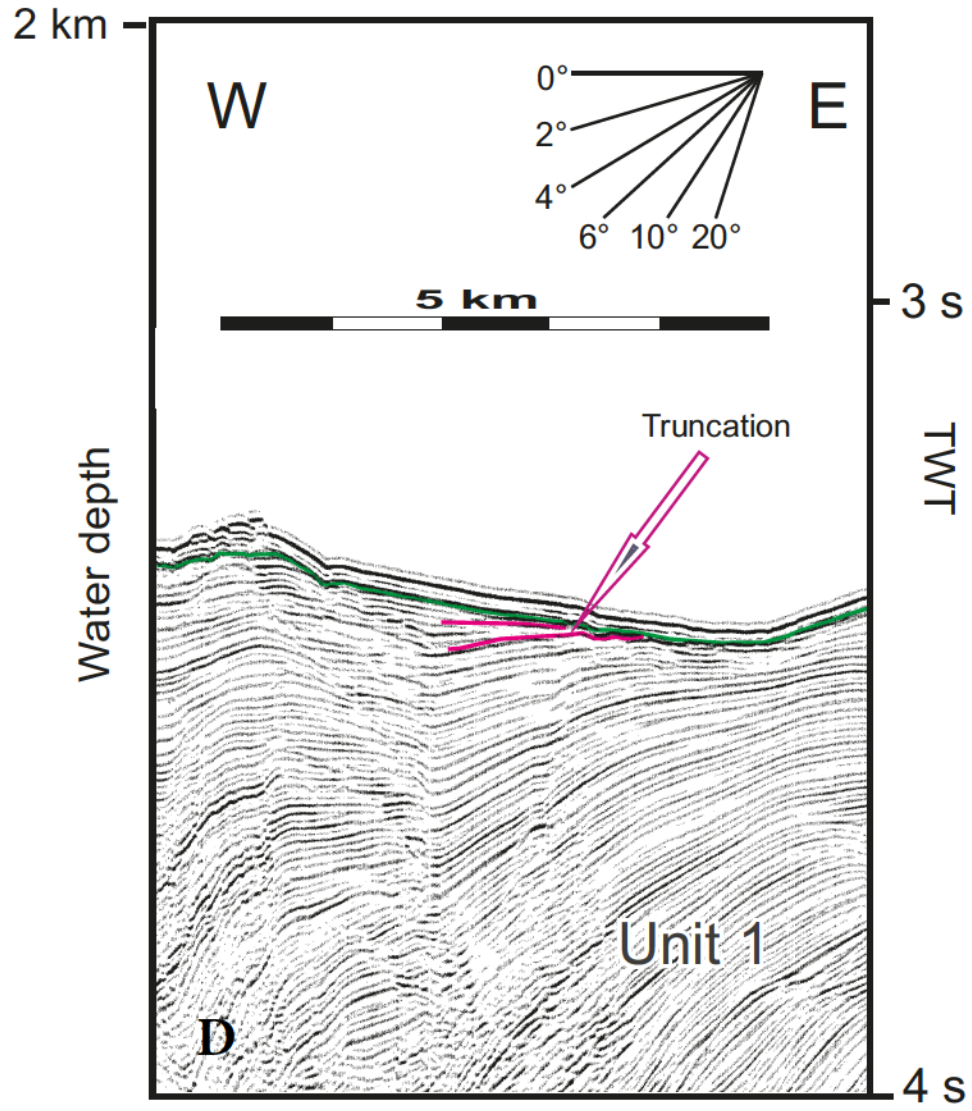

Figure 3.6 Multichannel seismic reflection profile D showing an example of a local unconformity within Unit 1. Note onlap in the middle of Unit 1 is also shown (Plate 29, Fixes 103-99).

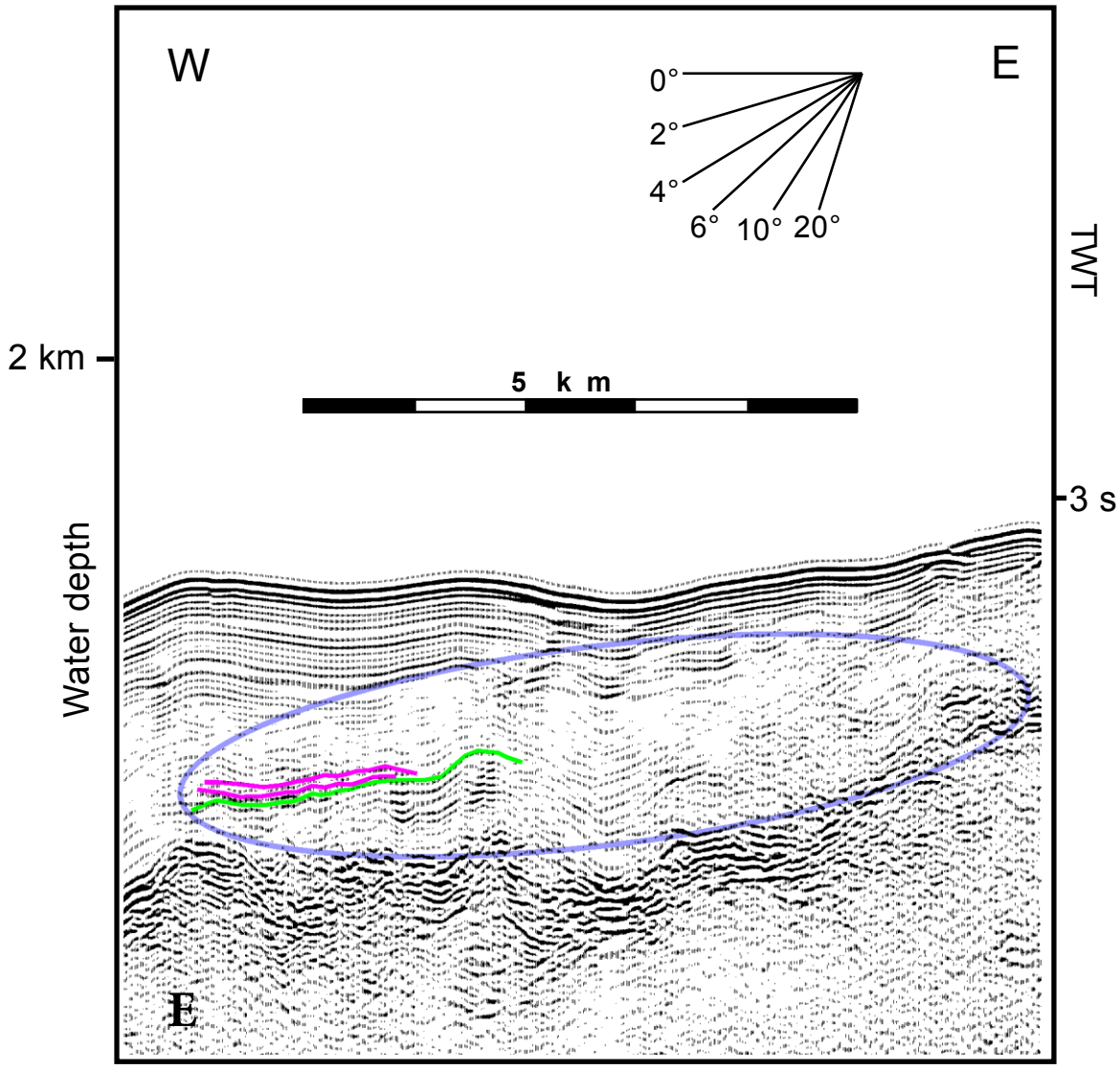

Figure 3.7 Multichannel seismic reflection profile E showing another example of a local unconformity (green) within Unit 1 in circle (blue). Note the thinning eventually pinching out sedimentary layers in pink (Plate 24, Fixes 182-176).

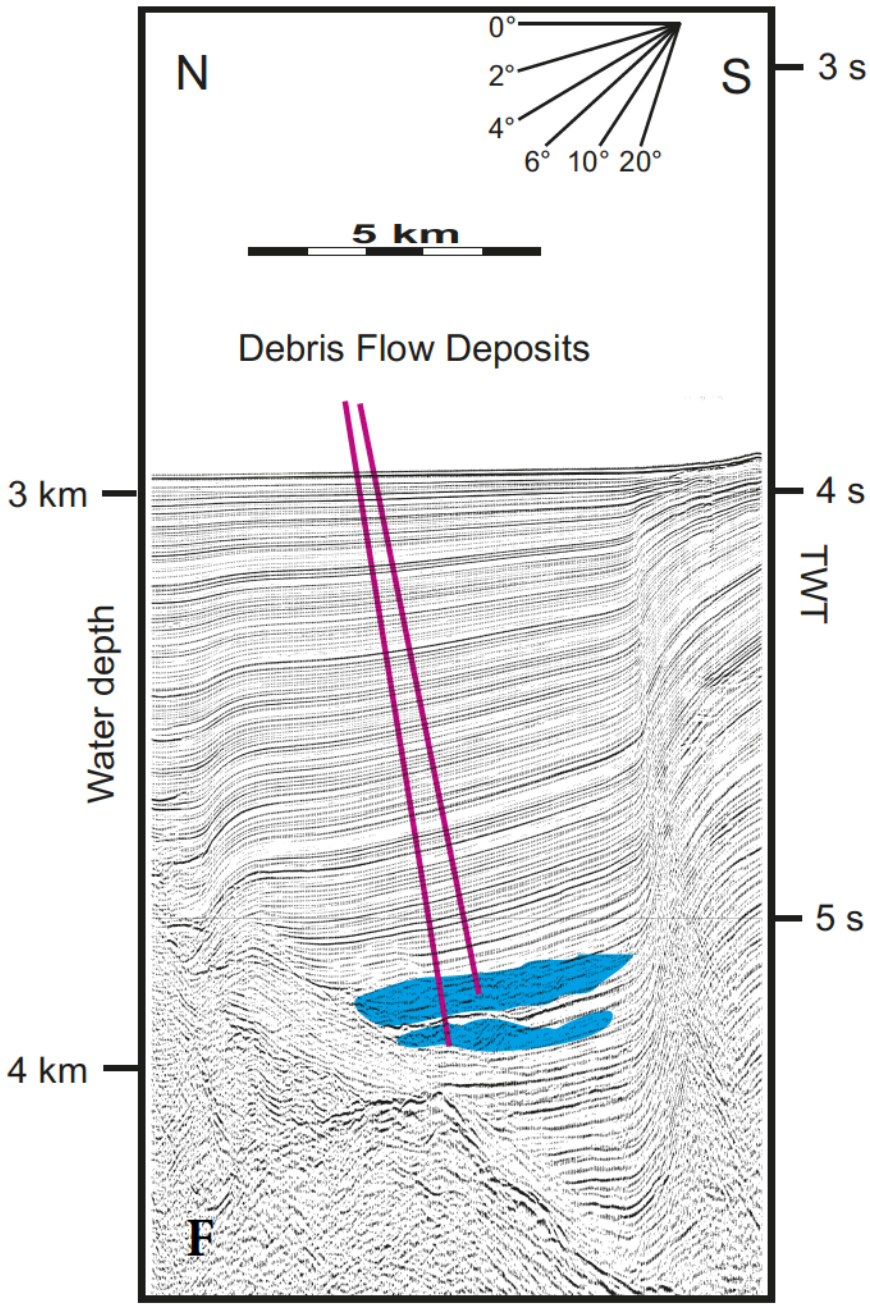

Figure 3.8 Seismic cross-section Fdemonstrating the chaotic and dis-ordered reflections of debris flows within Unit 1 highlighted by blue shading (Plate 19a, Fixes 956-949) .

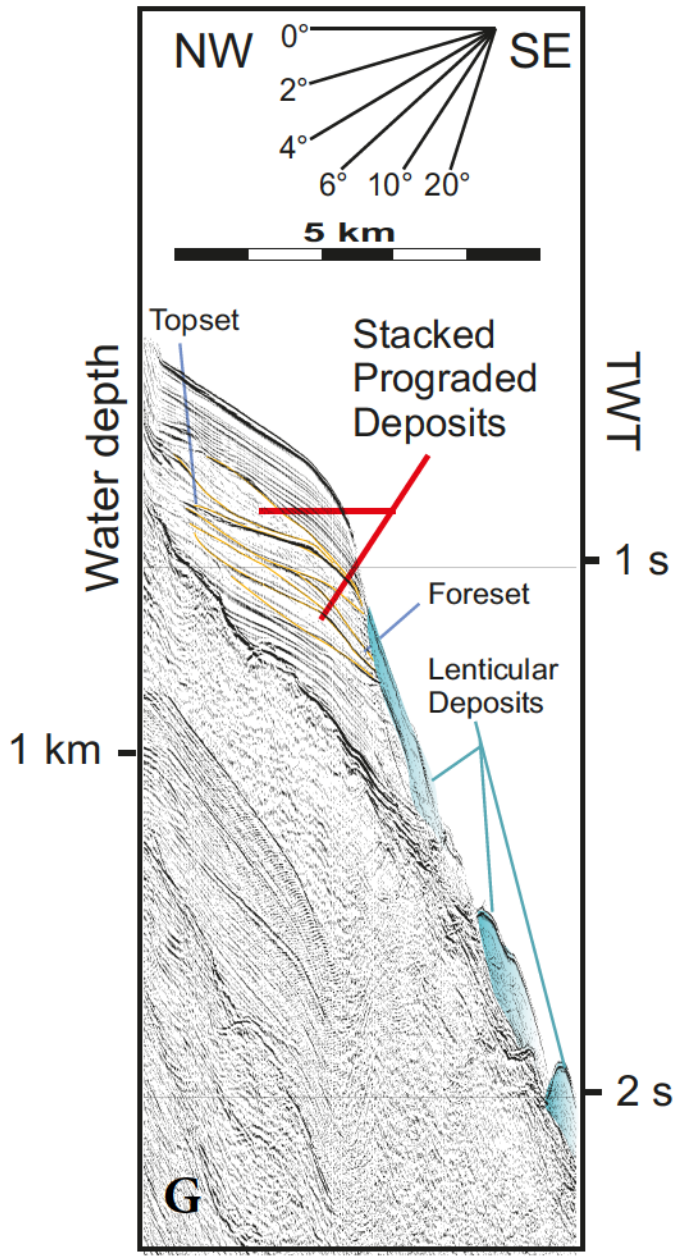

Figure 3.9 Seismic cross-section G showing the stacked prograded shelf deltas on the continental margin of the Finike Basin, within Unit 1 (Plate 21, Fixes 972-977).

shoreline can be readily determined in the seismic reflection profiles (Fig. 3.9). The sedimentological interpretation and the tectonic implication of these deposits are further discussed in Chapters 4 and 5.

Along the steep continental slope, Unit 1 is composed of a series of generally thin lens-like deposits that rest over the M-reflector. The internal character of these deposits ranges from undeformed stratified successions to heavily disturbed and poorly stratified or chaotic in appearance (Fig. 3.9). They are further described in Chapter 4.

Comparison between the detailed multibeam imagery and seismic reflection profiles show that along the Turkish continental margin, Unit 1 is cut by numerous submarine canyons (Figs. 3.10, 3.11). Orientation of these canyons appears to be down the slope of the continental margin and the canyons are observed along the margins of both Finike and Antalya basins (Fig. 3.10).

Figure 3.11 shows the thickness variations in Unit 1 across the study area. In the western portion of the study area, the Pliocene-Quaternary succession is thickest along a narrow trough across the Finike Basin, reaching thicknesses 2200 ms (Fig 3.12). Unit 1 thins toward the Turkish continental margin where it is either absent or shows maximum thickness less than ~300 ms. Unit 1 gradually thins toward the south onto the Sırrı Erinç Plateau. In the eastern and northeastern portion of the study area, the thickness of Unit 1 ranges between 400 and 600 ms. The isochron map illustrates the rapid change in the thickness of this unit at the NW and SE boundaries of the Finike Basin and the gradual decrease NE-SW (Fig 3.12).

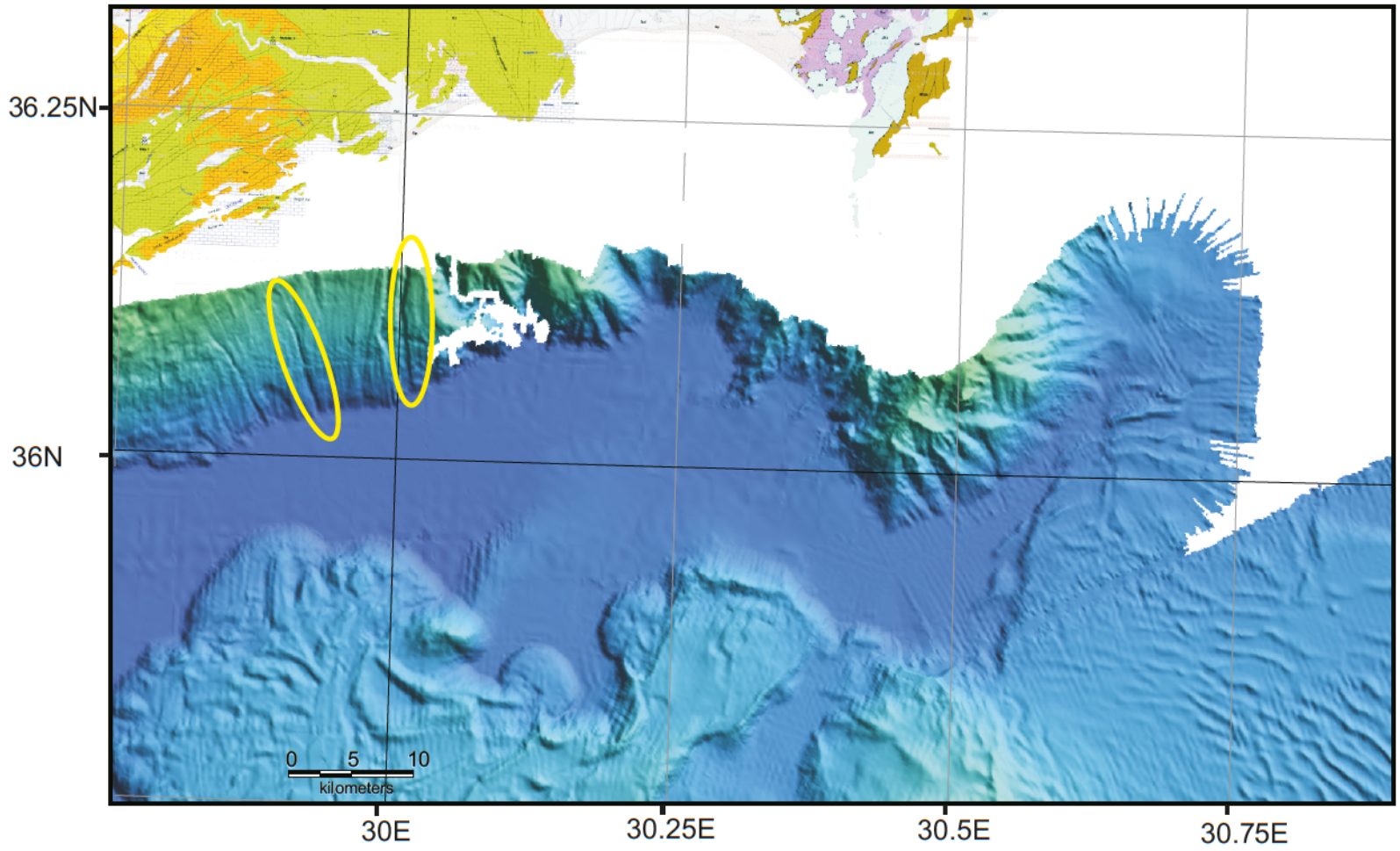

Figure 3.10 Multibeam bathymetry map of the study area highlighting some submarine canyons with a yellow circle.

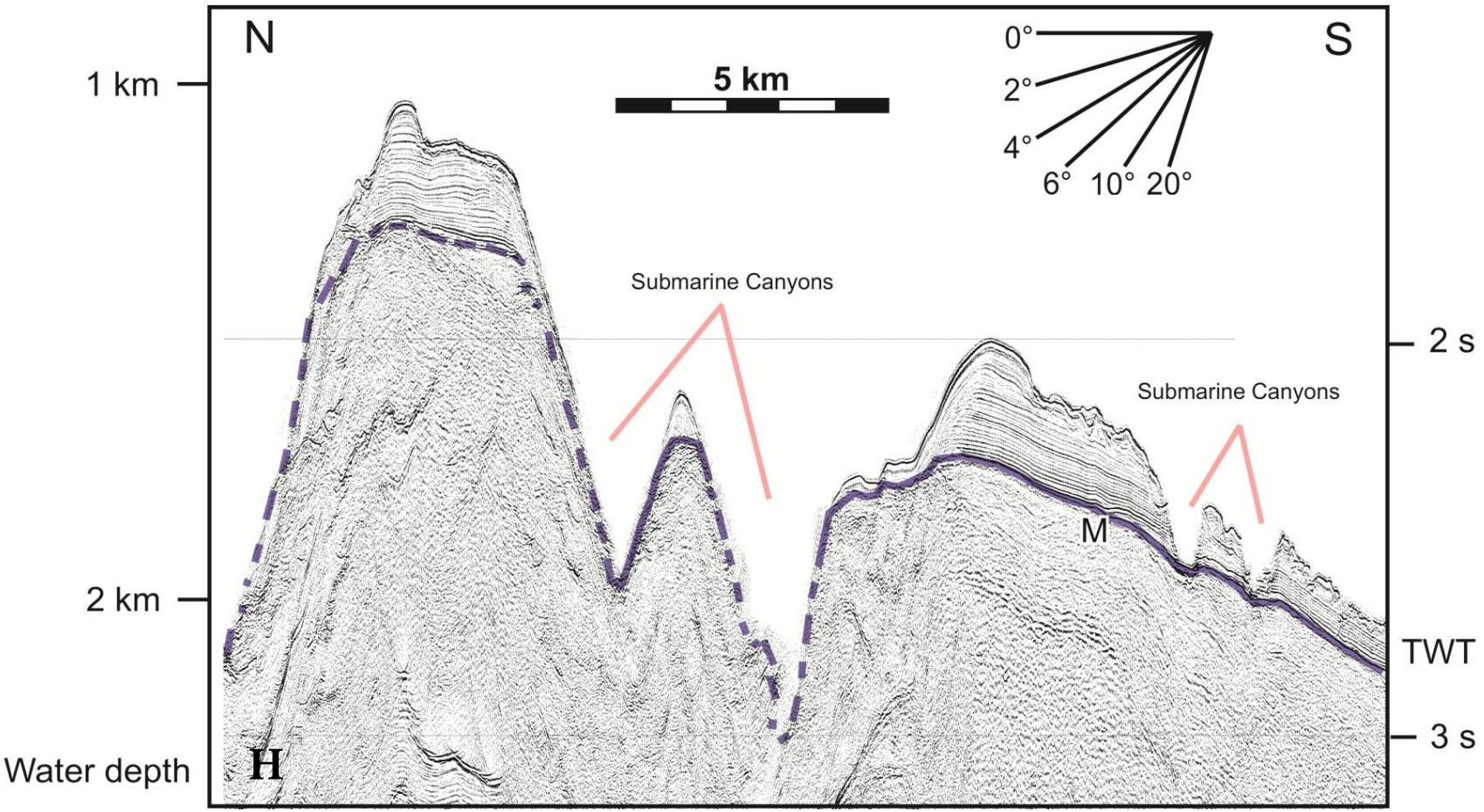

Figure 3.11 Seismic reflection profile H illustrating the submarine canyons that cut the Turkish continental margin (Plate 6, Fixes 2024-2009).

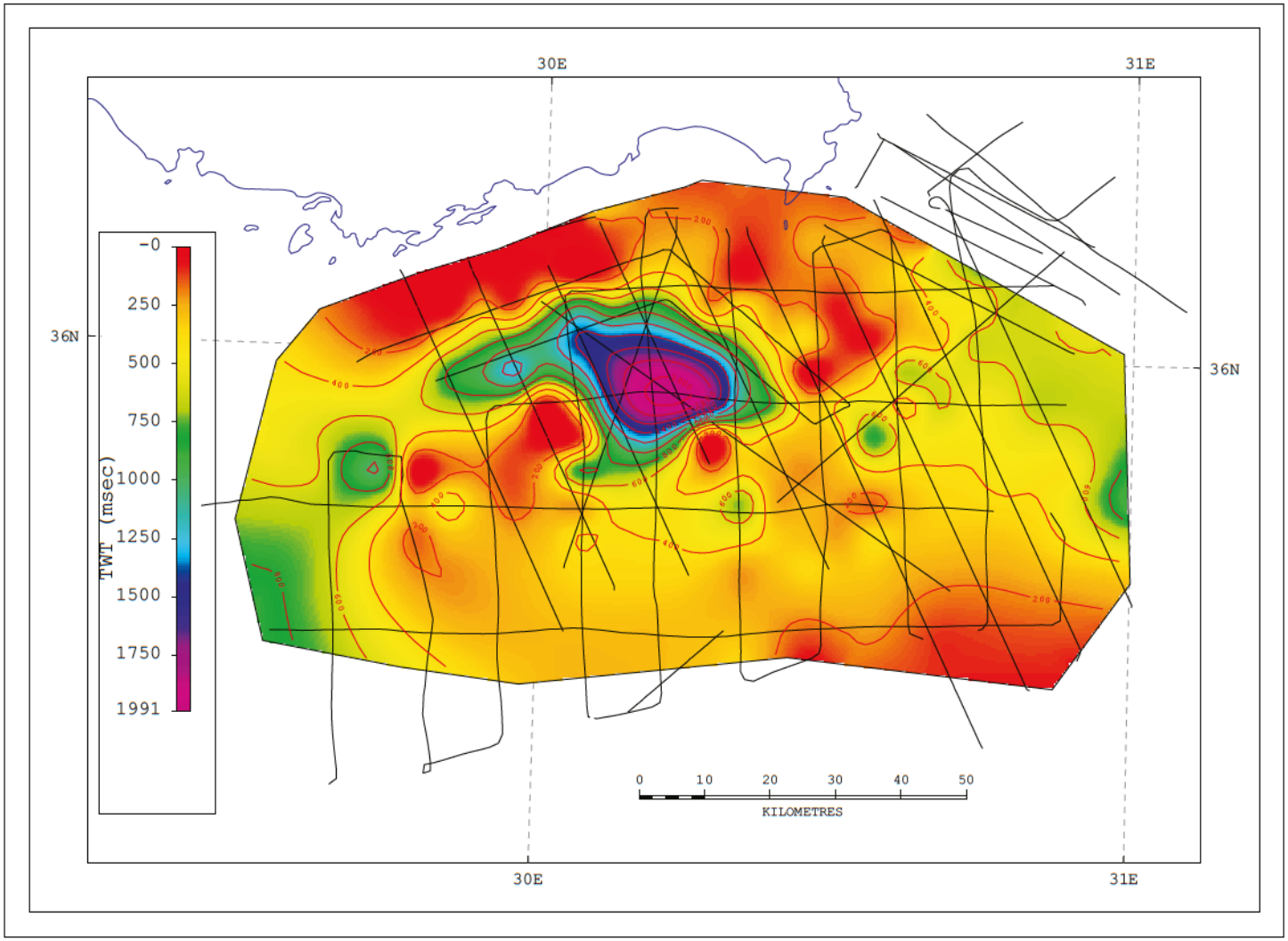

Figure 3.12 Isopach map showing the thickness in the two way travel time (msec) of the Pliocene-Quaternary succession across the study area

3.3.2 Unit 2: Late Miocene (Messinian)

Unit 2 is an acoustically transparent package which displays faint discontinuous reflectors and internal deformation (Figs. 3.12, Işler et al., 2005, Aksu et al., 2009). The M-reflector is the top of this unit, and the N reflector defines its base (Fig 3.13). Careful examination of the seismic reflection profiles shows that Unit 2 prominently occurs in the deep basinal settings of the southwestern Antalya Basin at depths 3700 ms (Fig. 3.15). It is also present at the transition zone from the Antalya Basin to the Anaxagoras Mountain as well as the easternmost fringes of the Finike Basin at depths 4000 ms (Figs. 3.15, 3.16). Unit 2 shows thinning and pinch-out through the eastern part of the Finike Basin and it is not present in the greater Anaximander Mountains (Aksu et al., 2009). In the southern part of the study area, the M-reflector stands as a highly reflective erosional surface, combining the M- and N-reflectors, similar to its occurrence in the deep Rhodes Basin (Hall et al., 2009).

Long-distance seismic stratigraphic correlations with the DSDP Sites 375 and 376 on the Florence Rise, reveal that Unit 2 is a predominantly evaporite succession consisting of halite, alternating with lesser quantities of anhydrite, limestone and dolomites with minor siliciclastic interbeds (Shipboard Scientific Party, 1978). The presence of this evaporitic succession, deposited during the Messinian Salinity crisis is extensively documented across the eastern Mediterranean basins (Hsü et al., 1973; Cita et al., 1978; Unit 2 of Hall et al., 2005a,b, 2009, Işler et al.; 2005 and Aksu et al. 2009; Piercey, 2011).

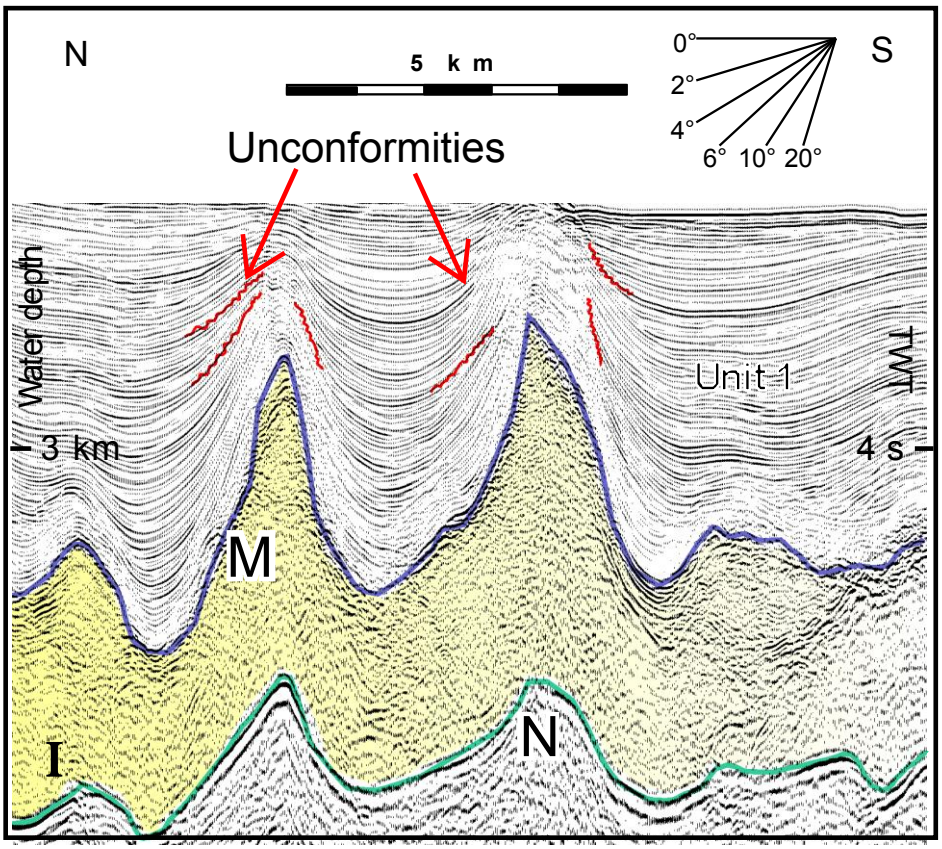

Figure 3.13 Seismic reflection profile I. Note the unconformities in Unit 1 on the crest of the salt are shown in red. Note the velocity pull-up on the base of salt (N-reflector in green) resulting from the high velocity contrast between the units and N-reflector depicts the shape of top of the salt (M-reflector in purple; Plate 30, Fixes 94-85).

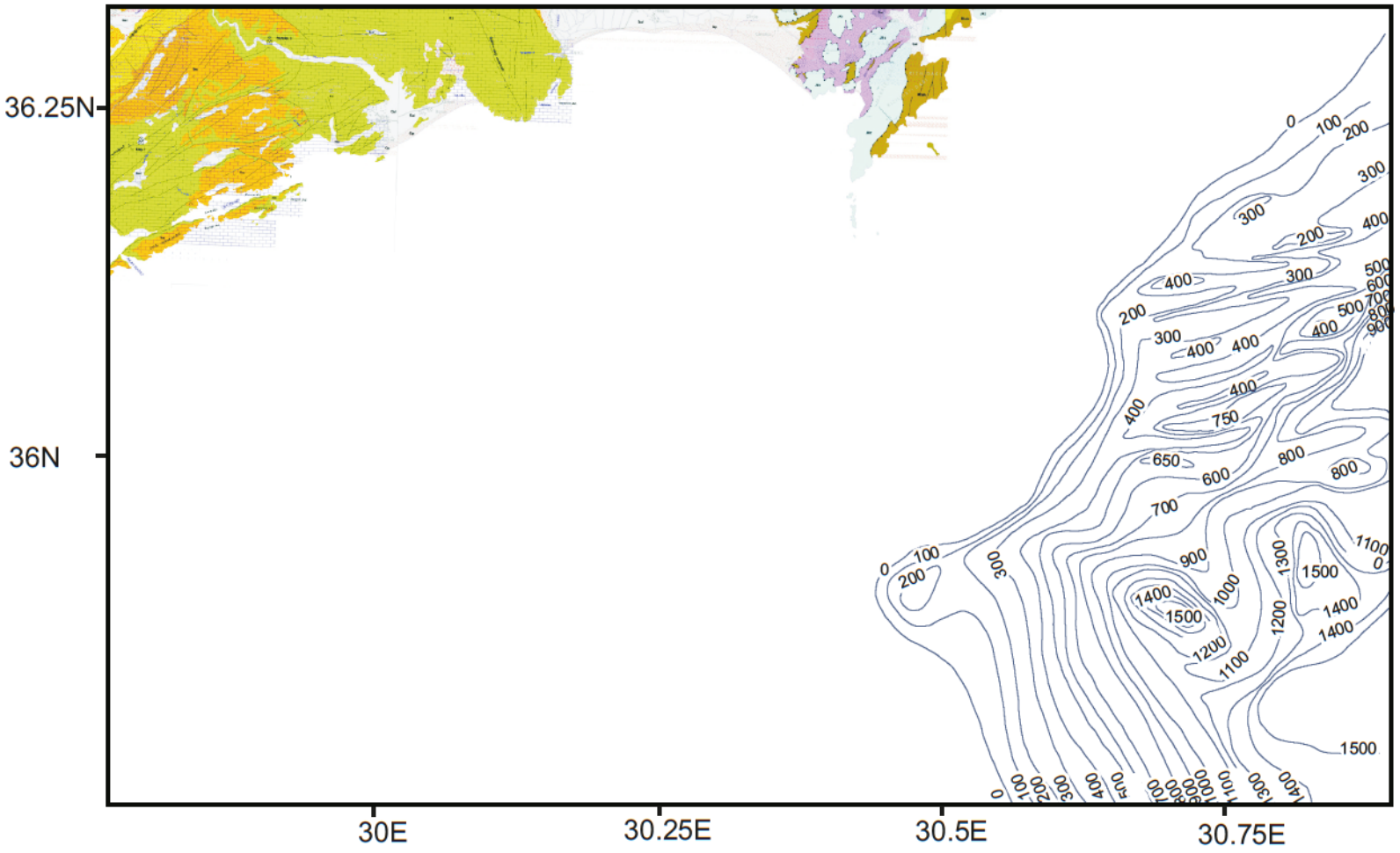

Figure. 3.14 Isopach map (in ms) showing the thickness distribution of the Messinian succession of Unit 2. Note that Unit 2 is ubiquitous in the southwestern Antalya Basin, but dramatically thins to form a basin edge westward. It is notably absent in the Finike Basin, except for its easternmost fringe. Also note that there are broadly east-west trending thick Unit 2 zones associated with large halokinetic structures (see text for explanations).

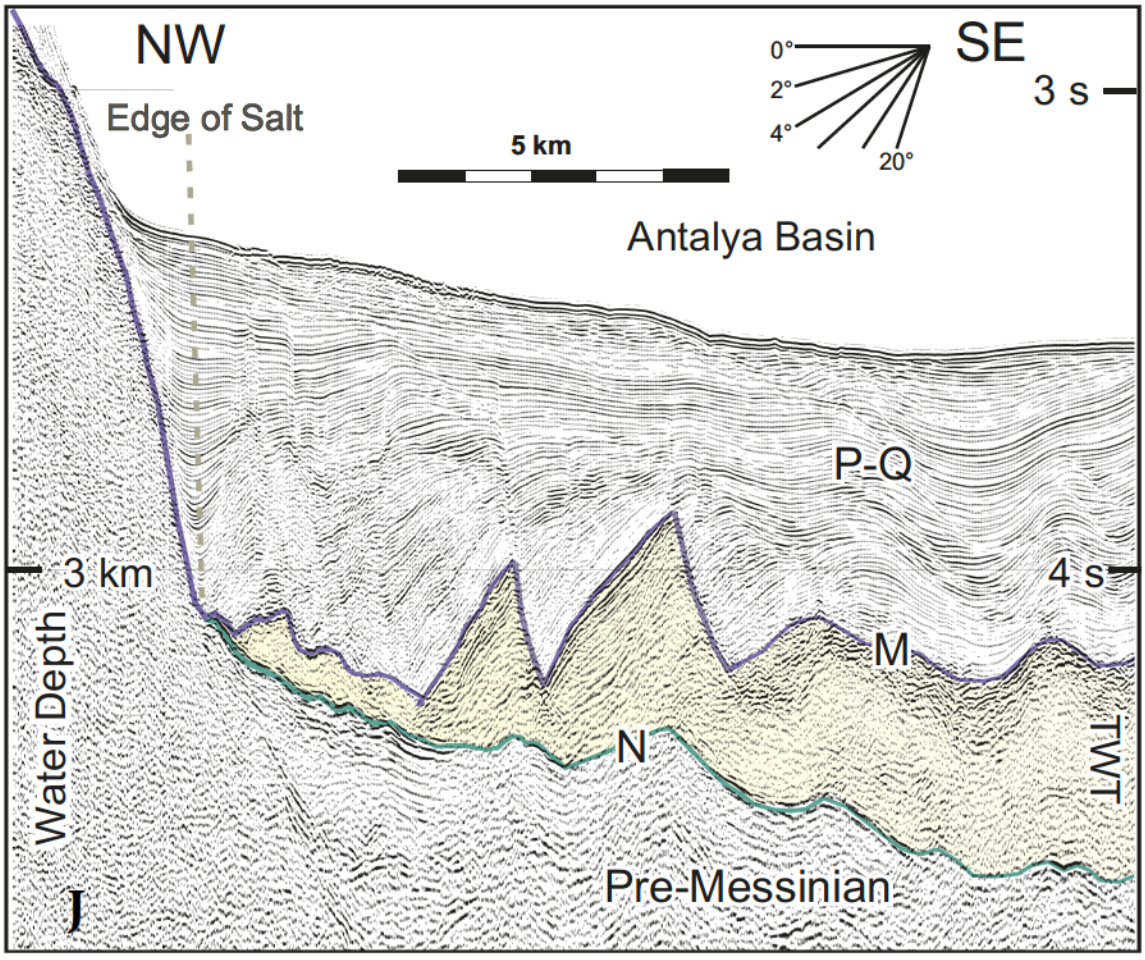

Figure 3.15 Seismic section profile J showing the architecture of the evaporate succession (Unit 2) coloured in yellow. M reflector indicates the top of salt and N reflector indicates the bottom. Note the partially continuous to discontinuous reflectors within Unit 3 (Pre-Messinian; Plate 28, Fixes 111-121).

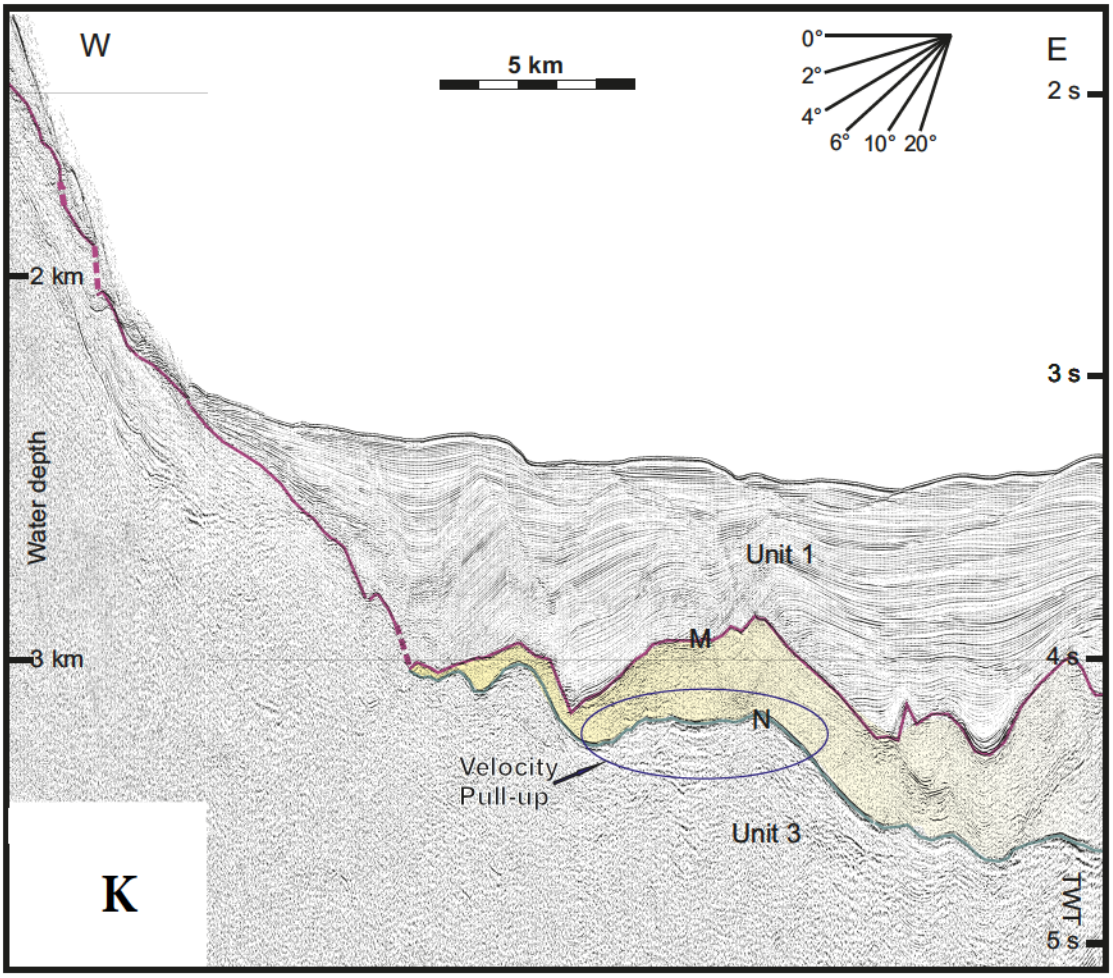

Figure 3.16 Seismic section profile K shows the architecture of the evaporite succession (Unit2) coloured in yellow. Note the velocity pull-ups along the N-reflector (base salt) which is partially highlighted within blue circle (Plate 15, Fixes 346-330).

Although some mud structures have been previously observed in the Florence Rise area (Woodside et al., 2000), the findings in this study show that these structures are largely associated with evaporites. Detailed velocity analysis of the structures across key regions in the study area gave interval velocities ranging between 3500 and 5000 m/s, with an average of ~4500 m/s (Figs. 3.17, 3.18). The velocity contrast with layers above and below show that the top of the salt layer (i.e., the M-reflector) and the base of the salt layer (i.e., the N-reflector) exhibit strong reflectivity with prominent velocity contrasts (e.g., Fig. 3.17) with velocity pull-ups on the base of Unit 2 (e.g., Fig. 3.16). These characteristics are clearly associated with salt in seismic reflection profiles, but never with mud. For example, because there is very little velocity contrast with mud and the surrounding siliciclastics, mud diapirs never show pull-up structures: in fact pull-down structures are often associated with mud intrusions U(Dimitrov 2002). Unit 2 varies in thickness from 1500 ms in southwestern Antalya Basin to 0 ms along a line that defines the edge of salt in the study area (Fig. 3.14). Examination of the seismic reflection profiles showed no clear evidence for weld structures along the margin of the western Antalya Basin (e.g., Figs. 3.15, 3.16). A number of highly reflective and relatively thin packages are occasionally observed on the edge of the continental slope in the Antalya Basin (Fig. 3.16). These highly reflective packages could be interpreted as weld structures, but poor imaging prevents clear determination of this interpretation. Even if they represent weld structures, the very small horizontal distances between 200 and 500 metres suggest that the original edge of the salt basin may have

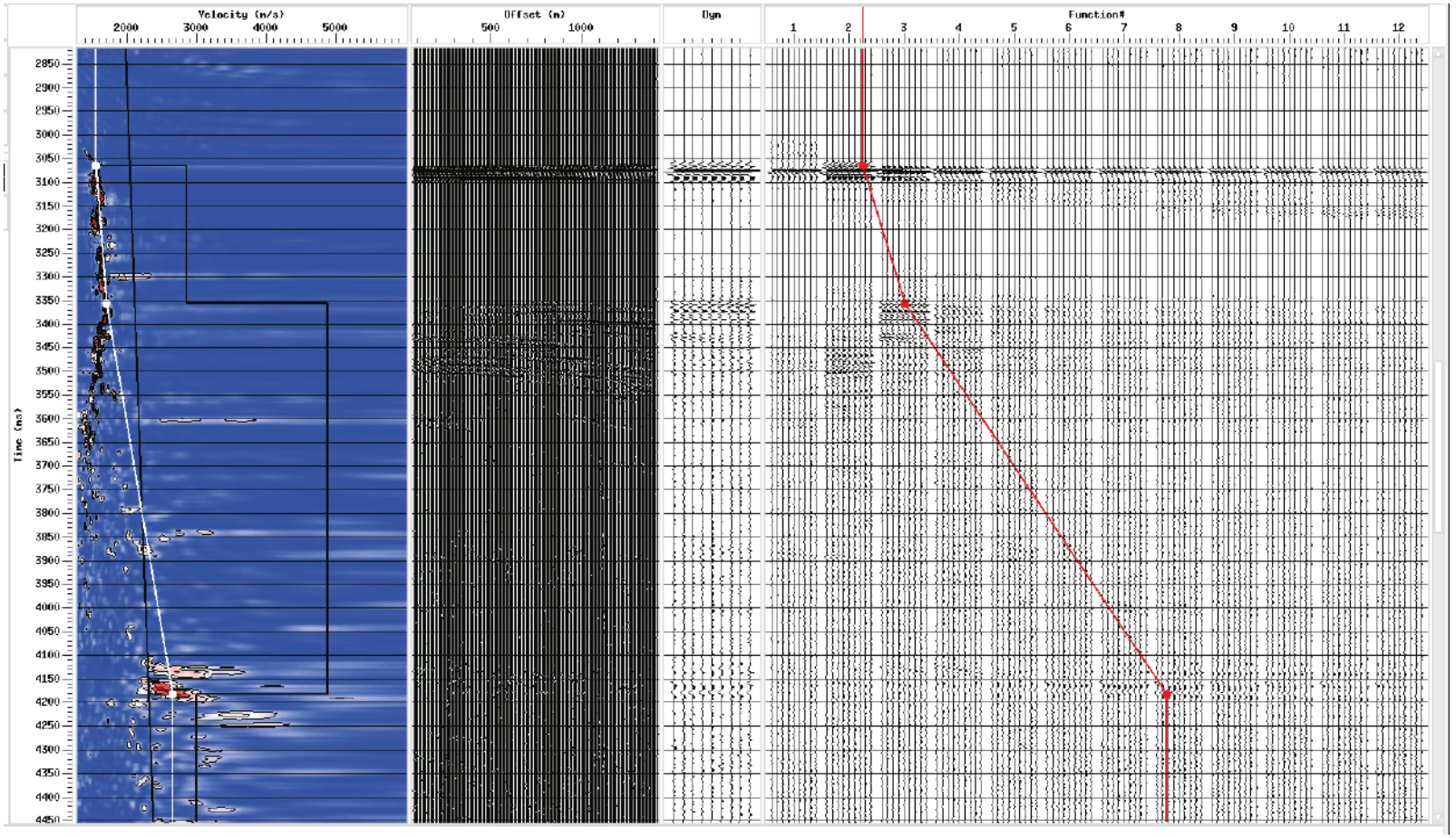

Figure 3.17 Velocity analysis with samblance spectrum (left) and velocity functions (right). Note that the interval velocity (black line superimposed on samblence plot) shows a marked increase to values exceeding 4500 m/s at the level of the M-reflector. This interval velocity cannot be reconciled with siliciclastic sediments, but is best explained by salt.

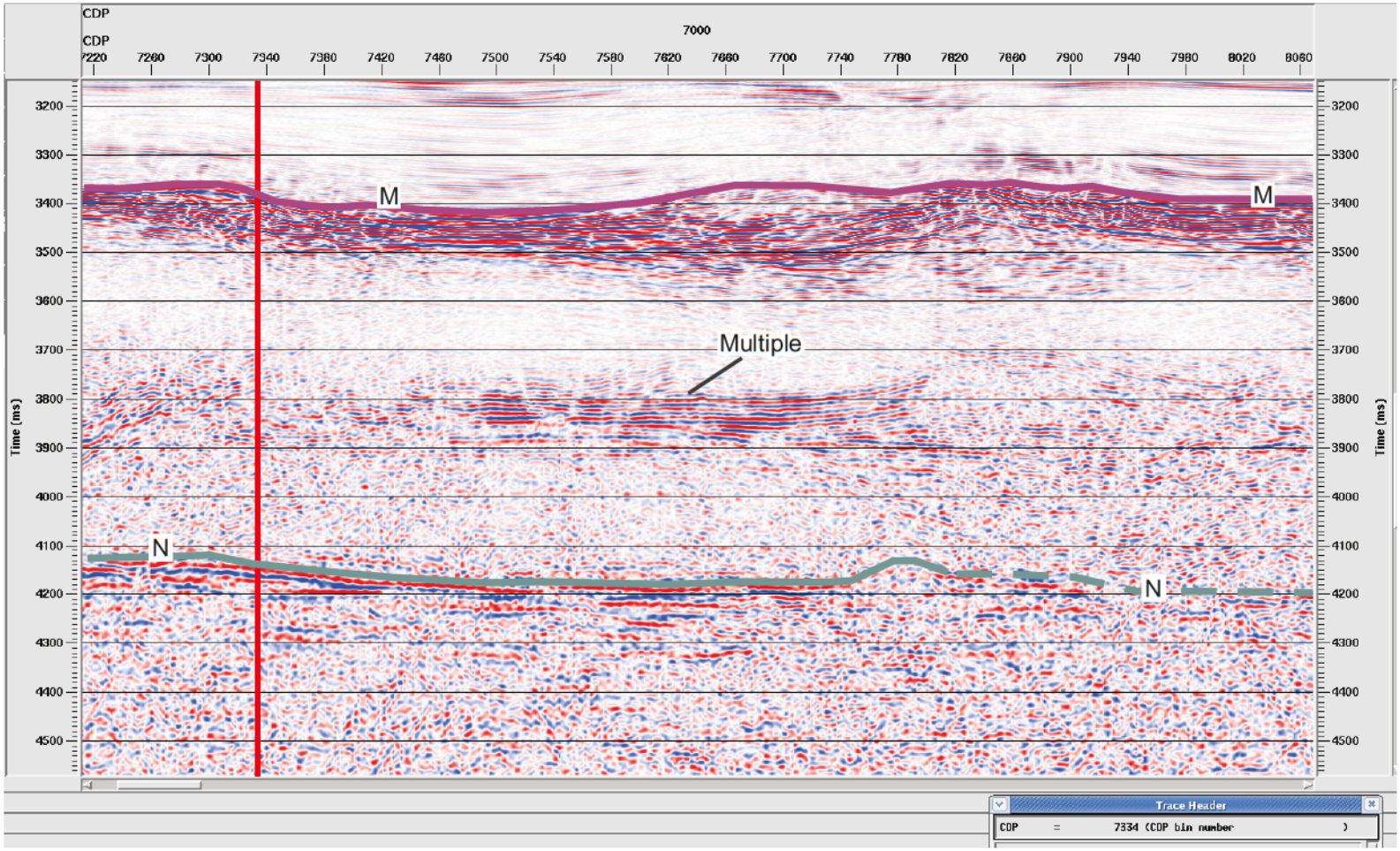

Figure 3.18 Kirchoff time migrated multichannel seismic reflection profile showing the locations of CDPs. Also marked is the CDP corresponding to the location of the velocity analysis shown in Figure 3.17. The M- and the N-reflectors are marker horizons discussed throughout the text.

been situated only a few hundred metres up-slope from the present-day edge. Therefore, the present day outline of the salt basin following the 0 ms contour also broadly depicts the shape of the ancestral Messinian basin (Fig. 3.14). Careful examination of the seismic reflection profiles and detailed mapping of Unit 2 collectively showed that the western boundary of the salt basin extends into the eastern edge of the Finike Basin, but Unit 2 is clearly absent within the deep Finike Basin further west (Fig. 3.15). For example, a seismic profile along the eastern margin of the Finike Basin clearly shows the thinning and eventual pinch-out of the Messinian succession of Unit 2 westward in the Finike Basin (Fig. 3.19). The ramification of the absence of the salt in Finike Basin and its regional tectonic implications are further discussed in Chapter 5.

3.3.3 Pre-Messinian successions and acoustic basement

Unit 3 is the oldest and deepest unit of the study area and consists of acoustically weak and partially continuous to discontinuous reflectors (Fig 3.15). The reflectors have low frequency content with low temporal and spatial resolution, which makes both stratigraphic and structural interpretation challenging. In regions where Unit 2 is missing, the M-reflector represents the top of Unit 3, whereas the N-reflector marks the top of this unit where the Messinian evaporite succession is present. Below the deep Finike Basin, Unit 3 occasionally includes well-defined internal layering (Fig 3.20). There are no dredge samples or drill cores in the Finike Basin, thus the age of the successions below the M-reflector can not be unequivocally determined. However, these sediments are clearly older than Pliocene, and because there are no Messinian

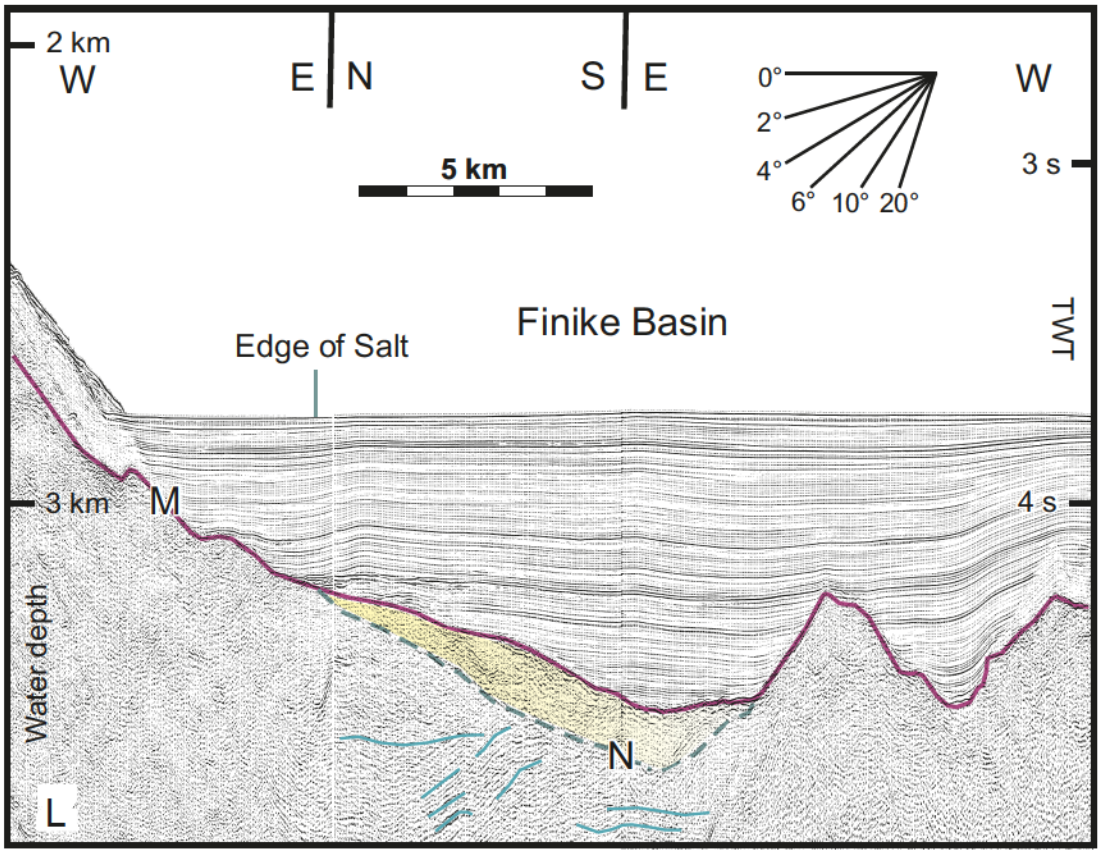

Figure 3.19 Multichannel seismic reflection profile L (a combination of three different lines) showing the thinning and pich out of the Messinian Unit 2 in easternmost Finike Basin (from left Plate 7, Fixes 2045-2050; Plate 8, Fixes 2050-2055; Plate 9, Fixes 2055-2062).

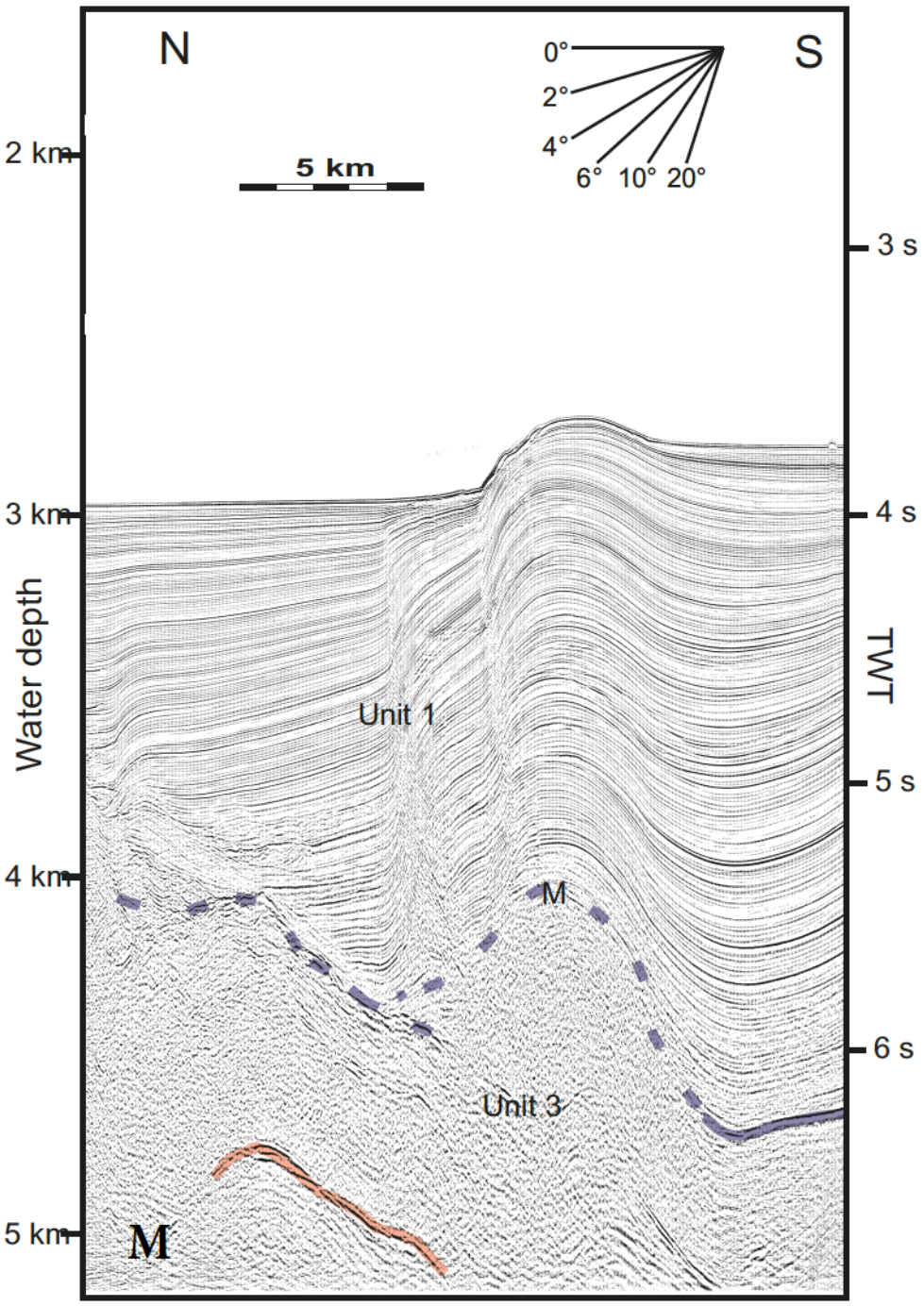

Figure 3.20 Seismic cross-section M demonstrates the internal lithologies of Unit 3 in pink (Plate 19a, Fixes 955-943).

evaporite succesions in thedeep Finike Basin, these sediments are also probably older than Messinian. Here in, they are assumed to be pre-Messinian Miocene. The widespread occurrence of pre-Messinian Miocene siliciclastics in the eastern Mediteranean, including the Kasaba Basin (Şenel and Bölükbaşı, 1997a,b) immediately north, Aksu, Köprü, Manavgat basins (Akay and Uysal, 1985; Akay et al., 1985; Işler et al. 2005; Turkish Petroleum Corporation, unpublished data) to the east of the study are a strongly suggests that Unit 3 successions are most probably Tortonian and older Miocene in age. Across a small area where Finike Basin connects to Antalya Basin, Unit 3 shows horizontally continuous reflections. These reflections are interpreted as the remnants of a pre-Messinian basin (Fig. 3.21).

3.4 Core Samples

In the course of Leg-1 of the ANAXIPROBE/TTR-6 cruise, 28 core samples were collected from the greater Anaximander Mountains and the surrounding areas, including the Sırrı Erinç Plateau and the southwestern Turkish continental margin (Fig. 3.22; Akhmanov et al. 1997; Cranshaw 2010). The sampling concentrated on slopes and mud volcanoes: the detailed summary of a selected number of samples is presented in Table 3.1.

3.5 Dredge Samples

During the ANAXIPROBE/TTR-6 cruise 17 dredge samples were collected from Anaximander Mountains and the Turkish continental slope (Fig. 3.22). Although a significant number of dredges were empty, the rest were adequate to provide an insight

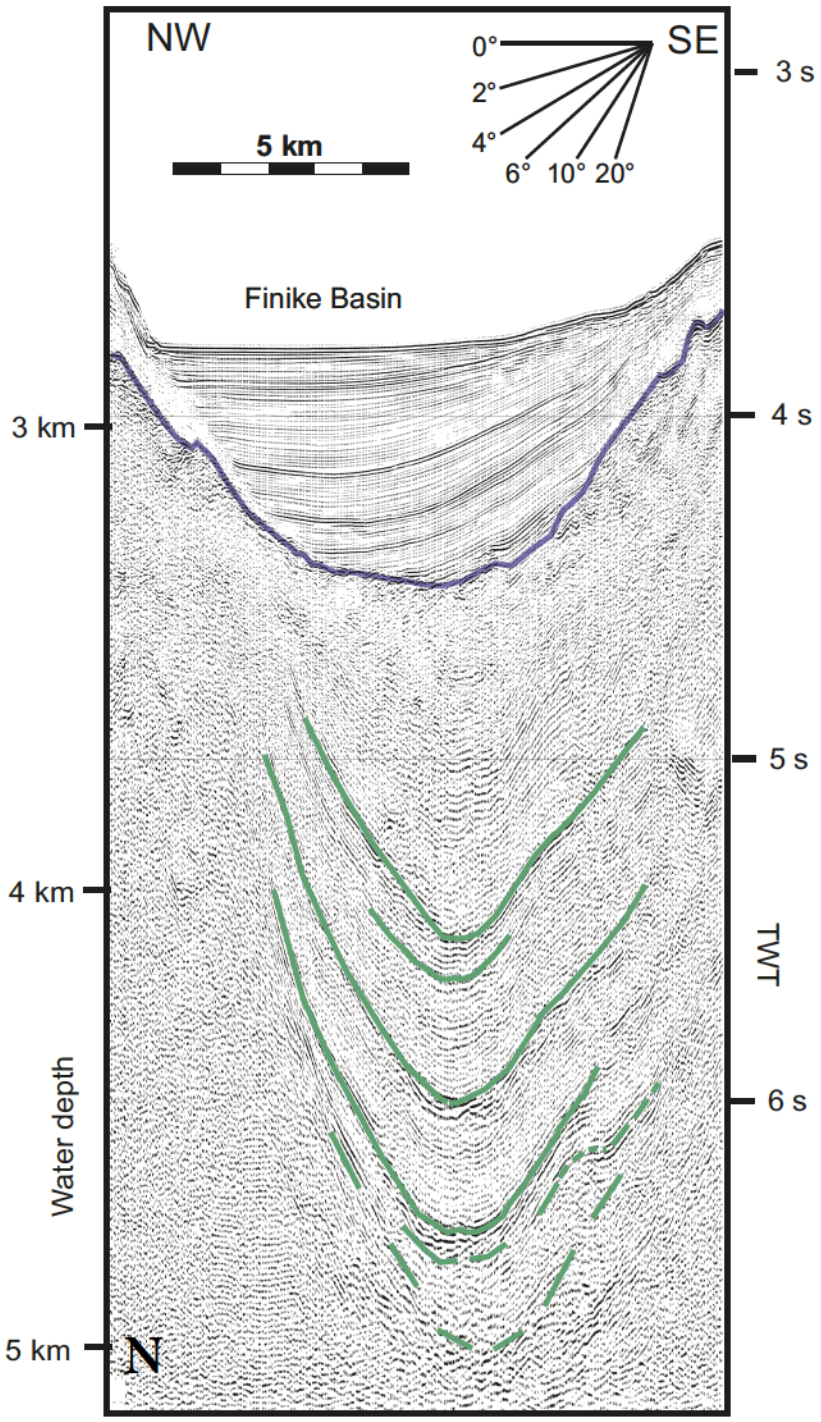

Figure 3.21 Seismic cross-section N demonstrating the strong reflectors in green present under the M-reflector (Plate 23, Fixes 842.3-850.3).

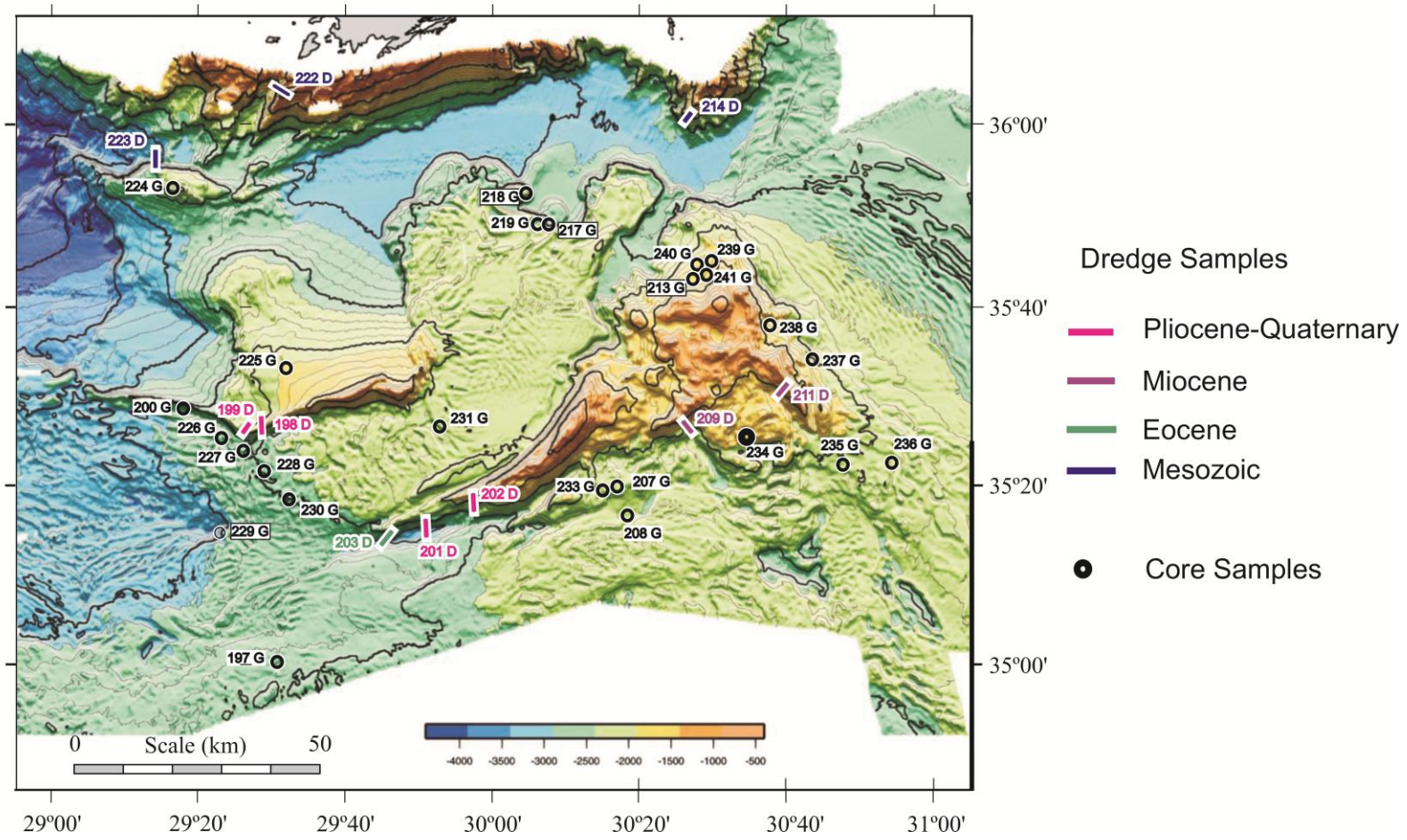

Figure 3.22 Bathymetry map showing the locations of the cores and the dredge samples (data from Woodside et al., 1997).

Location	Cores	Lithology	Chronology	Description
Anaximender Mountain	224G, pg. 92	Marly pelagic sediments,carbonate clay, clay with tephra and sapropels	Pleistocene-Holocene	
Sırrı Erinç Plateau	231G, pg. 78	Foram rich marl with tephra and saprosel layers, foram rich clay, slump mud breccia	Pleistocene-Holocene	- Evidence of reworked Eocene-Miocene strata , suggests the same history for Anaximenes and Anaximender - Wash-out of post-Miocene sediments into the Finike Basin
	219G, pg. 70, 90	Marl and mud consisting forams and petropod, clay, silty mud, silt with clasts of sandstone		
	217G, pg.80, 89	Foram and pteropod rich marl, structureless poorly sorted mud breccia		
Anaximenes Mountain	205G, pg. 79	Slump sediments with clay, marl, mud and carbonate peddles, silty sediments with shells	Pleistocene-Holocene	-Active slope processess
	206G, pg. 81	Marl with tephra layer,silty mud with shells, sapropel clasts		
Anaxagoras Mountain	213G, pg.68, 79, 87, 108	Pteropods rich marl, mud breccia, internal gas hydrates abundence	Jurrasic-Cretaceous	- Kula Mud Volcano, internal gas hydrates abundence, serpentined peridotide implying Antalya Nappes
	234G, pg. 82 95	Thin- soupy Pelagic sediments, grey mud breccia with hard rocks up to 7cm and large number of shells	Pleistocene-Holocene	- Kozan Mud Volcano
	235G, pg 69 82, 96	Pelagic marls with saprapel and tephra layers and dark grey mud breccia		- Tuzlukush Mud Volcano
	207G, pg. 69 82, 94	Mud breccia with hard rocks up to 9cm with oxidated upper part and large number of shells and living bivalves		- Amsterdam Mud Volcano

Table 3.1 A brief description of the core samples collected from Turkish continental slope, Anaximenes and Anaxagoras Mountains and the vicinity (pg.=page numbers and data from Woodside et. al., 1997).

into the subsurface geology of the region (Dumont and Woodside, 1997). Rocks encountered in these dredges included Eocene to Pleistocene siltstones, sandstones, limestones, mid-Miocene flysch, early Pliocene and Mesozoic conglomeratic sandy limestones and Jurassic-Cretaceous ophiolitic rocks (Fig. 3.22, Table 3.2; Hendericks and Singhal, 1997).

On the eastern Turkish continental slope, dredge 214D recovered a small amount of rock fragments (Fig. 3.22). However, these rocks provided important information as they contained predominantly Jurassic and Cretaceous ophiolitic rocks, suggesting a genetic linkage of the slope successions with the Antalya Nappes unit (Dumont and Woodside, 1997) situated north and northeast of the Finike Basin. The four core samples collected along the northern slopes of the Anaxagoras Mountain over the Kula mud volcano bear strong resemblance to dredge samples collected from the western Turkish continental slope and suggest an affinity to the Antalya Nappes (Fig. 3.22, Tables 3.1, 3.2; Dumont and Woodside, 1997).

On the western slope of the Turkish continental margin two dredge samples, 222D and 223D included mostly limestone fragments of Mesozoic age (Fig. 3.22). These two samples provided strong evidence of a genetic relationship of the Turkish continental margin with the Mesozoic Beydağları unit. Woodside et al. (1997) used the breccia containing terrigenous sediments now located at 2500 m depth and possibly formed during the Pliocene in a shallow marine environment to suggest that there is vertical tectonics or downward gravitational movement along the oceanic wall of the Beydağları massif.

Location	East Turkish Continental Slope	West Turkish Continental Slope	Anaxagoras Mountain	Anaximenes Mountain
Dredge	214D	223D, 222D	209D, 211D	201D, 202D, 203D
Lithology	Ophiolitic Rocks	Conglomeratic finer "sandy" limestone	Black Siltstone, Flysch, Sandstone and Limestone	Siltstone, Sandstone, Limestone
Chronology	Mesozoic	Early Pliocene and Mesozoic	Middle Miocene	Early-Mid Pliocene-Pleistocene, Eocene, Early-Mid Miocene
Description	Connection to the Antalya Napes considered	Limestone resembling the onland Bey Dağları Mountains; neritic facies with rudistids	High consistency of Mid Miocene Flysch along the area, Reworking of Eocene-Miocene material, Slickensides evidence of compression tectonics	Southeastern margin dominated by Eocene rocks

Table 3.2 A brief description of the dredge samples collected from Turkish continental slope, Anaximenes and Anaxagoras Mountains and the vicinity (data from Woodside et al., 1997).

Dredge samples 209D and 211D were collected over the Anaxagoras Mountains (Fig. 3.22). The samples showed middle Miocene age flysch facies. The limestone samples were found periodically similar to the samples collected over the Anaximenes Mountain (i.e., 202D-2; Hendricks et. al., 1997). The sporadic occurrence of a flysch succession atop Eocene limestones along the Anaximender and Anaximenes Mountains was an important discovery, and suggested a possible linkage with the Beydağları massif of southwestern Turkey (Woodside et al., 1997).

3.6 Kaş-1 and Demre-1 Wells

Two wells, Kaş-1 and Demre-1, were drilled in the onland Kasaba Basin situated in the west of the study area, for exploration purposes by the Turkish Petroleum Cooperation (Fig. 3.23). Kaş-1 well was drilled to a depth of 5298 meters and Demre-1 well was drilled to 6110 meters. Both wells encountered 2800-2900 m thick succession of thickly-bedded gray and light brown neritic limestones correlated with the Lower Jurassic-Upper Cretaceous Beydağları Formation (Fig. 3.24; Şenel and Bölükbaşı a, b, 1997). In both wells the Beydağları Formation is underlain by a massive, dark grey coloured, coarse grained dolomites succession, correlated with the Kuyubaşı Formation (Fig. 3.24; Şenel and Bölükbaşı, a, b, 1997, Şenel, 1997). The Demre-1 and Kaş-1 wells cut across a major thrust surface, as indicated by a reversal of stratigraphy where the Kuyubaşı Formation is underlain by 200-300 m thick gray and light brown neritic limestones of the Beydağları Formation (Fig. 3.24).

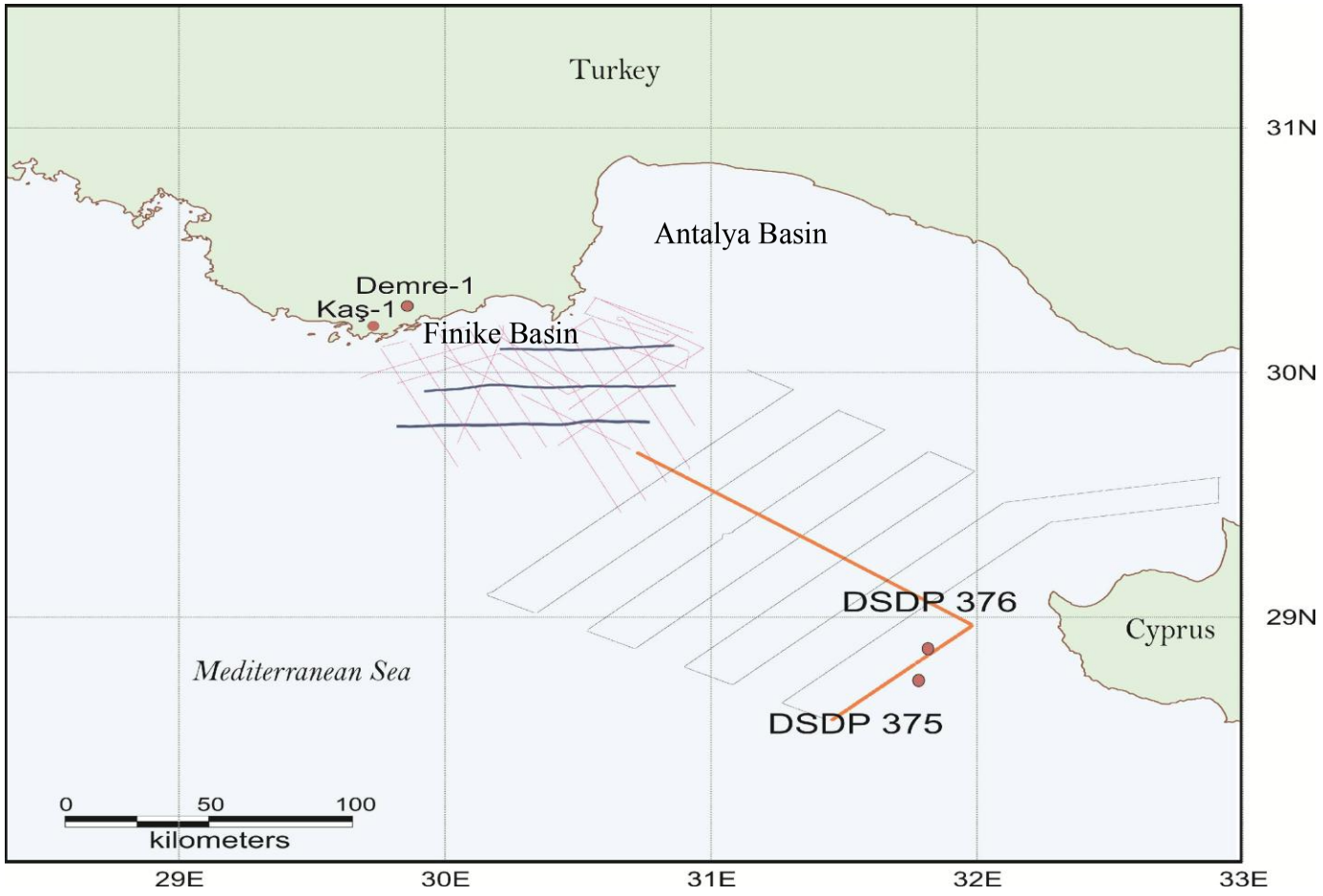

Figure 3.23 Map showing the long-distance correlation of DSDP boreholes over the Florence rise with the Sırrı Erinç Plateau, Finike Basin and the western Antalya Basin. The pink lines indicate the data belong to the author. The location of the Kaş-1 and the Demre-1 are also shown.

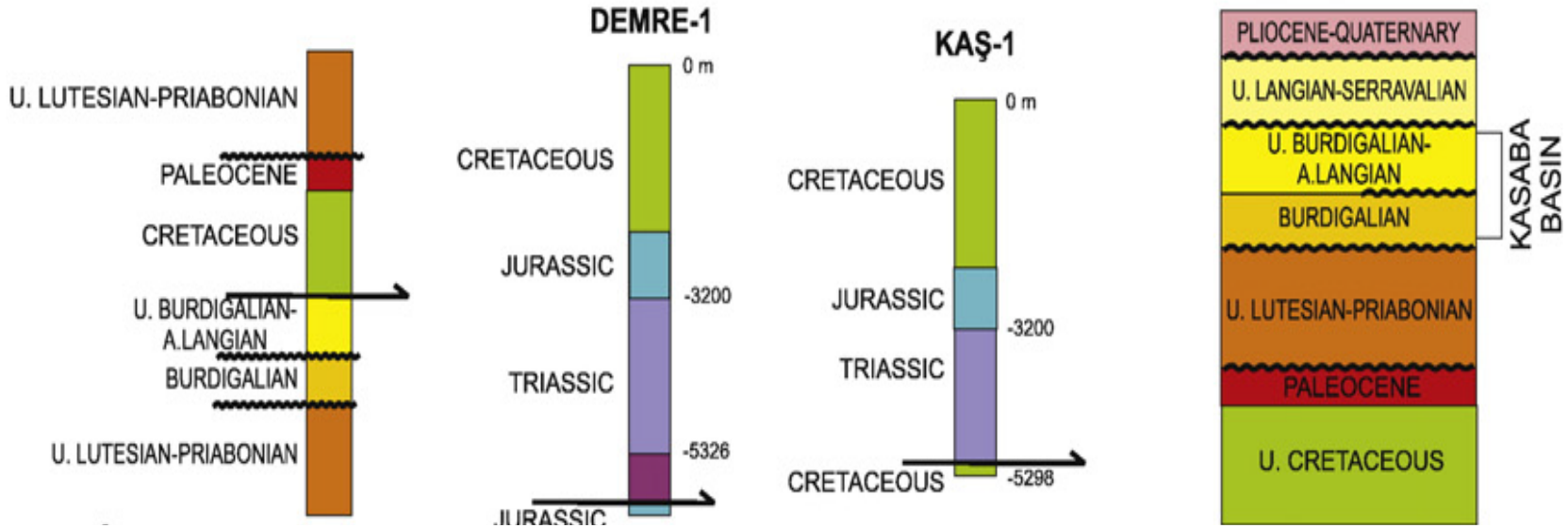

Figure 3.24 The stratigraphy of Demre-1 and Kaş-1 wells that are located in the onland Kasaba Basin. Location of the wells are shown in Figure 3.23. The columns on the left and the right end show general section from the northern margin of the Kasaba Basin and general stratigraphy of the Kasaba Basin. Note the repation of the stratigraphic units suggesting major thrusting in wells (from Aksu et al., 2009, Hall et al., 2009, data from Şenel and Bölükbaşı, 1997a,b)

According to these two onland exploration wells, the Serravallian-Langhian sedimentary successions in the Kasaba Basin and the Western Tauride Mountains were exposed to the Middle-Late Miocene phase of deformation. Data from Kaş-1 and possibly Demre-1 showed the presence of a notable south-verging thrust, dipping about 10 N, which shows similarities with the fold-thrust geometries observed in marine areas (Fig. 3.24). The implications of this major thrust are further discussed in Chapters Four and Five.

3.7 Chronostratigraphy

During the Deep Sea Drilling Project, boreholes 375 and 376 (Shipboard Scientific Party 1978) were drilled on the Florence Rise, west of Cyprus (Fig. 3.23). These two boreholes have penetrations of 216.5 (376) and 821.5 (375) meters below seabed and provide crucial information regarding the Miocene to Recent evolution of the eastern Mediterranean Sea. Eleven lithological units are identified (Shipboard Scientific Party, 1978). Seismic data collected along Florence Rise, with the data collected from the Finike Basin and vicinity, supplies a long distance correlation, as shown in Fig. 3.23 A preliminary chronology is generated for the seismic stratigraphic units defined in the study area based on the information above (Fig. 3.25). Accordingly, Unit 1 is correlated with Antalya Tufa, Alakilise and Yenimahalle formations of the Aksu, Antalya, Köprü and Manavgat basins from younger Quaternary to older Pliocene, respectively. Unit 1 is further correlated with Fanglomerate Athalansa,

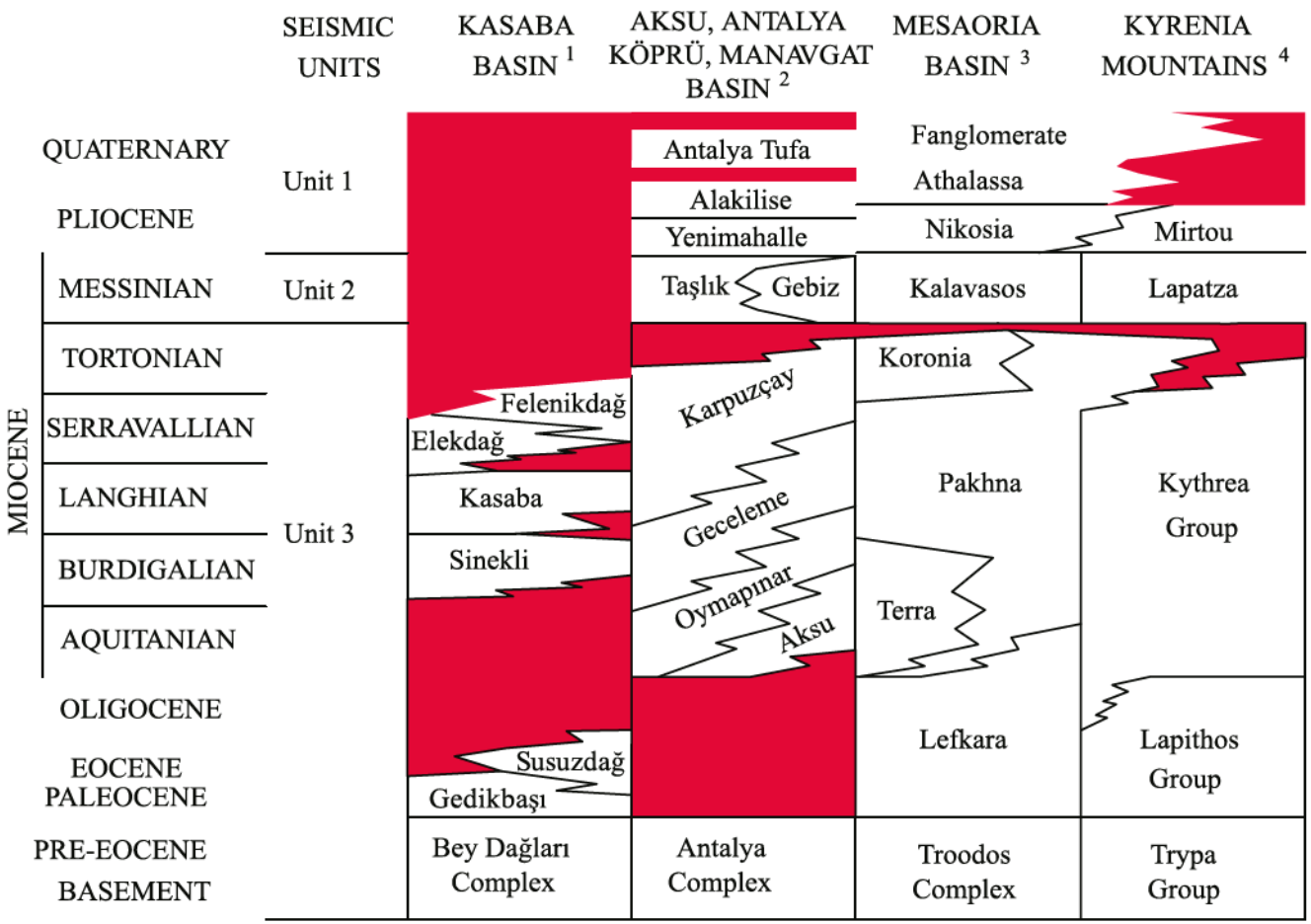

Figure 3.25 Stratigraphy of the Anaximander Mountains and the Finike Basin showing the correlations between seismic stratigraphic units 1–3 and the sedimentary successions of the on-land Kasaba Basin (Hayward, 1984; enel,1997a,b; enel and Bölükba , 1997a,b, Islamo lu and Taner, 2002, Hinsbergen et al., 2010); the marine Antalya Basin (I ler et al., 2005) the onland Aksu, Köprü and Manavgat Basins (Akay et al., 1985; Karabıyıkoğlu et al., 2000), and the onland Mesaoria Basin and theKyrenia Mountains (Cleintaur et al., 1977; Robertson et al., 1995; Robertson et al., 1998).

Nikosa and Kavalasos formations of the Mesaoria Basin, and the Pliocene-age Mirtou Formation of Kyrenia Mountains of northern Cyprus.

Unit 2 is correlated with the anhydrite- and selenitic gypsum-bearing siliciclastic deposits of the Gebiz Formation of the onland Aksu, Köprü and Manavgat basins as well as Taşlık Formation. (Akay and Uysal, 1985; Akay et al., 1985; Işler et al. 2005; Turkish Petroleum Corporation, unpublished data). It is also correlated with Kalavasos and Lapatza formations of the Mesaoria Basin and the Kyrenia Mountains.

In the Kasaba Basin, the Gedikbaşı Formation was deposited during the Paleocene and the Susuzdağ Formation lies over it creating a transgressive unconformity (Önalan, 1979; Şenel et al., 1989, 1994). Above these formations lie the Sinekli and Kasaba and Elekdağ formations. On the top of the Elekdağ Formation, the Felenkdağ conglomorate lies unconformably over the Miocene units (İslamoğlu and Taner, 2002). These formations belong to Unit 3 and they are correlated with Aksu, Oymapınar, Geceleme and Karpuzçay formations of Aksu, Antalya, Köprü, Manavgat basins. Further correlation carried out with Lefkara, Terra, Pakhna and Koronia units of Mesaoria Basin, and Lapithos and Kythrea groups of Kyrenia Mountains. It is also possible that Unit 3 may consist of the Beydağları and Antalya complexes of the western Tauride Mountain because it represents the acoustic basement (Cranshaw, 2010).

Chapter Four: Structural Architecture

The structural architecture of the Finike Basin and vicinity is presented in three time slices: (A) the Pliocene-Quaternary, (B) the Messinian and (C) the pre-Messinian Miocene.

4.1. Pliocene-Quaternary

On the basis of the seabed morphology and the internal structural elements, the Pliocene-Quaternary geology of the Finike Basin and vicinity is divided into five morpho-tectonic domains: Domains 1-5 (Fig. 4.1).

4.1.1 Domain 1 – Southwestern Antalya Basin

Domain 1 is bounded by the Turkish continental slope on the west and northwest, the Finike Basin on the south and southwest and Domain 2 on the south and southeast (Fig 4.1). It is located in the northeastern portion of the study area and includes the south western Antalya Basin, as well as the deeper portion of the Turkish continental slope and the continental rise. The Pliocene-Quaternary succession in Domain 1 includes three main structural elements: (i) slope-parallel relatively low-angle (20-30 degrees) normal faults, (ii) listric normal faults and (iii) bedding parallel detachments (Figs. 4.2-4.5). There are several superficial detachment faults at the base of the slope in this domain: these faults are described in Domain 5 below.

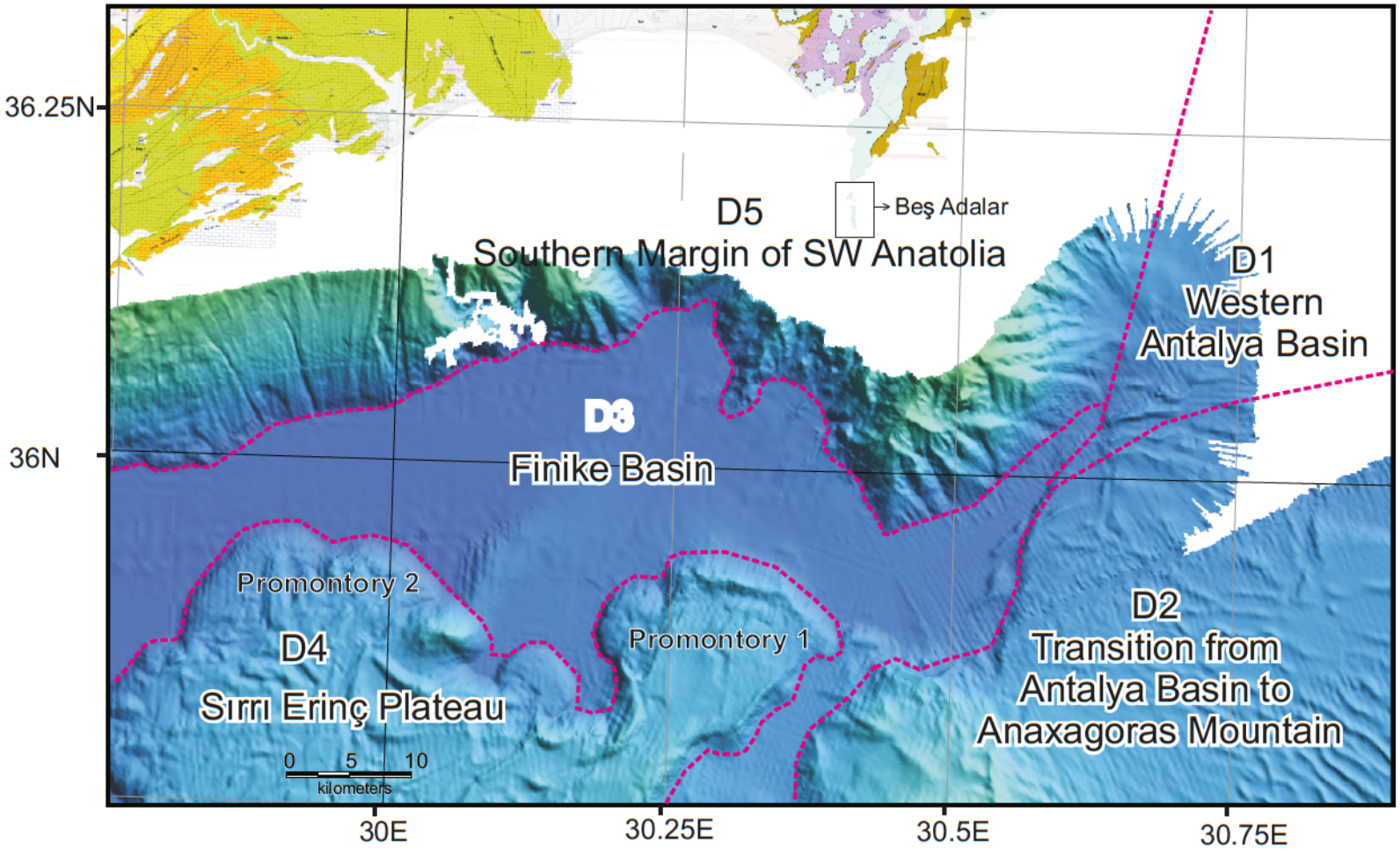

Figure 4.1 Multibeam map showing the morphology of the seafloor and the Pliocene-Quaternary morpho-tectonic Domains 1-5 in the Finike Basin and environs. The eastern portion of Sırrı Erinç Plateau is called Promontory 1 whereas the western portion is called Promontory 2. The black box shows the location of Beş Adalar.

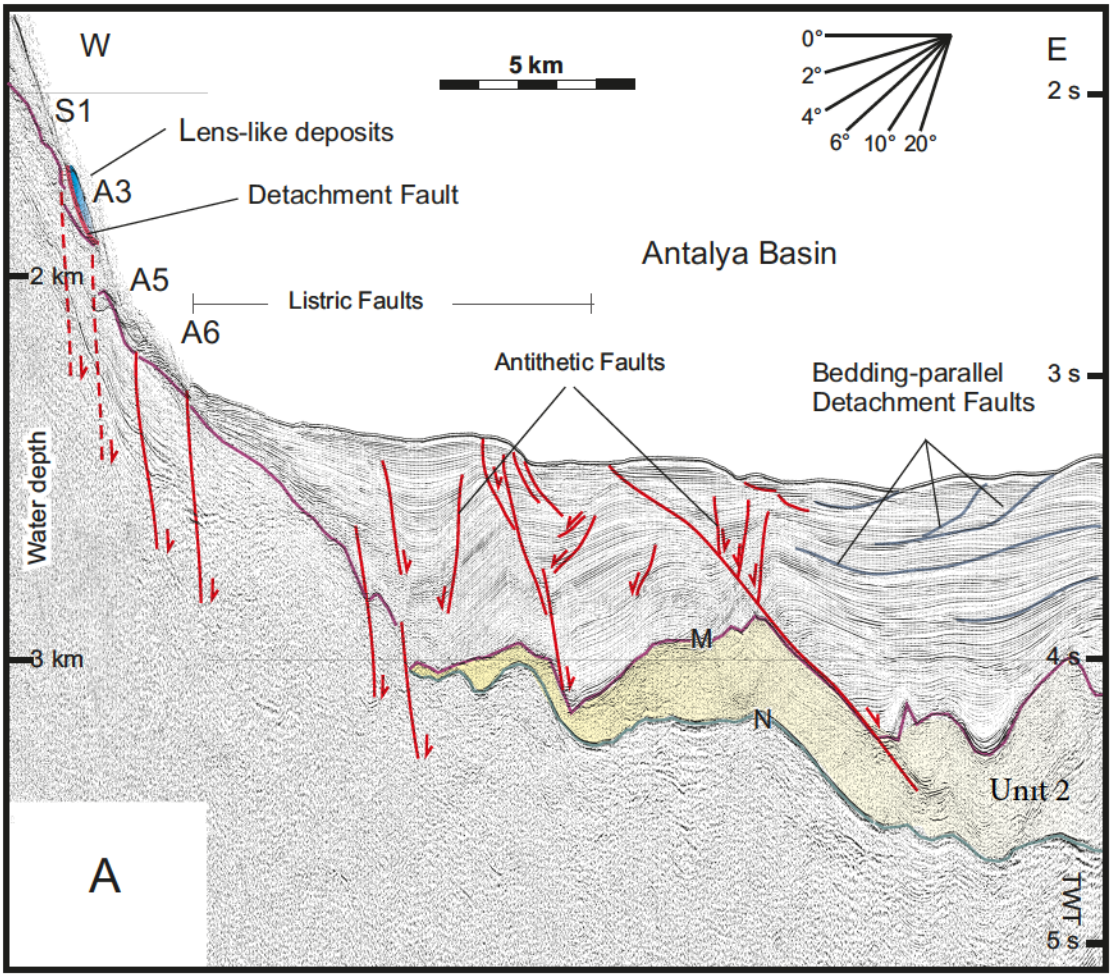

Figure 4.2 Multichannel seismic reflection profile A showing the internal architecture of morpho-tectonic Domain 1. Note the slope-parallel relatively low angle faults that define the structures along the lower slope. Also note the bedding-parallel detachment faults (in dark blue) that occur on the eastern portion of the large evaporite mound developed in Unit 2. Location is shown in Figure 4.3. (Plate 15, Fixes 346-330).

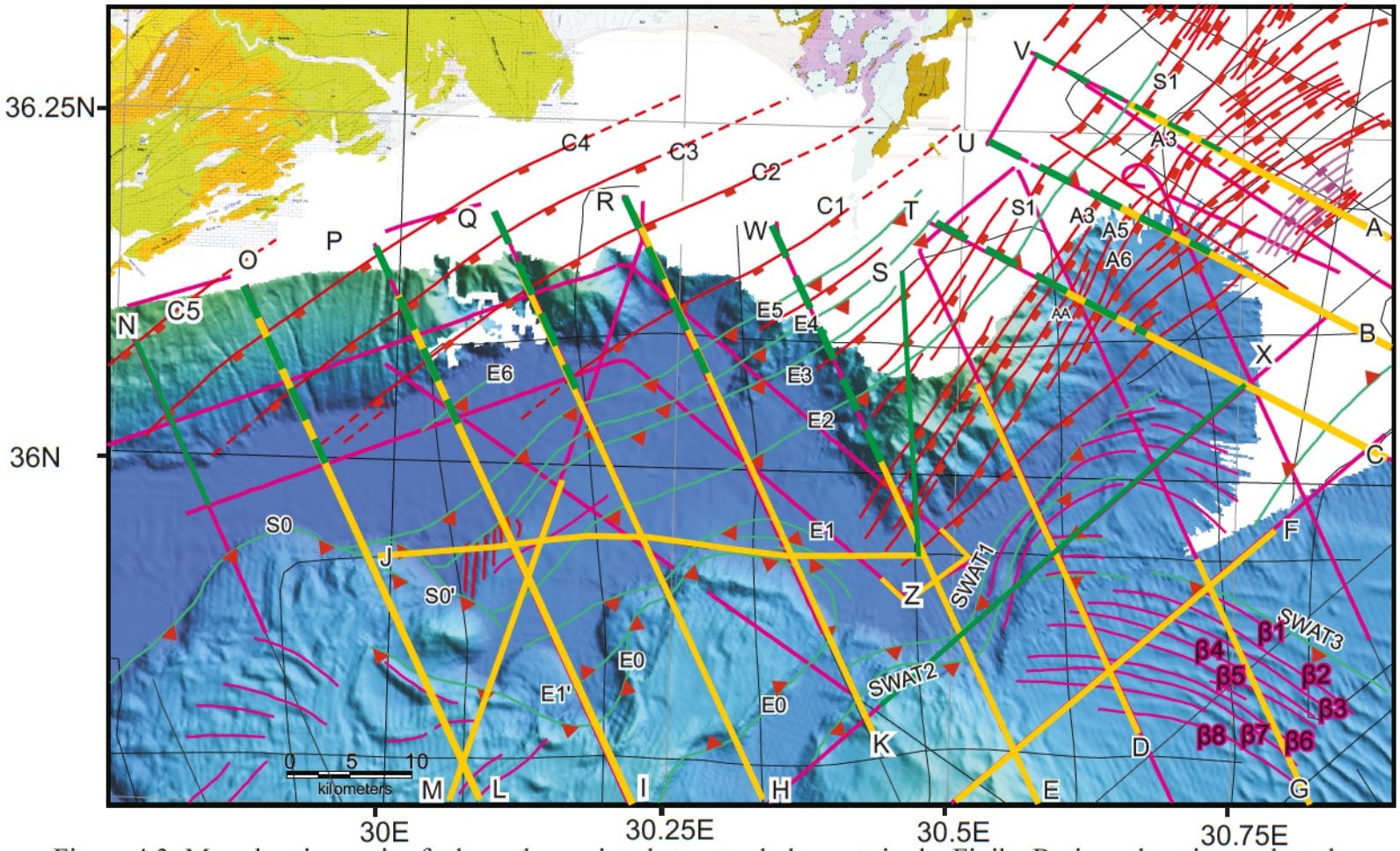

Figure 4.3 Map showing major faults and associated structural elements in the Finike Basin and environs plotted over the multibeam map of the region. Lines with square ticks are normal faults with ticks on the hanging wall block; lines with triangular ticks are thrust faults with ticks on the hanging wall block. The intepreted version of the seismic lines in magenta are not illustrated. The lines in green and yellow are the sections that are used to guide the interpretation and illustrated in this chapter and named alphabeticly. The dashed green line is used when there is an overlay between the sections that are used as two different figures.

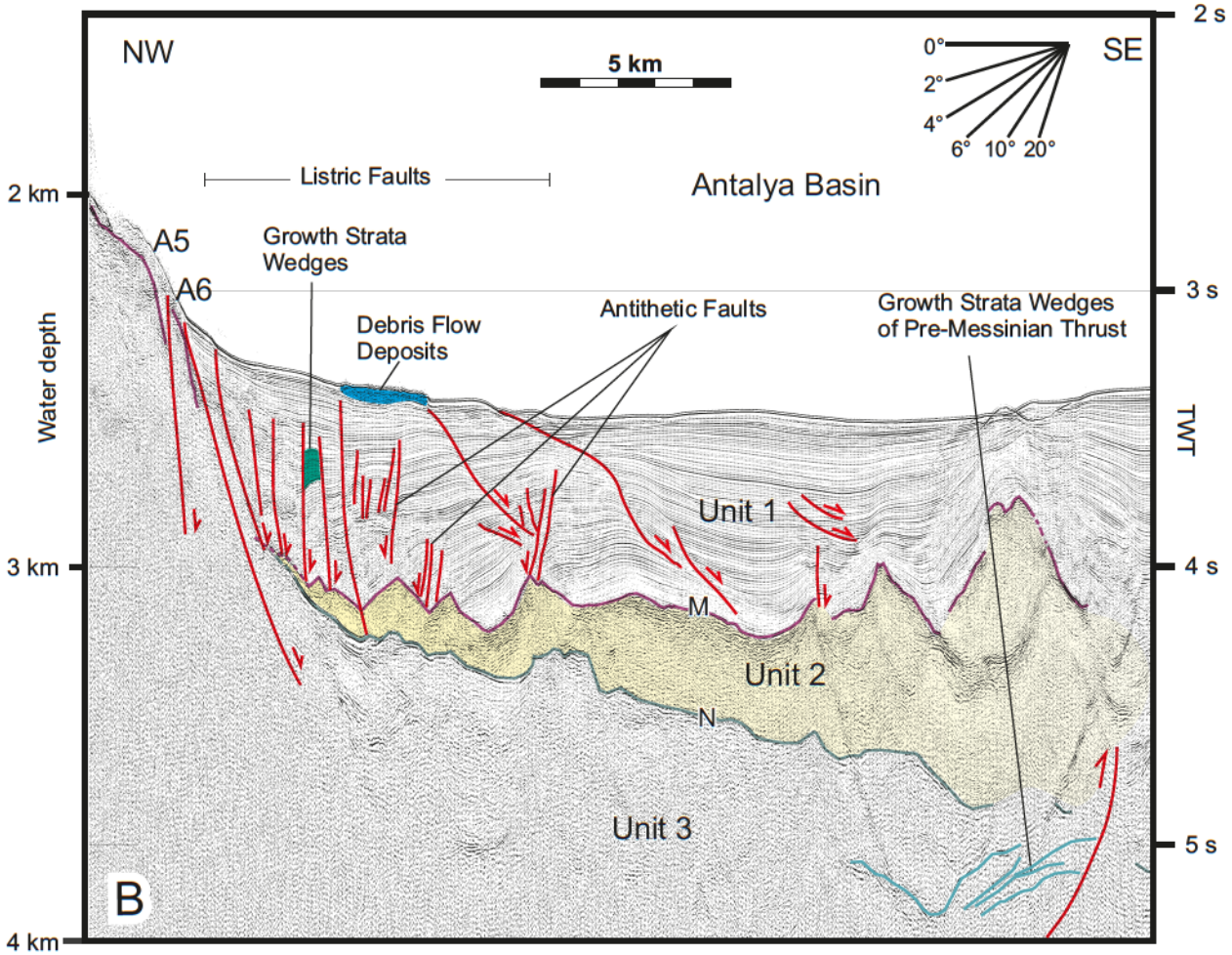

Figure 4.4 Multichannel seismic reflection profile B showing the internal architecture of morpho-tectonic Domain 1. Note that a series of normal faults with listric trajectories characterize the western margin of the Antalya Basin: these faults sole into the evaporite succession of Unit 2. Note the growth strata wedges on the hangingwall of these faults (i.e., in green shading) as well as the growth strata wedges on the backlimb of Pre-Messinian thrust within Unit 3. Also note the large very low-angle detachment faults within the basinal succession of Unit 1. Location is shown in Figure 4.3 (Plate 13, Fixes 370-388).

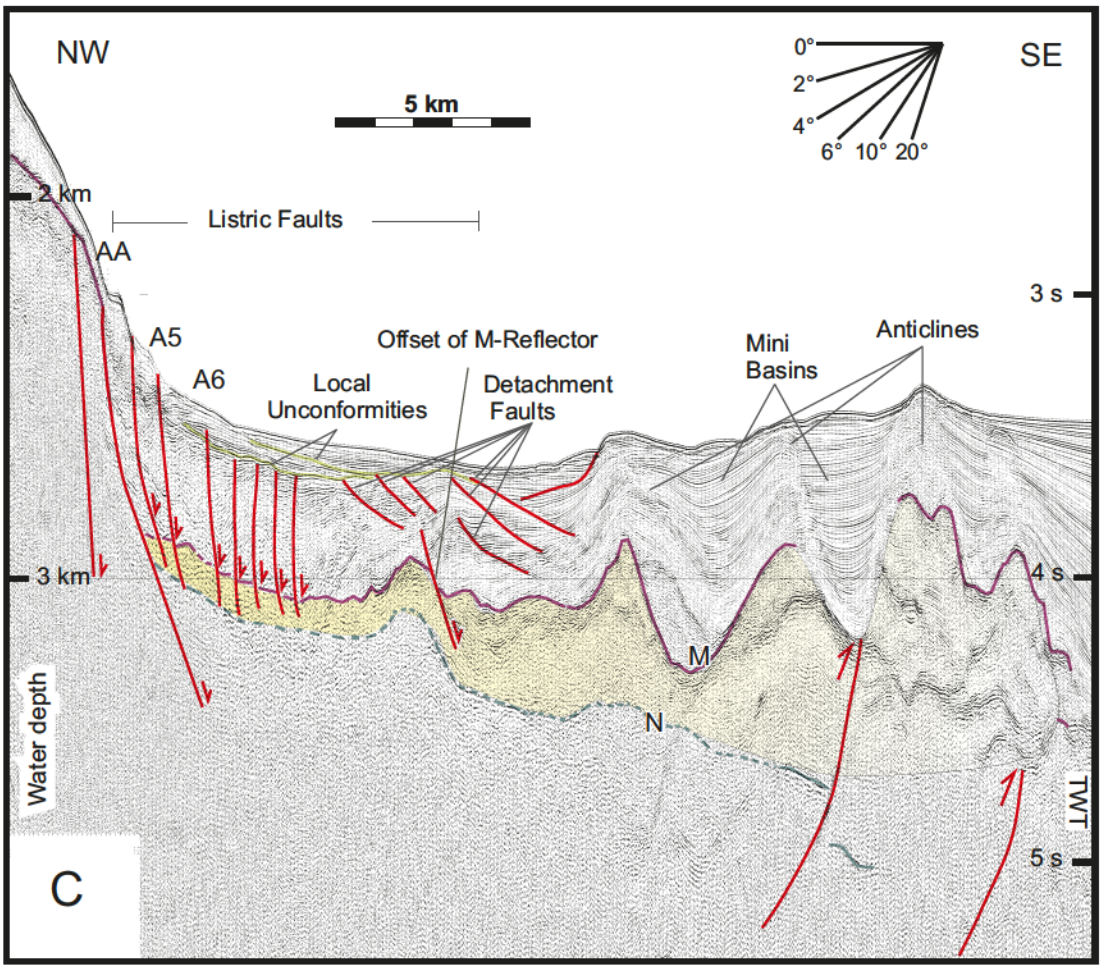

Figure 4.5 Multichannel seismic reflection profile C showing the internal architecture of morpho-tectonic Domain 1. Note that a series of normal faults with listric trajectories characterize the western margin of the Antalya Basin: these faults sole into the evaporite succession of Unit 2 occasionally creating ~ 150ms offset on M-reflector. Also note the large very low-angle detachment faults within the basinal succession of Unit 1. Location is shown in Figure 4.3 (Plate 11, Fixes 417-399).

4.1.1.1 Slope-parallel relatively low angle (20-30 degrees) normal faults

Seismic reflection profiles from morpho-tectonic Domain 1 show that there are several slope-parallel relatively low angle normal faults that are situated along the edge of the continental slope (Figs. 4.2-4.6). The prominent M-reflector and the other reflectors in Units 1 and 3 are cut by these faults (Fig. 4.5). The footwall – hanging wall relationships and cutoffs show that these faults have extensional stratigraphic separations. Interpretation of the dense grid of high-resolution seismic reflection profiles shows that they define a prominent family of northeast-southwest trending, southeast-dipping extensional faults (Fig. 4.3).

The slope-parallel relatively low-angle normal faults imaged along the lower portion of the continental slope have dip angles of ~20-30 degrees (Figs. 4.2, 4.4, 4.5). They are often situated immediately below the lens-like deposits described below; however, some of the slope-parallel relatively low angle normal faults cut the seabed, creating steps on the seafloor (e.g., Fig. 4.6). These faults invariably extend into the pre-Messinian Unit 3. They exhibit 100 ms to ~200-300 ms offsets at the M-reflector (e.g., faults A3 and S1; Fig. 4.6).

4.1.1.2 Listric normal faults

The structural architecture of the base of the continental slope and the western margins of the Antalya Basin is characterized by a fan of listric extensional faults (Figs. 4.2-4.5). These faults occur predominantly within the lower and middle portion of the Pliocene-Quaternary Unit 1 (Figs. 4.4, 4.5). The tip points of these faults are invariably

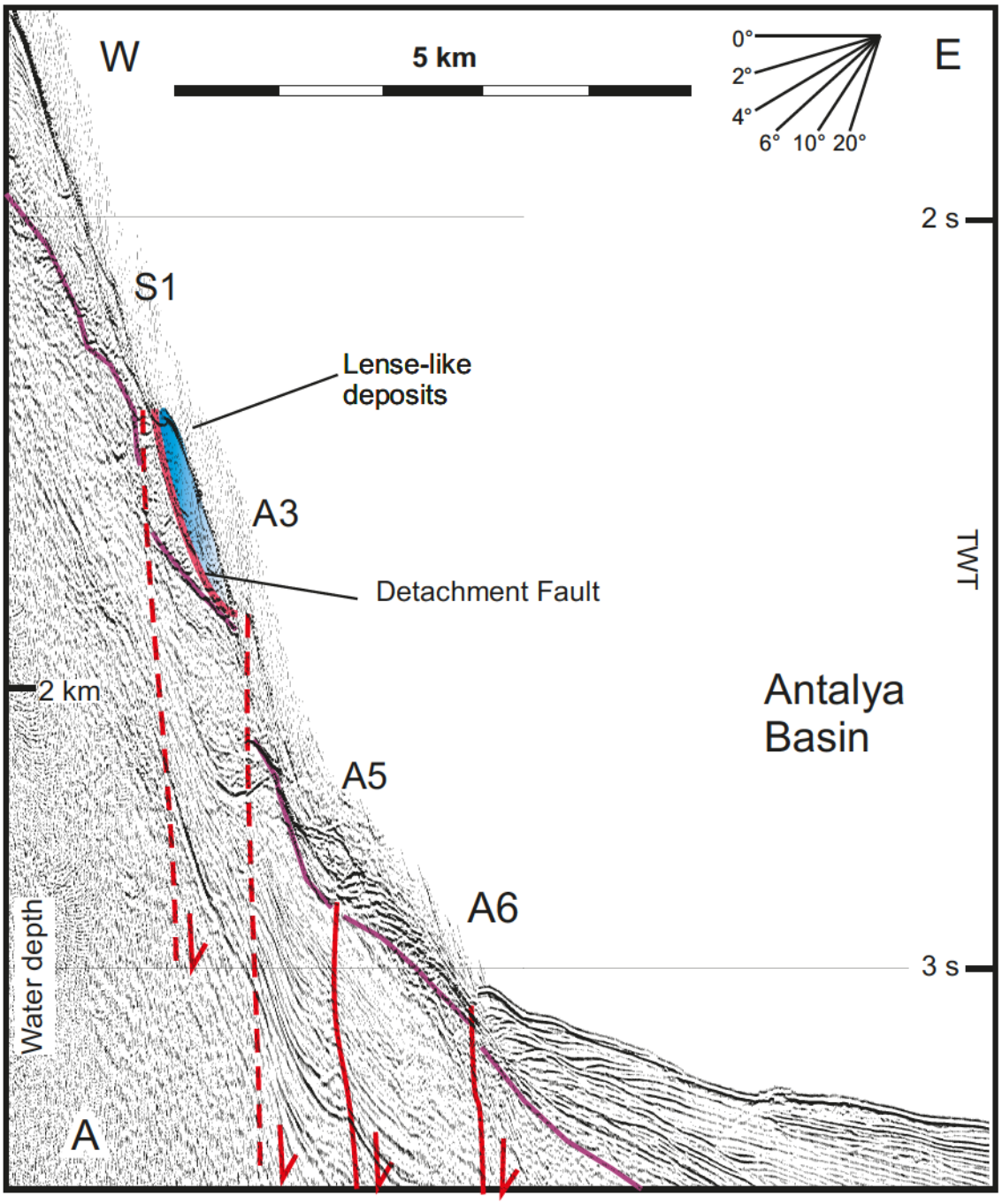

Figure 4.6 A segment of the multichannel seismic reflection profile A showing the internal architecture of thin lens-like deposits resting over the M-reflector along the steep continental slope of the westernmost Antalya Basin. Also note the 100 ms to ~200-300 ms offsets on the M-reflector created by the slope-parallel relatively low angle normal faults (From Figure 5.2).

within the upper portion of Unit 1. The faults show gently curved concave-up trajectories where dips are ~10 degrees near the M-reflector, and increase to ~20 degrees up-section (Figs. 4.4, 4.5). The interpretation of where these faults sole is debatable due to the complications of velocity pull-up of the Messinian succession and low seismic resolution. However, it is observed that all these listric faults generally sole into the Mesinian evaporites of Unit 2. The Pliocene-Quaternary successions of Unit 1 are well-stratified along the western portion of the Antalya Basin with numerous strong reflectors, which are cut by these listric fault fans. The hanging wall blocks of these faults show clear growth strata wedges developed within the lower and middle portion of the Pliocene-Quaternary Unit 1 (Fig. 4.4). These growth strata wedges clearly show that the development of the listric extensional fault fan was synsedimentary. A number of these faults also cut the M-reflector, creating offsets ~ 20-150 ms at this level (Fig. 4.5).

Mapping shows that these listric extensional faults define a prominent northeast-southwest trending fan near the base-of-slope region in western Antalya Basin (Fig. 4.3). The overwhelming majority of these faults display southeast dips, yet a few antithetic faults show northwest dips (Figs. 4.4, 4.5). There is a local unconformity within the upper portion of the Pliocene-Quaternary sediments of Unit 1 (Fig. 4.5). The tip points of the majority of the listric extensional faults are situated beneath this local unconformity, although the unconformity surface itself is clearly affected by faulting as indicated by the corrugation of the reflectors at and above the unconformity.

4.1.1.3 Bedding parallel detachments

The structural framework of the deeper Antalya Basin, away from the continental slope and rise is characterized by very prominent bedding-parallel detachments that occur within the entire Pliocene-Quaternary Unit 1 (Figs. 4.2 4.4, 4.5). When examined in detail, these bedding-parallel detachments compartmentalize Unit 1 into several nearly-equally-separated sections (Fig. 4.2). The base of each compartment is delineated by a reflector, representing the surface of detachment. The reflectors above the detachment appear to abut the detachment, whereas those below the detachment are clearly truncated by the detachment (Fig. 4.2). Yet, except for regions of limited areal extent, the detachment surface is perfectly parallel to the bedding planes, indicated by internally parallel reflectors (Fig. 4.2). Careful examination of these detachment faults and the surrounding sediments appears to show very little growth, if any. The region of the seafloor overlying these detachment faults is sufficiently distant from the continental slope and rise to preclude the development of these detachment surfaces as related to sliding and slumping. The evolution of these structures is further treated in the discussion.

4.1.2 Domain 2 –Transition from Antalya Basin to Anaxagoras Mountain

Domain 2 is situated immediately south of Domain 1 (Fig. 4.1). It is bounded in the west by the easternmost extent of the Finike Basin, and in the southwest by the Anaxagoras Mountain of the Anaximander Seamounts (*sensu lato*). To the east it extends into the deep central Antalya Basin. The Pliocene-Quaternary succession of the domain

is characterized by a corrugated seafloor morphology that developed over a prominent salt-cored fold belt.

4.1.2.1 Salt-cored fold belt

The structural architecture of the northwestern portion of Domain 2 is controlled by two very prominent northeast-southwest trending and southeast verging thrusts (SWAT: Southwestern Antalya Yhrust; SWAT1 and SWAT2; Figs. 4.3, 4.7, 4.8). Both thrusts clearly cut the M-reflector, extending into the Pliocene-Quaternary succession of Unit 1 (Figs. 4.7, 4.8). Thrust SWAT1 occasionally creates ~200 ms offset at the M-reflector (e.g., Fig. 4.7). The tip point of the thrust SWAT2 in the southerly seismic reflection profile (i.e., Fig. 4.8) lies within the lower-middle Pliocene-Quaternary where it creates ~200 ms offset, whereas that in the northerly profile appears to extend all the way to the depositional surface (Fig. 4.7). These thrusts have very shallow dips at depth (~5). The thrust trajectories are probably listric with thrusts cutting the salt unit and soling deep into Unit 3. This thrust system carries the salt-cored fold belt that developed within the Pliocene-Quaternary succession. These faults also carry the Antalya Basin over the Finike Basin. Across the boundary between Domains 2 and 3, the M-reflector rises from ~4.5 s in the Finike Basin to ~3.0 s over the northern hills of the Anaxagoras Mountain (Fig. 4.8). Some of this elevation difference may be depositional and/or erosional; however a large portion is believed to have been provided by the offset of thrusts SWAT1 and SWAT2 (i.e., ~1400- 1200 ms offset at the pre-Messinian level, also discussed later).

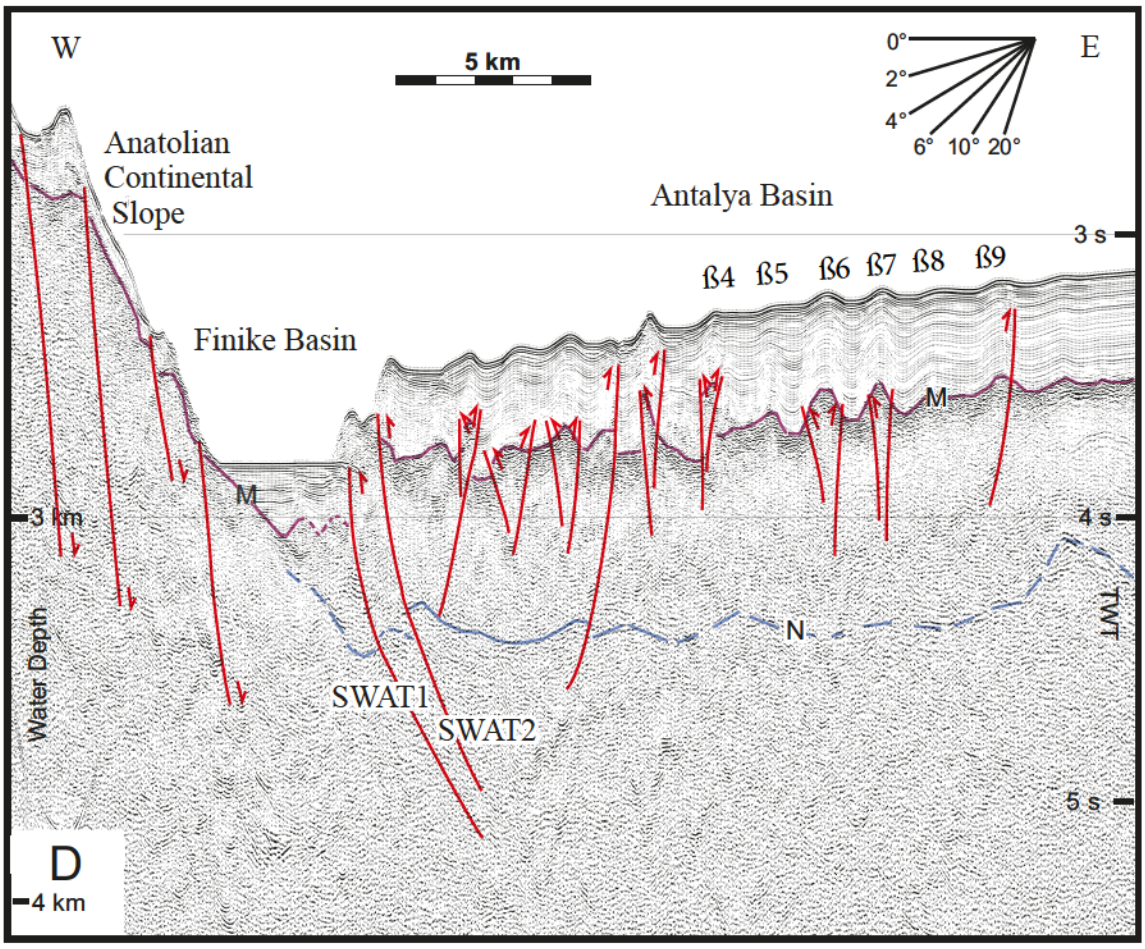

Figure 4.7 Multichannel seismic reflection profile D showing the internal structural framework of the northwestern margin of morpho-tectonic Domain 2. Note the presence of two large thrusts that delineate the boundary between morpho-tectonic Domains 2 and 4. Also note that the structures of the Pliocene-Quaternary succession above the listric thrust trajectory are dominated by numerous upright anticlines (shown with ß symbol) an their intervening synclines, these are mapped rıdges and troughs in Fig. 4.3 (discussed in text). Location is shown in Figure 4.3 (Plate 24, Fixes 203-185).

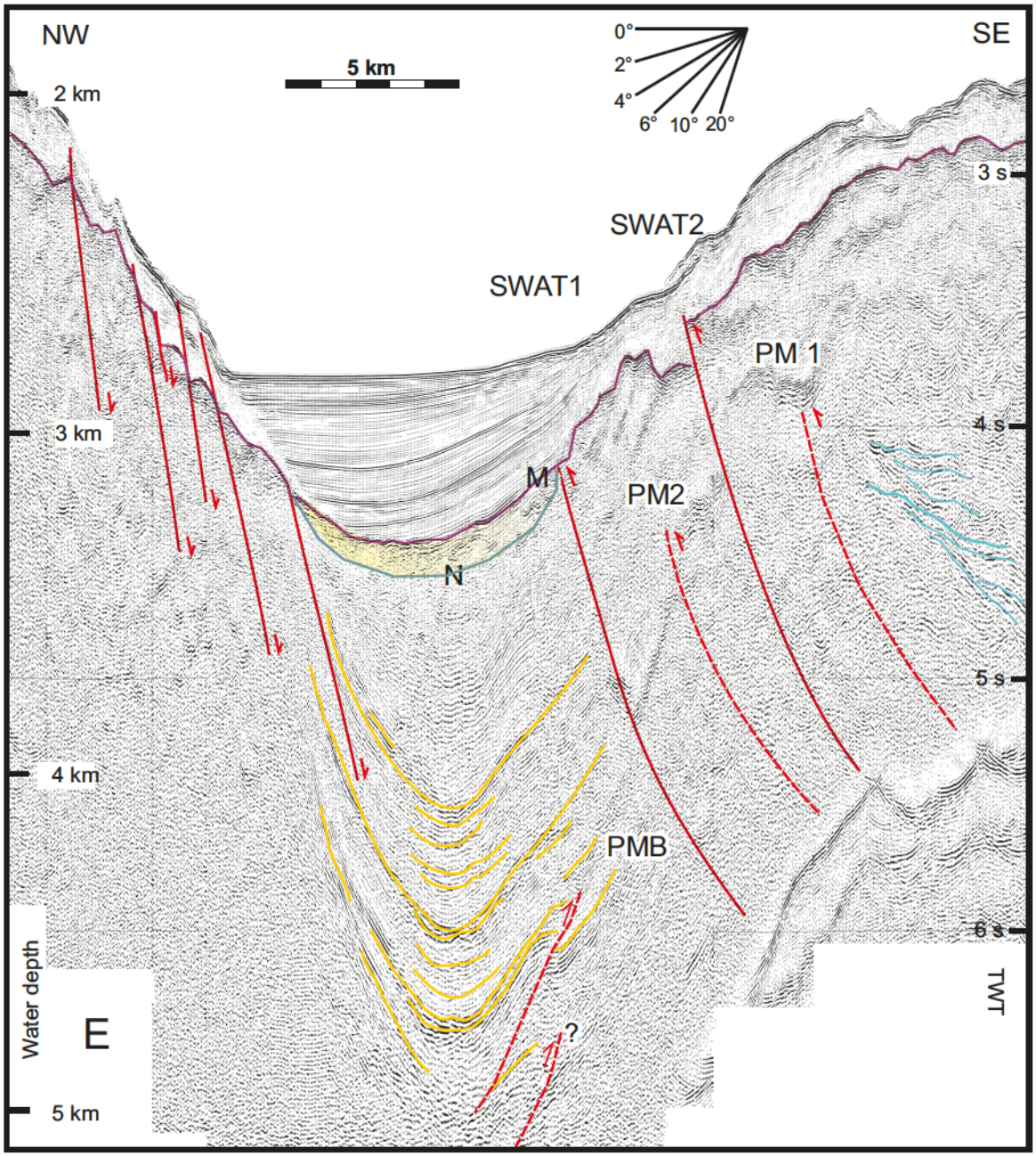

Figure 4.8 Multichannel seismic reflection profile E showing the internal structural framework of the northwestern margin of morpho-tectonic Domain 2. Note the presence of two large thrusts (SWAT1, SWAT2) that delineates the boundary between morpho-tectonic Domains 2 and 4. PM1 and PM2 represents Pre-Messinian Thrust and PMB is Pre-Messinian Back-thrust. Location is shown in Figure 4.3 (Plate 23).

The structural architecture of the southern portion of Domain 2 is characterized by the northwest-southeast trending foothills in front of the Anaxagoras Mountain (Figs. 4.3, 4.9). Here the M-reflector is a prominent marker, which rises from ~5 s in the deep Antalya Basin to ~3 s near the northern foothills of the Anaxagoras Mountain. This progressive southerly rise of the M-reflector is accompanied with concomitent thinning of the Pliocene-Quaternary succession of Unit 1 (Fig. 4.9). The Pliocene-Quaternary succession is very thin (200 ms) across the rugged morphology of the M-reflector over the Anaxagoras Mountain.

The morphology of Domain 2 is delineated by a corrugated seafloor, which defines large north-convex features bounded at the northwest and southeast margins by the eastern fringes of the Finike Basin and the northwest-southeast trending foothills of the Anaxagoras Mountain, respectively (Figs. 4.1, 4.3). Comparison between the multibeam bathymetry map and the seismic reflection profiles shows that this corrugated seafloor morphology is the surface expression of the structural architecture of Pliocene-Quaternary Unit 1 (Fig. 4.1, 4.3, 4.9). The ridges and troughs in the multibeam map nicely correspond with the upright anticlines and their intervening synclines (Figs. 4.3, 4.9, 4.10). These structures form internally-parallel features, hence the corrugation of the seafloor.

Examination of the seismic reflection profiles shows that the upright anticlines are bounded at their margins by prominent faults (e.g., Fig. 4.10). Footwall – hanging wall relationships on the M-reflector clearly shows that most of these faults are thrusts, which

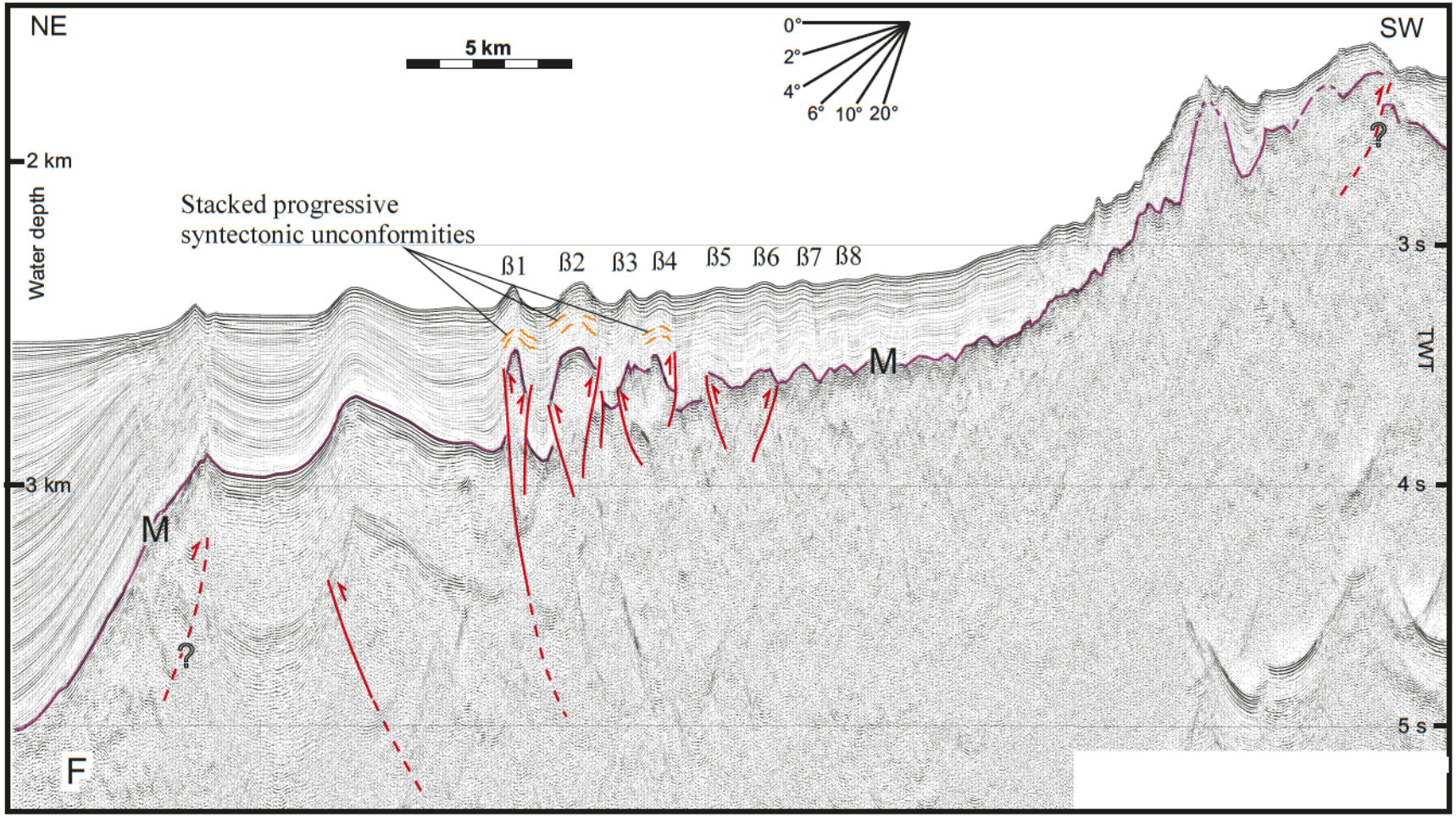

Figure 4.9 Multichannel seismic reflection profile F showing the internal structural framework of the southwestern margin of morpho-tectonic Domain 2. Note that the M-reflector becomes progressively shallower toward the Anaxagoras Mountain, and the accompanying thinning of the Pliocene-Quaternary succession of Unit 1. Also note that the seafloor morphology is corrugated and that there are upright anticlines and synclines (ß1-ßß8) within the Pliocene-Quaternary succession of Unit 1. Location is shown in Figure 4.3 (Plate 4, Fixes 1287-1258).

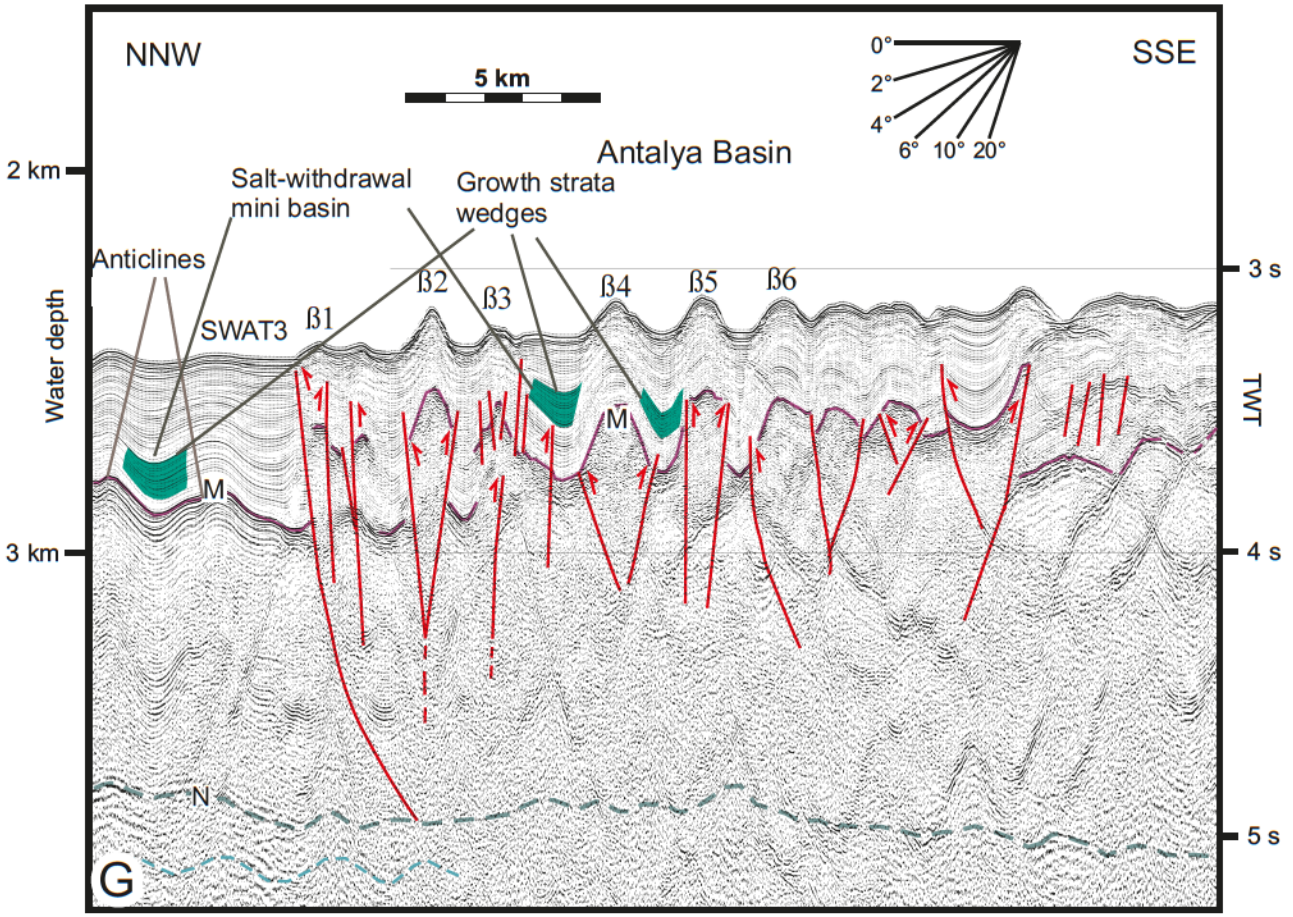

Figure 4.10 Multichannel seismic reflection profile G showing the internal structural framework of the southern and southeastern segment of the morpho-tectonic Domain 2. Note the corrugated seafloor morphology and the upright anticlines (ß1-ß6) and synclines and the growth strata wedges (partially shown in green shading) within the mini basins that chracterize the structural architecture of the Pliocene-Quaternary succession of Unit 1. Note the simple anticlines on the NNW portion of the section that are not cut by faults. Location is shown in Figure 4.3 (Plate 26, Fixes 240-258).

create displacements of 100-400 ms on the M-reflector. The thrusts that define the margins of a given broadly northwest-southeast trending upright anticline have northwest vergence on the western margin of the structure and southeast vergence on the structures eastern margin. Thus, the upright anticlines are bounded by two oppositely verging thrusts, creating positive flower structures (Fig. 4.10). The thrusts clearly extend into the upper portion of the Pliocene-Quaternary succession (e.g., the thrusts beneath ß2 Fig. 4.10). Here they create significant rises and falls on the seafloor, corresponding with the crests of the upright anticlines and the troughs of the intervening synclines, respectively.

In the seismic reflection profiles the salt-cored fold belt shows seafloor elevations ranging between ~50 and ~200 ms relative to the adjacent troughs (Figs. 4.7, 4.10). Nine individual fold structures are mapped from this belt and named as ß1-ß9 (Figs. 4.7, 4.9, 4.10). Most of the folds are symmetrical structures (e.g., ß6 in Fig. 4.10), but a few asymmetrical structures are also observed (e.g., ß1, Fig. 4.10). It is further noted that some of the structures are symmetrical in one place, but become clearly asymmetrical along strike (compare ß4 in Figs. 4.7, 4.10). The northern margin of this ~30 km wide fold belt is marked by a major thrust fault, SWAT3 (Fig. 4.10). The thrust has a broadly westnorthwest-eastsoutheast strike and southsouthwest dip, which parallels the general strike of the fold belt (Fig. 4.3).

The internal makeup of the Pliocene-Quaternary succession within the folds displays acoustically-transparent zones with little coherent reflectivity in the flanks of the folds (Figs. 4.7, 4.9). This seismic signature is very typical in many similar fold

structures mapped in various eastern Mediterranean basins, such as the Antalya Basin (e.g., İşler et al., 2005), Cilicia Basin (Bridge et al., 2005, Aksu et al., 2005) and the Latakia Basin (Hall et al., 2005). Similar structures are also observed and mapped over the Florence Rise (e.g., Zitter et al., 2003, ten Veen et al. 2004). In all these regions, the weakness of coherent reflections along the flanks of the folds, the characteristic tear-drop shape of these structures, the association of these structures with growth strata wedges on the margins of the folds and the presence of notable progressive syntectonic unconformities over the crestal regions of these folds collectively suggest that these structures are formed as the result of mobilization and migration of the Messinian evaporite succession of Unit 2.

Not all fold structures are cut by thrusts: some of these upright anticlines are simple symmetrical or asymmetrical folds (Fig. 4.10). In such structures the M-reflector shows undulating morphology with wavelengths of ~500 m and amplitudes of ~200 m. The Pliocene-Quaternary succession of Unit 1 immediately above the M-reflector is also undulated with similar wavelengths but progressively decreasing amplitudes toward the seafloor. Only some of these folds have seafloor inflections (e.g., Fig. 4.10). The troughs between the folds show clear development of growth strata wedges within the lower and middle portions of the Pliocene-Quaternary. These growth strata wedges result from the withdrawal of salt followed by synkinematic sinking of the mini basin and infilling by additional sediments: they are thus interpreted as salt-withdrawal mini basins.

Although these structures are cored with Messinian evaporites of Unit 2, they are not diapirs because in most places the supra salt-strata (i.e., the Pliocene-Quaternary of Unit 1) overlying the M-reflector are not intruded by the evaporites (e.g., ß6-9 in Fig. 4.7 in ß5-8 Fig.4.9). However, there are several structures which may be diapirs, such as ß1, ß2 (Fig. 4.9), ß2, ß5 (Fig. 4.10). In these structures, if the apparent termination of Unit 1 strata against the lower portion of the upright anticline is caused by the intrusion of the evaporite succession, then the structure can be called a diapir. However, if the apparent termination of Unit 1 strata against the lower portion of the upright anticline is simply caused by thinning of the Unit 1 strata, the structure is not a diapir. The temporal resolving power of the seismic method is very limited in evaporite deposits in general, the Mediterranean examples are not an exception.

The timing of the fault activity can be determined using the growth strata wedges within the salt withdrawal synclines. Examination of the seismic reflection data shows that most of the fault activity took place during the early Pliocene-Quaternary (e.g., Figs. 4.9, 4.10). However, the overall growth strata development observed in many synclines, extending all the way to the uppermost Pliocene-Quaternary suggested that fault activity continued across the Pliocene-Quaternary. This interpretation is further corroborated by the stacked progressive syntectonic unconformities that developed along the flanks of the fold structures adjacent to the growth strata wedges in the Pliocene-Quaternary succession (Figs. 4.9). The fact that the correlative conformities of these progressive syntectonic unconformities can be readily correlated into the lower-upper Pliocene-

Quaternary succession further testifies that growth of the folds must have been occurring during the entire Pliocene-Quaternary.

The roots of the oppositely-verging thrusts extend deep into the Messinian evaporite Unit 2, and possibly below (Figs. 4.7, 4.9, 4.10). The oppositely-dipping thrust trajectories appear to merge at depth and continue as a single stem further into the section. It is believed that these faults further merge at depth on the large listric thrusts of SWAT1, SWAT 2 and SWAT3 (e.g., Figs. 4.7, 4.10), translating the stress to these major thrusts (further elaborated in the Chapter 5).

4.1.3 Domain 3 –Finike Basin

Domain 3 is situated south of the Turkish continental margin (i.e., Domain 5) and north of the Sırrı Erinç Plateau (i.e., Domain 4; Fig. 4.1). It is bounded in the east by Domains 1 and 2, and merges with the northern slopes of the Anaximander Mountain (*sensu stricto*) in the southeast. It includes the ENE-trending deep trough known as the Finike Basin and the fringes of the Turkish continental slope in the north, and the Sırrı Erinç Plateau and the Anaxagoras Mountain in the south (Fig 4.1). To the southwest, the domain extends into the narrow and deep trough referred to as the Anaximander Basin (Aksu et al., 2009). The Pliocene-Quaternary succession in Domain 3 is characterized by a series of thrusts faults that are largely imaged within the Pliocene-Quaternary succession of Unit 1 (e.g., Figs. 4.3, 4.11-4.14).

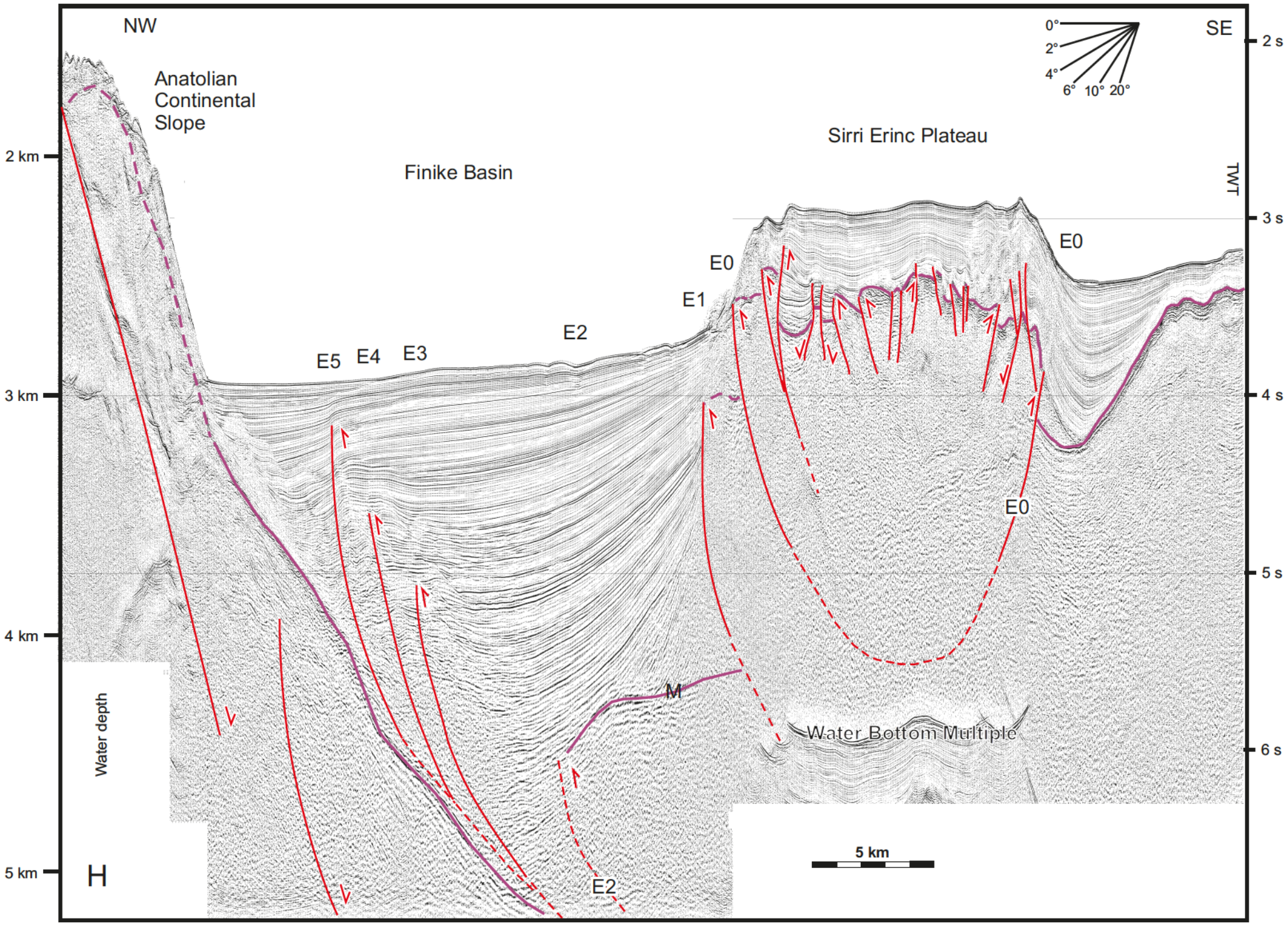

Figure 4.11 Multichannel seismic reflection profile H showing the internal structural framework of morpho-tectonic Domain 3. Note that in the northern portion of the domain, the structural elements of the Turkish continental margin delineated by the M-reflector in purple dip with 10-20 angles deep into the Finike Basin. Further note the major offsets of the M-reflector by two oppositely verging thrusts that define a very prominent pup-up structure along the northern portion of the Sırrı Erinç Plateau. Within the Finike Basin there are several northwest-verging thrusts that cut the Pliocene-Quaternary successions of Unit 1.E0 through E5 are thrusts described in text. Location is shown in Figure 4.3 (Plate 21a, Fixes 977-1007.5).

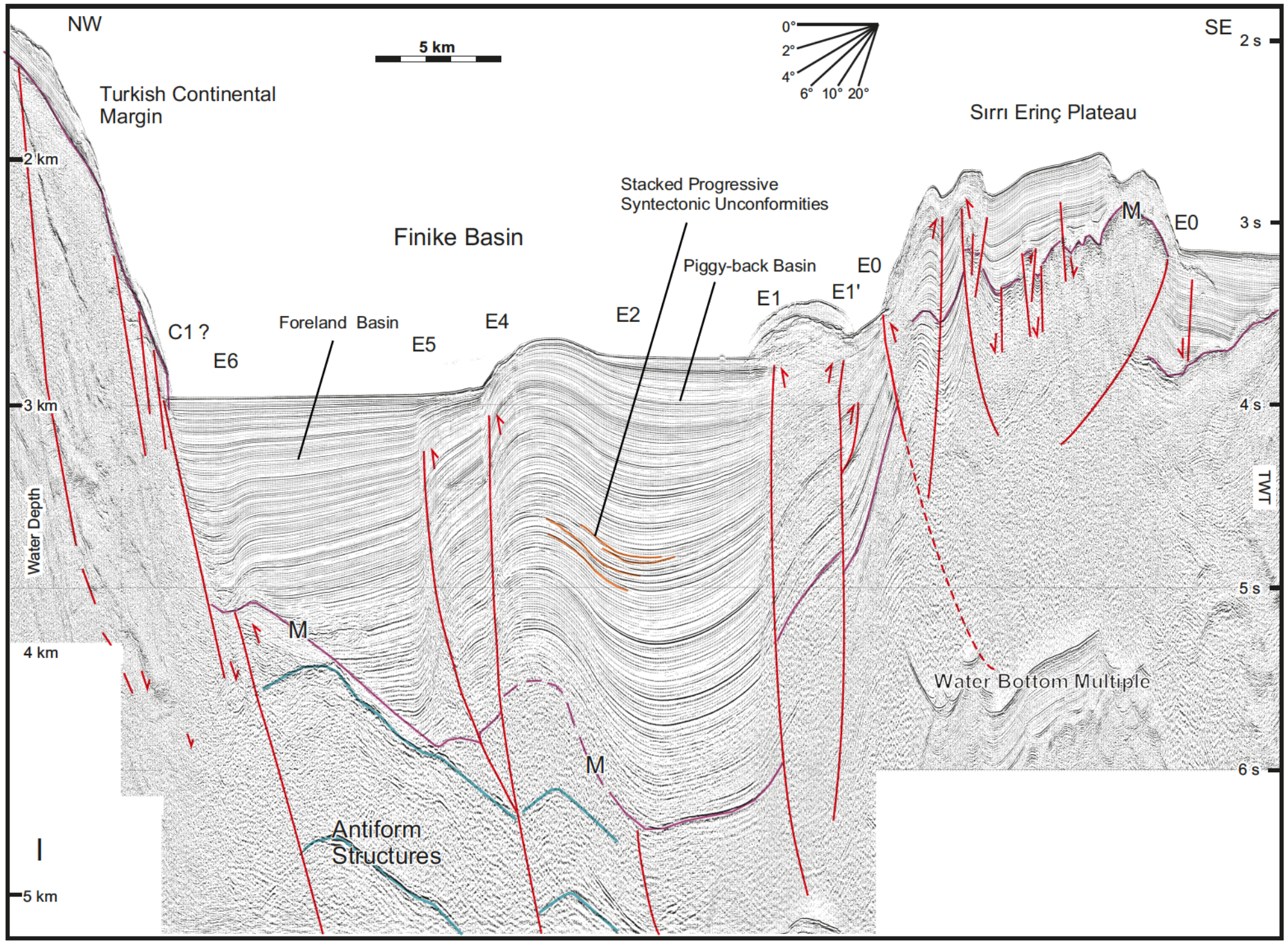

Figure 4.12 Multichannel seismic reflection profile I showing the internal structural framework of Domain 3. Note that two major thrusts are prominently imaged within the central Finike Basin. Also note that both the southern and northern margins of the Finike Basin are marked by steep discontinuities, explained in text. E0 through E2, E4 through E6 and the antiform structures are thrusts described in text. Location is shown in Figure 4.3 (Plates 19a, Fixes 960-930).

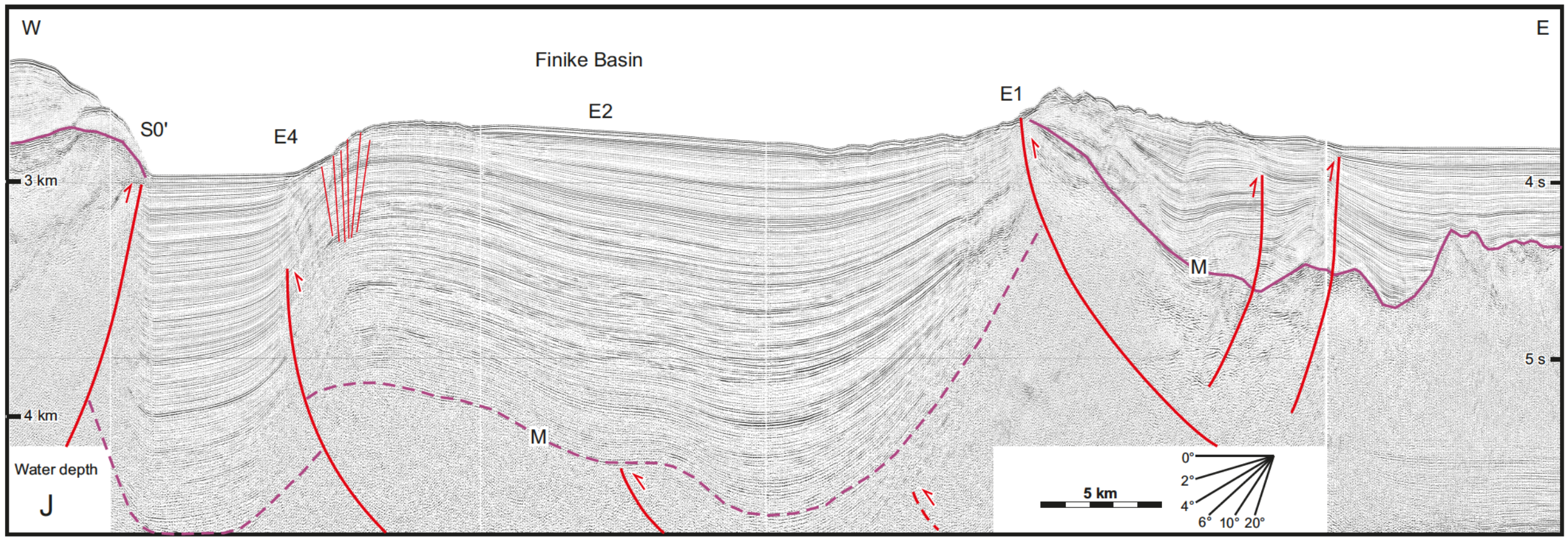

Figure 4.13 Broadly east-west trending multichannel seismic reflection profile J showing the internal architecture of the southern portion of the Finike Basin, immediately north of the S ır Erinç Plateau. Note the major offsets of the M-reflector by the oppositely verging thrusts. E1, E2, E4 and SO' are thrusts described in text. Location is shown in Figure 4.3 (Vintage data).

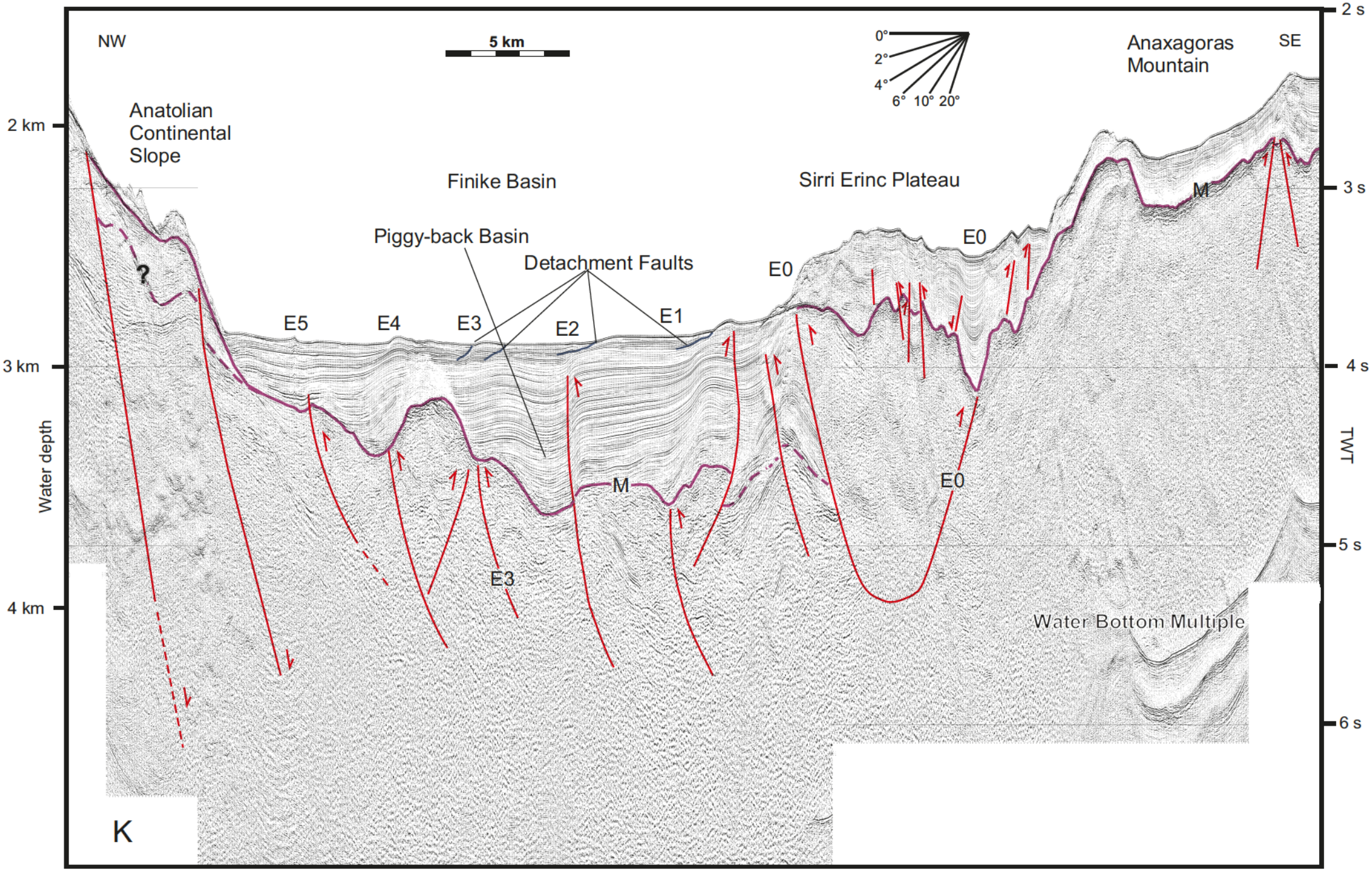

Figure 4.14 Northwest-southeast trending multichannel seismic reflection profile K showing the internal structural framework of the eastern portion of Domain 3. Note that the northern region of the Finike Basin contains notably thinner Pliocene-Quaternary sediments, and that the M-reflector is much shallower in the seismic profile. E0 through E5 are thrusts described in text. Location is shown in Figure 4.3 (Plate 22, Fixes 349-314).

4.1.3.1 Pliocene-Quaternary thrust faults

The structural architecture of Domain 3 is controlled by at least six large northeast-southwest trending and northwest verging thrusts, labeled as E1 through E6 (Figs. 4.3, 4.11-4.14). Detailed examination of the seismic reflection data shows that all these thrusts clearly cut the M-reflector, extending into the Pliocene-Quaternary succession of Unit 1 (e.g., Figs. 4.11-4.12). The tip points of these thrusts occur predominantly within the middle to upper portion of the Pliocene-Quaternary succession. However, in some cases, the tip points of the thrusts are found beneath the M-reflector (i.e., E2 in Figs. 4.12-4.13; E1, E3, E4 in Fig. 4.14). All thrusts in this domain have shallower dips at depth (~10) and concave-up trajectories where the dip amounts increase significantly up section to ~20 (Figs. 4.11-4.14). Thus, the thrust trajectories are invariably listric and the thrusts sole deep into Unit 3 within the Finike Basin, extending beyond the penetration of the seismic profiles (Figs. 4.11-4.14).

Mapping of thrusts E0 through E6 reveal that there are three distinctly separate families of thrusts within Domain 3. Family 1 is solely associated with the southeastern Finike Basin and northeastern margin of the Sırrı Erinç Plateau, and includes thrusts E0 and E1 (Fig. 4.3). Family 2 is associated with the southwestern Finike Basin and the northwestern margin of the Sırrı Erinç Plateau, and includes S0 and S0' (Fig. 4.3). Family 3 is entirely confined to the Finike Basin and the southern portion of the Turkish continental margin, and includes thrusts E2 through E6 (Fig. 4.3).

Family 1 – curvi-linear thrusts in southeastern Finike Basin

There are two large thrusts that exhibit significant vertical stratigraphic separations on the M-reflector: these are thrusts E0 and E1 (Fig. 4.3). These thrusts clearly extend into the pre-Messinian Miocene and older Unit 3. Mapping showed that these two thrusts form a structural as well as a morphological boundary along the southern portion of the Finike Basin and the northwest promontory of the Sırrı Erinç Plateau (Fig 4.3). Thrust E0 invariably cuts the M-reflector and extends to or near the seafloor (Figs. 4.11, 4.12, 4.14). The tip point of thrust E1 lies beneath the M-reflector and rests under an approximately 800 ms thick Pliocene-Quaternary succession on profile K (Fig. 4.12). Toward the southwest, thrust E1 progressively cuts further upward into Unit 1 (sequentially compare Figs. 4.14, 4.11 and 4.12), so that the tip point of the thrust is at the seafloor where it creates a distinct step (Fig. 4.12). Here it creates a positive flower structure with a minor, but oppositely verging E1' thrust (Fig. 4.12). Examination of the hanging wall-footwall relationships of the prominent markers cut by thrust E1 suggests that there is up to 1200 ms offset at the M-reflector, decreasing up section to up to 350 ms offset at the seabed. These offsets clearly increase from northeast to southwest (Figs.4.3, 4.11, 4.12, 4.14).

Family 2 – curvi-linear thrusts in southwestern Finike Basin

The second family of thrusts is called thrusts S0 and S0' and they carry the northwestern portion of the Sırrı Erinç Plateau over the Finike Basin by creating significant offsets on the M-reflector (Fig. 4.3). This architecture of Family 2 is very

similar to that observed in Family 1. The roots of these thrusts lie beneath the M-reflector in pre-Messinian Miocene and older succession of Unit 3 (Figs. 4.13, 4.15). Mapping showed that thrusts S0 and S0' resemble thrusts E0 and E1 in their geometry and their structural and morphological architecture. It is believed that these four thrusts are genetically related as major structures that define the boundary between the northwestern portion of the Sırrı Erinç Plateau and southwestern Finike Basin (Fig 4.3). The tip points of these thrusts occur within the upper portion of the Pliocene-Quaternary succession at the morphological boundary between the Finike Basin and the Sırrı Erinç Plateau. They have concave-up trajectories with shallower dips at depth (~10) and dip amounts increase up section to 20 (Figs. 4.13, 4.15) indicating the listric trajectories of the thrusts, and their soling into Unit 3 (Figs. 4.13, 4.15). Thrusts S0 and S0' similarly cut the M-reflector and they tip at or near the seafloor (Figs. 4.13, 4.15). The hanging wall-footwall relationships of the prominent markers cut by the thrusts suggest they create up to 1500 ms offset at the M-reflector (Fig. 4.15).

Family 3 – northeast-southwest trending thrusts

Several northeast-southwest trending and southeast-verging thrusts are mapped within the central Finike Basin: they are labeled as E2 through E6 (Fig. 4.3). These thrusts form internally parallel map traces that extend from the southernmost portion of the Finike Basin toward the northeast where they continue as a distinct family into the shallower Turkish continental margin (Fig. 4.3). In their southwestern segments, these thrusts abut the broadly east-west trending curvi-linear thrusts SO and SO'.

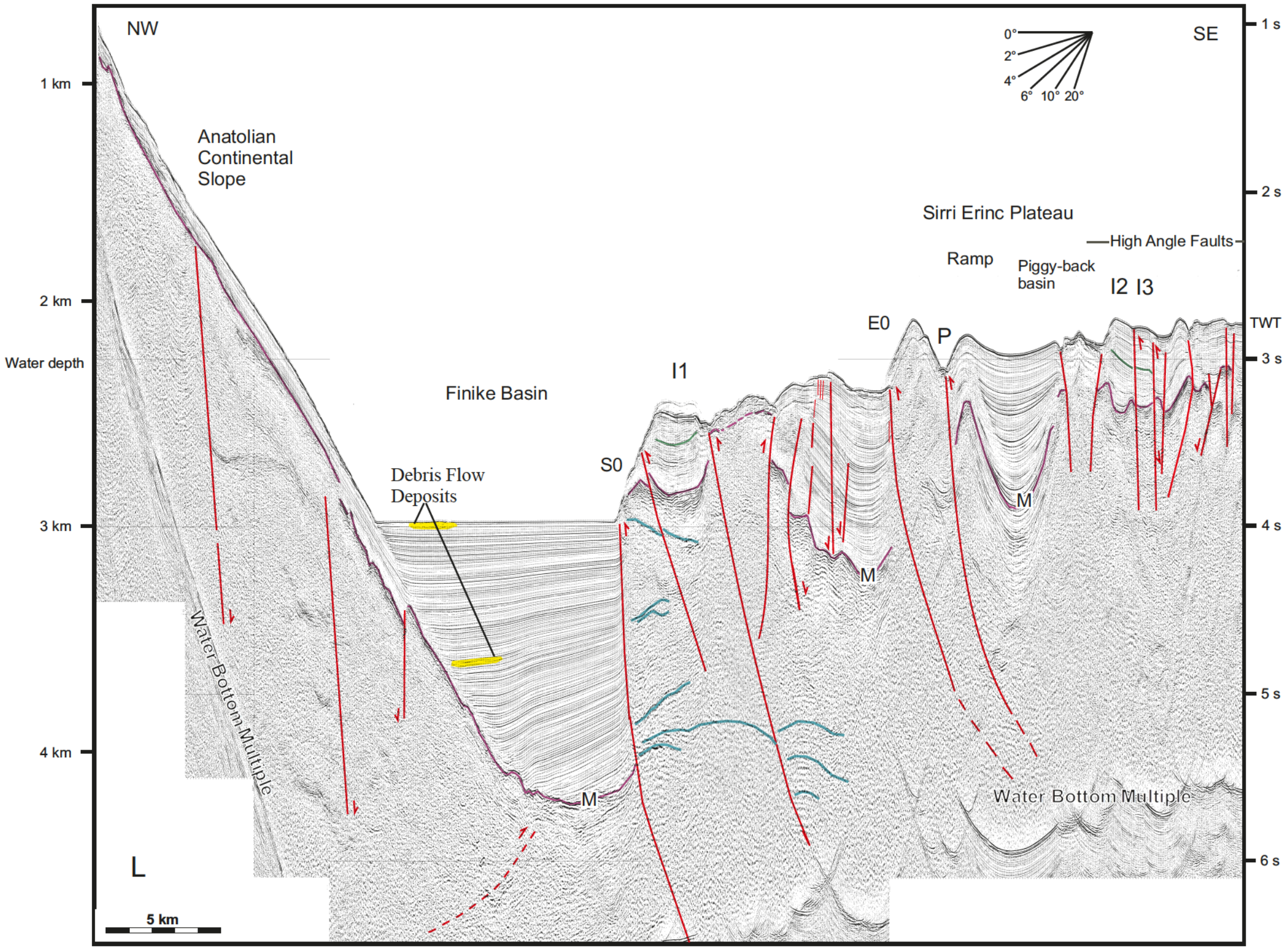

Figure 4.15 Multichannel seismic reflection profile L showing the internal structural framework of the northwestern margin of morpho-tectonic Domain 2. Note the major offsets of the M-reflector by the oppositely verging thrusts. Also note that the core of the upright anticlines (i.e., folds) are composed of acoustically-transparent zones. Location is shown in Figure 4.3 (Plate 18, Fixes 1116-1151).

Thrust E2 defines the trailing portion of the northeast-southwest trending thrust family. It generally shows tip points deep within the Pliocene-Quaternary, except in the eastern portion of the Finike Basin where it cuts through much of Unit 1 (Figs. 4.3, 4.14). Here, thrust E2 lies within the upper-middle Pliocene-Quaternary where it creates ~100 ms offset. A profile within the deep Finike Basin shows that E2 creates its largest offset of ~1200 ms at the M-reflector in the middle of the basin (Figs. 4.4, 4.11) where the Pliocene-Quaternary succession reaches its maximum depth ~6000 ms (Fig. 4.11). An adjacent profile show that the tip point of thrust E2 appears to lie beneath the M-reflector (Fig. 4.12). Here, thrust E2 does not cut the Pliocene-Quaternary, but the presence of growth strata wedges in the lower portion of Unit 1 on the backlimb of the thrust culmination, as well as the inflection and folding created on the M-reflector suggest the presence of thrust E2 and its activity during the early Pliocene-Quaternary (Figs. 4.11-4.14).

In the deep Finike Basin, approximately 5 km northwest of thrust E2, a set of three similarly trending thrusts are mapped: E3, E4 and E5. These thrusts show internally parallel map traces, and verge toward the northwest. The tip points of these thrusts lie within the middle to upper Pliocene-Quaternary succession (except Fig. 4.14). The thrusts create 50-200 ms offsets on strong marker reflectors within the Unit 1 (Figs. 4.12, 4.14) and cause a significant rise on the seafloor (e.g. thrust E4 in Figs. 4.12, 4.13). Traced toward the northeast, these thrusts progressively lose their expression and become buried below the M-reflector (sequentially compare Figs. 4.12, 4.11, 4.14). The hanging

wall blocks of these thrusts show clear growth strata wedges developed within the Pliocene-Quaternary Unit 1 (Fig. 4.12, 4.14). Careful examination of these thrusts, particularly in the deep Finike Basin shows that the thrust trajectories are listric and that the trajectories converge at depth to possibly form a single stem (e.g., Figs. 4.11, 4.12). Thus, thrusts E3, E4 and E5 may be splays of a single large thrust that sits within the central Finike Basin, where thrusts E5 and possibly E6 forming the leading portion of the thrust family. Traced progressively toward the northwest, thrusts E3, E4 and E5 extend from the northwestern fringe of the Sırrı Erinç Plateau across the Finike Basin onto the southeastern slopes of the Turkish continental margin (Fig. 4.3).

Thrust E4 is particularly significant because of its geometry (e.g., Figs. 4.12, 4.14). Seismic profiles shows that this thrust created an approximately 5 km wide ramp in its hanging wall. The offlap reflection terminations of strata on the piggy-back basin toward the ramp as well as a series of stacked progressive syntectonic unconformities on the backlimb of the thrust culmination collectively suggest that the thrust activity continued during the Pliocene-Quaternary. Comparison of strong marker reflectors in the piggy-back basin and the foreland basin (Fig. 4.12) shows that the sediments are consistently thicker in the foreland basin as opposed to the piggy-back basin, suggesting a higher sediment supply from the Turkish continental margin. Thus, comparison of the depth of the seabed between foreland and piggy-back basin of E4 shows that the basin is ~200 ms shallower on the backland indicating an approximate uplift of 200 ms on the seafloor.

4.1.4 Domain 4 – Northern fringes of Sırrı Erinç Plateau

Domain 4 is situated on the south-southwest portion of the study area. It includes the northern fringes of the Sırrı Erinç Plateau (Fig. 4.1). It is bounded by the southern margin of Domain 3 (i.e., the Finike Basin) in the north and the western portion of Domain 2 (i.e., the transition from the Antalya Basin to the Anaxagoras Mountain). The Pliocene-Quaternary succession of the northern margin of Domain 4 is characterized by a major thrust fault zone, fully described in section 4.1.3 (i.e., Families 1 and 3). The structural architecture of the core of Domain 4 is defined by numerous normal faults (e.g., Figs. 4.3, 4.11-4.15). For the purpose of description, the northern margin of the domain is divided into two promontories: Promontory 1 on the east and Promontory 2 on the west (Fig. 4.1).

4.1.4.1 Promontory 1

Promontory 1 is located on the eastern portion of the domain (Fig. 4.1). It has a narrow neck on its southern part and extends toward the northeast broadening gently (Fig. 5.1). The northern fringes of the promontory are bounded by a set of thrust faults that are discussed as Family 1 (i.e., E0-E1 in Figs. 4.3, 4.11-4.14). Seismic reflection profiles show that the M-reflector rises from the deep Finike Basin southward onto the Sırrı Erinç Plateau, and that the large vertical stratigraphic separation on the M-reflector is also accompanied by a notable reverse-sense stratigraphic separation (fully discussed above). This architecture shows that the uplift of the eastern promontory of the Sırrı Erinç Plateau occured as the result of thrusting associated with thrusts E0 and E1. These two thrusts

created on average ~1200-2500 ms offset at the M-reflector between Finike Basin and Sırrı Erinç Plateau (Figs. 4.11, 4.12, 4.14).

4.1.4.2 Promontory 2

Promontory 2 is located in the western portion of Domain 4 (Fig. 4.1). It is a wide zone that occupies the northwestern portion of the Sırrı Erinç Plateau (Fig. 4.1), and is bounded by two prominent thrust faults (i.e., S0 and S0', described in Family 2 above; Figs. 4.3, 4.13, 4.15, 4.16). Careful examination of the multibeam bathymetry map shows that these thrusts draw a convex to north arc extending both southwest and southeast from the apex of the promontory. This arc delineates the boundary between the Sırrı Erinç Plateau and Finike Basin (Fig. 4.3).

Seismic reflection profiles show that the M-reflector rises from the Finike Basin toward the south onto the Sırrı Erinç Plateau, similar to that described above for E0 and E1. This rise is also associated with significant reverse-sense stratigraphic separation clearly visible on the M-reflector. This architecture shows that the uplift of the western promontory of the Sırrı Erinç Plateau occured as a result of thrusting, associated with thrusts S0 and S0'. These two thrusts created ~1200-1500 ms offset at the M-reflector between Finike Basin and Sırrı Erinç Plateau (Figs. 4.13 4.15, 4.16). Therefore, similar to thrusts E0 and E1 which control the uplift of the eastern portion of the Sırrı Erinç Plateau, thrusts S0 and S0' control the uplift of the western portion of the Sırrı Erinç Plateau. The northern boundary of the Sırrı Erinç Plateau is sinuous. This suggests that the dip of the bounding thrusts E0, E1, S0, and S0 is modest.

4.1.4.3 Sırrı Erinç Plateau south of the promontories

The seafloor morphology reveals the existence of a number of E-W and N-S trending lineations at the seafloor. These lineations are the surface expressions of subsurface structures associated with relatively high-angle faults that define the framework of the Pliocene-Quaternary succession (Figs. 4.11-4.15). The tip points of these faults generally lie within the Pliocene-Quaternary succession of Unit 1. The faults clearly cut the M-reflector and create variable offsets, ranging from 50 to 200 ms at this level (Figs. 4.14, 4.11, 4.12). The faults further extend into the pre-Messinian, Unit 3. Examination of the Pliocene-Quaternary marker reflectors as well as the M-reflector shows that there are several faults that display contractional stratigraphic separations as well as the ones that display extensional stratigraphic separations (Figs. 4.14, 4.11, 4.12, 4.15, 4.17). Comparison between the seismic reflection profiles and the multibeam bathymetry map shows that the corrugations on the seabed are the surface expression of the horst-graben structures in the subsurface.

The seabed morphology reveals that seafloor lineations predominantly occur in the western portion of the Sırrı Erinç Plateau (Fig. 4.3). Seismic reflection profiles from Promontory 2 display several large thrust faults and numerous relatively high-angle faults similar to those described above (Fig. 4.15). These large thrust faults invariably cut the M-reflector and create offsets between 200-400 ms at this level, and sole in to the pre-Messinian, Unit 3 (Figs. 4.13, 4.15).

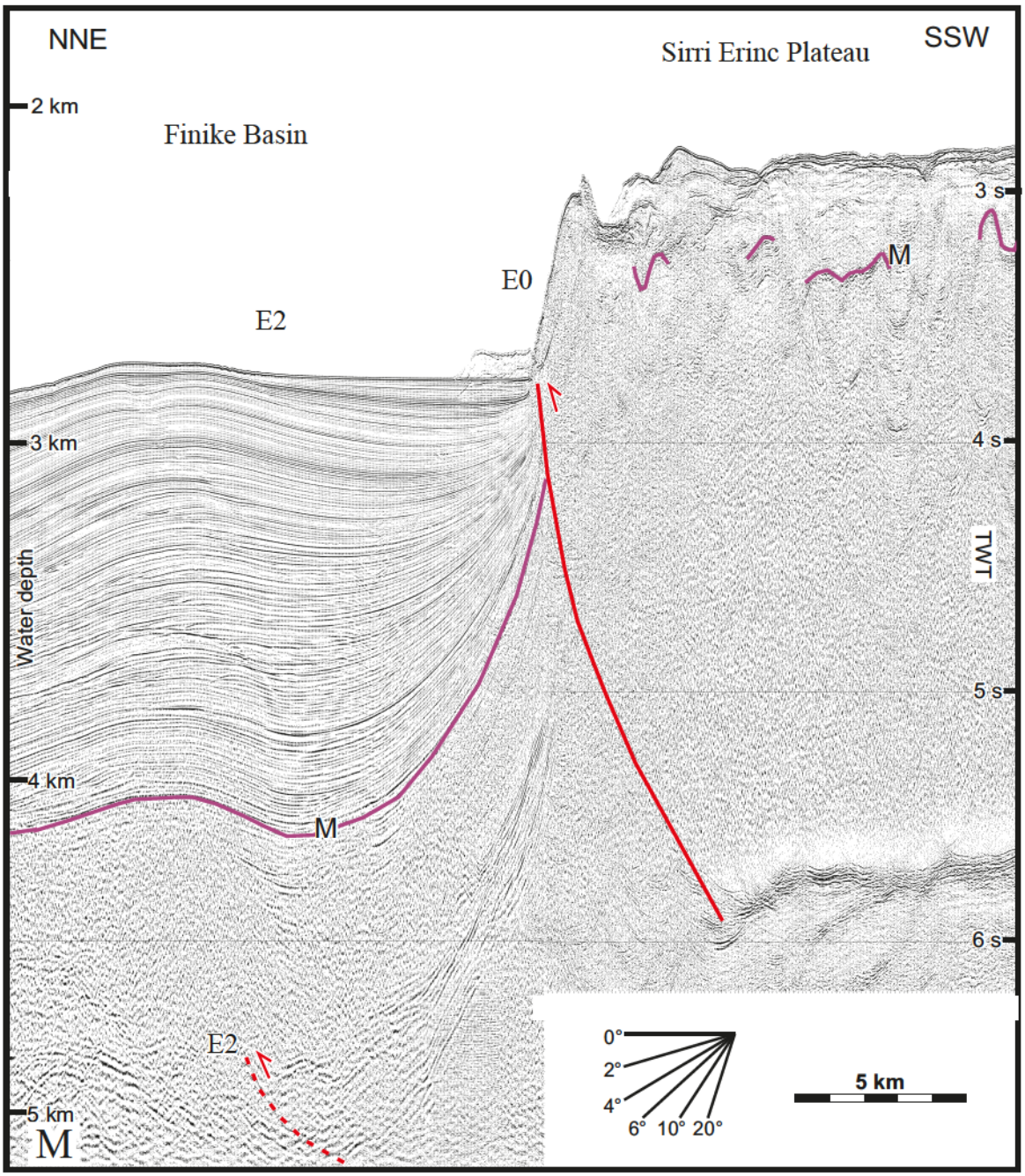

Figure 4.16 Multichannel seismic reflection profile M showing the internal structural framework of the northwestern margin of morpho-tectonic Domain 4. Note the major offsets of the M-reflector. Also note that the core of the upright anticlines (i.e., folds) are composed of acoustically transparent zones. Location is shown. in Figure 4.3 (Plate 16, Fixes 364-383).

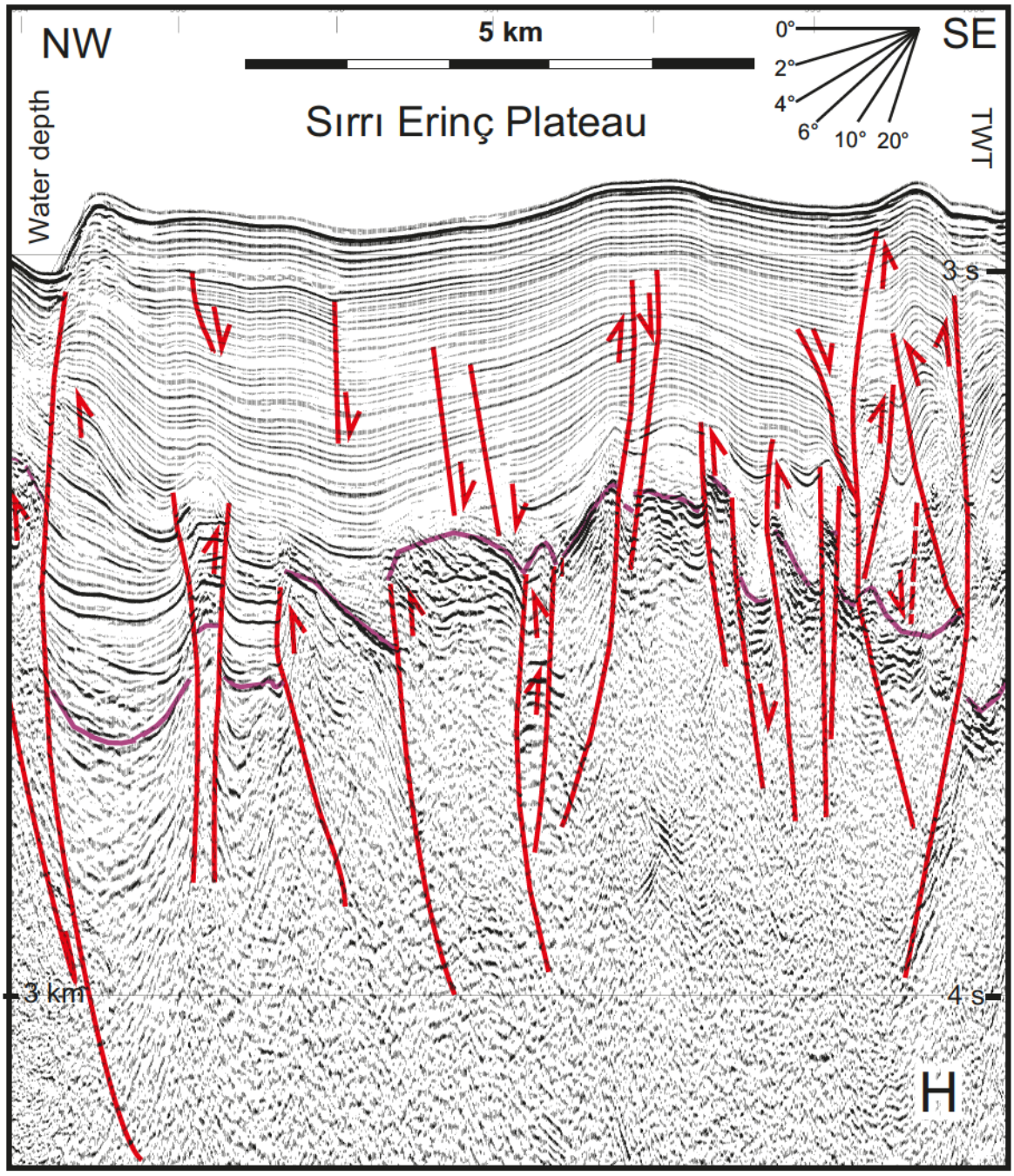

Figure 4.17 A segment of the multichannel seismic reflection profile from Line H showing the prominent high angle faulting over Sırrı Erinç Plateau that creates both contractional and extensional stratigraphic separations. Location is shown in Figure 4.3 (Plate 21a, Fixes 995-1002).

They define broadly east-west and/or northwest-southeast trending map traces, south of the leading thrusts E0, E1, S0 and S0' which are already described in Domains 3 and 4 above. Comparison between the multibeam map and the seismic reflection profiles shows that the large seafloor lineations perfectly correlate with the ramp anticlines created by the large thrust culmination. For example, the tip points of thrusts E0 and P lie at the depositional surface. These thrusts have prominant ramp anticlines, and thrust P developed a major piggy-back basin (Fig. 4.15). The ridges created by the ramp anticlines as well as the trough of the piggy-back basin are clearly visible in the multibeam map as prominent morphological features (Fig. 4.18). Thus, the lineations associated with asymmetrical and occasionally symmetrical fold structures are clearly the result of uplift of the seafloor during continued thrusting in the Pliocene-Quaternary (Fig. 4.15). This will be further discussed in Chapter 5.

A number of smaller relatively high-angle faults occur in this region. Most of these faults show extensional seperations on prominent marker beds and extend into the lower portion of Pliocene-Quaternary succession of Unit 1 (Fig. 4.15). These faults show tip points in the upper portion of the Pliocene-Quaternary succession, and often rise to the seafloor where they create steps. Comparison between multibeam and seismic reflection profiles further show that they create significant lineations on the seafloor.

One of the striking internal architectures of these normal faults is the inverted folding between the M-reflector and the seafloor. For example, in Figure 4.19 there are three structures labeled as I1, I2 and I3 (Fig. 4.15).

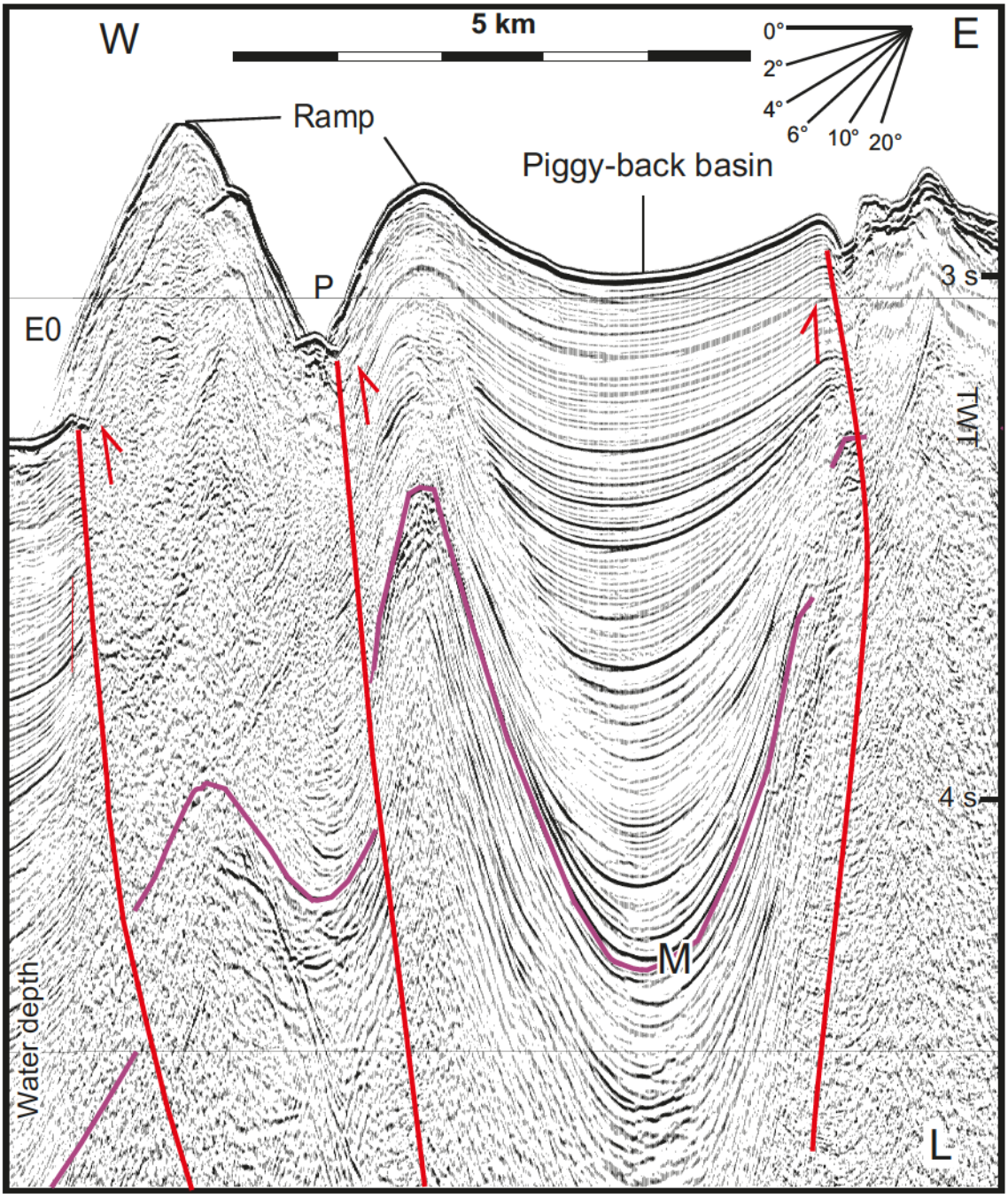

Figure 4.18 A segment of the multichannel seismic reflection profile L showing the prominent thrusts faults and their associated ramp anticlines and piggy-back basin over Sirri Erinc Plateau (From Fig. 5.15, Plate 18, Fixes 1137-1144).

In these structures the regions where the M-reflector shows a concave down morphology, the seafloor shows an opposite convex up morphology. Careful examination of the seismic reflection profiles shows that a mid-Pliocene-Quaternary unconformity separates the concave down and convex up reflector packages in these structures. These structures are interpreted as inversion structures as further addressed in Chapter 4.

4.1.5 Domain 5 – Turkish Continental Margin

Domain 5 is situated north of the Finike Basin (i.e., Domain 3) and west of the southwestern Antalya Basin (i.e., Domain 1; Fig. 4.1). It is bounded in the north by the onland Western Taurus Mountains and the Beydağları Complex. On the northern fringes of the Finike Basin, the domain extends from west to east and in the western neighborhood of the Antalya Basin it exhibits a southwest-northeast trend, with a prominent continental shelf extending from the Beşadalar (Fig. 4.1). The Pliocene-Quaternary succession of Domain 5 includes four main structural elements: (i) superficial detachment faults, (ii) normal faults, (iii) stacked prograded deposits and (iv) large thrust faults.

4.1.5.1 Superficial detachment faults

Along the steep continental slope of the Finike Basin and the westernmost Antalya Basin, thin lens-like deposits rest over the M-reflector (Figs. 4.20, 4.21). In seismic reflection profiles, these deposits exhibit prominently concave bases and gently convex and/or corrugated tops. The internal character of these deposits ranges from undeformed stratified successions to heavily deformed and poorly stratified or chaotic in appearance

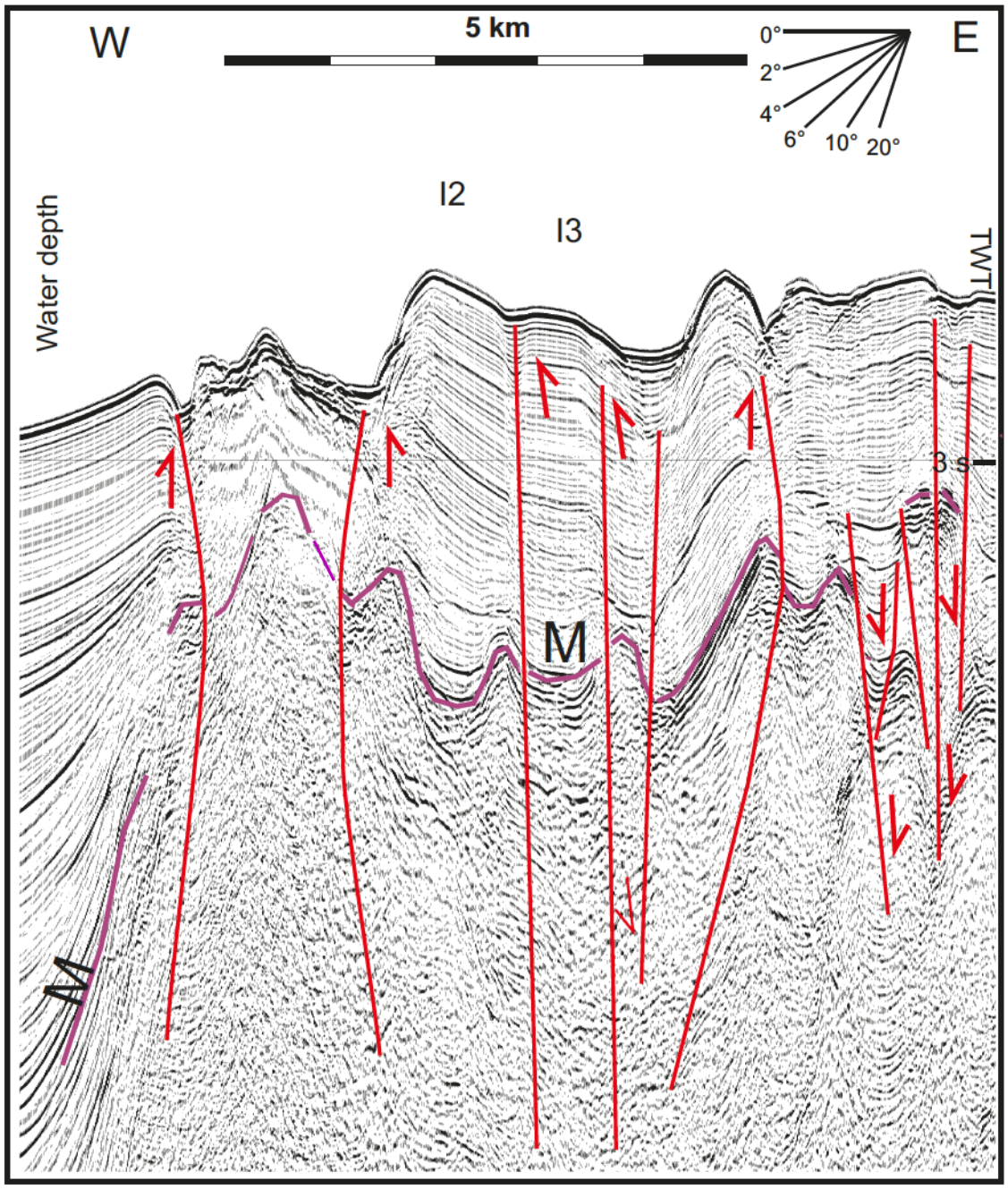

Figure 4.19 A segment of the multichannel seismic reflection profile L showing the prominent inversion structures I2 and I3 over S rr Erinç Plateau (From Fig. 4. 15, Plate 18, Fixes 1142-1147).

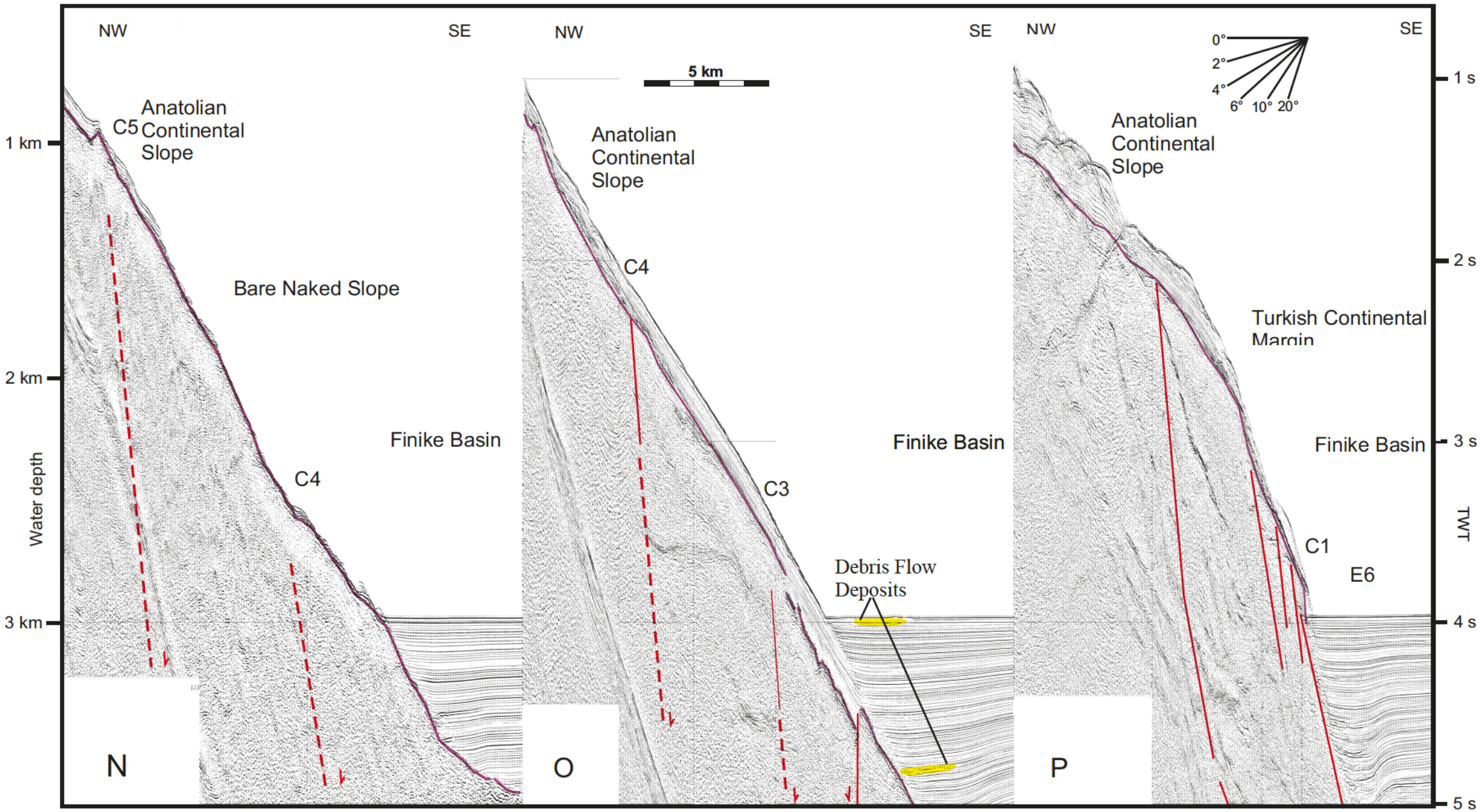

Figure 4.20 Multichannel seismic reflection profiles N, O, P showing the internal structural framework of the western margin of morpho-tectonic Domain 5. Location is shown in Figure 4. 3 (N: Plate 17, Fixes 1107-1095; O: Plate 18, Fixes 1116-1127.5; P: Plate 19a, Fixes 963-953).

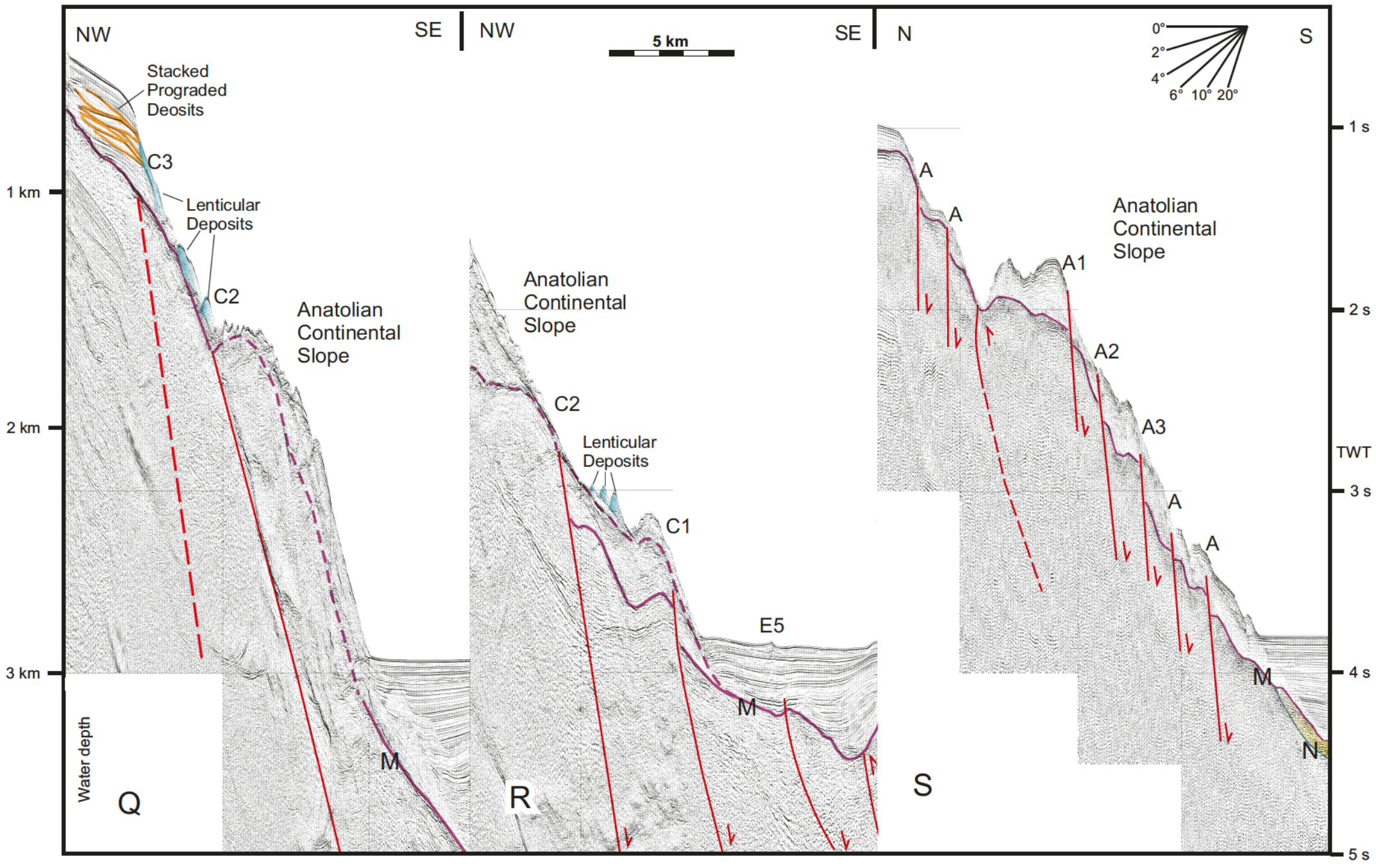

Figure 4.21 Multichannel seismic reflection profiles Q, R, S showing the internal structural framework of the central margin of morpho-tectonic Domain 5 (Fig, 4,1). Location is shown in Figure 4.3 (Q: Plate 21a, Fixess 973-984; R: Plate 22, Fixes 349-339) .

(e.g., shaded in blue, Figs. 4.21, 4.22 sections Q, R, V). The concave base of these deposits is clearly the reflection of concave-up detachment faults (Figs. 4.21, 4.22 sections Q, R, and V). These detachment faults display listric trajectories that either sole on the M-reflector, or extend to cut the seafloor. In this morpho-tectonic domain the lens-like structures are only observed at water depths between 1725 m and 2400 m (2300 and 3200 ms); however, they occur ubiquitously along the Turkish continental margin. A quick glance at the seismic reflection profiles reveals that these deposits and the shallow detachment faults occur immediately above a family of normal faults that define the architecture of the continental slope.

On the basis of the similarities between the lens-like deposits described above and previously described seismic images of slump and slide deposits, they are interpreted as deposits associated with various stages of slope failure (e.g., Aksu and Hiscott, 1992; Hiscott and Aksu, 1994). The largely undeformed lenses with well stratified internal architecture, showing step-like separations on the seafloor are interpreted as slide deposits. It is believed that these deposits have been mobilized, as indicated by the steps on the seafloor, but did not move very far down along the slope, as indicated by their internal stratification. The lenses which show heavily deformed internal architecture and are poorly stratified or chaotic in appearance are interpreted as slide-slump transitions. These deposits are believed to have moved further down the slope and experienced varying degrees of internal mixing as they glided along the slope. The presence of lenticular deposits within the abyssal depths in Antalya Basin (see below) are clear indications that

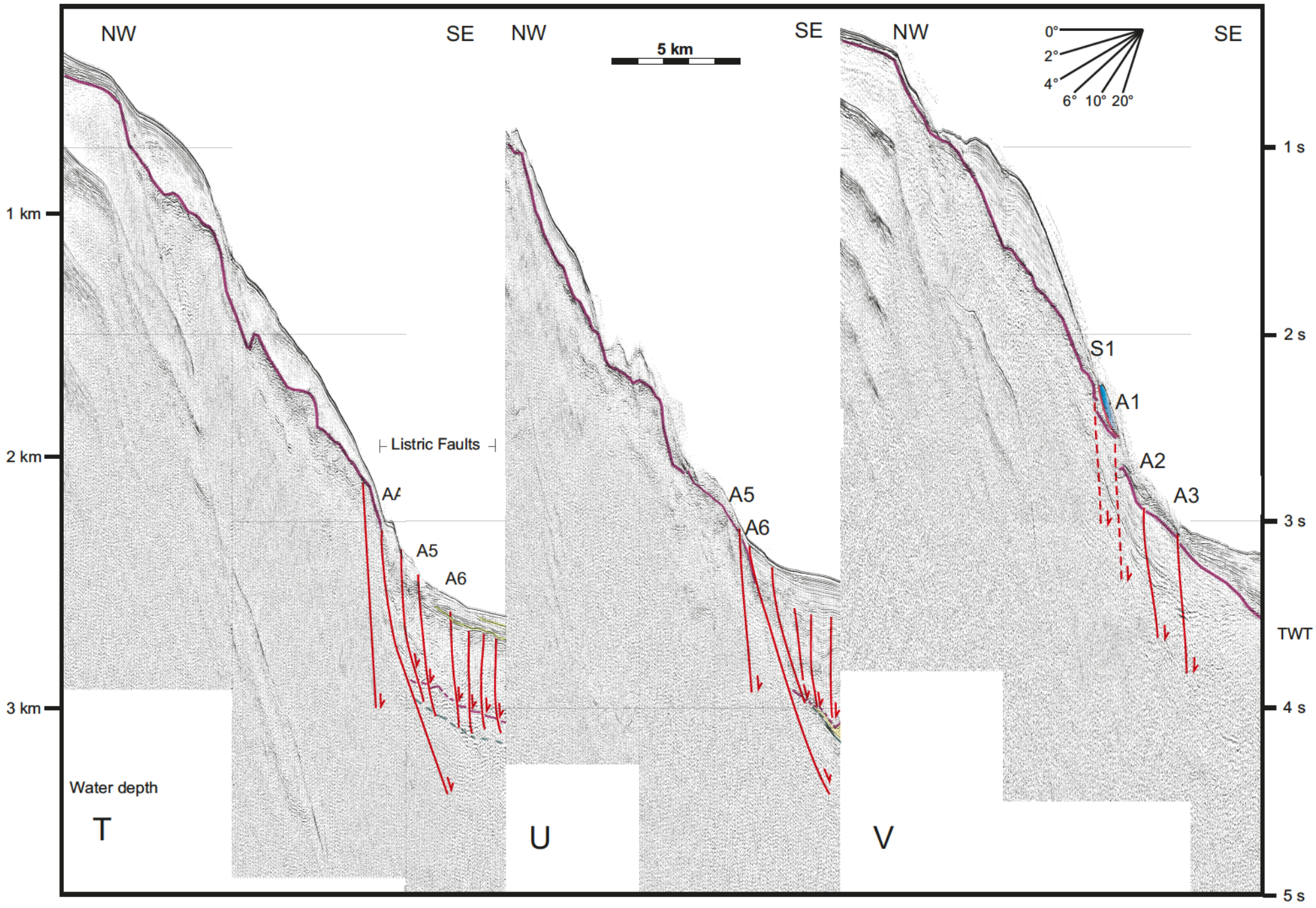

Figure 4.22 Multichannel seismic reflection profiles T, U, V showing the internal structural framework of the northeastern margin of morpho-tectonic Domain 5 (Fig. 4.1). The purple marker shows M-reflector and the green marker shows N-reflector. Location is shown in Figure 4.3 (T: Plate 11, Fixes 424-412; U: Plate 13, Fixes 365-374.5; V: Plate 15, Fixes 352-341).

some of these slump deposits moved all the way down the slope, generating debris flows (discussed later).

4.1.5.2 Normal faults

The multibeam map shows that the Turkish continental margin (i.e., morpho-tectonic Domain 5) is cut by several submarine canyons that have different sizes and depths (Fig. 4.3). Seismic reflection profiles from this region show that there are several normal faults situated at various levels along the continental margin, often controlling the location of these canyons (Figs. 4.3, 4.20-4.22). These faults predominantly cut the M-reflector and tip either at the seafloor (e.g., Fig. 4.19, sections Q, R, S) or in the upper portion of Pliocene-Quaternary succession of Unit 1 (e.g., Fig. 4.20, sections N, O, P). Footwall-hanging wall relationships and cut offs of prominent reflectors show that these faults display extensional stratigraphic separations, with 100-700 ms vertical offset at the M-reflector. Interpretation of a tight grid of seismic reflection profiles and mapping show that these faults define a prominent family of northeast-southwest trending and invariably southeast-dipping extensional faults (Fig. 4.3).

The structural architecture of the southern portion of Domain 5 is controlled by five large northeast-southwest trending and southeast dipping normal faults, labeled from east to west as C1 through C5 (Figs. 4.3, 4.20, 4.21). The faults have dip angles ranging between 15 and 20 . The faults in the westernmost portion of the domain are entirely confined to the pre-Messinian Miocene Unit 3. In this region none of the relatively high-angle faults appear to cut the M-reflector, although some inflection possibly due to the

southeast drop of the hanging wall is observed in a couple of the faults (e.g., Fig. 4.20, faults C1, C2 in section P). Seismic reflection profiles show that from southwest to northeast, the faults progressively cut stratigraphically higher in the Pliocene-Quaternary (sequentially compare Figs. 4.20-4.22). In the eastern segment of the domain these normal faults create variable offsets, ranging from 50 ms to ~300 ms at the M-reflector (Figs. 4.20, 4.21). The seismic data from the southwesternmost section of Domain 5 reveal that there is only a very thin veneer of Pliocene-Quaternary succession over the slope (Fig. 4.20, section N). Here, the slope face includes a few isolated irregular packages consisting of Unit 1 sediments. The Pliocene-Quaternary succession becomes slightly thicker toward the upper portion of the slope. Across most of this region the slope face corresponds to the M-reflector, thus Unit 3 successions are largely exposed on the depositional surface or situated beneath a thin veneer of Unit 1 sediments (Fig. 4.20).

4.1.5.3 Stacked Prograded Deposits

On the continental slope of the Finike Basin within Domain 5 a seismic reflection profile shows the presence of a number of vertically stacked and seaward prograded successions within the Pliocene-Quaternary Unit 1 (Figs. 4.21, 4.23). These prograded successions are 120-200 ms thickness and are composed of seaward-dipping oblique-prograded clinoforms. They are separated from one another by prominent shelf-crossing unconformities as also previously described in Chapter Three (Fig. 4.21). The internal architecture of these deposits with clear topset beds leading to foreset beds (but not showing the bottomset strata) are very similar to delta successions described elsewhere in

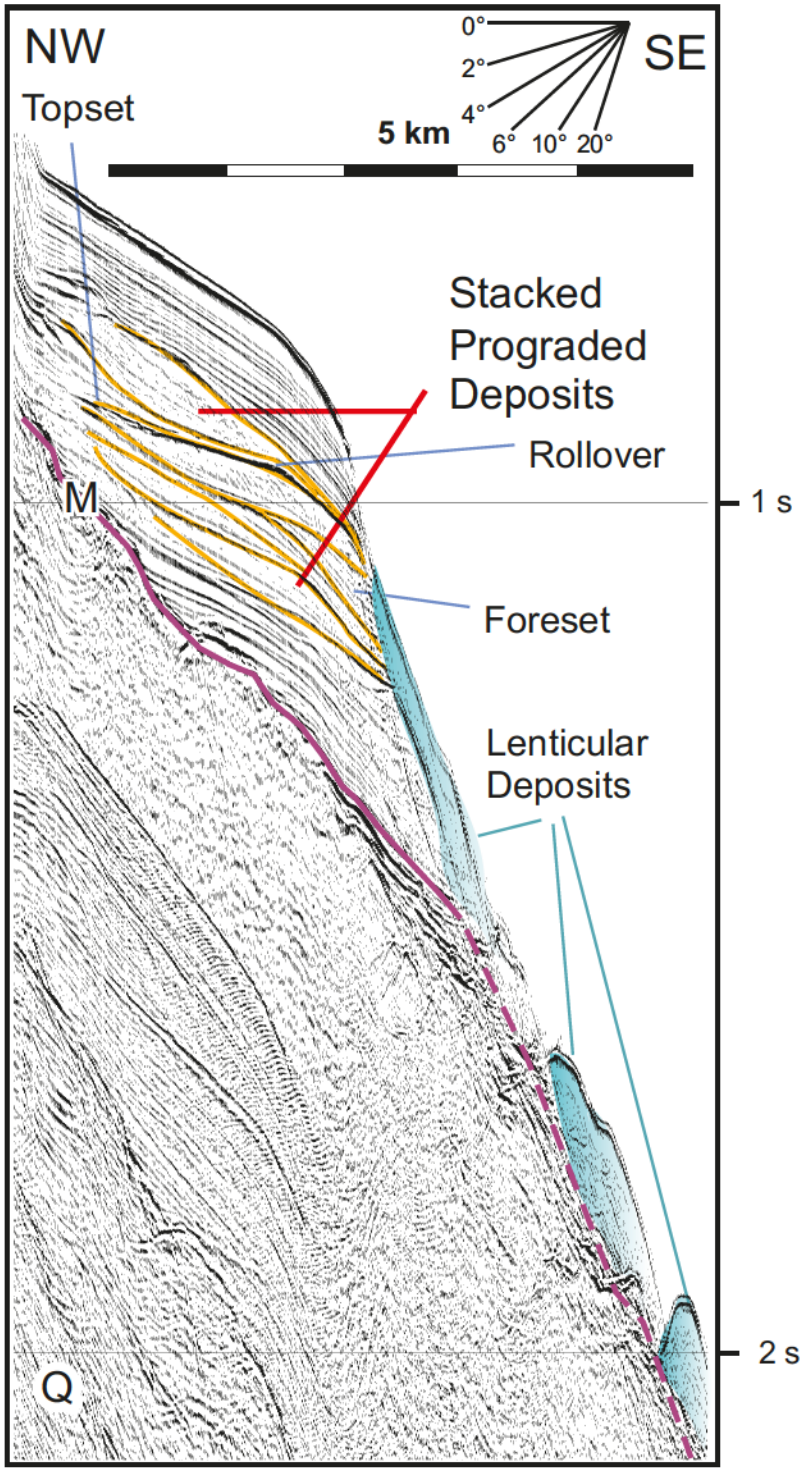

Figure 4.23 A segment of the multichannel seismic reflection profile Q showing the shelf deltas and slope deposits (Plate 21a, Fixes 973-977).

the eastern Mediterranean Sea (e.g., Aksu et al., 1992a,b). On the basis of these strong similarities between the previously imaged and described successions, these deposits are interpreted as shelf-edge deltas. This architecture is characteristic of Quaternary stacked delta successions developed at rapidly subsiding continental shelves (Aksu et al., 1992a,b; Hiscott, 2001). The stacked, progradational geometry and near equal thicknesses of each package suggests that they were deposited during successive glacial sea-level low stands, with the offlap break (i.e., the topset to foreset transition) in each succession representing the last phase of delta progradation prior to the following sea-level rise (e.g., Aksu et al., 1992a,b). The present day position of the topset-to-foreset transitions of the stacked prograded deltas in the Finike Basin margin ranges in depth between 800 and 1500 ms (Figs., 4.21, 4.23).

A similar set of vertically stacked and seaward prograded successions are also described from the margin of the Rhodes Basin at deeper water settings ranging from ~1425 m to ~2475 m (Hall et al., 2009). These authors also interpreted these deposits as shelf-edge deltas, and suggested that their present-day occurrences at such depths imply up to ~2400 m of subsidence in the Rhodes Basin since the early-middle Pliocene at a rate of subsidence of ~600-800 m/Ma (Hall et al., 2009). The sedimentological interpretation of these vertically-stacked and prograded delta successions and their tectonic ramifications to the basin evolution are discussed in detail in Chapter 5.

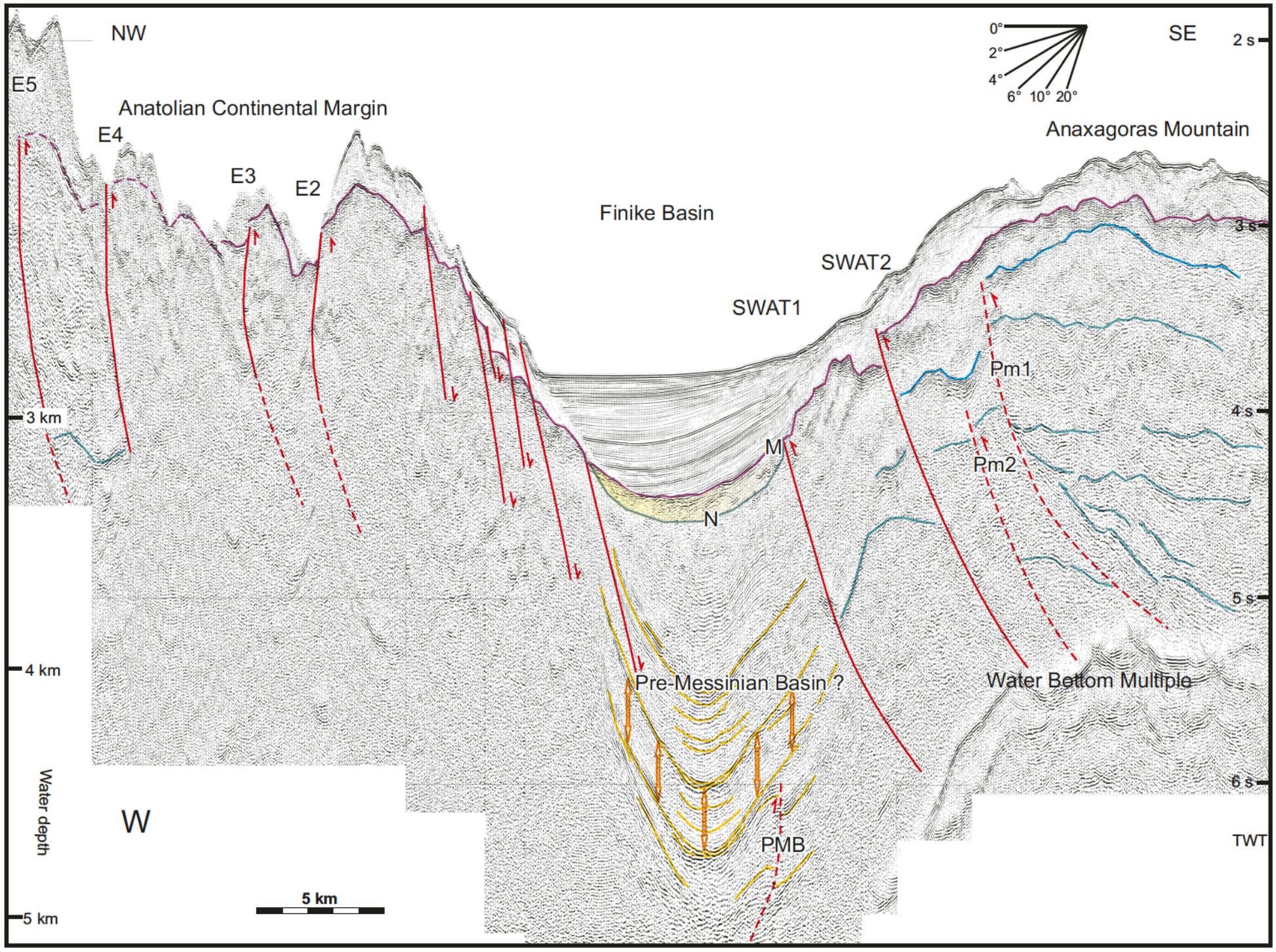

Figure 4.24 Multichannel seismic reflection profile W showing the internal structural architecture of the northern portion of morpho-tectonic Domain 5. Note the highly irregular seafloor morphology, created by the submarine canyons cutting the continental margin. Also note the deeply-seated thrusts that define the framework of the region. The vertical arrows in red show that the thickness of successions within the Pre-Messinian basin indicates no growth. Location is shown in Figure 4.3 (Plate 23, Fixes 827-870) .

4.1.5.4 Large thrust faults

Along the continental slope of the Finike and westernmost Antalya Basin there are several deep-seated northeast-striking and northwest-verging thrust faults (Figs. 4.3, 4.24,). Seismic reflection profies show that the tip point of the thrusts is within the lower-middle Pliocene-Quaternary succession. The thrusts create ~100 ms – 500 ms offset at the M-reflector. The tip points of some of the thrusts lie beneath the highly irregular seafloor morphology created by submarine canyon cutting the continental margin (e.g., Fig. 4.24). These thrusts show similiar trends to that of thrust E2-E5 in the Finike Basin (as previously discussed above). These thrusts have dip angles ranging between 15 and 20 along concave-up trajectories. Seismic stratigraphy and mapping suggest that these thrusts are the extension of the thrust family 2 of the Finike Basin and further extend toward the northeast possibly linking with thrusts mapped onland (further elaborated in Chapter Five). All these thrusts were active in the Pliocene-Quaternary.

4.2 Messinian Succession

The structural architecture of the Messinian succession in the Antalya Basin is comprised of several anticlines and their intervening synclines. These structures are interpreted as salt diapirs and walls (e.g., Işler et al., 2005; Aksu et al., 2005; Hall et al., 2005), and not as mud volcanoes and/or mud diapirs (e.g., Woodside et al., 2000, Zitter et al., 2003), as discussed in Chapter Three.

4.2.1 Salt Anticlines/Diapirs

Seismic reflection profiles show that the structural framework of the Messinian succession includes east-northeast – west-southwest trending, generally non-cylindrical internally parallel anticlines and synclines (Figs. 4.25, 4.26). These anticlines are delineated by the morphology of the M-reflector at their tops and, the internal architecture of the Messinian evaporites of Unit 2 and the late Miocene succession of Unit 3 at their bases. They are mainly developed on the northern portion of the salt basin (Figs. 4.2, 4.4, 4.5, 4.25, 4.26). The anticlines are seperated from each other by mini basins (i.e., their intervening synclines). The crests of the anticlines rise 200-600 ms above the floors of the adjacent mini basins (Figs. 4.2, 4.4, 4.5, 4.26, 4.26) resulting in occasional seafloor elevations (i.e., compare $_1$ and $_2$, Fig. 4.26) caused as the result of the uplifting of the overburden succession associated with salt migration and form broadly linear map traces (Fig. 4.26). These corrugations can also be followed on the multibeam map clearly in the southern area of the salt basin (Figs. 4.3, 4.25). The halokinetic sequences within the Pliocene-Quaternary succession on the crest of the salt wall (e.g., Fig. 4.2) and diapirs (Fig. 4.26) and the growth strata wedges on the hanging walls of the normal faults and the progressive syn-tectonic unconformities (e.g., Figs. 4.2, 4.4) are the consequences of the upward movement of the Messinian salt.

The northern edge of the salt basin shows the presence of a thin (~150 ms) succession of Messianian. Here, the succession is cut by numerous listric normal faults which either sole into Unit 2 or define the boundary of the salt basin (Figs. 4.2-4.5, 4.25)

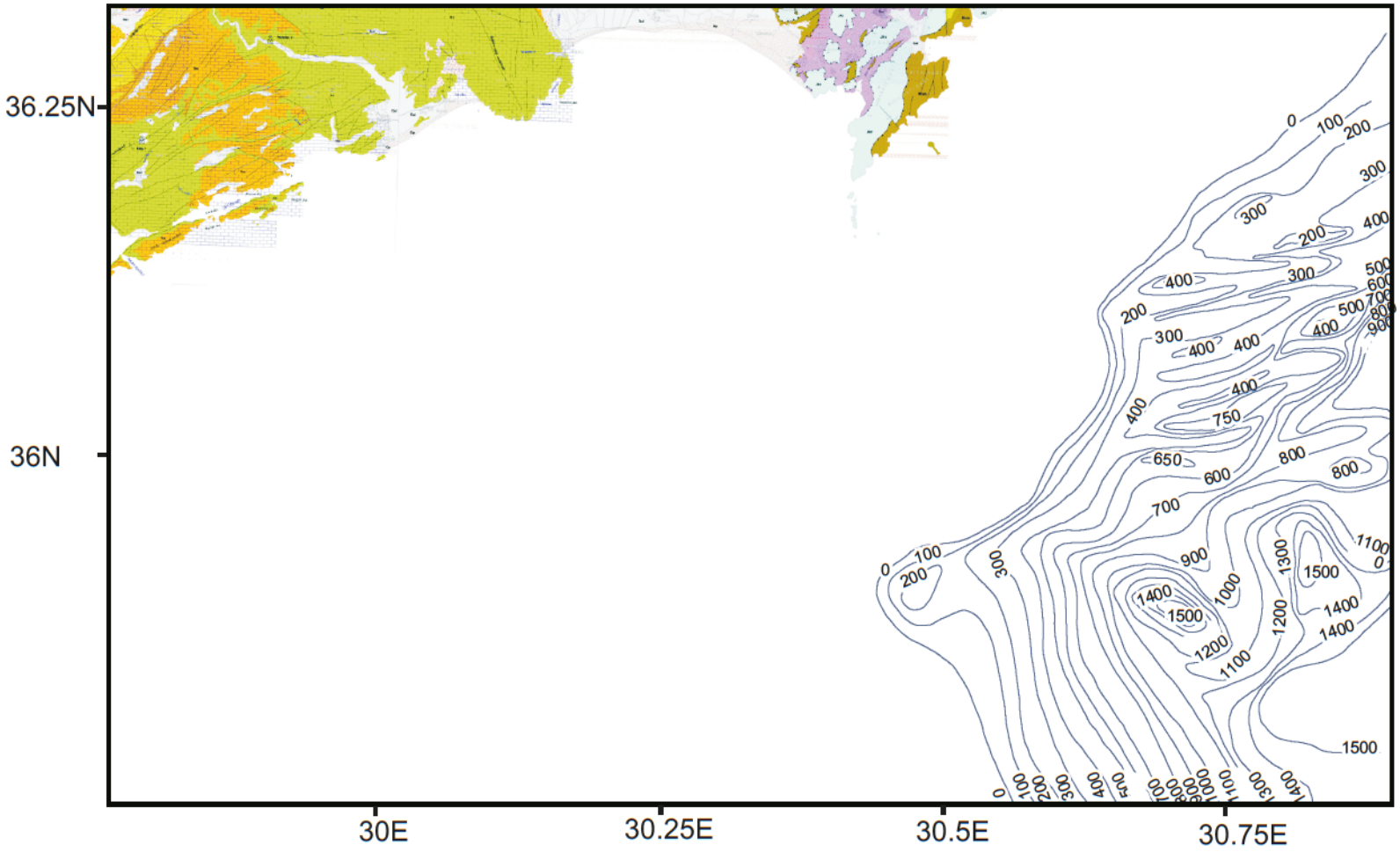

Figure. 4.25 Isopach map (in ms) showing the thickness distribution of the Messinian succession of Unit 2. Note that Unit 2 is ubiquitous in the southwestern Antalya Basin, but dramatically thins to form a basin edge westward. It is notably absent in the Finike Basin, except for its easternmost fringe. Also note that there are broadly east-west trending thick Unit 2 zones associated with large halokinetic structures (see text for explanations).

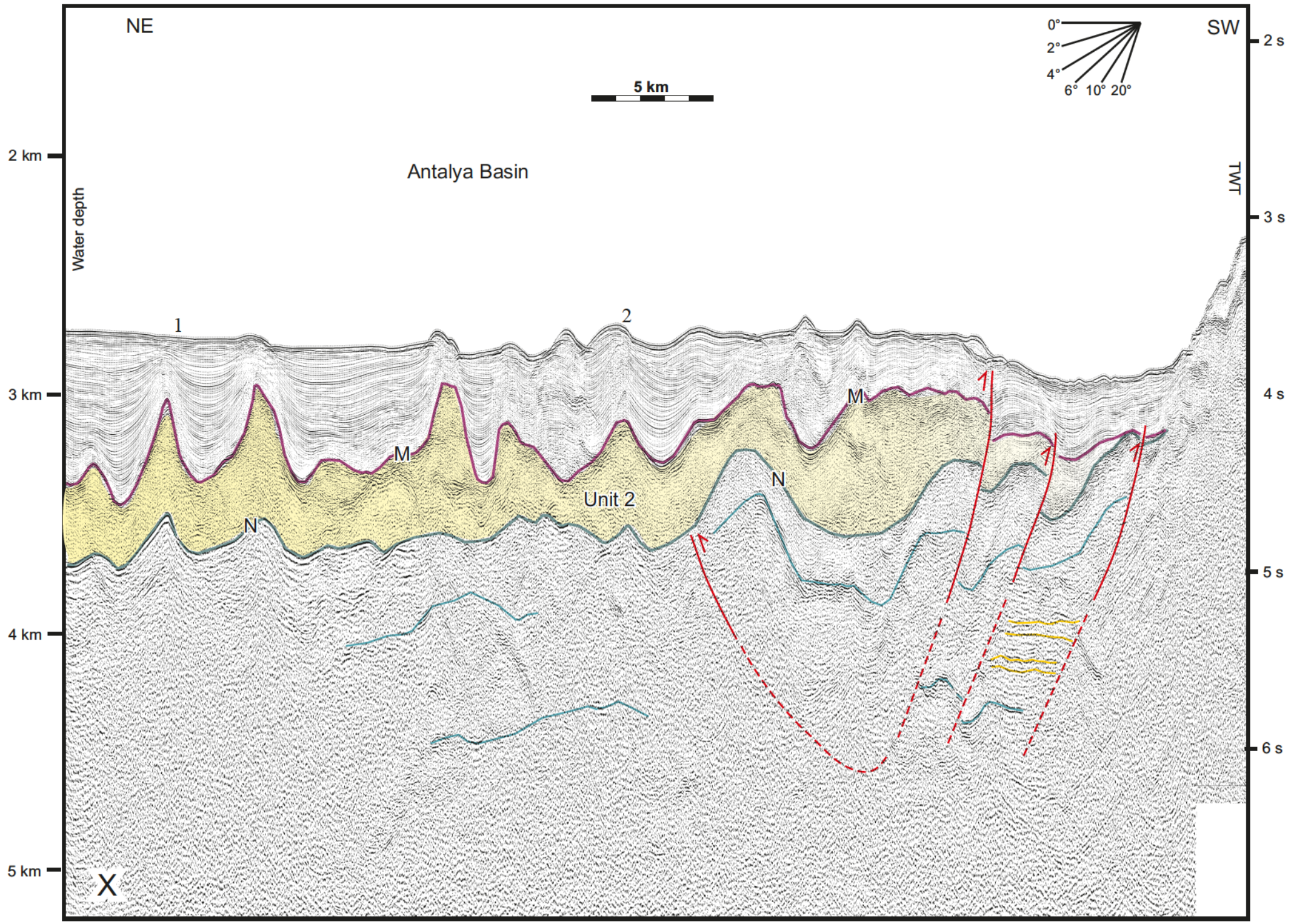

Figure 4.26 Multichannel seismic reflection profile X showing the the thick Messinian Unit 2 in morpho-tectonic Domain 2. Note that Unit 2 clearly thins and pinches out toward the eastern Finike Basin. Location is shown in Figure 4.3 (Plate 30, Fixes 94-65).

at the edge of the continental slope and sole directly into older successions of Unit 3. Seismic reflection profiles show that Unit 2 is absent below both the continental shelf and continental slope. Hence, the succession gets thicker moving downslope and reaches ~800 ms within the Antalya Basin (Fig 4.25). In seismic profiles A, B and C (i.e., Figs. 4.2, 4.4, 4.5), thick salt pillows are clearly developed associated with listric normal faults (compare Figs. 4.3 and 4.25).

4.3 Pre-Messinian Successions

The structural architecture of the pre-Messinian successions of Unit 3 (Chapter Three) is comprised of a prominant fold/thrust belt which extended across the entire study area (Figs, 4.5, 4.10, 4.12, 4.24). The age of the deformation of these structures is clearly pre-Messinian, although some of these structures are reactivated during the Pliocene-Quaternary (Fig. 4.24; see above).

The pre-Messinian structural architecture of the southwestern Antalya Basin consists of northeast-southwest trending and southeast-verging thrusts (Fig. 4.27). These faults generally cut the N-reflector and tip at or immediately beneath the M-reflector (Fig. 4.5). The thrusts sole deep within the pre-Messinian Unit 3 (Fig. 4.4). They have concave-up listric trajectories where their dip amounts increase up section from 15 to 20 (Figs. 4.4, 4.5). Seismic reflection profiles show that some of these thrusts display growth strata wedges developed within Unit 3 on their piggy-back basins (Fig. 4.4). Thus, it is believed that these thrusts are pre-Messinian in age. The growth strata wedges at the level of the Pliocene-Quaternary succession at the top of these thrust faults might

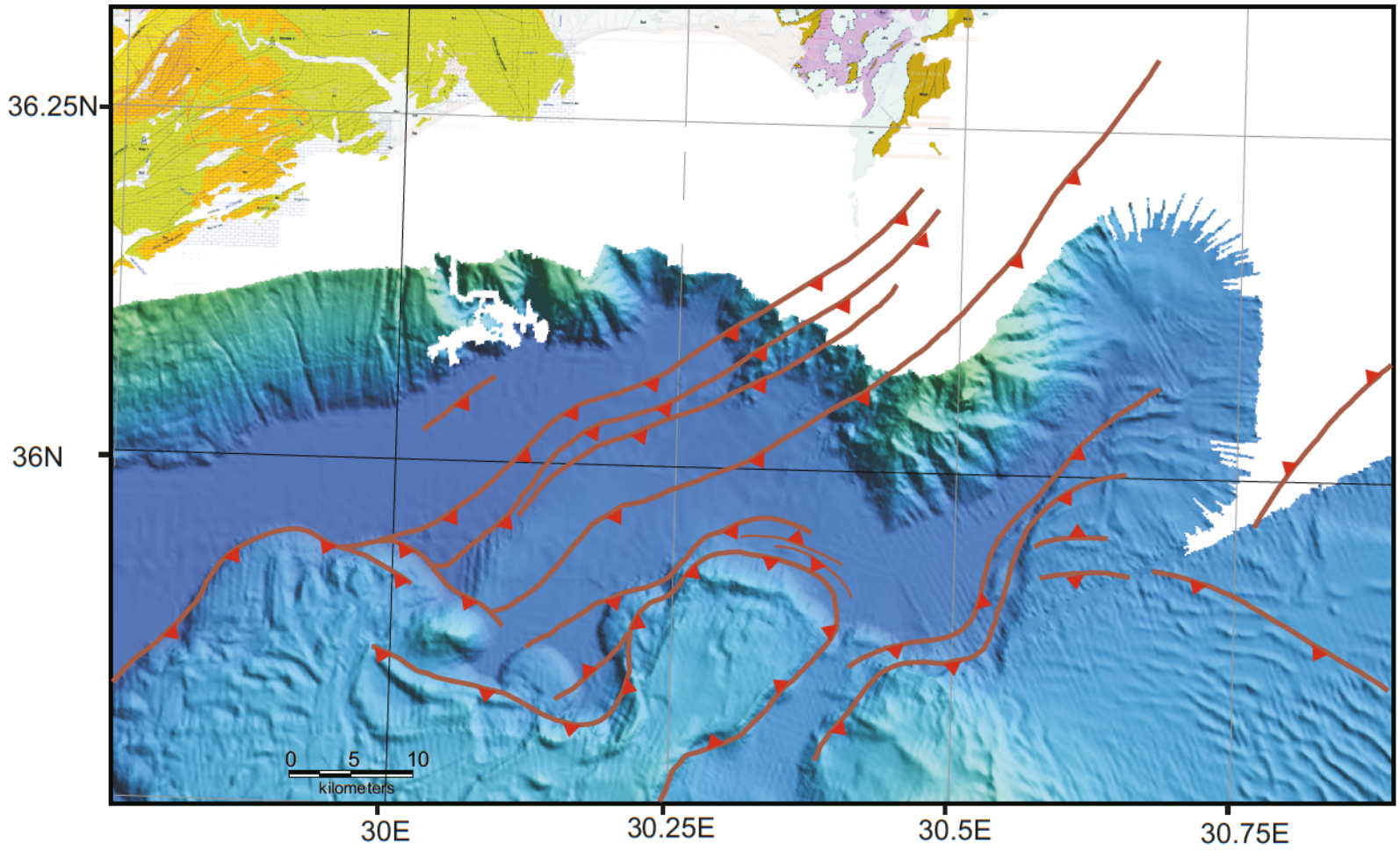

Figure 4.27 Map showing pre-Messinian origin faults and associated structural elements in the Finike Basin and environs plotted over the multibeam map of the region. Lines with triangular ticks are thrust faults with ticks on the hanging wall block.

indicate the upward movement of salt as a result of the sediment load. However, these thrusts might also play a role in the upward movement of the Messinian evaporites in addition to the sediment load. If so, this suggests that these faults are reactivated in the Pliocene-Quaternary, during the deposition of Unit 1 (Figs. 4.4, 4.5).

Traced further toward the south the pre-Messinian structural framework is characterized by four prominent northeast-southwest trending and northwest verging thrusts SWAT1, SWAT2, PM1 and PM2 (Figs. 4.10, 4.24). These thrusts have listric trajectories with dip angles that range between 10 and ~20 . They tip beneath the M-reflector and create significant offsets within Unit 3 reaching ~500 ms (Fig. 4.24). The tip points of the thrusts rest beneath the M-reflector. The growth strata wedges on the backlimb of thrust PM1 and the antiform structures on the hanging wall of thrust PM2 suggest that these thrusts were highly active during early Miocene (Fig. 4.24).

A pre-Messinian basin existed as a deep narrow hole situated in the eastern portion of the Finike Basin between the forelimb of SWAT1 and the Turkish continental margin (Fig. 4.24). Seismic reflection data revealed that Unit 3 successions exhibit almost no growth across the thrusts (Fig. 4.24). This architecture suggests that the presence of the basin dates back to pre-Messinian Miocene. In the deeper settings of the Finike Basin a prominent thrust is mapped beneath this pre-Messinian basin (PMB in Fig. 4.24). It is interpreted as a possible back thrust of a more prominent thrust verging oppositely through the Turkish continental margin. This thrust has a dip angle of ~20 and verging southeast. It creates ~100 ms offset within the pre-Messinian successions of

Unit 3. The absence of growth strata wedges on the pre-Messinian successions suggests that the timing of the thrust activity of PMB is younger than the pre-Messinian basin (Fig. 4.24).

The middle and the westernmost portion of the Finike Basin does not show any evidence of a pre-Messinian basin. The middle portion of Finike Basin illustrates a series of thrust faults verging northwest with big antiform structures observed on the hanging wall of the thrusts (Fig. 4.12). Although the seismic reflection profiles were carefully examined, it was not possible to detect growth strata wedges within Unit 3. However, on the westernmost Finike Basin the correlation of the data with unpublished seismic reflection profiles from the Turkish Petroleum Company suggests that thrusts S0 and S0 are may be of pre-Messinian origin which were reactivated during the Pliocene-Quaternary (Fig. 4.15). The seismic reflection profiles across the Sırrı Erinç Plateau also illustrate these thrust faults which display antiform structures on their hanging walls (unpublished data from Turkish Petroleum Company, Fig. 4.15). These faults are discussed further in Chapter Five.

Chapter Five: Discussion

5.1 Previous Studies

The tectonic evolution of the Eastern Mediterranean has been studied extensively (e.g., Jongsma and Mascle, 1981, Hayward, 1984, Anastasakis and Kelling, 1991, Woodside et al., 1998, Papazachos and Papaioannou, 1999, Zitter et al., 2000, Woodside et al., 2000, 2002, ten Veen and Kleinspehn, 2002, Poisson et al., 2003, Zitter et al., 2003, ten Veen, 2004, Savaşçın et al., 2005, van Hinsbergen et al., 2007, Aksu et. al., 2009). However, these studies mostly focused on the tectonic architecture of the larger eastern Mediterranean region, leaving our knowledge of the structural and stratigraphic evolution of the Finike Basin incomplete (e.g., Woodside et al., 1998, Zitter et al., 2003, ten Veen et al., 2004, Aksu et. al., 2009). This is the first study that discusses the detailed structural and the stratigraphic evolution of the Finike Basin and its genetic relationships with the surrounding regions, such as the western Taurus Mountains, the Anaximander Mountains (*sensu lato*), the Antalya Basin in the east and the Rhodes Basin in the west. Before a detailed discussion of the findings of this dissertation, a summary of the previous studies in the eastern Mediterranean surrounding the Finike Basin region is given below.

Woodside (1977) used low-resolution single channel seismic reflection profiles and gravity data to describe the large-scale tectonic elements and the nature of of the crust in the eastern Mediterranean region. Combining the results of the both onland and offshore geological and geophysical data from Levantine and Heredotus basins, he

suggested that the crust in the eastern Mediterranean is the northern continuation of the African continental crust. He noted the character of the Florence Rise and the Anaximander Mountains, the northward tilting and subsidence of the Antalya and Finike Basins, and the apparent continuation of the Strabo Trench south of the Florence Rise and further suggested that the African Plate is under-thrusting the Turkish Plate (i.e., the Aegean-Anatolian Microplate). He pointed out the lack of intense seismicity between the African and Turkish plates, the absence of an active volcanic arc, and the presence of a poorly-developed trench to suggest that active subduction must have ended along the Cyprus Arc within the past 5 Ma, but the convergence of two plates must be continuing along zones of weak regional deformation.

Jongsma and Mascle (1982) used seismic reflection data to study the Pliny-Strabo trenches that forms the eastern margin of the Hellenic Arc and suggested that the deformation observed in this area is very complicated and contains regions of extension and compression as well as strike-slip deformation. They concluded that the collision of the African continental margin with the Hellenic Arc is still in progress, causing the overriding of the Mediterranean Ridge along the southeastern branch of the Hellenic Trench system.

The Hellenic Arc and Pliny-Strabo trenches were studied more extensively than the Cyprus Arc until the early 1990s. Anastasakis and Kelling (1991) used single channel seismic reflection profiles to explain the main tectonic elements of the Cyprus Arc, including the Cyprus and Pytheus trenches. They suggested that the Cyprus Trench

displays evidence of underthrusting and morphostructural features typical of subduction zones, and that the Pytheus Trench is associated with dextral strike-slip movement and connects the western end of the Cyprus Trench to the Strabo Trench sector of the Hellenic Trench system.

Papazachos and Papaioannou (1999) attempted to delineate the plate boundaries and the nature of the plate motions on the Island of Cyprus and vicinity by using the locations of earthquakes recorded by seismographs and fault plane solutions of large recent earthquakes. They suggested that the African and Eurasian plates in this region display a continuous boundary creating two north concave arcuate structures that are linked with a NNE trending dextral transform fault (i.e., Paphos Transform Fault) situated on the western margin of Cyprus, linking the Florence Rise in the west with the Cyprus Arc in the east (Fig. 5.1). Furthermore, they suggested that the Florence Rise joins the Rhodes thrust fault, a previously undefined structure along the southern margin of the Turkish continental slope.

During the UNESCO-supported Training-Through-Research cruises substantial new single channel low-resolution seismic reflection profiles were collected from the eastern Mediterranean, including the Rhodes and Antalya basins, Anaximander Mountains, Florence Rise and Pliny-Strabo Trenches. in Mediterranean, using the RV *Gelendzhik* (Woodside et al., 1997, 1998).

The first documentation of the gas hydrates related to the mud volcanism in the Anaximander Mountains was made by Woodside et al. (1998). They used multibeam

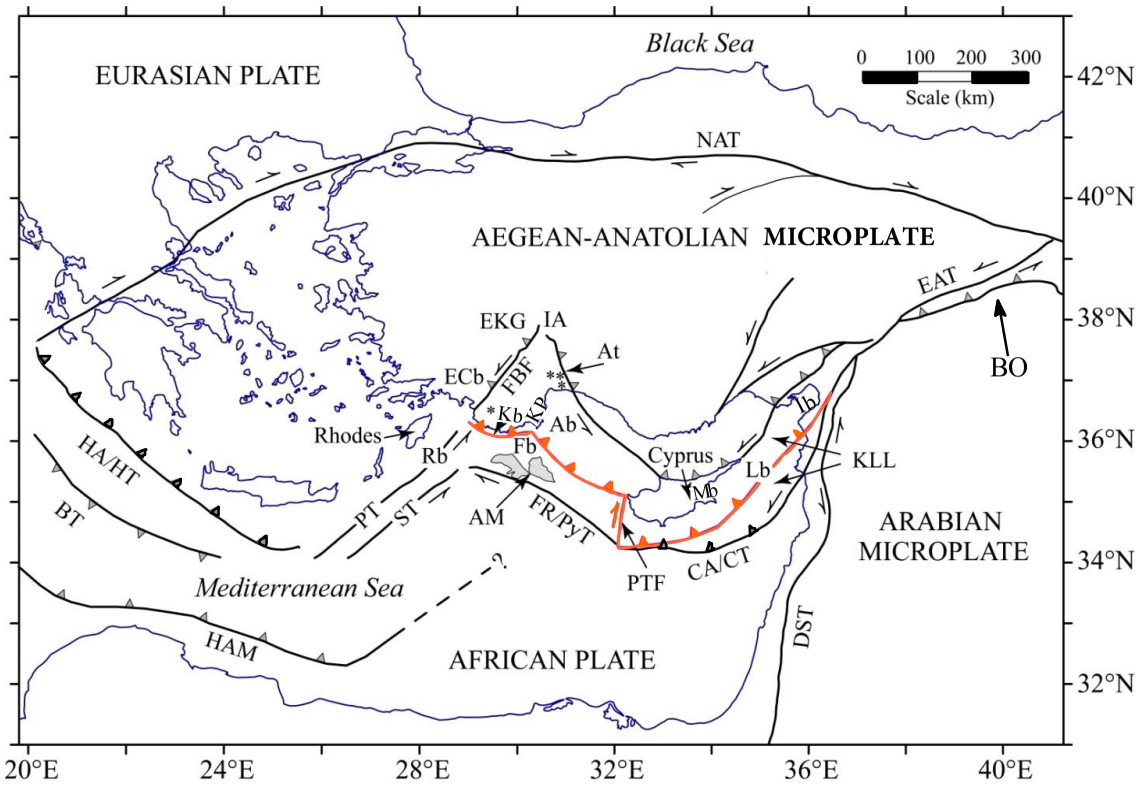

Figure 5.1 Locations-1 Map showing the location of Ab=Antalya Basin, AM=Anaximander Mountains At=Aksu Thrust, BO=Bitlis Ocean, BT=Back thrust, CA/CT=Cyprus Arc/Cyprus Trench, DST=Dead Sea Transform fault, EAT=East Anatolian Transform fault, ECB= Esen Cay Basin, EKG= Egridir-Kovada Graben, FB=Finiki Basin, FBF=Fethiye-Burder Fault zone, FR/PyT=Florence Rise/Pytheus Trench, HA/HT=Hellenic Arc/Hellenic Trench, HAM=Hellenic Active Margin, Ib=Iskenderun Basin, Kb=Kasaba Basin, KLL=Kyrenia/Larnaca/Latakia Ridges, Kp=Kemer Peninsula, LB=Latakia Basin, Mb=Mesaria Basin NAT=North Anatolian Transform fault, PT=Pliny Trench, PTF= Paphos Transform Fault, Rb=Rhodes Basin, Rt=Rhodes Thrust, ST=Strabo Trench, *=Wells (Modified from Cranshaw 2010)

bathymetry and seismic data to suggest that the Anaximander Mountains are characterized by individual blocks defined by the cross-cutting strike-slip faults. They further suggested that these faults may be the cause of the mud volcanoes by allowing over-pressured fluids to be expelled to the shallower subsurface. They used pockmarks and mud volcanoes with carbonate crusts and benthic communities to suggest the presence of gas in the sediments. Woodside et al. (1998) further suggested the under-thrusting of the Anaximander Mountain by the Anaximenes Mountain, causing crustal shortening and the rising and northwest-tilting of the Anaximander Mountain. They also proposed a massive gravitational slide, in the region between the Anaximander Mountain and Anaximenes/Anaxagoras Mountains, and referred it as the Great Slide (Fig. 5.2). They speculated that the sliding occurred during the Late Pliocene or Pleistocene as a gravitational flow to the north and south. They anticipated that the flow was initially started under the effect of the presence of gas hydrates in poorly consolidated sediments with higher than normal water content. They suggested that the active compressional tectonics resulted in deformation of the sediments which started releasing gas from decomposing gas hydrates as it was elevated above the gas hydrate stability zone, thus the Great Slide.

Woodside et al. (2000) used gravity and magnetic data, swath bathymetry and seismic reflection profiles to show that the deep Rhodes Basin contains no Messinian evaporites and only a thin Pliocene–Quaternary sedimentary succession overlying the acoustic basement. They associated the acoustic basement to the pre-Miocene rocks

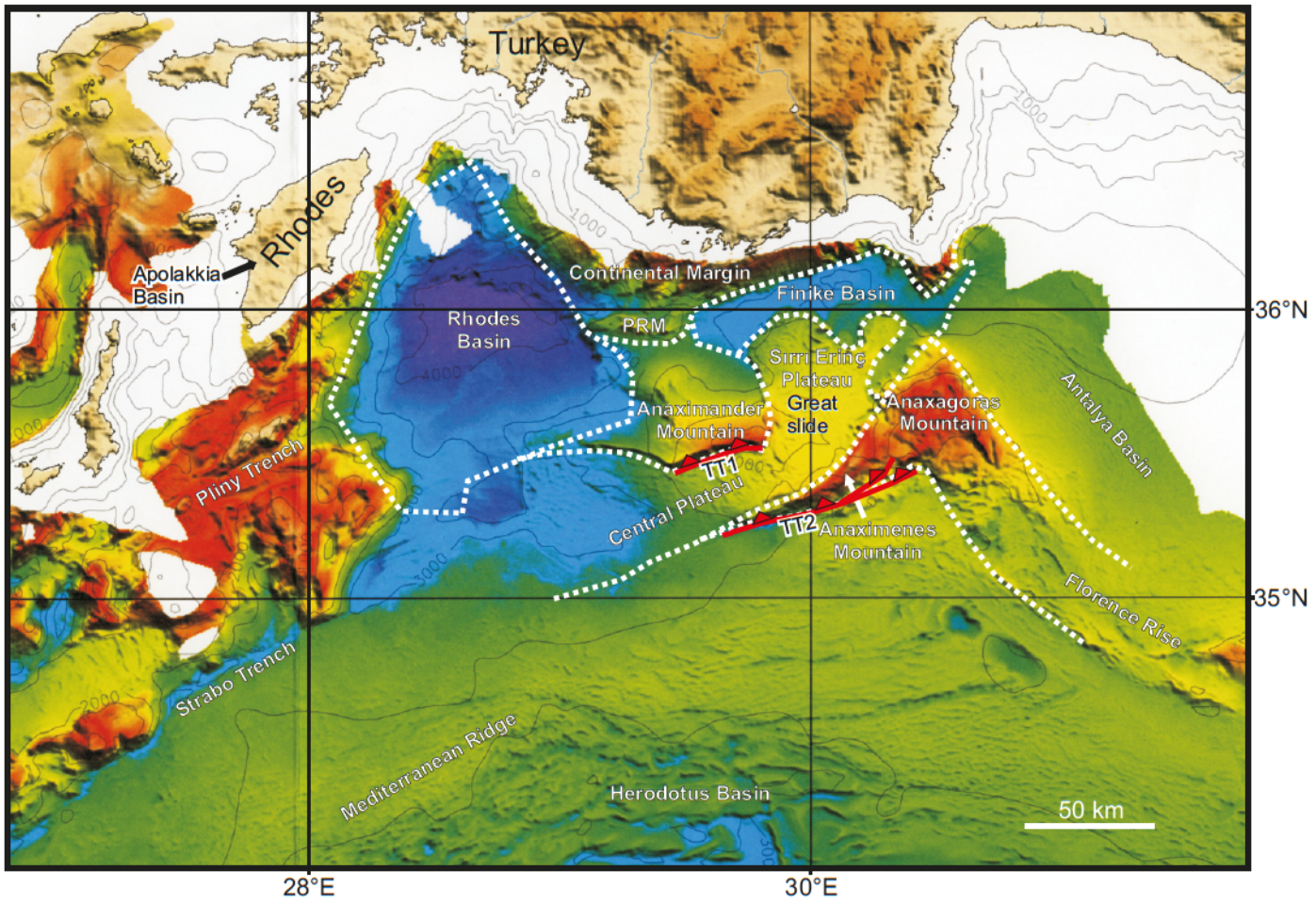

Figure 5.2 Map showing the location of the Anaxagoras Mountain, Anaximander mountain, Anaximenes Maountain, Antalya Basin, Apolakkia Basin,Turkish Continental Margin, Florence Rise, Rhodes Basin, Rhodes Island, S rr Erinç Plateau, TT1 and TT2 thrusts (Modified from Hall et al., 2009).

which may be related to the Hellenide–Tauride alpine orogens. They suggested that reverse faulting, strike-slip faults, sedimentary nappe-formations and mass sliding are presently occurring in the Rhodes Basin, and comparably high seismic activity on its northwestern margin show the continuation of the evolution of this basin. They proposed that the Rhodes Basin developed as the result of a collapse of its present brittle basement, in connection with the progressive development of transform motion along the eastern branch of the Hellenic Arc. They pointed out the similarities between the Rhodes Basin and pull-apart basins along the transpressive branch of the Hellenic Arc and speculated that the Rhodes Basin may also be a post-Miocene foundered trough (i.e., like the Pliny Trench).

During the ANAXIPROBE 95 and PRISMED II 98 surveys, Zitter et al., (2000, 2003) collected seismic reflection profiles, multibeam and gravity data to show that there is no evidence for present-day thrusting along the Anaxagoras Mountain and Florence Rise. They defined the deformation along and across the Florence Rise as anastomosing faults and pop-up structures. They claimed that the reactivation of preexisting thrusts and normal faults caused the deformation of this region in a major strike-slip system. This deformation is described as a broad zone of northwest–southeast dextral wrenching. Zitter et al. (2003) remarked on the similarities between the Hellenic and Cyprus Arcs, with sinistral strike slip faulting along their eastern segments such as the Strabo/Pliny Trenches and Kyrenia, Larnaca, Latakia Ridges versus dextral faulting along their western segments, such as the Florence Rise and the Matapan Ridge (Fig.5.1). They used

the multibeam data to point out the similarities between the eastern Anaximander Mountains and the Florence Rise, and speculated that the western Anaximander Mountains may have opened up from the Rhodes and Finike basins in a transtensional setting in southwest Turkey, possibly associated with the Fethiye–Burdur Fault Zone. They concluded that the Anaximander Mountains and the Isparta Angle together form a tectonic accommodation zone between the active deformation in southwestern Turkey and the Aegean region and the tectonically quieter Cyprus region.

Woodside et al. (2002) used EM12D multibeam bathymetric data, high speed seismic refection profiles, and continuous gravity and magnetic data from the eastern Mediterranean Sea and described the Florence Rise as a submarine feature extending from the northwest of Cyprus to the northwest end of the Cyprus Arc which is formed by the Anaximander Mountains. They suggested that Florence Rise is a surviving remnant of a prior subduction zone, separating the passively-subsiding Antalya Basin from the southern and southwestern collisional tectonics. They brought forward the idea that the boundary between the Aegean-Anatolian Microplate and the African Plate is probably sutured, but that continuing deformation has resulted in the development of a broad dextral wrench zone extending across the Florence Rise toward the Anaximander Mountains. They also linked the tectonic deformation to the westward movement of the Cyprus domain and the northeast movement of the African Plate along the Florence Rise, thus the progressive adjustment of the collisional/compressional plate interaction. Woodside et al. (2002) attributed an important proportion of the current deformation to

the passive superficial deformation caused by the invasion of thick sediments from the Herodotus Basin and Mediterranean Ridge into the area of the Florence Rise. They concluded that the present-day deformation along the Florence Rise is related to the presence of the Eratosthenes continental block at the subduction zone which might have stopped the subduction along the Cyprus Arc, as well as to the geometry of the subducting African slab beneath the Florence Rise which has been stretched and detached from the main part of the plate.

Ten Veen et al. (2004) used multibeam bathymetry, backscatter images, seismic reflection profiles and gravity and magnetic data to study the neotectonic evolution of the Anaximander Mountains and vicinity and suggested that the western and eastern Anaximander Mountains are correlated with the Bey Dağları unit of southwest Turkey, and the ophiolitic Antalya Nappe Complex, respectively. They further suggested that the development of several grabens extending from the southern Aegean to southwestern Turkey took place in the Serravallian–Tortonian times. During the Late Miocene differential subsidence resulted in the formation of the Anaximander Mountains which is reflected by an unconformity between the Lower–Middle Miocene and Pliocene–Quaternary successions. They further stated that during the Messinian–Quaternary, the western part of the Anaximander Mountains was characterized by distributed sinistral shear parallel to N70 E, which was marked by the onset of an extension on N20 E-striking normal faults that formed long graben-like depressions. However, during the Pliocene, these basins were transected by N70 E-striking sinistral strike-slip faults, but

continued crustal extension suggestive of mainly transtensional deformation. They suggested that the eastern part of the Anaximander Mountains is characterized by N150 E-striking normal and/or oblique normal faults, which lack significant evidence of strike-slip deformation, whereas a consistent sinistral faulting is observed on the western mountains along the Hellenic Arc that merges with the extensional domain in the eastern mountains.

There are also a number of studies onland Turkey immediately north of the study area, which provide important information for the understanding of the evolution of the Finike Basin and the surrounding environs (Hayward, 1984, Yağmurlu et al., 1997, Savaşçın and Oyman, 1998, ten Veen and Kleinspehn, 2002, Poisson et al., 2003, ten Veen, 2004, van Hinsbergen et al., 2007, Toker and Yağmurlu, 2010.)

Hayward (1984) studied the Kasaba Basin, a former Tertiary marine depocentre which is presently nestled on the foothills of the western Taurus Mountains. He suggested that it is a pheripheral foreland basin created as a result of the thrusting, associated with the emplacement of the Lycian Nappes and ophiolites onto a previously stable carbonate platform during the Miocene. Hayward (1984) suggests that the carbonate platform foundered and irregularly subsided during the primary phase of the ophiolite emplacement in the late Aquitanian, and continued loading during the Burdigalian causing the basin development. He argued that fan-deltas originating at the leading edge of the nappes moved towards the basin into a series of small submarine fans.

Meanwhile, in central areas of the carbonate platform along the margin of the basin opposite the nappe pile, the loading of the nappes and its downward flexural response created a peripheral bulge. A thick wedge of carbonate-platform-derived sediments were shed northwestwards into the dominantly ophiolite derived basin fill. The Kasaba Basin remained as a marine depocentre until the Serravallian indicated by the shallow marine successions (Hayward, 1984), but became subareally exposed during the Tortonian as shown by the thick alluvial fan complexes. This exhumation of the Kasaba Basin is associated with the rise of the western Taurus Mountains.

Savaşçın et al. (1995), Yağmurlu et al. (1997) and Savaşçın and Oyman (1998) studied the evolution of the Isparta Angle by using the differences between coeval calcalkaline/alkaline volcanics to the east and west the Kırka-Afyon-Isparta region. They showed that alkaline volcanics are located on the west in side of the Isparta Angle forming a north-south trend paralleling the Eğridir-Kovada graben (Fig. 5.3). They indicated that the Kirka-Afyon-Isparta volcanism mainly developed following the northward subduction of the Africa Plate beneath the Eurasian Plate. They showed that this volcanism occurred ~21 Ma in the north, progressively becoming younger to ~4 Ma in the south. They showed that the volcanism was clearly associated with a major N-S trending fault zone, bounding several half graben. They further showed that this fault zone has notable dextral strike slip movements (Fig. 5.3). They suggested that the evolutionary characteristics of the Cyprus Arc is controlled by the southward migration of the plate boundry and the lateral change in the mode of convergence along this arc was

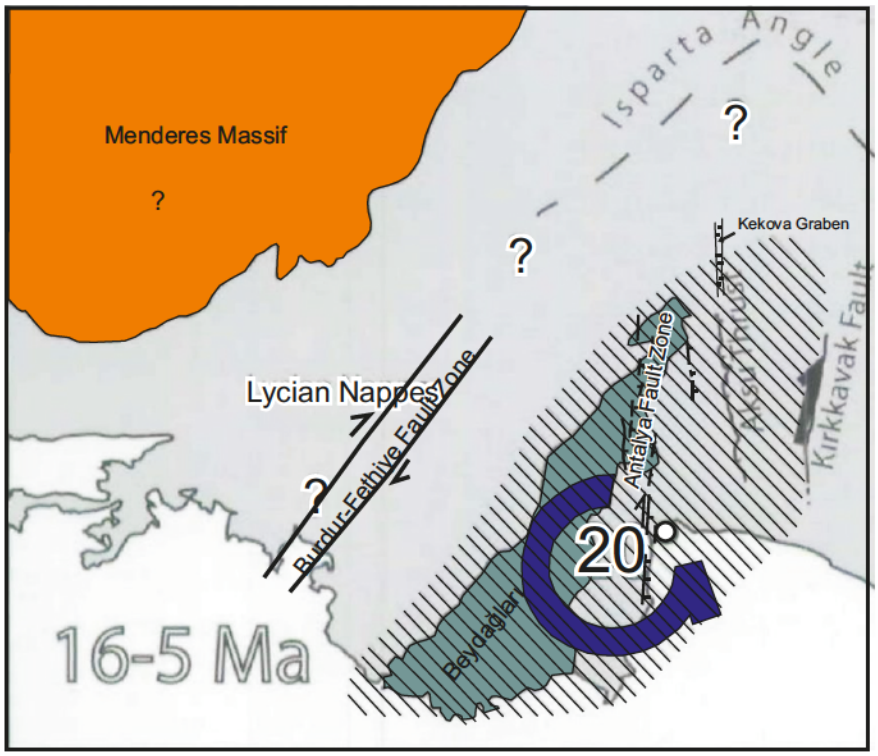

Figure. 5.3 Map showing the locations of Aksu thrust, Antalya fault zone, Beyda lar Isparta Angle, Kekova Graben, K r kkavak Fault, Lycian Nappes. The shaded area is referred to as Beydağları Block and the blue arrow shows the direction of rotation between 16-5 Ma (modified from van Hinsbergen etl. al., 2010 ; Ya murlu et.al., 1997). The question marks indicate that the exişstance of Burdur Fethiye Fault Zone, weather it is dextral or sinistral and its linkage to the Isparta Angle is still an ongiong discussion.

due to differences in the crustal structure of the underthrusting plate. Furthermore, they suggested that the volcanic centres are on the synthetic fault elements of the Eğridir-Kovada intra-continental rifting in connection to the northward movement of the African Plate.

Dilek and Rowland (1993) suggested that a NE trending rift zone developed between the Beydağları and Anamas-Akseki platforms during the Early Triassic-Jurassic and that rift assemblages and oceanic crust were developed in this triangular-shaped rift zone. They indicated that this ocean started to close by east-west compression during the uppermost Cretaceous and the rift sediments and ophiolites were thrust over the Beydağları and Anamas-Akseki platforms in the west and east, respectively, forming the Antalya nappes. They further suggested that the Beyşehir-Hoyram Hadim and Lycian nappes were placed over the carbonate platforms during the middle to late Tertiary, in turn suggesting that the Burdur and Akşehir oblique faults, bounding the Isparta Angle were developed parallel to the suture zones during the Late Maastrichtian and represent the reactivated Neotectonic lineations (Yağmurlu et al., 1997)

Glover and Robertson (1998a,b), Robertson (1998) used low-resolution seismic reflection profiles to suggest that the western margin of the Antalya Basin is characterized by a series of generally north-south trending east-dipping extensional faults.

Çiçek and Koçyiğit (2009) highlighted the presence of four tectonic models to explain the extensional regime in southwestern Turkey as (1) the tectonic escape

(extrusion) model (Dewey and Şengör, 1979), where the extension in southwest Turkey originated as a result of intracontinental collision between the European Plate to the north, the Arabian Microplate to the south, and the associated escape of the Aegean-Anatolian Microplate along the North Anatolian and East Anatolian transform faults in the Late Miocene, (2) the backarc spreading model (Le Pichon and Angelier, 1979), which suggests that the migration of the trench system to the south and southwest gave rise to an extensional regime in the back-arc region in the Hellenic Arc, (3) the orogenic collapse model (Seyitoğlu et al., 1992) where the extension has been attributed to the cessation of the Paleogene shortening as a consequence of the ongoing over-thickening of the soutwest Turkish lithosphere that started in Late Oligocene-Early Miocene and (4) the episodic two-stage extension model (Koçyiğit et al., 2000) which suggests that the extensional regime has not been continuous since Late Oligocene-Early Miocene, but instead is linked with the development history of the southwest horst-graben system in Turkey, where the extension occurred in two phases separated by a short-lived contractional interval. Çiek and Koçyiğit (2009) further suggested that phase-I extension is restricted to Early Miocene to Early Pliocene and issued from the orogenic collapse, while the current phase-II extension is dominated by the tectonic escape of the Aegean-Anatolian Microplate and the roll back in the Hellenic trench since the Late Pliocene. They indicated that the short-lived intervening contractional phase occurred from Middle Miocene to Middle Pliocene.

Poisson et al. (2003a) also showed that the tectonic history of the Isparta Angle region has several phases, with the main events in the Late Cretaceous (initial shortening), pre-Miocene (Antalya Nappe emplacement), and Late Miocene/Pliocene (Aksu thrusting). They demonstrated that the Aksu phase of thrusting reactivated older thrusts, giving rise to the most prominent relief of the area, the Davras Dağ. Poisson et al. (2003b) showed that the mid-Pliocene successions are clearly involved in the Aksu Thrust phase. They documented that the Aksu Thrust is younger than previously believed (i.e., post-Late Pliocene), and suggested that the east-west compressional Aksu phase must be synchronous with the north-south sinistral strike-slip along the Dead Sea transform fault system, as well as the north-south compression and uplift which affected the Pliocene successions in north Cyprus. Poisson et al. (2003a) also noted that the two N–S-trending Aksu and Köprüçay basins developed as half grabens controlled by extensional and.or strıke-slip faults such as the Kırkkavak Fault and the Aksu Thrust.

Ten Veen and Kleinspehn (2002) used land investigations to delineate two phases of neotectonic deformation in the Apolakkia Basin on the Island of Rhodes, separated by a kinematic change at ~4.5 Ma (Fig. 5.2). They suggested that the Apolakkia Basin developed as a Late Miocene fault wedge basin in response to the syn-depositional southwest-northeast D1 extension with similar strain patterns in the adjacent inner Hellenic Arc. They attributed the kinematic change at ~4–5 Ma to a threshold of obliquity whereby the inner forearc started to experience sinistral-oblique divergence. They suggested that the Pliocene-Pleistocene D2 transtensional phase reoriented the basin

and resulted in the combined syn-depositional west-north – westeast-southeast extension and 070 sinistral shear. They further suggested that the principal shear zones offshore also occur consistently at ~070 , mimicking the D2 kinematic history of the Apolakkia Basin (Fig. 5.2). They concluded that the upper crust of the expanding Aegean-Anatolian block behaved independently at its leading edge, and the Pliny trench constitutes a major boundary separating partitioned forearc slivers, a post-4.5 Ma partitioning recorded reliably by the Pliocene fill of the Apolakkia Basin.

Van Hinsbergen et al. (2007) showed that the Island of Rhodes represents an uplifted block in the largely submerged southeastern Aegean forearc. They used palaeomagnetic data to document that the island experienced two phases of counterclockwise rotation: a 9 6 rotation between 3.8 and 3.6 Ma, and a 17 6 rotation since 0.8 Ma. They showed that between these two phases of rotation, the Island of Rhodes tilted to the southeast, drowning the southeastern coast to a depth of 500–600 m between 2.5 and 1.8 Ma, then to the northwest, which resulted in the re-emergence of the drowned relief between 1.5 and 1.1 Ma. They suggested that these rotations are related to the formation of the south Aegean sinistral strike-slip system and the foundering of the Rhodes Basin.

Aksu et al. (2009) used high-resolution multi-channel seismic reflection profiles to show that the Anaximander Mountains experienced a Miocene contractional tectonic phase characterised by an east-west trending and south-verging fold-thrust belt. They suggested that this compressional tectonic phase finalised in the latest Miocene is

replaced by a tectonic regime dominated by transpression and rotation in the Pliocene. They speculated that the Anaximander and the Anaximenes Mountains developed as the result of the reactivation, uplift and rotation of a linked, thick-skinned pre-Messinian imbricate thrust fan. They further commented that the Anaximander and Anaximenes Mountains experienced a progressive counterclockwise rotation. On the other hand, they suggested clockwise rotation of the Anaxagoras Mountain and the Florence Rise. They interpreted the Sırrı Erinç Plateau as a major Pliocene-Quaternary transpressional fault system.

Hall et al. (2009) used high-resolution multi-channel seismic reflection profiles to study the evolution of the Rhodes Basin. They suggested that the basin evolved during a period of Miocene convergence which resulted in the development of a south-southeast verging fold-thrust belt, which ended in the late Miocene. They raised the absence of the Messinian evaporites in the Rhodes Basin, thus suggesting that the region must have remained above the depositional base of marine evaporitic environment during the Messinian crisis. They further suggested that a second phase of deformation started in the middle Pliocene-Quaternary and that it is characterized by a northeast-southwest sinistral transpression, and rapid regional subsidence. They attrubuted the evolution of the Rhodes Basin to the subsidence which is associated with loading of the large imbricate thrust panels that carry the western Tauride Mountains in the north (Fig. 5.1).

Van Hinsbergen et. al. (2010) reevaluated the timing and amount of rotation of the eastern limb of the Aegean orocline, located in SW Turkey by conducting a

detailed paleomagnetic study on lower Miocene strata in the Bey Dağları area. They acquired a large scale paleomagnetic array and sampled two composite sections over Korkuteli and Doğantaş including the lower Miocene foreland basin stratigraphy from the Aquitanian unconformity with the Bey Dağları limestones to the uppermost Burdigalian-lowermost Langhian. They also used pre-existing data to combine with their new data to have better data coverage and with their reassessment they suggested that the Bey Dağları region underwent no rotation between the late Cretaceous and late Burdigalian, and 20 counterclockwise rotation between 16 and 5 Ma. i.e. during the middle to late Miocene and prior to deposition of previously reported non-rotated Pliocene sediments north of Antalya. Thus, they suggest that the rotation of the eastern and the western limbs of the Aegean orocline was simultaneous with their new age constraints of 16-5 Ma in the east, compared with (largely) 15-8 Ma in the west, as previously published. They further speculate that the rotation of the Bey Daglan was bounded in the south at the plate boundary with Africa, and in the east by the Aksu thrust and Kirkkavak dextral strike-slip fault, which together partitioned dextral transpression induced by the rotating block.

Poisson et. al. (2003a, 2011) indicated that the rifting and creation of the Pamphylian Basin occurred in the Late Permian-Early Triassic which was situated between the two continental blocks (Beydağları and Anatolian) was named the Isparta Angle , Late Cretaceous-Early Paleocene convergence and collision closing of the basin and expelled it over continental blocks and the Antalya Nappes. They stated that the Neogene Antalya Basin developed above this paleogeography. They suggested that the

final collision of the continental microplates and closure of Isparta Angle occured in Late Miocene-Early Pliocene and the final position of the Antalya Complex over Beydaglari occured in Langhian, thus, the Neogene basins are associated with the latest compressional events. They concluded with suggesting that the orientation of the basins was affected by the early tectonism and that the infill of the basins was affected by the erosion of the uplifted continental areas. (Fig.5.4)

5.2 Structural evolution of the Finike Basin and environs

The structural architecture of the Finike Basin and vicinity is fully described in Chapter 4 and is summarized here to provide a precise framework and for the development of a tectonic model. Despite the fact that the tectonic and structural architecture of the study area is described under the heading of five morpho-tectonic domains (i.e., Domain 1 -Southwestern Antalya Basin, Domain 2 -Transition from Antalya Basin to Anaxagoras Mountain, Domain 3 -Finike Basin, Domain 4 -northern fringes of Sırrı Erinç Plateau, Domain 5 -Turkish Continental Margin), the following discussion will be done holistically using three temporal divisions: pre-Messinian, Messinian and post-Messinian (i.e., Pliocene-Quaternary).

5.2.1 Pre-Messinian

The pre-Messinian successions across the entire study area show the presence of a very prominent, generally northeast-southwest trending and invariably northwest-verging fold-thrust belt, except in the southern fringes of the Antalya Basin where there is a small

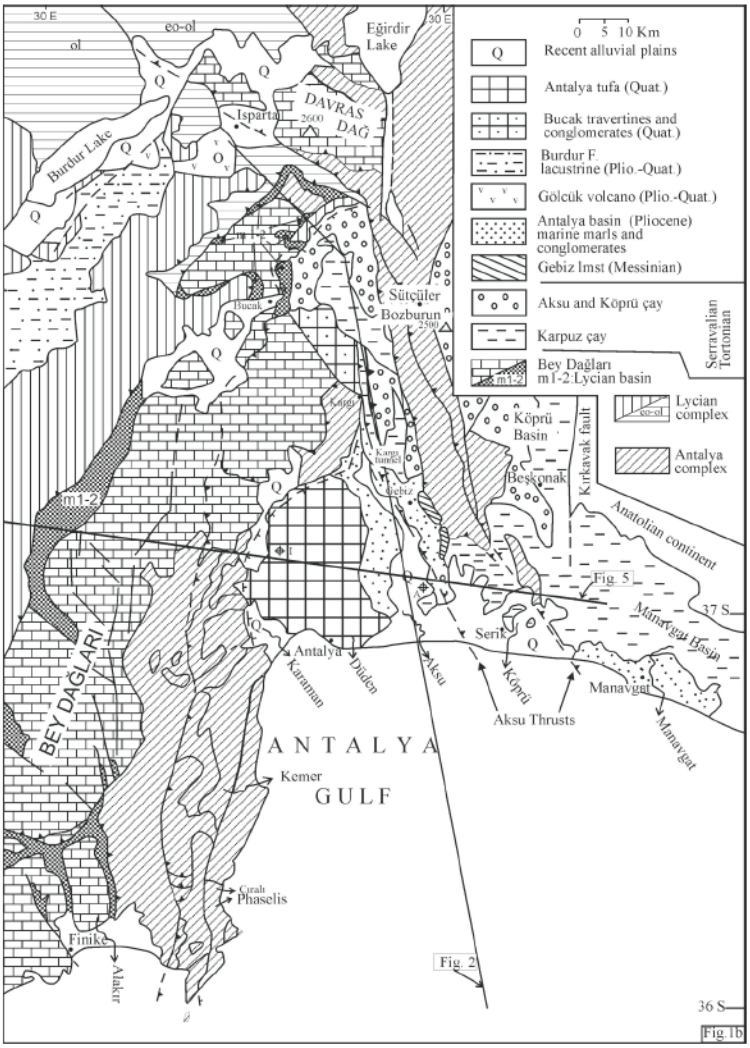

Figure 5.4. Map showing geology of the Isparta Angle (from Poisson et. al., 2011)

northeast-southwest trending and southeast-verging thrust. This major fold-thrust belt shows similar trend and vergence with the fold-thrust belt mapped in the inner portion of the western Antalya Basin (e.g., Işler et al., 2005; King in progress), as well as across the entire Kemer Peninsula (Dilek and Rowland, 1993). The thrusts in this belt are largely pre-Messinian structures. In the southwestern Antalya Basin, these thrusts generally cut the N-reflector and tip at or immediately beneath the M-reflector, soling deep within the pre-Messinian Unit 3. Across the northern fringes of the Anaxagoras Mountain, the entire Finike Basin, the northern margin of the Sırrı Erinç Plateau, as well as the eastern portion of the Turkish continental margin these thrusts display growth strata wedges developed within Unit 3, on their piggy-back basins, thus are also pre-Messinian in origin. However, this fold-thrust belt was reactivated in the Pliocene-Quaternary, as elaborated below. The prominent unconformities at the N-reflector (where Messinian evaporites are present) and the M-reflector (where Messinian evaporites are absent) decapitated the uppermost portion of the pre-Messinian successions (see Chapter 4). Therefore, the growth stratal development in the pre-Messinian cannot be determined. Because the thrusts often cut the M-reflector and extend into the Pliocene-Quaternary, the timing of thrusting cannot be clearly delineated. The fact that growth strata wedges are developed in the pre-Messinian Unit 3 in the Antalya Basin (this study, King in progress) and the Sırrı Erinç Plateau (Aksu et al., 2009), and possibly in the Finike Basin (this study) suggest that the fold-thrust belt was clearly active during the Miocene.

During the Miocene, a major foredeep existed between the Eurasian Plate in the north and the north-moving African-Arabian Plate in the south. This foredeep extended from the former Bitlis Ocean, across the present-day eastern Mediterranean toward the Ionian Sea (Faccenna at al., 2006), and constituted the eastern arm of the Tethys Ocean. During the initial collision between the Eurasian and African-Arabian Plate, the eastern promontory collided with the Eurasian Plate, creating the Bitlis-Zagros suture and closing the communication of the Tethys Ocean with the larger Panthalassa Ocean to the east. This collision is the tectonic event that fragmented the northern margin of the African Plate and the southern margin of the Eurasian Plate, creating several smaller continental blocks, namely the Arabian, Aegean-Anatolian, Black Sea and the Apulian Microplates. This event culminated in the Messinian, and profoundly influenced the tectonic framework of the entire eastern Mediterranean Sea. For example, there are broadly east-west and/or northeast-southwest trending fold thrust belts mapped in the Iskenderun Basin (Aksu et al., 2005a), Latakia and Mesaoria Basins (Hall et al., 2005a, Calon et al., 2005a,b), Cyprus Basin (Hall et al., 2005b), the Antalya Basin (Işler et al., 2005), Rhodes Basin (Hall et al., 2009), the greater Anaximander Mountains (Aksu et al., 2009), as well as the Florence Rise and the greater Cyprus Arc (Sellier et al., 2011, Sellier et al., 2012). Across these basins, the common structural theme has been the presence of very large ramp anticlines which developed over crustal-scale imbricate thrusts. The present day sedimentary framework in the regions is dominated by the development of piggy-back basins associated with these thrusts.

The study area was a segment within this very large foredeep that occupied the narrow corridor which developed during the initial closure of the Tethys Ocean. The smaller-scale irregularities along the plate margins invariably created regionally restricted tectonic provinces. One such province is the Isparta Angle (Yağmurlu et al., 1997). The Isparta Angle is a north-convex triangular-shaped tectonic province in southern Turkey. It constitutes one of the most important features in southern Turkey which can be correlated with other major lineaments in the eastern Mediterranean such as the Kyrenia Range of northern Cyprus (e.g., King, in progress). The Isparta Angle is bounded to the west by the Lycian Nappes, beyond which, the Burdur-Fethiye Fault zone is characterized by sinistral strike-slip faults with considerable normal dip-slip component (Şaroğlu et al., 1987; Price and Scott, 1994; Barka et al., 1997). The Isparta Angle is bounded to the east by the Beyşehir, Hoyran and Hadim Nappes (Monod, 1977). During the Miocene, the western limb of the Isparta angle, including the Beydağları carbonate massif experienced a 30° counterclockwise rotation (Kissel and Poisson, 1987; Morris and Robertson, 1993), whereas the eastern limb experienced a 40° clockwise rotation since the Eocene (Kissel et al., 1990). The Isparta Angle was developed as the result of the Tertiary closure of the Pamphylian Basin, which originally separated the Beydağları and the Western Taurus platforms during the Mesozoic (Poisson et al., 2003b).

In a recent work van Hinsbergen et. al. (2010) indicated that the western limb of the Isparta Angle near the Beydağları complex (hereafter referred to as the Beydağları Block) experienced a 20 counterclockwise rotation between 16 and 5 Ma. If this rotation

is correct, then it is critical that the kinematic model developed in the study area accommodes this rotation, but more importantly that the boundaries of the rotating crustal fragments be firmly delineated. The western boundary of the Beydağları Block was probably accommodated by the prominent Burdur-Fethiye Fault Zone, a 40-50 km wide zone that occupies the Eşen River valley in southwestern Turkey and extends toward the apex of the Isparta Angle (Fig. 5.4 from Hall et al.2014). The Burdur-Fethiye Fault Zone is characterized by numerous NE-SW trending normal faults with sinistral strike slip deformation, as well as a series of northwest-southeast trending normal faults (Fig. 5.5 from Hall et al. 2014; Şenel, 1997 a,b; Şenel and Bölükbaşı, 1997). For example, the hippodrome of the ancient Lycian town of Cibyra is sinistrally offset by 50 cm (Akyüz and Altunel, 2001), confirming that the Burdur-Fethiye Fault is a presently active sinistral strike-slip fault zone. First motions of recent earthquakes do not readily corroborate this (Hall et. al., 2009). A mix of motions is observed, as discussed later. Hall et al. (2009) suggested that the Burdur Fethiye Fault Zone evolved through the reactivation of the pre-Messinian contractional structures. van Hinsbergen et al. (2010) speculated that the eastern margin of the Beydağları Block was probably accommodated by the dextral transpressional shear along either the Kırkkavak Fault and/or the Aksu thrust in the greater onland Antalya Basin. The critical question here is whether the eastern boundary of the Beydağları Block extends this far to the east or if it occurs along the present-day continental margin of the westernmost Antalya Basin, east of the Kemer Peninsula.

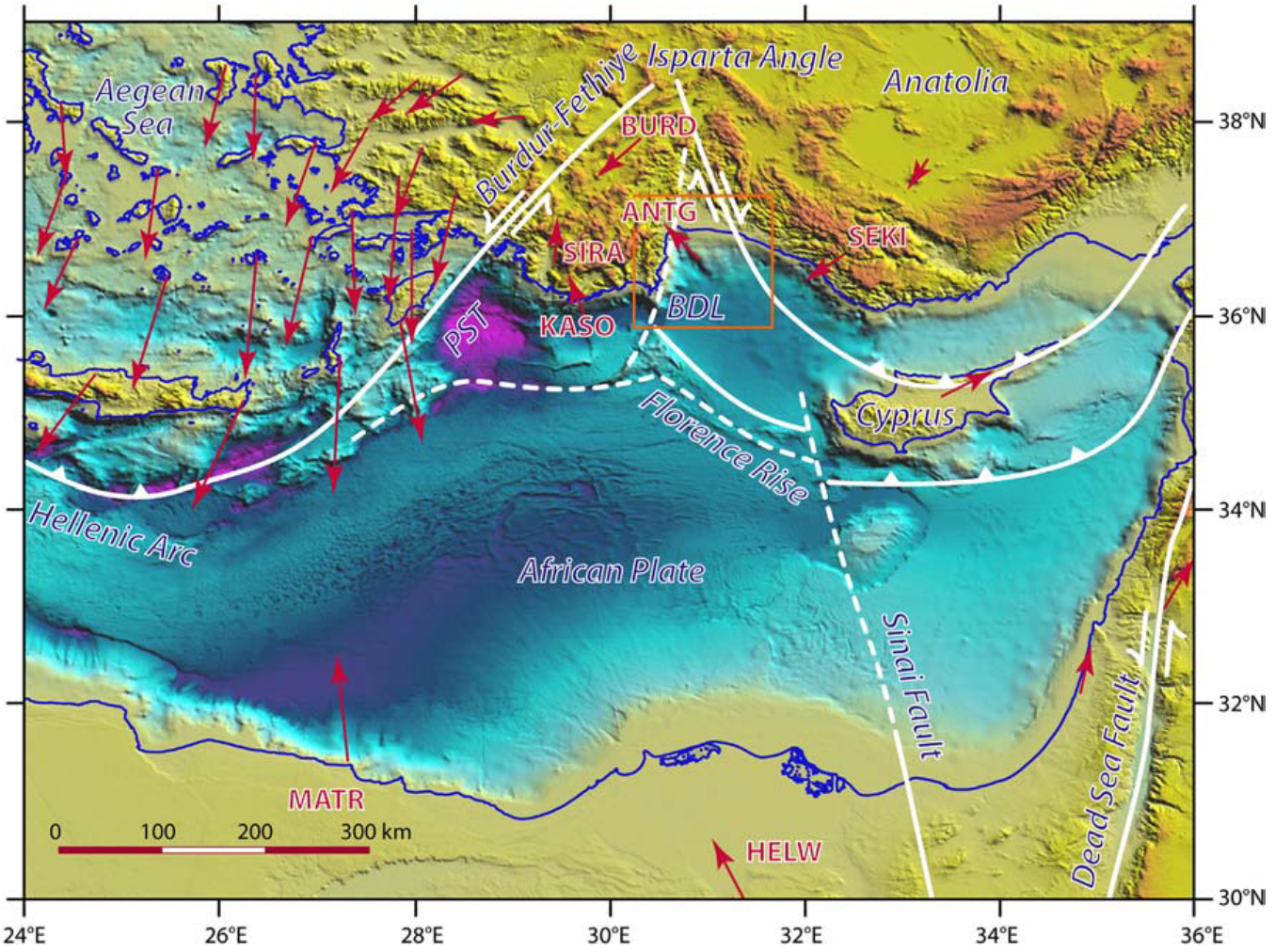

Fig. 5.5. Physiography of the easternMediterranean Sea showing a selection of GPS vectors, relative to a fixed Anatolia, redrawn from McClusky et al. (2000). The topography and bathymetry are compiled from GeoMapApp (Ryan et al., 2009), the coastline and the selected isobaths contours are from the International Oceanographic Commission (1981). PST = Pliny–Strabo trenches, BDL = Beydağları Lineament. Strike-slip motions across major lineaments indicated by GPS vectors are shown in red,with possible extensions indicated with dashed arrows in the triangular area south of the Isparta Angle. (Hall et.al 2014)

Savaşçın et al. (1995), Yağmurlu et al. (1997) and Savaşçın and Oyman (1998) showed that the volcanism along the apex of the Isparta angle was clearly associated with a major N-S trending fault zone and that this fault zone has notable dextral strike slip movements (Fig. 5.3). Barka et al. (1995) and Barka et. al. (1997) also identified a major strike-slip fault extending from the apex of the Isparta Angle southward into the eastern Mediterraenan Sea; however they indicated this zone as a sinistral strike slip system (e.g., Fig 14 of Barka et al., 1997). Aksu et al. (2009) also speculated in their model that a major sinistral strike-slip system may have developed along the westernmost Antalya Basin, although the suggested sinistral sense of the zone is not in keeping with the onland data from Savaşçın et al. (1995), Yağmurlu et al. (1997) and Savaşçın and Oyman (1998). The data presented in this dissertation also suggest the presence of a major fault zone along the westernmost Antalya Basin, extending with a north northeast-south southwest trend into the easternmost Finike Basin (also see Pliocene-Quaternary below). This fault zone occupies the present-day continental margin, east of the Antalya Complex onland, and is referred to as the Antalya Fault Zone (Savaşçın et al., 1995). If the Antalya Fault Zone is a dextral strike-slip fault, then it is possible that the eastern margin of the Beydağları Block is situated along this north northeast-south southwest trending zone, and not the Kırkkavak Fault and/or the Aksu thrust as suggested by van Hinsbergen et al. (2010). However, because the seismic data in this area are poor in the deeper portions, the Miocene tectonic activity cannot be confirmed, rendering the eastern boundary of the Beydağları Block speculative.

Furthermore, if the Antalya Fault Zone is a sinistral strike-slip system, then it cannot be the eastern boundary of the Beydağları Block: in this scenario, the most likely candidates are the Kırkkavak Fault and/or the Aksu Thrust as initially suggested by van Hinsbergen et al. (2010).

A critical question here is where is the southern boundary of the Beydağları Block The possible candidates for this are (i) the boundary between the Sırrı Erinç Plateau and the deep Finike Basin or (ii) the southern margin of the Anaximenes Mountain and the lineation that defines the boundary between the Anaxagoras Mountain in the east and the Sırrı Erinç Plateau and the Anaximander Mountain in the west. The southern boundary of the Beydağları Block can be comfortably placed at the northern fringes of the Sırrı Erinç Plateau. The suggested 20 counterclockwise rotation of the Beydağları Block in the Late Miocene (i.e., 16 and 5 Ma) necessitates a major contraction south of the Beydağları Block (Fig. 5.3). The data presented in this thesis support the presence of large, crustal-scale thrusts at the boundary between the Finike Basin and the Sırrı Erinç Plateau. These thrusts are clearly pre-Messinian in origin (Aksu et al., 2009), and they appear to be independent of the younger northeast-southwest trending and northwest-verging thrusts that cut the Pliocene-Quaternary successions in the Finike Basin. Aksu et al. (2009) proposed that the major thrust zone that defines the frontal segment of the Sırrı Erinç Plateau links with the major thrust that cores the southern margin of the Anaximander Mountain (*sensu stricto*) by a sinistral strike slip fault that

marks the western margin of the Sırrı Erinç Plateau (Fig. 5.2). It is possible that the southern margin of the Beydağları Block is delimited by this thrust/strike-slip fault zone.

The southern boundary of the Beydağları Block can also be situated at the southern margin of the Anaximenes Mountain. Aksu et al. (2009) showed that a crustal-scale imbricate thrust pair, thrust TT1 and thrust TT2 carry the Anaximander Mountain (*sensu stricto*) and the Anaximenes Mountain, respectively. They further showed that the southern thrust (i.e., TT2) of this pair can be readily traced toward the northeast defining the boundary between the Anaxagoras Mountain in the east and the Sırrı Erinç Plateau in the west. This boundary trends toward the northeast where it appears to link with the north northeast-south southwest trending zone that is characterized by relatively high-angle deeply seated extensional faults. Recall that this north northeast-south southwest trending zone is the boundary that is correlated with the dextral Antalya Fault Zone. If correct, the Antalya Fault Zone links with thrust TT2, defining the eastern and southern boundaries of the Beydağları Block.

However, these two scenarios may not be mutually exclusive, and both the boundary between the Sırrı Erinç Plateau and the deep Finike Basin and the southern margin of the Anaximenes Mountain and the lineation that defines the boundary between the Anaxagoras Mountain in the east and the Sırrı Erinç Plateau and the Anaximander Mountain in the west may form the southern boundaries of the Beydağları Block.

5.2.2 Messinian

Various previous studies in the eastern Mediterranean documented the presence of a tectonically quiet period during the Messinian interval, including the Adana, Cilicia, Iskenderun, Latakia, Cyprus, Mesaoria, Antalya and Rhodes Basins, as we as the Anaximander Mountains and the Sırrı Erinç Plateau (Aksu et al., 2005a,b, 2009; Hall et al., 2005a,b, 2009; Calon et al., 2005a,b, Burton-Ferguson et al., 2005, Işler et al., 2005). These studies related the tectonic quiescence to the final collision and suturing of the Arabian Microplate and the Aegean-Anatolian Microplate along the Bitlis-Zagros zone, and the initiation of the west-directed escape of the Aegean-Anatolian Microplate. During this interval the tectonism switched from a phase of contractional deformation into a phase of partitioned stress where contraction, extension and strike-slip deformation all occurred in regionally confined zones.

The data presented in this dissertation clearly shows that there is a major difference in the style of deformation between the pre-Messinian Miocene successions and the post-Messinian successions. The data from the western Antalya Basin show halokinetic features in Unit 2, which are developed during the Pliocene-Quaternary, and not during the Messinian. The thrusts that bound the flanks of the salt pillows and walls are also associated with halokinetic movements and are likely to be Pliocene-Quaternary in age. Other than the above, Unit 2 in the Antalya Basin contains no stratification of structures. The observations from the easternmost Finike Basin support this

interpretation. Therefore, it can be argued that the data from this study also support the period of tectonic quiescence, at least for the western Antalya Basin.

5.2.3 Pliocene-Quaternary

Previous studies clearly documented that the Pliocene-Quaternary tectonic architecture of the eastern Mediterranean basins is characterized by diverse structural elements, which are notably regionally confined. For example, gravitationally-driven extension dominates the Inner Cilicia and Inner Latakia Basins (e.g., Aksu et al., 2005a, Hall et al., 2005a), whereas contraction and halokenetic deformation dominate the Outer Cilicia and Outer Latakia Basins (Bridge et al., 2005). Similarly, deeply seated thrusting and contractional deformation dominate large-scale tectonic zones, such as the Misis-Kyrenia, Amanos-Larnaka, Aksu-Kyrenia (Aksu et al., 2005, Hall et al., 2005, Işler et al., 2005).

The study area similarly shows a distinctly partitioned strain, with normal faults occupying the westernmost Antalya Basin and the continental margin off the Kemer Peninsula, listric normal faults and associated bedding parallel detachments occupying the region that is affected by halokinetic movements in deeper western Antalya Basin (see Chapter 4). Similarly, prominent thrusts dominate the structural architecture of the Finike Basin, as well as the Sırrı Erinç Plateau (see Chapter 4). The occurrence of these diverse and seamingly conflicting structures occupying zones that are adjacent to one another appears counter intuitive. However, it shows the complexity of the tectonism and the provincialisation of the strain into distictly unique domains.

5.2.3.1 Westernmost Antalya margin normal faults

A prominent family of northeast-southwest trending, invariably southeast-dipping extensional faults define the structural architecture of the westernmost Antalya Basin, occupying a region that extends from the base of slope to the present-day shelf-to-slope break. The tip points of these faults either lie on the depositional surface where they create distinct steps on the seabed or high in Pliocene-Quaternary Unit 1 where they still created an inflection at the seabed. They invariably extend into the pre-Messinian Unit 3. These faults define a 15-25 km wide zone in the offsore. Detailed geological maps on the Kemer Peninsula onland immediately west of this fault zone show the presence of numerous north-south and/or north northeast-south southwest trending and east and/or east southeast dipping extensional faults (Şenel 1995a,b; 1997; Koçyiğit and Deveci, 2007). Similar to the northeast-southwest trending and southeast-dipping extensional faults mapped in the marine areas, these faults are also developed over the pre-existing Miocene and older thrusts. On the basis of the similarities in their trends and dip directions and their stratigraphic occurrence cutting the Pliocene-Quaternary (or being active onland today), the 15-25 km wide zone in the marine realm is extended to include the 10-20 km wide zone mapped over the onland Kemer Peninsula. Thus, the zone of high-angle extensional faults delineates a major 25-45 km wide broadly north northeast-south southwest trending zone that extends across the entire length of the Kemer Peninsula paralleling the trends of the Antalya Complex. It is readily correlated with the Antalya Fault Zone defined on the basis of the ages of the calcalkaline volcanism along

the apex of the Isparta Angle (i.e., Savaşçın et al., 1995, Yağmurlu et al., 1997, Savaşçın and Oyman 1998). This fault zone is also identified by Barka et al. (1995) and Barka and Reilinger (1997); however, they show this zone as a major sinistral strike-slip fault (e.g., Fig 14 of Barka and Reilinger, 1997).

It is clear that the Antalya Fault Zone is a major, possibly crustal-scale structure that extends from the apex of the Isparta Angle, near the town of Burdur, southward into the eastern Mediterranean Sea, delineating the broadly north northeast-south southwest trending coastline in the Antalya Bay. It is also clear that this fault zone developed during the Pliocene-Quaternary, overprinting the pre-existing Miocene and older fold-thrust belt in both the onland and the marine portions. However, there is no concensus regarding the sense of slip of the Antalya Fault Zone: while Barka et al. (1995) and Barka and Reilinger (1997) shows this as a sinistral strike slip system, Savaşçın et al. (1995), Yağmurlu et al. (1997) and Savaşçın and Oyman (1998) show it as a dextral strike slip fault zone. The data presented in this dissertation do not provide supporting evidence for either slip direction.

5.2.3.2 Halokinetic movements

One of the most prominent features of the seismic stratigraphic and structural architecture of the eastern portion of the study area is the presence of various structures associated with the mobilization of the Messinian evaporites of Unit 2 during the Pliocene-Quaternary. These structures include (i) a prominent northeast-southwest trending, generally southeast dipping fan of listric extensional faults characterizing

the Pliocene-Quaternary structural architecture near the base-of-slope region in western Antalya Basin, (ii) a series of bedding parallel detachments which divide the Pliocene-Quaternary Unit 1 into several distinct segments, and (iii) a major zone characterized by numerous salt- and/or mud-cored folds in the southwestern segment of the Antalya Basin, north of the foothills of the Anaxagoras Mountain.

During the Messinian, the eastern segment of the study area was one of the numerous isolated Messinian depocentres which received evaporite sediments. These deposits were laid down horizontally. During the Pliocene-Quaternary, the Antalya Basin received significant sedimentation from the adjacent landmass, as well as the pelagic rain from the water column. When the Pliocene-Quaternary sediments reached a critical thickness, the underlying evaporites became mobilized, creating the above indicated halokinetic structures, such as the development of the salt pillows and walls in southwestern Antalya Basin, and the developement of the west northwest-east southeast trending internally-parallel salt-cored folds that are bounded by their northern and southern margins by bi-vergent thrusts forming positive flower structures. A number of these structures appear to have been also affected by the ongoing regional deformation. For example, the considerably wide zone of bi-vergent positive flower structures developed along the foothils of the Anaxagoras Mountain running parallel to the general trend of the Florence Rise are distinctly similar to structures developed across major strike slip zones (Sellier et.al., 2011; 2012). Zitter et al. (2003) imaged similar structures in their seismic reflection profiles across the entire Florence

Rise and suggested the development of a dextral wrench to explain the Pliocene-Quaternary evolution of the greater Cyprus Arc. Therefore, it is likely that in addition to the overburden or the Pliocene-Quaternary successions, the salt-core (or mud-cored) fold-belt mapped in this study is developed in response to the strike slip deformation associated with the evolution of the Florence Rise.

The prominent northeast-southwest trending, generally southeast dipping fan of listric extensional faults are another example of deformation being affected by two distinctly different processes. The tilted domino-like architecture of the faults in this fan, and their trends paralleling the relatively high-angle faults that delineate the architecture of the western Antalya continental margin strongly suggest that this fault fan is associated with the development of the north northeast-south southwest trending Antalya Fault Zone. However, the listric trajectories of these faults soling into the Messinian evaporite Unit 2 further suggest that they are clearly affected by the Pliocene-Quaternaryt halokinetic movements.

Finally, the bedding-parallel faults that are developed solely within the Pliocene-Quaternary and are confined to the base-of-slope region in western Antalya Basin are also examples of deformation associated with halokinesis. In this region, these faults are invariably linked with the development of similar trending salt walls and/or pillows. Their tip points are situated in the upper portion of Unit 1 and generally sole into common bedding-parallel detachment surfaces. These bedding parallel detachments divide Unit 1 into several nearly-equally separated sections limited on the top and base by abutting and

truncating the surface of detachment and suggested to be a result of gravitanional sliding and slumping.

5.2.3.3 Thrusting in Finike Basin and Sırrı Erinç Plateau

The Pliocene-Quaternary architecture of the Finike Basin immediately west of the region dominated by halokinetic structures is characterized by 5-6 large thrusts that rise from the pre-Messinian successions, extending into the Pliocene-Quaternary. Growth stratal architecture in the piggy-back basins developed on the hanging wall of these thrusts clearly documented that they were active during the Pliocene-Quaternary. The development of a predominantly contractional domain, immediately west of an extensionally- or strike-slip dominated domain may appear to be counter intuitive. However, this and similar settings illustrate how profoundly the strain is partitioned in the Pliocene-Quaternary. The thrusting that is observed in Unit 1 in the Finike Basin can be explained by the continued rotation and relative southward migration of the Beydağları Block during the Pliocene-Quaternary. This 20 rotation was proposed by van Hinsbergen et al. (2010) for the Late Miocene (i.e., from 16 to 4 Ma). However, the absence of Pliocene-Quaternary successions across the Beydağları Block may have obscured age of termination of this rotation. It is possible that the rotation of the Beydağları Block continued during at least the Pliocene and possibly extending into the Quaternary. If true, the continued rotation of the Beydağları Block, will create a northwest-southeast-directed contractional regime, regardless where the southern boundary of the block may be located (i.e., either the Sırrı Erinç Plateau or the

Anaximenes Mountain). It is believed that these Pliocene-Quaternary thrusts are developed as reactivated structures over the pre-existing pre-Messinian thrusts. Similarly, the Pliocene-Quaternary thrusting observed in the Sırrı Erinç Plateau can also be explained by the accommodation of the rotation of the Beydağları Block.

Within the core of the Sırrı Erinç Plateau the structural architecture is characterized by numerous bi-vergent thrust faults where thrust surfaces converge to form the single stem of positive flower structures. This region is beyong the boundary of this dissertation. However, a quick review of the literature shows that the region is interpreted as a major shear zone developed during the Pliocene-Quaternary (e.g., Aksu et al., 2009).

5.2.4 Evolution of the Finike Basin

The Finike Basin is an enigmatic depression south of the Turkish continental margin. The basin has no Messinian evaporites of Unit 2 (except its easternmost corner), but contains a very thick Pliocene-Quaternary succession of Unit 1. The fact that there is no Unit 2 in the Finike Basin, but a thick succession of Unit 2 in the Antalya Basin to the east suggest that the Finike Basin was largely above the depositional base of the evaporites during the Messinian salinity crisis. The evolutionary history of the Finike Basin must therefore account for the elevated morphology of the region during the Messinian and the development of a deep depression with a thick siliciclastic succession during the Pliocene-Quaternary. The stacked prograded shelf deltas that are now situated in water depths of 1000-1200 m along the continental margin north of the Finike Basin suggest that the basin and its northern margin rapidly collapsed during the Quaternary. In

fact approximately 700 m of subsidence occurred in the upper Pliocene-Quaternary. The absence of detailed chronostratigraphy precludes any refinement of the onset of this rapid subsidence.

The important qauestion here is this: what mechanism was responsible for the rapid collapse of the Finike Basin during the Pliocene-Quaternary Is there evidence to support that this collapse can be readily related to structures mapped in the study area Unfortunately the data are inconclusive regarding the possible mechanism which resulted in the rapid Pliocene-Quaternary subsidence of the Finike Basin. In the absence of unequivocal structural data along the northern margin of the basin, the following speculations can be made for the possible mechanism(s) for the evolution of the Finike Basin: (1) it may have developed associated with a major south-dipping extensional fault that may be situated beneath the present-day continental margin, or (2) it may have evolved as a sag-basin associated with the loading of the evolving Taurus Mountains to the north of the basin during the Miocene and Pliocene. Both of these scenarios have pros and cons, as explained below.

Scenario 1: The high-resolution seismic reflection profiles show that the northern margin of the Finike Basin is sharp and relatively steep compared to the southern margin (see Chapter 4). The slope face is nearly barren, only covered by a very thin veneer of Pliocene-Quaternary succession. Several scoop-like detachments further superficially scraped the existing Pliocene-Quaternary succession. Several acoustically transparent lenses interpreted as debris deposits occur at

different levels within the Pliocene-Quaternary, indicating that there were mass wasting events along the relatively steep slopes of the northern Finike Basin margin. Slope instabilities may be related to overbuilding of the slope by sediments, or by a mechanical response to seismic triggering associated with earthquakes. On the basis of similarities with previously described gravity driven sediment flows (e.g., Aksu and Hiscott, 1992; Hiscott and Aksu, 1994), they are interpreted as debris flow deposits.

In the detailed descriptions of the structures, it was implicit that the architecture of the northern basin margin does not include prominent south-dipping basin bounding extensional faults. However, it is conceivable, although not probable that a low-angle listric extensional fault may be present along the northern margin of the Finike Basin. To further this speculation, a horizontally stretched seismic reflection profile is shown here (Plate 19b). The original interpretation was made in seismic profiles with 7x vertical exaggeration; whereas this horizontally stretched profiles has 3x vertical exaggeration. This more realistic profile reveal three critical inconsistencies with regard to the presence of a south-dipping extensional fault: (i) the basinal sediments can be occasionaly traced upslope, which clearly precludes the existence of a down-to-basin fault, (ii) careful calculations of the slope angles reveal that the dip of this speculated fault varies between 8.9 and 11.3 , much lower than the generally expected 30-70 dip angles on major basin-bounding faults, and (iii) there is no indication that the M-reflector is cut at the base of the Pliocene-Quaternary succession.

In one seismic reflection profile, it is possible to place an extensional fault along the northern margin of the Finike Basin (Plate 19b). This fault would be placed at the base of slope, and would dip at ~20 angle. On the basis of the presence of a clearly delineated ramp anticline imaged in the pre-Messinian successions of Unit 3, it was suggested that there is a north-verging thrust at this location (see Chapter 4). The ramp anticline and the thrust trajectory are very similar to those observed and mapped in the southern portion of the Finike Basin, thus are believed to be correct. If there is an extensional fault at the same location, it is conceivable that the extensional fault may have utilized the pre-existing zone of weakness associated with the older thrust during the Pliocene-Quaternary. However, the lack of similar possible extensional faults in the adjacent seismic reflection profiles ~5 km east and west is unsettling, because if true, such a large extensional fault ought to have been clearly imaged in these profiles as well. A possible explanation of this is that a series of such extensional faults en echelon defines the margin and that there are transfer zones between them.

Scenario 2: The development of the Finike Basin and the Rhodes Basin to the west as sag-basins are already proposed by Hall et al. (2009) and Aksu et al. (2009). They similarly showed the lack of evidence for extensional faults along the northern margins of these basins. Hall et al. (2009) documented the presence of a prominent NE-SW trending and SE verging fold-thrust belt within the Rhodes Basin. They showed that the middle Pliocene-Quaternary was marked by a transpressional episode. This architecture is nearly identical to that observed across the Sırrı Erinç Plateau, as well as

the Finike Basin. Hall et al. (2009) and Aksu et al. (2009) speculated that the Pliocene-Quaternary subsidence observed within the piggy-back basins associated with thrusts in both the Rhodes Basin, as well as the Anaximander Mountain (*sensu stricto*) is probably created by the regional flexural response associated with the thrust-loading in the evolving Taurus Mountains to the north of these basins.

It is quite possible that the rapid collapse of the Finike Basin may indeed be related to the loading of the imbricate thrust sheets across the southern segment of the western Taurus Mountains (Fig. 5.6). In this study, part of the tectonism is attributed to the development of a block rotation also centered over the western Taurus Mountains (van Hinsbergen et al. 2010, Fig. 5.3). Despite the fact that new seismic reflection profiles were collected from the Finike Basin in 2010 with a much longer streamer in order to better image the deeper structures, the tectonic architecture of the northern margin of the Finike Basin remains unresolved. A detailed kinematic study may be helpful in the deciphering of the Pliocene-Quaternary evolution of this complicated region.

5.3 Regional Synthesis

Following from Aksu et al. (2008**)** and Hall et al. (2009**)**, but adding the rotation of dextral strike slip on the Antalya Fault Zone, the following possibility of Miocene to Recent evolution can be proposed (Fig. 5.7).

During the Pliocene-Quaternary the Isparta Angle was subjected to a pincer-type squeeze resulting in the wedge to the south being pushed to the south, resulting in compression at the southern end of the Beydağları Block in the Finike Basin, sinistral

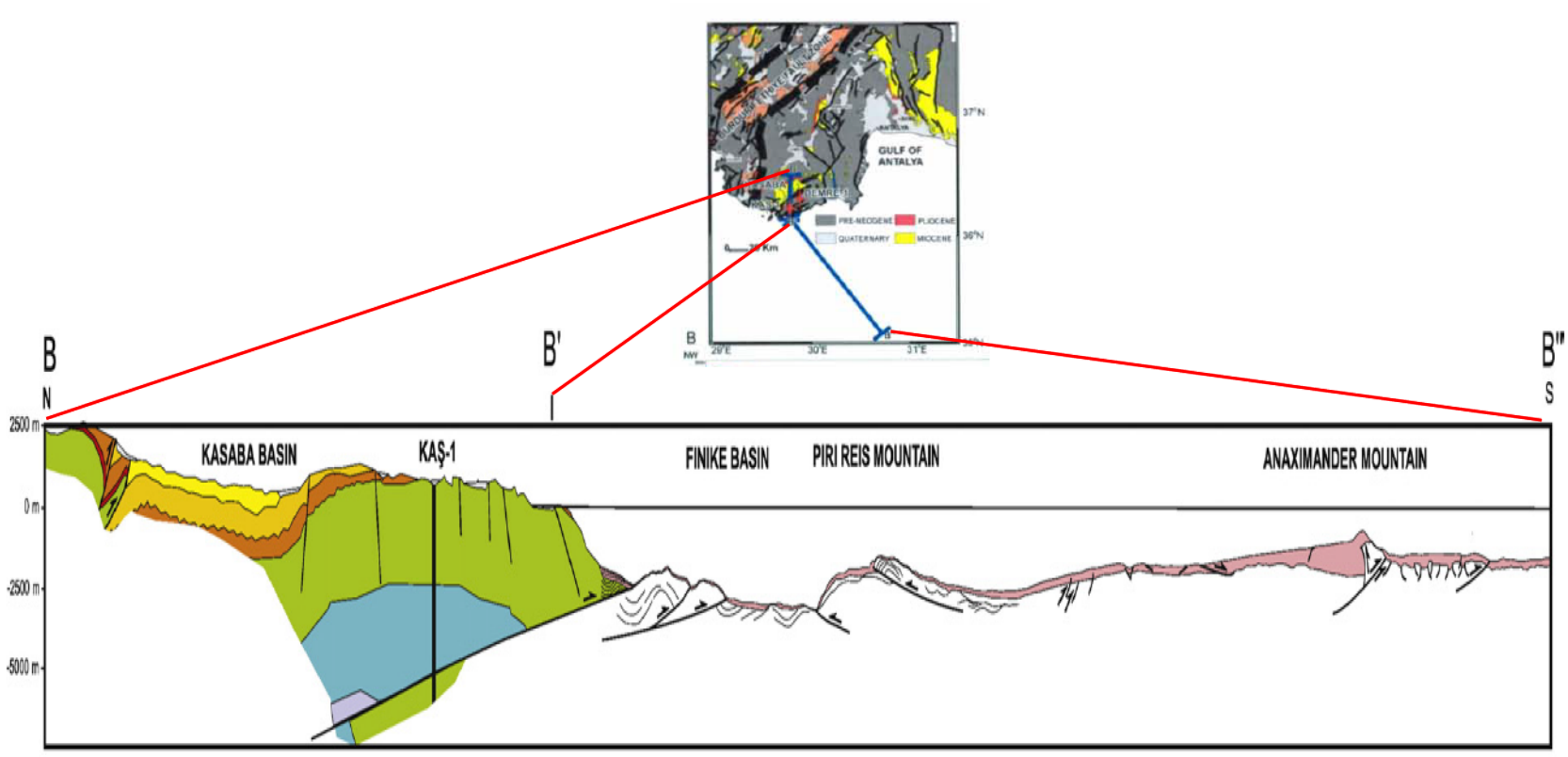

Figure 5.6 True-scale cross-section from SW Turkey to theAnaximander Mountain, based on land geology and the seismic profiles interpreted in Jeremy et. al (2009). Land cross-sections based on Şenel et al. (1994) and Şenel (1997c). Location of the cross-section is shown on the map above the cross-section (modified from Cranshaw 2010). Note the thrusting across the southern segment of the western Taurus Mountains and its suggested consequent, the uplift of the Kasaba Basin and due to its related loading. the subsıdence of the Finike Basin as a flexural response.

transpression along the Aksu Thrust and dextral strike slip along the Antalya Fault Zone and Burdur Fethiye Fault Zone. Burdur Fethiye Fault Zone also shows sinistral strike slip related to rollback of the Hellenic subduction and so first rotation along this fault is mixed-perhaps sinistral dominating to the south and dextral to the north. The origin of the P-Q subsidence of the Finike Basin in this picture would more likely relate to a sag in front of Tauride thrusting rather than extension (but the latter cannot be discounted at this stage).

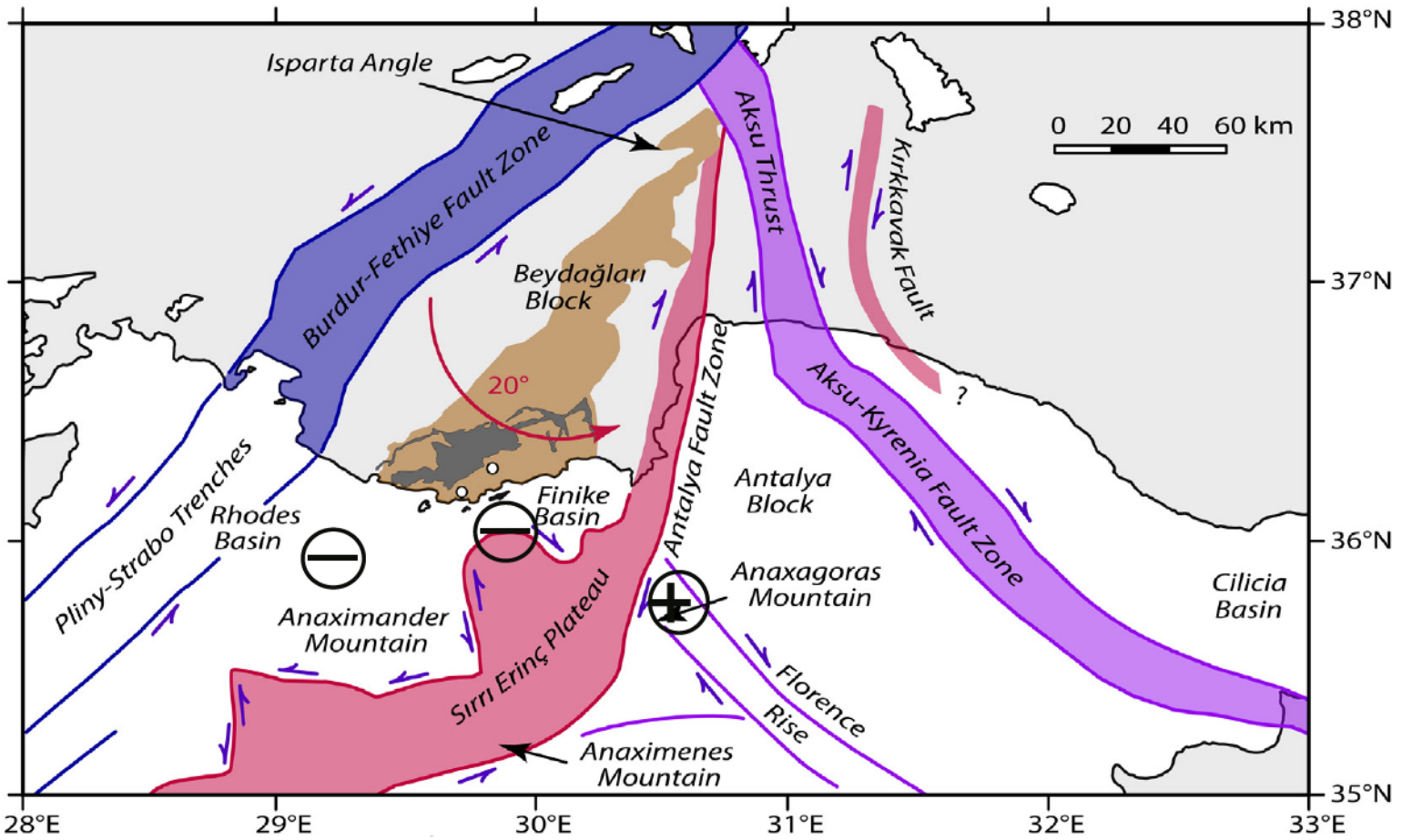

Figure. 5.7 Synthesis of the tectonic framework of the Finike Basin and environs. AB=Antalya Basin. AFZ=Antalya Fault Zone, AM=Anaximander Mountain, BFFZ= Burdur Fethiye Fault Zone, FB=Finike Basin, FR= Florence Rise, IA=Isparta Angle, PST=Pliny-Strabo Trenches, RB=Rhodes Basin, - and + signs indicate the location of subsidence and uplift, respectively. Antalya Fault Zone re-drawn from Hall et al. (2014), Savaşçın et al. (1995), Barka et al. (1995) and Barka and Reilinger (1997); the geometry of the Beydağları Block and its rotation are from van Hinsbergen et al. (2010a,b); Kırkkavak Fault is from van Hinsbergen et al. (2010a,b); Aksu–Kyrenia Fault zone is from Işler et al. (2005); Pliny–Strabo Trenches and the Burdur Fethiye Fault zone are from Hall et al. (2009); the geometry of the Sırrı Erinç Plateau is from Aksu et al. (2009), modified from Aksu et al. (2014)

Chapter Six: Conclusions

The interpretation of 3500 km of high-resolution seismic reflection profiles revealed the following salient conclusions:

- The pre-Messinian structural architecture of the Finike Basin and its immediate environs are dominated by contractional tectonics. A prominent belt of southwest-northeast trending fold-thrust belt was developed in the Early-Middle Miocene, associated with the regional contractional tectonism of the entire eastern Mediterranean. This fold-thrust belt extended northeast into the western segment of the Antalya Basin. In a regional context, this belt was part of the reactivated thrusts of the western margin of the Isparta Angle.
- During the Messinian and Early Pliocene, there was a major switch in the tectonism from contraction to distinctly partitioned strain, including extension in western Antalya Basin, to continued contraction and possible rotation in the Finike Basin, to transpression in the northern fringes of the Anaxagoras Mountains and the Sırrı Erinç Plateau.
- In the western Antalya Basin the Pliocene-Quaternary deformation is associated with listric extensional faults that invariably sole into the M-reflector and the underlying evaporite Unit 2. Mapping showed that these faults define a broad zone of extension and/or transtension along the westernmost segment of the Antalya Basin, including the continental margin. This fault zone is interpreted to define a major broadly north-south trending fault zone, linking with the dextral

Antalya Fault identified in the onland Antalya Basin, running through the apex of the Isparta Angle.

- The presence of five to six large northeast-southwest trending and northwest-verging thrusts variably cutting the Pliocene-Quaternary succession of Unit 1 in the Finike Basin indicated continued contractional deformation in this portion of the study area, west of the extensional faults of the Antalya Fault zone.
- van Hinsbergen et al (2010) suggested that the Beydağları Block experienced a 20 counterclockwise rotation during the Late Miocene to Early Pliocene. In my scenario the western and eastern margins of the block are delineated by the Burdur-Fethiye Fault Zone and the dextral Antalya Fault, whereas the southern margin of the block is speculated to be defined by the northern margin of the Sırrı Erinç Plateau and/or the southern margin of the Anaximenes and Anaxagoras Mountains.
- Previous studies suggested that the northern margin of the Finike Basin is delineated by a major south-dipping extensional fault. If there was such a fault it possibly utilized the pre-existing zone of weakness associated with the older thrust during the Pliocene-Quaternary. However, the seismic reflection data were mute regarding the presence of a major extensional fault along the northern margin of the Finike Basin, strongly suggesting that an alternative mechanism must be responsible for the development of the basin.

- The presence of stacked prograded delta successions, presently sitting in water depths of 700-1200 m depth indicate that the Finike Basin rapidly collapsed during the Pliocene-Quaternary. This rapid subsidence and the evolution of the Finike Basin is best explained by the flexural response of the crust to the loading of the thrust sheets associated with the development of the Western Taurus Mountains.

References

Akay, E. and Uysal, S., 1985. Orta Toroslar n bat s ndaki (Antalya) Neojen çökellerinin stratigrafisi, sedimantolojisi ve yap sal jeolojisi. Mineral Research Exploration Institute (MTA), unpublished report, 276 pp.

Akay, E., Uysal, S., Poisson, A., Cravette, J., Müller, C., 1985. Antalya Neojen havzas n n stratigrafisi. Bulletin of the Geological Society of Turkey, 28: 105-119.

Akhmanov, G.G., Akhmetjanov, A.M., Ivanov, M.K., Mazzini, A., van der Bosch, H., Kleeven, T.P., Korkin, A.V., Ivanova, E.K., Kozlova, E.V., Gablina, S.S., Yu Belen kaya I., van der Schans, E., Stadnitskaya, A.N. and Sautkin, A.P., 1997. Coring Results. *In*:

Akhmanov, G.G., Akhmetjanov, A.M., Ivanov, M.K., Mazzini, A., van der Bosch, H., Kleeven, T.P., Korkin, A.V., Ivanova, E.K., Kozlova, E.V., Gablina, S.S., Yu Belen kaya I., van der Schans, E., Stadnitskaya, A.N. and Sautkin, A.P., 1997. Coring Results. *In*: Woodside, J.M., Ivanov, M.K. and Limonov, A.F., ŞEds.) Neotectonics and fluid flow through seafloor sediments in the Eastern Mediterranean and Black Seas. Part 1: Eastern Mediterranean Sea. Intergovernmental Oceanographic Commission Technical Series, 48: 72-120, 128 pp.

Aksu A.E. and R.N. Hiscott, 1992. Shingled Upper Quaternary debris flow lenses on the NE Newfoundland slope. Sedimentology, 39: 193-206.

Aksu, A.E., Hall, J. and Yaltırak, C., 2005a. Editorial - Miocene to Recent tectonic evolution of the eastern Mediterranean: new pieces of the old Mediterranean puzzle. Marine Geology, 221: 1-13.

Aksu, A.E., Calon, T.J., Hall, J., Mansfield, S., and Yaşar, D., 2005b. The Cilicia–Adana Basin complex, Eastern Mediterranean: Neogene evolution of an active fore arc basin in an obliquely convergent margin. Marine Geology, 221: 121–159.

Aksu A.E., J. Hall, and Yaltırak, C., 2009. NNeogene evolution of the Anaximander Mountains and Finike Basin at the Junction of Hellenic and Cyprus Arcs, Eastern Mediterranean. Marine Geology, 258: 24-47.

Aksu, A.E., Hall, J., C. Yaltırak, Çınar, E., Küçük, M., Çifçi, G., 2014. Late Miocene–Recent evolution of the Finike Basin and its linkageswith the Beydağlari complex and theAnaximander Mountains, eastern Mediterranean, Tectonophysics, http://dx.doi.org/10.1016/j.tecto.2014.04.042

Akayüz, H.S. and Altunel, E., 2001. Geological and archaeological evidence for post-Roman earthquake surface faulting at Cibyra, SW Turkey, Geodinamica Acta, 14, 95–101.

Anastasakis, G., Kelling, G., 1991. Tectonic connection of the Hellenic and Cyprus Arcs and related geotectonic elements. Mar. Geol. 97, 261– 277.

Barka, A., Reilinger, R., Şaroğlu, F. and Şengör, A.M.C. 1995. The Isparta angle: its importance in the neotectonics of the eastern Mediterranean region, IESCA-1995 Proceedings, 3-17.

Barka, A., Reilinger, R., aroğlu, F., and engör, C. 1997. The Isparta Angle: Its importance in the neotectonics of the eastern Mediterranean region. *In*: O. Pi∏kin,

Bridge, C., Calon, T.J., Hall, J. and Aksu, A.E., 2005. Salt tectonics in two convergent margin basins of the Cyprus Arc, northeastern Mediterranean. Marine Geology 221: 223-259.

Burton-Ferguson, R., Aksu, A.E., Calon, T.J., and Hall, J., 2005. Seismic stratigraphy and structural evolution of the Adana Basin, Eastern Mediterranean. Marine Geology, 221: 189-222.

Calon, T.J., Hall, J. and Aksu, A.E., 2005. The Oligocene-Recent evolution of the Mesaoria Basin (Cyprus) and its western marine extension, Eastern Mediterranean. Marine Geology, 221: 95-120.

Calon, T.J., Aksu, A.E. and Hall, J., 2005. The Neogene evolution of the Outer Latakia Basin and its extension into the Eastern Mesaoria Basin (Cyprus), Eastern Mediterranean. Marine Geology, 221: 61-94.

Ciner, A., Karabiyikoglu, M., Monod, O., Deynoux, M. & Tuzcu, S., 2008. Late Cenozoic sedimentary evolution of the Antakya basin, southern Turkey. Turkish J. Earth Sci., 17, 1, 1-41.

Cita, M.B., Wright, R.C., Ryan, W.B.F. and Longinelli, A., 1978. Messinian Paleoenvironments. In: K. Hsü, L. Montadert et al., Initial Reports of the Deep Sea Drilling Project XLII, Part I, p. 1003-1035. U.S. Government Printing Office, Washington.

Cleintaur, M.R., Knox, G.J., Ealey, P.J., 1977. The geology of Cyprus and its place in the eastern Mediterranean framework. Geol. Mijnb. 56 (1), 66-82.

Çiçek, A., Koçyiğit, A., 2009. A NNE-trending active graben in the Isparta Angle, SW Turkey: Karamık Graben, its geometry, age and earthquake potential. Trabajos de Geologia, Vol. 29, 168-174.

Cranshaw, J., Aksu, A., Hall, J., Çifçi, G., Dondurur, D., Yaltırak, C., 2009. The junction of Hellenic and Cyprus arcs: a detailed study of the morphology and Neogene tectonic evolution of the Anaximander Mountains. EGU 2009, TS6.6/G27/GD21/SM3.1, Halls X/Y.

Cranshaw, J., 2010. Seismic acquisition, processing and Interpretation of the Anaximander Seamounts in the Eastern Mediterranean Sea. Master's thesis, Memorial University of Newfoundland, Newfoundland, Canada.

Dewey, J.F. and Şengör, A.M.C., 1979. Aegean and surrounding regions: complex multiplate and continuum tectonics in a convergent zone. Geol. Soc. Amer. Bull., 90, 84-92.

Dilek, Y. and Rowland, J.C. 1993. Evolution of conjugate passive margin pair in Mesozoic southern Turkey. Tectonics 12, 954-970.

Dimitrov, L. I., 2002. Mud volcanoes the most important pathway for degassing deeply buried sediments. Earth-Science Reviews, 59(1–4), 49–76.

Dobrin, M.B., 1976. Introduction to geophysical prospecting (3d ed.). New York, McGraw-Hill, 619 p.

Dumont, J.F., and Woodside, J.M., 1997. Dredging Results.*In*: Woodside, J.M., Ivanov, M.K. and Limonov, A.F., (eds.) Neotectonics and fluid flow through seafloor sediments in the Eastern Mediterranean and Black Seas. Part 1: Eastern Mediterranean Sea. Intergovernmental Oceanographic Commission Technical Series, 48: 65-71, 128pp.

Faccenna, C., Martinod, O.B.J., Regard, C.P.V. 2006. Slab detachment beneath eastern Anatolia: A possible cause for the formation of the North Anatolian fault. Earth and Planetary Science Letters 242 (2006) 85 – 97, Available online 10 January 2006

Gaullier, V., Mart, Y., Bellaiche, G., Mascle, J., Vendeville, B. C., Zitter, T., & Party, S. L. P. I. I. S., 2000. Salt tectonics in and around the Nile deep-sea fan: insights from the PRISMED II cruise. Geological Society, London, Special Publications, 174 (1), 111–129.

Glover, C.P., Robertson, A.H.F., 1998a. Role of regional extension and uplift in the Plio-Pleistocene evolution of the Aksu Basin, SW Turkey. J. Geol. Soc. (Lond.) 155, 364 – 387.

Glover, C.P., Robertson, A.H.F., 1998b. Neotectonic intersection of the Aegean and Cyprus tectonic arcs: extensional and strike-slip faulting in the Isparta Angle, SW Turkey. Tectonophysics 298, 103 – 132.

Govers, R., Wortel, M.J.R., 2005. Lithosphere tearing at STEP faults: Response to edges of subduction zones, Earth Planet. Sci. Lett. 236, 505–523.

Gunes, P., 2010. Miocene to recent stratigraphy, structural architecture and tectonic evolution of the Florence Rise, Eastern Mediterrenean Sea.Master's thesis, Dokuz Eylül University, İzmir, Turkey.

Hall, J., Aksu, A.E., Calon T.J., Yaşar, D, 2005a. Varying tectonic control on basin development at an active microplate margin: Latakia Basin Eastern Mediterranean. Marine Geology, 221: 15-60.

Hall, J., Aksu, A.E., King, H., Gogacz, A., Yaltırak, C., Çifçi, G., 2014. Miocene–Recent evolution of the western Antalya Basin and its linkage with the Isparta Angle, eastern Mediterranean Marine Geology 349, 1–23

Hall, J., Calon, T.J., Aksu, A.E., and Meade, S.R., 2005b. Structural evolution of the Latakia Ridge and Cyprus Basin at the front of the Cyprus Arc, Eastern Mediterranean Sea. Marine Geology 221: 261-297.

Hall, J., Aksu, A.E., Yaltırak, C., Winsor, J.D., 2009. Structural architecture of the Rhodes Basin: a deep depocentre that evolved since the Pliocene at the junction of Hellenic and Cyprus Arcs, eastern Mediterranean. Marine Geology, 258: 1-23.

Hayward., A.B. 1984. Miocene clastic sedimentation related to the emplacement of the Lycian nappes and the Antalya Complex, SW Turkey. In: Dixon., J.E & Robertson A.H.F (eds), The geological Evolution of the Eastern Mediterranean. Geological Society London, Special Publications 17, 287-300.

Hendricks, K.B., Singhal, V.R., 1997. Delays in new product introductions and the market value of the firm: the consequences of being late to the market. Management Science 43, 422–436.

Hinsbergen, D. J. J.., Dekkers, M. J., Koç, A., 2010. Testing Miocene Remagnetization of Bey Dağları: Timing and Amount of Neogene Rotations in SW Turkey. Turkish J. Earth Sci., 19, 123–156.

Hiscott, R.N., and Aksu, A.E., 1994. Submarine debris flows and continental slope evolution in front of Quaternary ice sheets, Baffin Bay, Canadian Arctic. American Association of Petroleum Geologists Bulletin, 78 (3): 445-460.

Hsüü, K.J., Cita, M.B. and Ryan, W.B.F., 1973. The origin of the Mediterranean evaporites. In: W.B.F. Ryan, K. Hsü, et al., Initial Reports of the Deep Sea Drilling Project 13 Ş1), p. 1203-1231. U.S. Government Printing Office, Washington.

Islamoğlu, Y. & Taner G., 2002. Molusc content and stratigraphy of the Uçarsu ve Kasaba formations in Kasaba Miocene basin. Bulletin of Mineral Research and Exploration 125: 31-57

Işler, F.I., Aksu, A.E., Hall, J., Calon T.J, and Yaşar, D., 2005. Neogene development of the Antalya Basin, Eastern Mediterranean: an active fore-arc basin adjacent to an arc junction. Marine Geology, 221: 299-330.

Jongsma, D., and J. Mascle 1981. Evidence for northward thrusting south-west of the Rhodes basin. Nature, 293, 49-51.

Karabıyıkoğlu, M., Çiner, A., Monod, O., Deynoux, M., Tuzcu, S., Örçen, S., 2000. Tectonosedimentary evolution of the Miocene Manavgat Basin, western Taurides, Turkey. Tectonics and Magmatism in Turkey and the Surrounding Area, Special Publication Geological Society, London, vol. 173, pp. 271 – 294.

Kissel, C. and Poisson, A., 1987. tude pal omagnetique preliminaire des formations C nozoiques des Beydağlar (Taurides ocidentales, Turquie). C. R. Acad. Sci. Paris 304 (8), 343-348.

Koçyiğit, A., nay, E. and Saraç, G., 2000. Episodic graben formation and extensional neotectonic regime in west Central Anatolia and the Isparta Angle: a case study in the Akşehir-Afyon Graben, Tukey. Geol. Soc. London Spec. Pbl. 173: 405-421.

Koçyiğit, A., Deveci, Ş., 2007. A N-S-trending Active Extensional Structure, the Şuhut (Afyon) Graben: Commencement Age of the Extensional Neotectonic Period in the Isparta Angle, SW Turkey. Turkish Journal of Earth Sciences, 16, p.391-416.

Krebes, E.S., and Hearn, D.J., 1985. On the geometrical spreading of viscoelastic waves. Bulletin of the Seismological Society of America, 75: 391-396.

Krebes, E.S., 1989. Seismic Theory and Methods: Geophysics 551 course notes, University of Calgary, 4.1 - 4.18.

Le Pichon, X., Angelier, J., 1979. The Hellenic Arc and Trench system: A key to the neotectonic evolution of the Eastern Mediterranean area. Tectonophysics, 60, 1-42.

Mascle, J., Le Quellec, P., Leite, O., and Jongsma, D., 1982. Structural sketch of the Hellenic continental margin between the western Peloponnesus and eastern Crete. Geology, 10, 113-116.

McClusky, S., Balassinian, S., Barka, A., Demir, C., Ergintav, S., Georgiev, I., Gurkan, O., Hamburger, M., Hurst, K., Kahle, H., Kastens, K., Kekelidze, G., King, R., Kotzev, V., Lenk, O., Mahmoud, S., Mishin, A., Nadariya, M., Ouzonis, A.M., Paradissis, D., Peter, Y., Prilepin, M., Reilinger, R., Sanli, I., Seeger, H., Tealeb, A., Toksöz, M.N., Veis, G., 2000. Global Positioning System constraints on plate kinematics and dynamics in the eastern Mediterranean and Caucasus. Journal of Geophysical Research 105 (B3), 5695–5719.

Mitchum, M. R., Jr., Vail, P. R. and Sangree, J. B., 1977a. Seismic stratigraphy and global changes of sea level, Part 6: Stratigraphic interpretation of seismic reflection patterns in depositional sequences. *In*: C. E. Payton (Editor), Seismic Stratigraphy Applications to Hydrocarbon Exploration. Memoir of the American Association of Petroleum Geologists, 26: 117-135.

Mitchum, R.A.Jr., Vail, P.R. and Thompson III, S., 1977b. Seismic stratigraphy and global change of sea level. Part 2: The depositional sequence as a basic unit for stratigraphic analysis. *In*: C.E. Payton (Editor), Seismic Stratigraphy Applications to Hydrocarbon Exploration. American Association of Petroleum Geologists. Memoir, 25: 53-62.

Monod, O., 1977. Recherces g ologiques dans le Taurus occidentales au sud de Beyşehir (Turquie). Th se de Doctorat d= tat s Sciences, Universit de Paris-Sud, Orsay, France. 442 pp.

Moores, E.M., Robertson, P.T., Malpas, J., Xenophontos, C., 1984. Model for the origin of the Troodos massif, Cyprus and other Mideast ophiolites. Geology 12, 223-226.

Morris, A., and Robertson, A.H.F., (1993). Miocene remagnetism of carbonate platform and Antalya Complex units within the Isparta Angle, southwest Turkey, I. Tectonophysics, 220:243-266.

Myers, K.J. and Milton, N.J., 1996. Concepts and principles of sequence stratigraphy. *In*: D. Emery and K.J. Myers (Eds.), Sequence Stratigraphy. Blackwell Science, p. 11-44, 297 pp.

Önalan, M., 1979. Geology of the field between Elmalı and Kaş (Antalya). Doctoral dissertation, YTU Monographies, 131 p.

Papazachos BC, Papaioannou CA. Lithospheric boundaries and plate motions in the cyprus area. *Tectonophysics*. 1999;308(1–2):193-204. doi: 10.1016/S0040-1951(99)00075-X

Piercey, T., 2011.A seismic reflection study of the Neogene sedimentary history of the outer Cilicia basin, Eastern Mediterranean. Master's thesis, Memorial University of Newfoundland, NNewfoundland, Canada

Pinous, O.V., M.A. Levchuk, and D.L. Sahagian, 2001, Regional synthesis of the productive Neocomian complex of West Siberia; sequence stratigraphic framework: AAPG Bulletin, v. 85/10, p. 1713-1730.

Poisson, A., Yağmurlu, F., Bozcu, M., Şentürk, M., 2003.New insight on the tectonic setting and evolution around the apex of the Isparta Angle, SW Turkey). Geological Journal, 38: 257-282.

Poisson, A., Wernli, R. Sağular, E.K. and Temiz, H., 2003. New data concerning the Age of the Aksu thrust in the south of the Aksu valley, Isparta Angle (SW Turkey): consequences for the Antalya Basin and the eastern Mediterranean. Geological Journal, 38: 311-327.

Poisson, A., Orszag-Sperber, F., Koskun, E., Bassetti, M., Muller, C., Wernli, R. and Rouchy, J., 2011.The late Cenozoic evolution of the Aksu basin (Isparta Angle; SW Turkey).New insights.Ball. Soc. Geol. Fr., t. 182, no 2, pp. 133-148

Price, S. and Scott, B., 1994.Fault-block rotations at the edge of a zone of continental extension; southwest Turkey. J. Struct. Geol., 16, 381-392.

Robertson, A.H.F., 1998. Mesozoic-Tertiary tectonic evolution of the easternmost Mediterranean area: integration of marine and land evidence. *In*: A.H.F Robertson, K.C.

Robertson, A.H.F., 2000. Mesozoic-Tertiary tectonic-sedimentary evolution of a south Tethyan oceanic basin and its margin in southern Turkey. *In*: E. Bozkurt, J.AQ. Winchester and J.D. Piper (Eds.) Tectonics and Magmatism in Turkey and the Surrounding Area. Geological Society, London, Special Publications, 173: 43-82.

Robertson, A.H.F. and Dixon, J.E., 1984. Introduction: aspects of the geological evolution of the Eastern Mediterranean. In: The Geological Evolution of the Eastern Mediterranean, J.E. Dixon and A.H.F. Robertson ŞEds), Blackwell Scientific Publications, Oxford, Geological Society Special Publication 17: 1-74, 824 pp.

Robertson, A.H.F., Eaton, S., Follows, E.J., Payne, A.S., 1995. Depositional processes and basin analysis of Messinian evaporites in Cyprus. Terra Nova 7, 233–253.

Robertson, A.H.F., 1998. Mesozoic–Tertiary tectonic evolution of the easternmost Mediterranean area: integration of marine and land evidence. In: Robertson, A.H.F., Emeis, K.C., Richter, C., Camerlenghi, A. (Eds.). Proceeding of the Ocean Drilling Program, Scientific Results, vol. 160, pp. 723–782.

Ryan, W.B.F., 1969. The floor of the Mediterranean Sea. PhD Thesis, Columbia University, New York, 236 pp.

Ryan, W.B.F., Carbotte, S.M., Coplan, J.O., O'Hara, S., Melkonian, A., Arko, R., Weissel, R.A., Ferrini, V., Goodwillie, A., Nitsche, F., Bonczkowski, J., Zemsky, R., 2009. Global multi-resolution topography synthesis. Geochemistry, Geophysics, Geosystems. http://dx.doi.org/10.1029/2008GC002332 (10: Q03014).

Sage, L., Letouzey, J., 1990. Convergence of the African and Eurasian plate in the eastern Mediterranean. In: J. Letouzey (Ed.). Petroleum and Tectonics in Mobile Belts, Edition Technip, Paris, pp. 49-68, 224 pp.

Savaşçın, M. Y., Francalanci, L., Innocenti, T., Manetti, P., Birsoy, R., Dağ., 1995.Miocene–Pliocene potassic–ultrapotassic volcanism of the Afyon–Isparta region (central western Anatolia, Turkey): Petrogenesis and geodynamic implications. International Earth Sciences Colloquium on the Aegean Region (IESCA-1995), Proceedings,V-II,pp.487–502.

Savaşçın, M. Y., Oyman, T., 1998. Tectono-Magmatic Evolution of Alkaline volcanics at the Kırka-Afyon-Isparta Structural Trend, SW Turkey. Turkish Journal of Earth Sciences, 7, 201-215.

Şaroğlu, F., Boray, A., Emre, O., 1987. Active faults of Turkey. Mineral Research Exploration Institute (MTA), Turkey, unpublishedreport 8643, 394 pp.

Sellier, N.C., Vendeville, B.C, Loncke, L., 2011. Interactions between deep-seated and salt tectonics along the Western Cyprus Arc (Florence ridge). Part II: experimental modelling. Tectonophysics, Available online 20 July 2011

Sellier Y.C., Loncke L., Vendeville B.C., Mascle J., Zitter T., Woodside J., Loubrieu B., 2012. Post-Messinian evolution of the Florence Ridge area (Western Cyprus Arc), Part I: Morphostructural analysis. Tectonophysics, Available online 13 April 2012.

Şengör, A.M.C., Görür, N. and Şaroğlu, F., 1976 Strike-slip faulting and related basin formation in zones of tectonic escape: Turkey as a case study. Society of Economic Paleontologists and Mineralogists, Special Publication 37: 227-264.

Şengör, A.M.C., Yılmaz, Y., 1981. Tethyan evolution of Turkey: a plate tectonic approach. Tectonophysics 75: 181-241.

Şengör, A.M.C., S. Ozeren, T. Genç, E. Zor, East Anatolia high plateau as a mantle supported, north–south shortened domal structure, Geophys. Res. Lett. 30 (2003) 8045.

Şenel, M., 1997a. Geological Map of Fethiye, L8 quadrangle, No:2, 1:100,000 General Directorate of Mineral Research and Exploration, Ankara, Turkey, 22 pp.

Şenel, M., 1997b. Geological Map of Fethiye, M8 quadrangle, No:4, 1:100,000 General Directorate of Mineral Research and Exploration, Ankara, Turkey, 15 pp.

Şenel, M., Bölükbaşı, A.S., 1997a. Geological Map of Fethiye, M9 quadrangle, No:5, 1:100,000 General Directorate of Mineral Research and Exploration, Ankara, Turkey, 11 pp.

Şenel, M. and Bölükbaşı, A.S., 1997b. Geological Map of Turkey, Fethiye – M9 Sheet, 1:100,000 scale. General Directorate of Mineral Research and Exploration ŞMTA), Jeoloji Etütler Dairesi, Ankara.

Şenel, M., Selçuk H., Bilgin, Z., Şen, M.A., Karaman, T., Dinçer, M.A., Durukan, E., Arbas, A., Örçen, S. ve Bilgi, C., 1989. Geology of Çameli (Denizli) - Yeşilova (Burdur) - Elmalı (Antalya). General Directorate of Mineral Research and Exploration, Ankara, Turkey, Report 9429.

Şenel, M., Akdeniz, N., Öztürk, E.M., Özdemir, T., Kadınkız, G., Metin, Y., Öcal, H., Serdaroğlu, M. ve Örçen, S., 1994. Geology of the northern part of Fethiye (Muğla) – Kalkan (Antalya). Directorate of Mineral Research and Exploration, Ankara, Turkey, Report 9761.

Shipboard Scientific Party, 1978. Sites 375 and 376, Florence Rise. *In*: K. Hsü, L. Montadert et al., Initial Reports of the Deep Sea Drilling Project 42 Ş1), p. 219-304. U.S. Government Printing Office, Washington.

Ten Veen, J.H., Kleinspehn, K.L., 2002. Geodynamics along an increasingly curved convergent plate margin: late Miocene–Pleistocene Rhodes, Greece. Tectonics 21 (3) 21 pp. (10.1029/2001TC001287).

Ten Veen, J.H., Woodside, M., Zitter, T.A.C., Dumont, J.F., Mascle, J., Volkonskaia, A., 2004. Neotectonic evolution of the Anaximander Mountains at the junction of the Hellenic and Cyprus Arcs. Tectonophysics, 391: 35-65.

Toker, E. and Yağmurlu, F., 2010. Tentono-sedimentary evolution of the Eocene transgressive deposits in the Acigol, Burdur and Isparta areas (SW Turkey). AG Lanscape & Environment 4(2), pg. 58-70.

Van Hinsbergen, D.J.J., Krijgsman, W., Langereis, C.G., Corn e, J.-J., Duermeijer, V.E. and van Vugt, N., 2007. Discrete Plio-Pleistocene phases of tilting and counterclockwise rotation of the southeastern Aegean Arc (Rhodos, Greece): early Pliocene formation of the south Aegean left-lateral strike-slip system. Journal of Geological Society London, 164: 1133-1144

Woodside, J.M., 1977. Tectonic elements and crust of the eastern Mediterranean Sea. Mar. Geophys. Res. 3, 317– 354.

Woodside, J.M., Ivanov, M.K. and Limonov, A.F., 1997. Neotectonics and fluid flow through seafloor sediments in the Eastern Mediterranean and Black Seas. Part 1: Eastern Mediterranean Sea. Intergovernmental Oceanographic Commission Technical Series, 48.

Woodside, J., Ivanov, M.K., Limanov, A.F., 1998. Shallow gas and gas hydrates in the Anaximander Mountains region, eastern Mediterranean Sea. *In*: Henriet, J.-P., Mienert, J. (Eds.), Gas Hydrates: Relevance to World Margin Stability and Climate Change. Geological Society, London, Special Publications, 137: 177–193.

Woodside, J., Mascle, J., Huguen, C., Volkonskaia, A., 2000. The Rhodes Basin, a post-Miocene tectonic trough. Marine Geology, 165, 1–12.

Woodside, J., Mascle, J., Zitter, T., Limonov, A., Ergün, M., Volkonskaia, A., 2002. The Florence Rise, the Western Bend of the Cyprus Arc. Marine Geology 185, 175–194.

Yağmurlu, F., Savaşcın, Y. and Ergün, M., 1995. Relation of alkaline volcanism and active tectonism within the evolution of Isparta Bend, SW-Turkey. International Earth Sciences Colloquium on Aegean Regions 9-14 October 1995, Güllük, Izmir-Turkey, Abstracts, p.58.

Yağmurlu, F., Savaşcın, Y. and Ergün, M., 1997. Relation of alkaline volcanism and active tectonism within the evolution of Isparta Angle, SW-Turkey. The Journal of Geology, v.105, 717-728.

Yılmaz, Ö., 2001. Seismic Data Analysis: Processing, Inversion and Interpretation of Seismic Data (2 Volumes). Investigations in Geophysics No: 10. Society of Exploration Geophysicists.

Zanchi, A., Kissel C., and Tapirdamaz, C., 1990. Continental deformation in Western Turkey: a structural and paleomagnetic approach. International earth sciences congress on Aegean regions, Oct 1990, 357-367.

Zitter, T., Woodside, J., Mascle, J., 2003. The Anaximander Mountains: a clue to the tectonics of southwest Anatolia. Geological Journal, 38, 375-394.

http://www.glossary.oilfield.slb.com/Display.cfm Term=bow%20tie

http://principles.ou.edu/seismic explo/reflect/reflect.html

http://www.glossary.oilfield.slb.com/DisplayImage.cfm ID=227

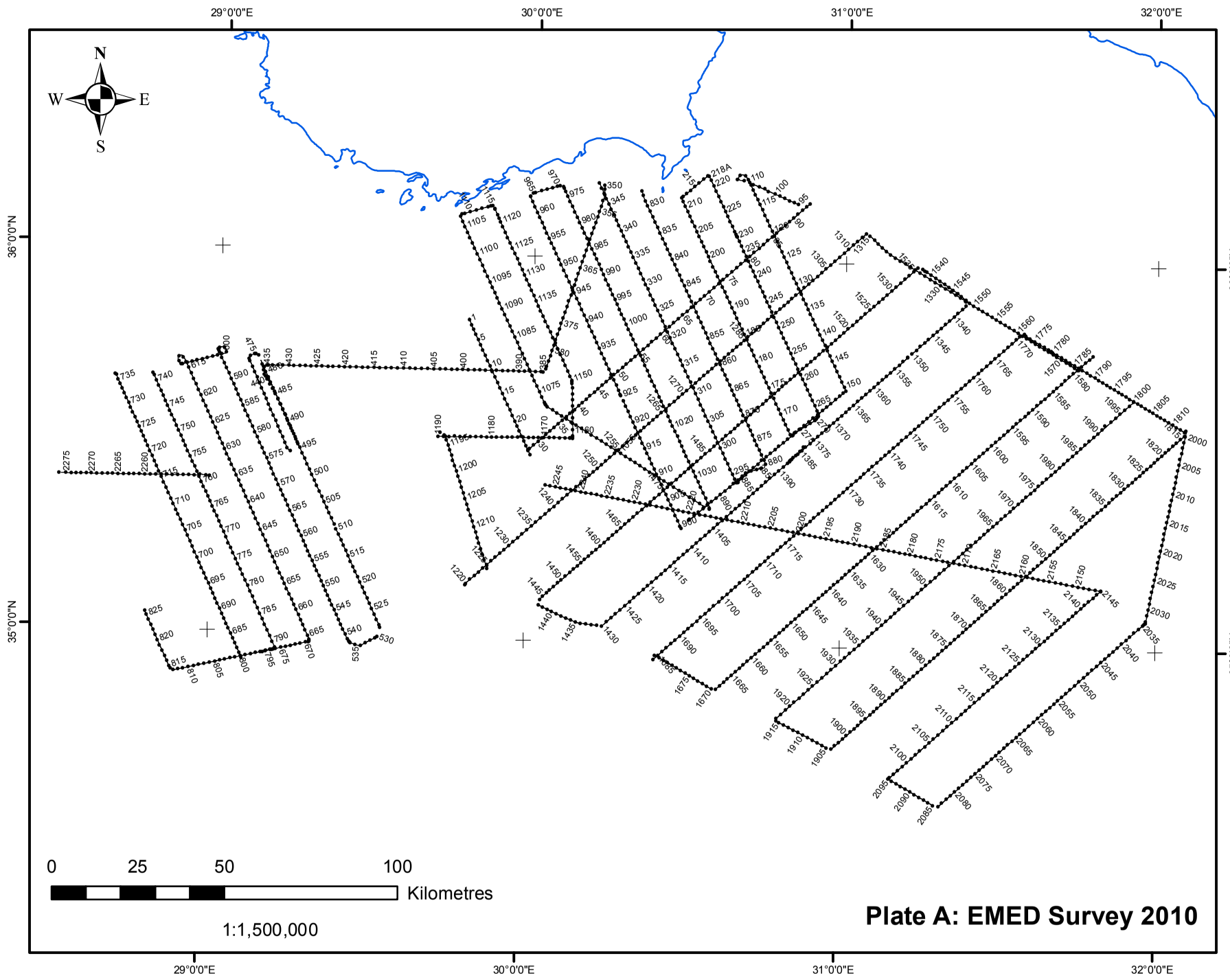
29°0'0"E
30°0'0"E
31°0'0"E
32°0'0"E
36°0'0"N
35°0'0"N
N
W
E
S
0
25
50
100
Kilometres
1:1,500,000
Plate A: EMED Survey 2010

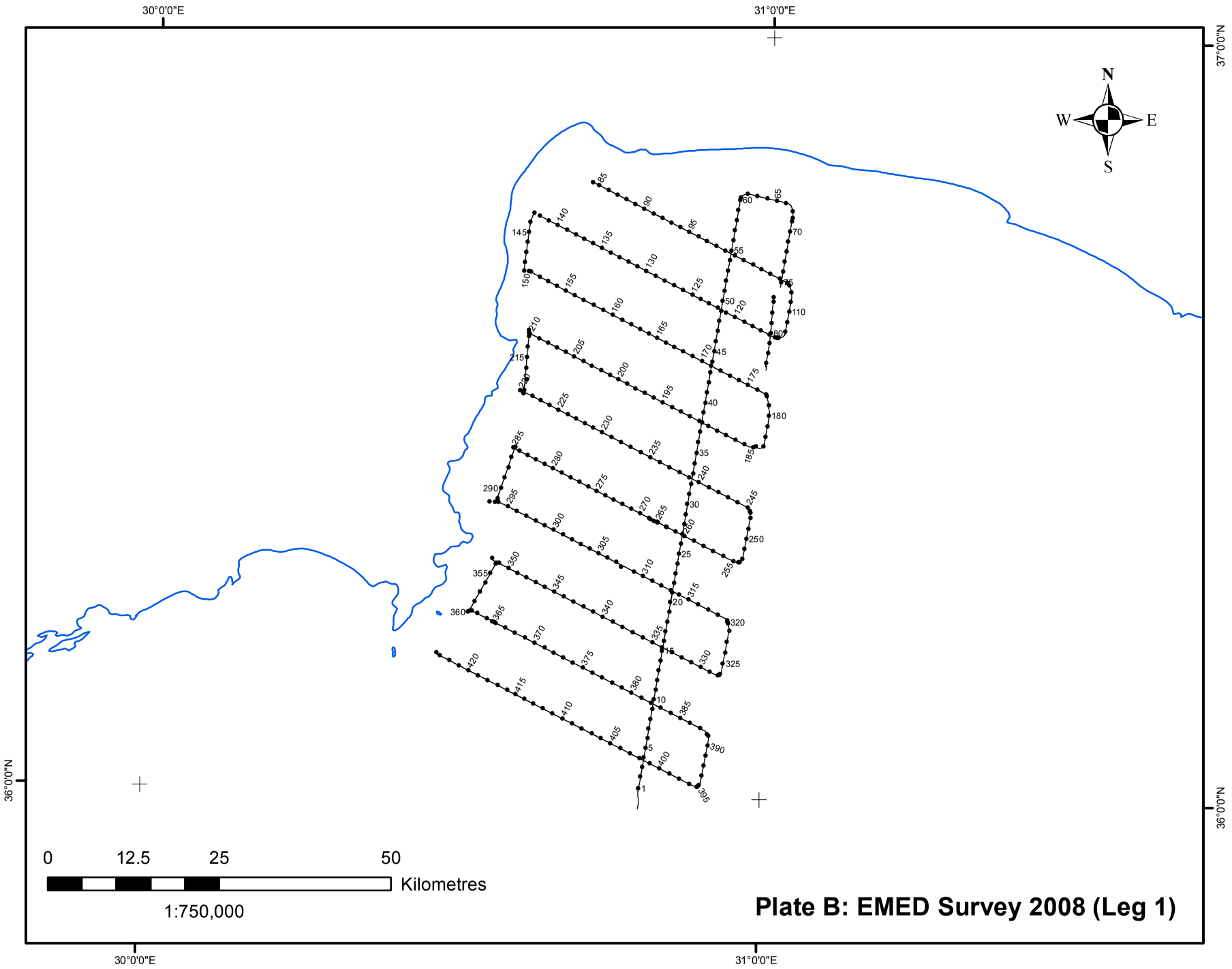

Plate B: EMED Survey 2008 (Leg 1)

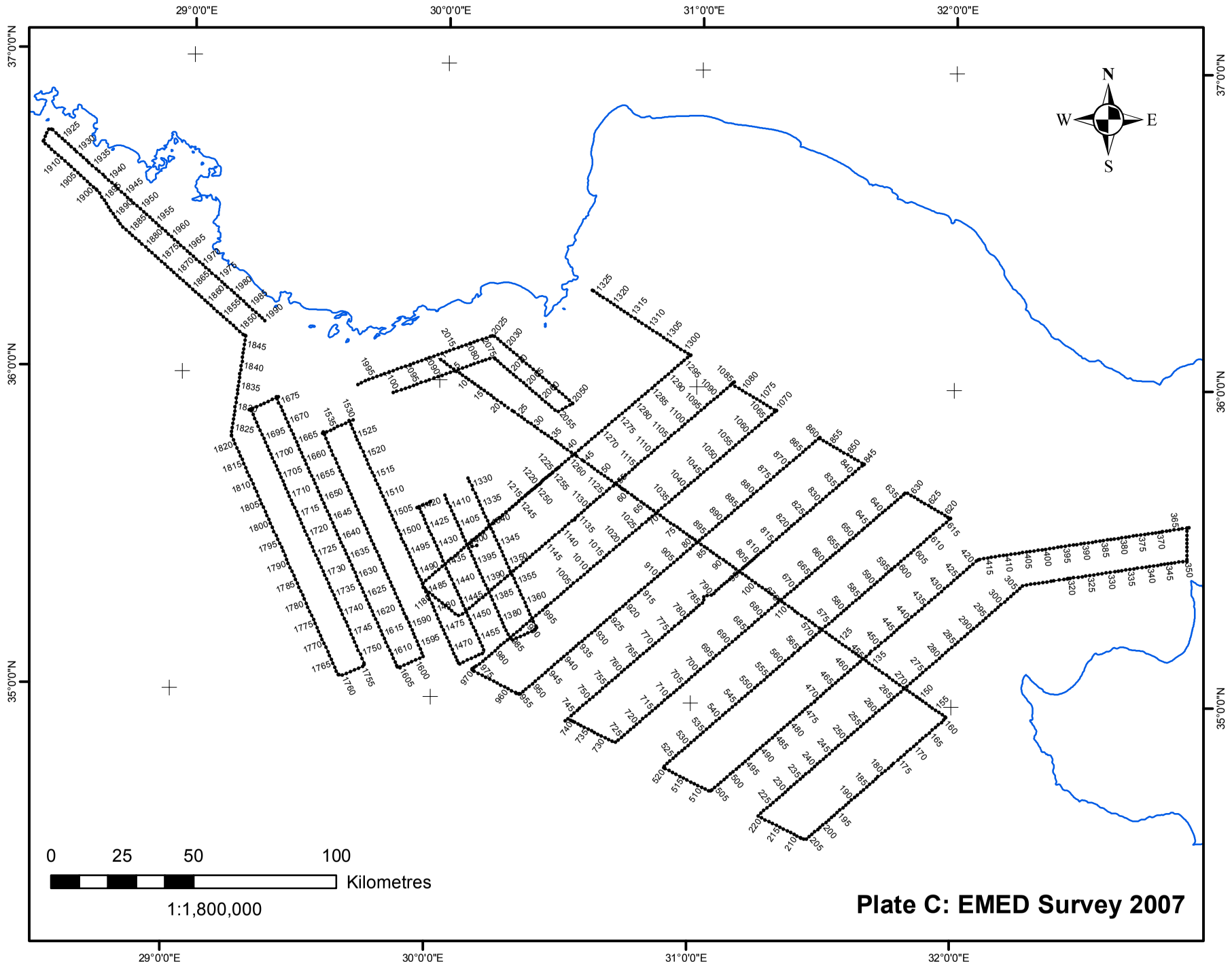
29°0'0"E
30°0'0"E
31°0'0"E
32°0'0"E
37°0'0"N
36°0'0"N
35°0'0"N
N
W
E
S
0
25
50
100
Kilometres
1:1,800,000
Plate C: EMED Survey 2007

Plate 1

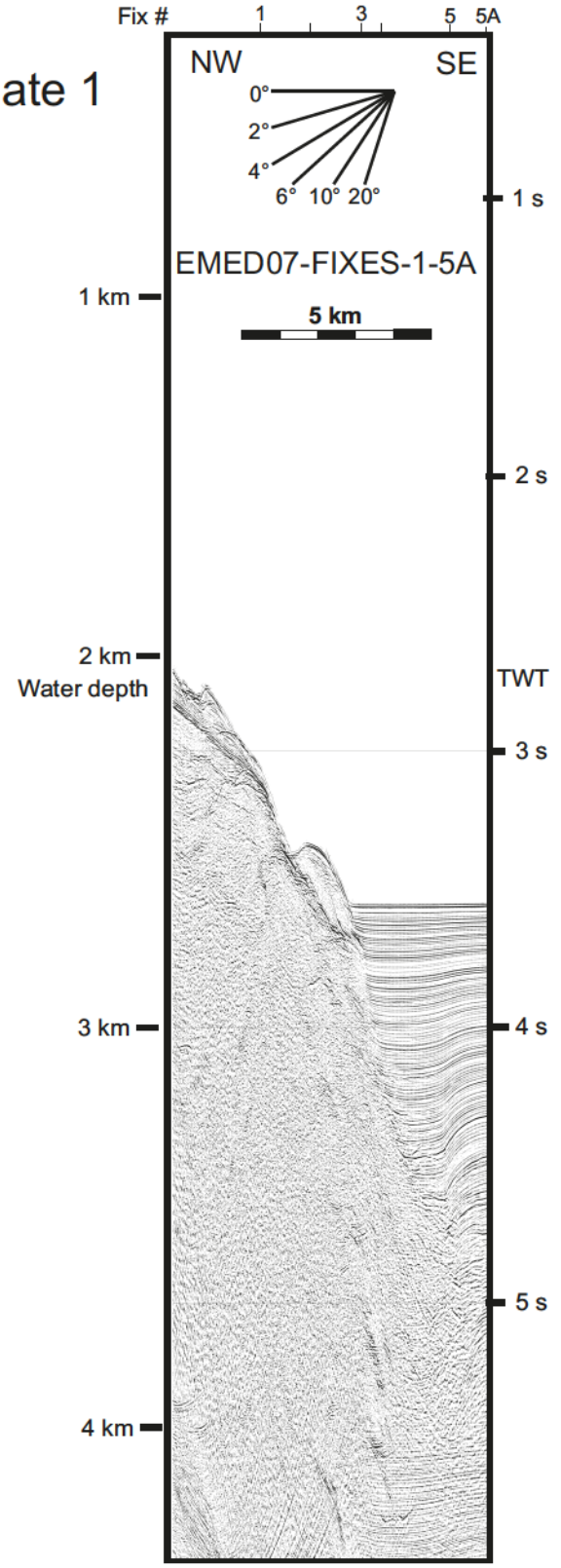
Fix #
1
3
5
5A
NW
SE
0°
2°
4°
6°
10°
20°
1 s
EMED07-FIXES-1-5A
1 km
5 km
2 s
2 km
Water depth
TWT
3 s
3 km
4 s
5 s
4 km

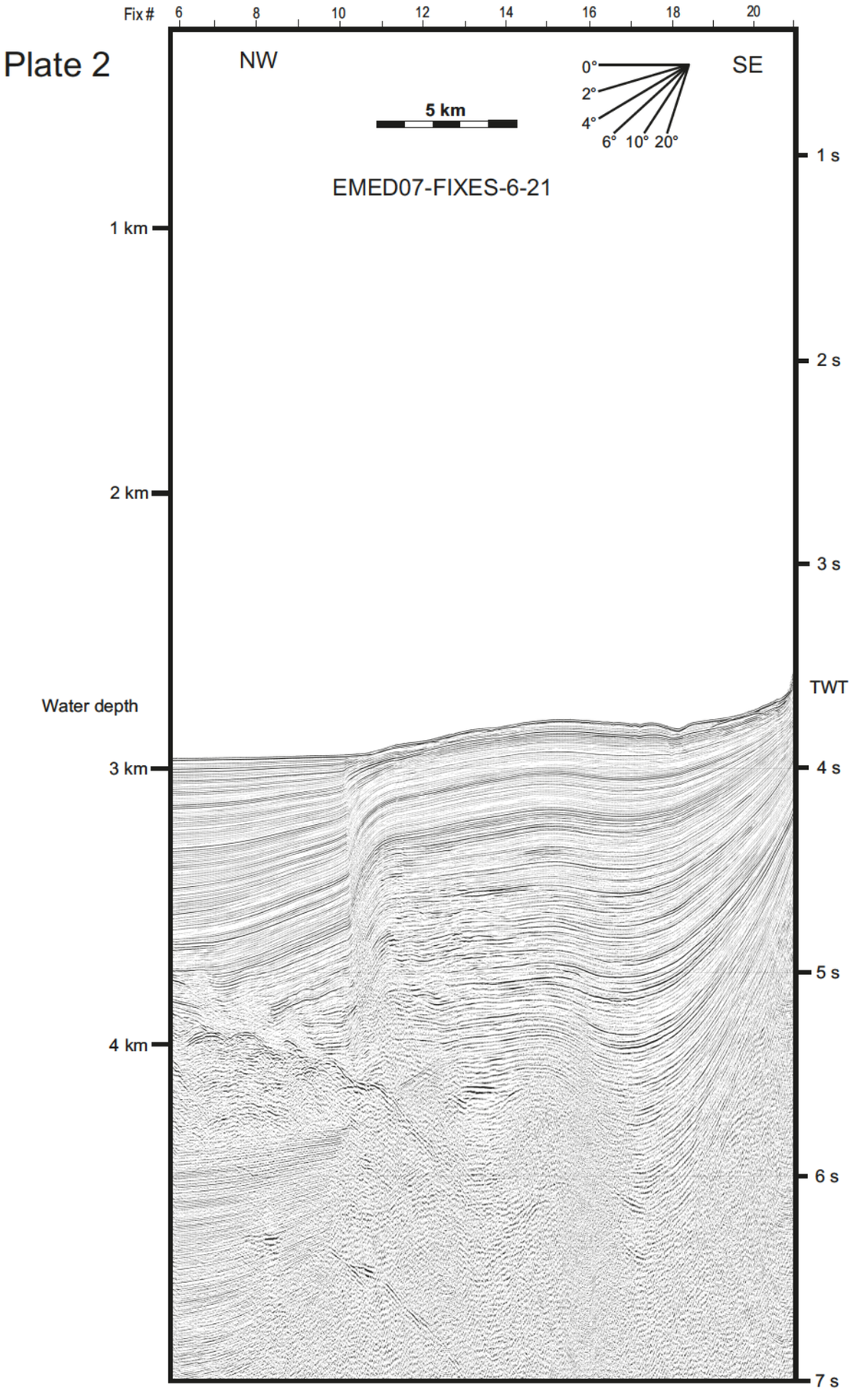
Plate 2
Fix #
6
8
10
12
14
16
18
20
NW
SE
0°
2°
4°
6°
10°
20°
5 km
EMED07-FIXES-6-21
1 km
2 km
3 km
4 km
Water depth
1 s
2 s
3 s
TWT
4 s
5 s
6 s
7 s

Plate 3

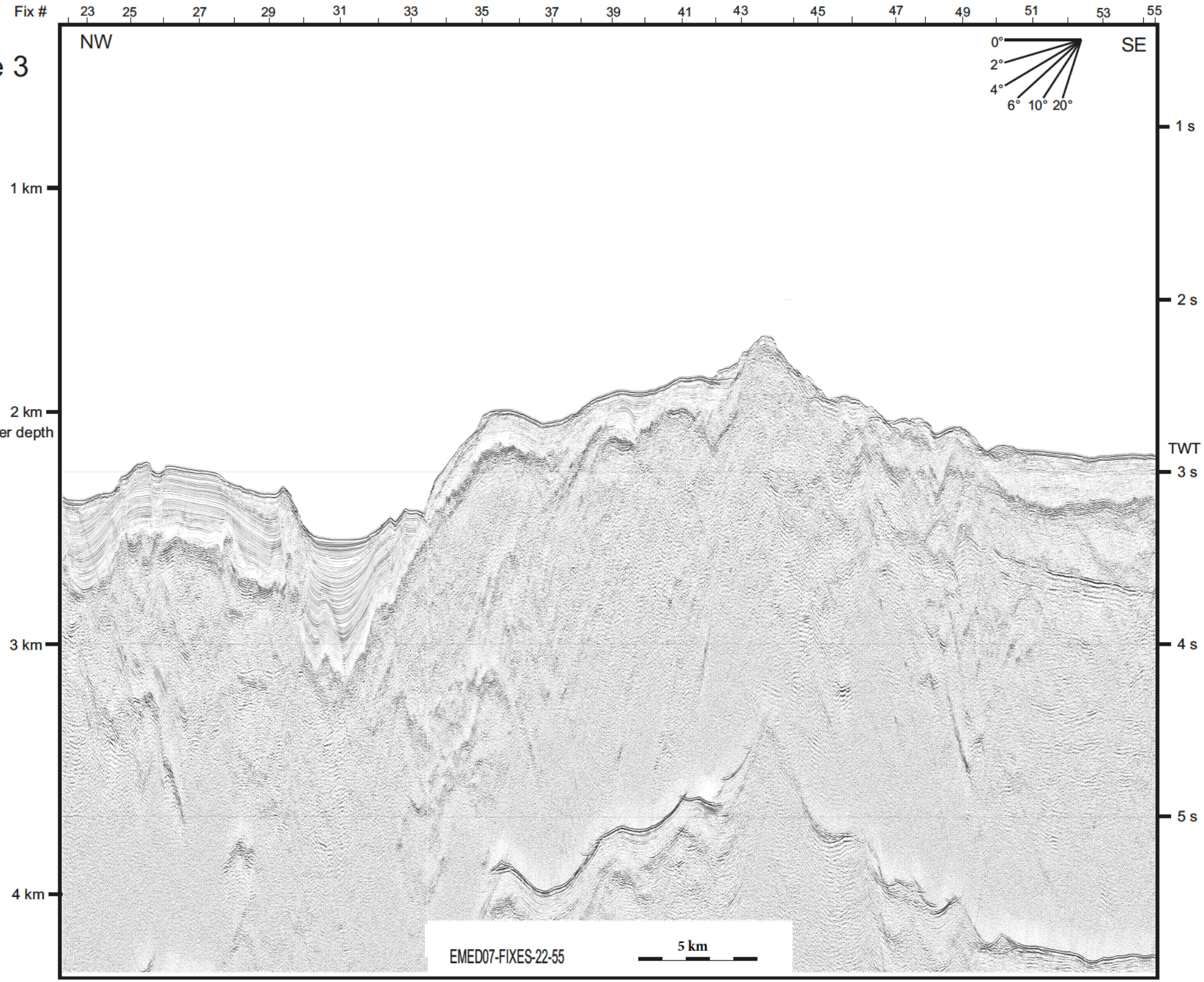
Fix #
23
25
27
29
31
33
35
37
39
41
43
45
47
49
51
53
55
NW
SE
0°
2°
4°
6°
10°
20°
1 s
1 km
2 km
Water depth
TWT
2 s
3 s
3 km
4 s
5 s
4 km
EMED07-FIXES-22-55
5 km

Plate 4

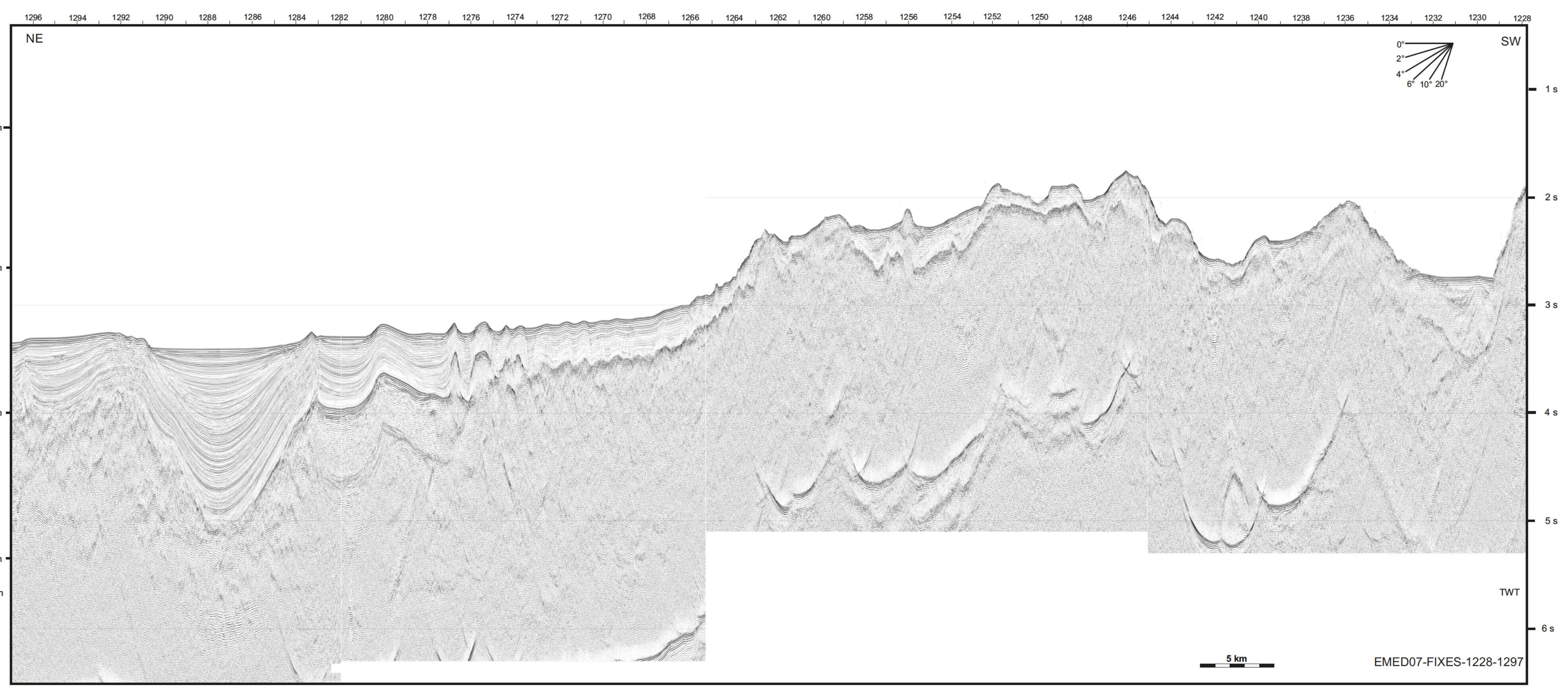
Fix #
1296 1294 1292 1290 1288 1286 1284 1282 1280 1278 1276 1274 1272 1270 1268 1266 1264 1262 1260 1258 1256 1254 1252 1250 1248 1246 1244 1242 1240 1238 1236 1234 1232 1230 1228
NE
SW
0°
2°
4°
6° 10° 20°
1 km
2 km
3 km
4 km
Water depth
1 s
2 s
3 s
4 s
5 s
6 s
TWT
5 km
EMED07-FIXES-1228-1297

Plate 5

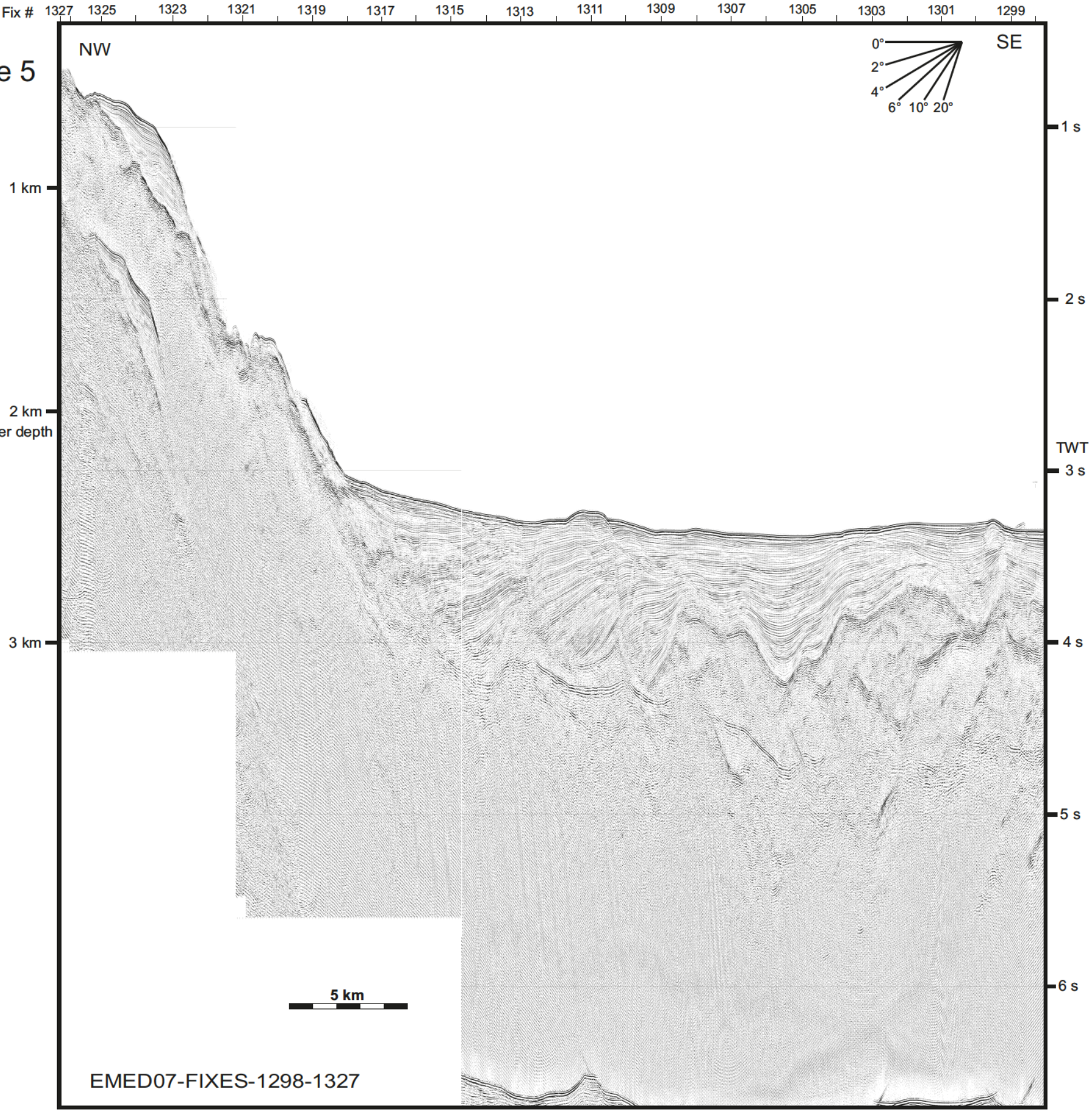
Fix #
1327
1325
1323
1321
1319
1317
1315
1313
1311
1309
1307
1305
1303
1301
1299
NW
SE
0°
2°
4°
6°
10°
20°
1 km
2 km
Water depth
3 km
1 s
2 s
TWT
3 s
4 s
5 s
6 s
5 km
EMED07-FIXES-1298-1327

Plate 6

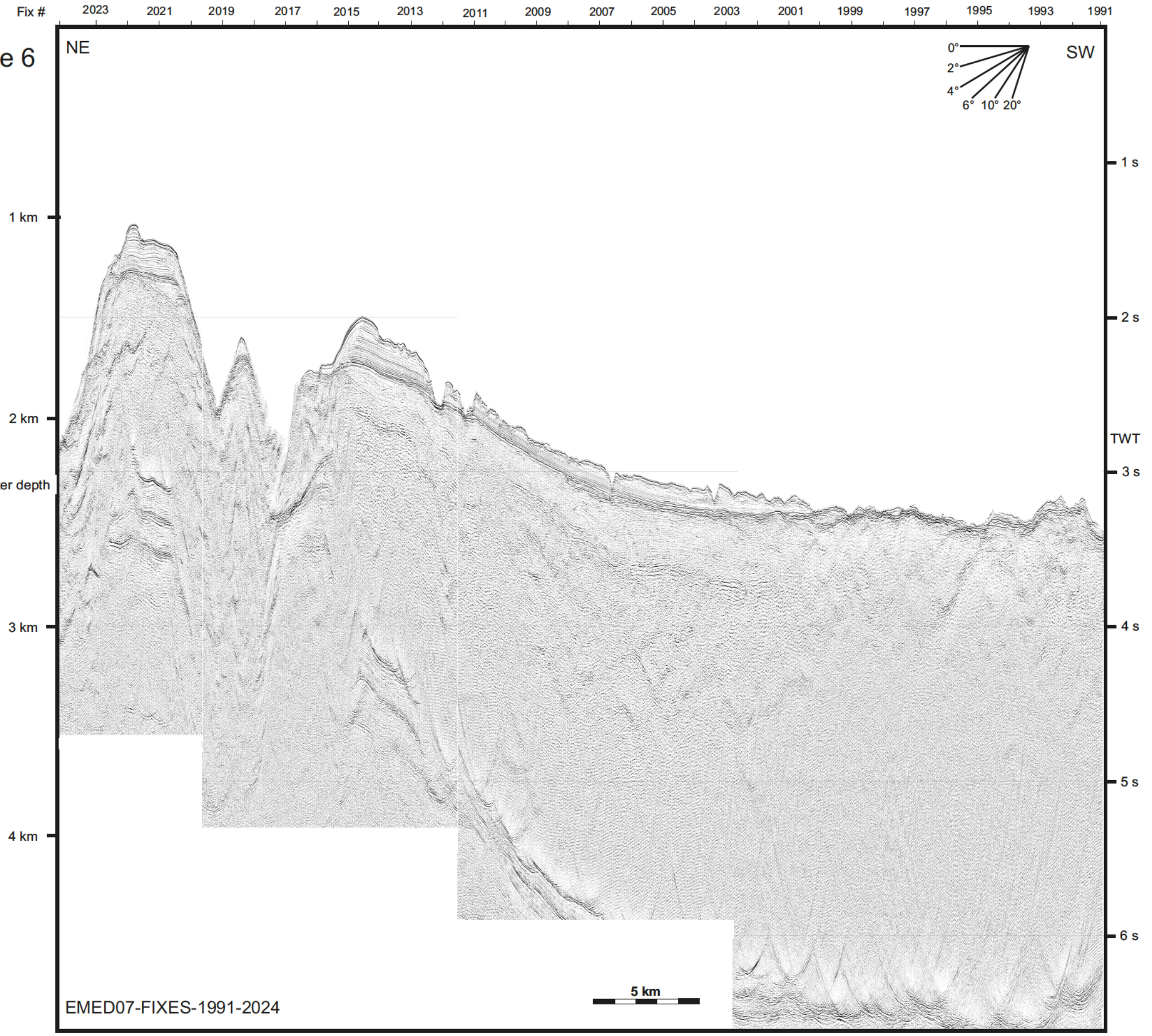
Fix #
2023
2021
2019
2017
2015
2013
2011
2009
2007
2005
2003
2001
1999
1997
1995
1993
1991
NE
SW
0°
2°
4°
6°
10°
20°
1 km
2 km
Water depth
3 km
4 km
1 s
2 s
TWT
3 s
4 s
5 s
6 s
5 km
EMED07-FIXES-1991-2024

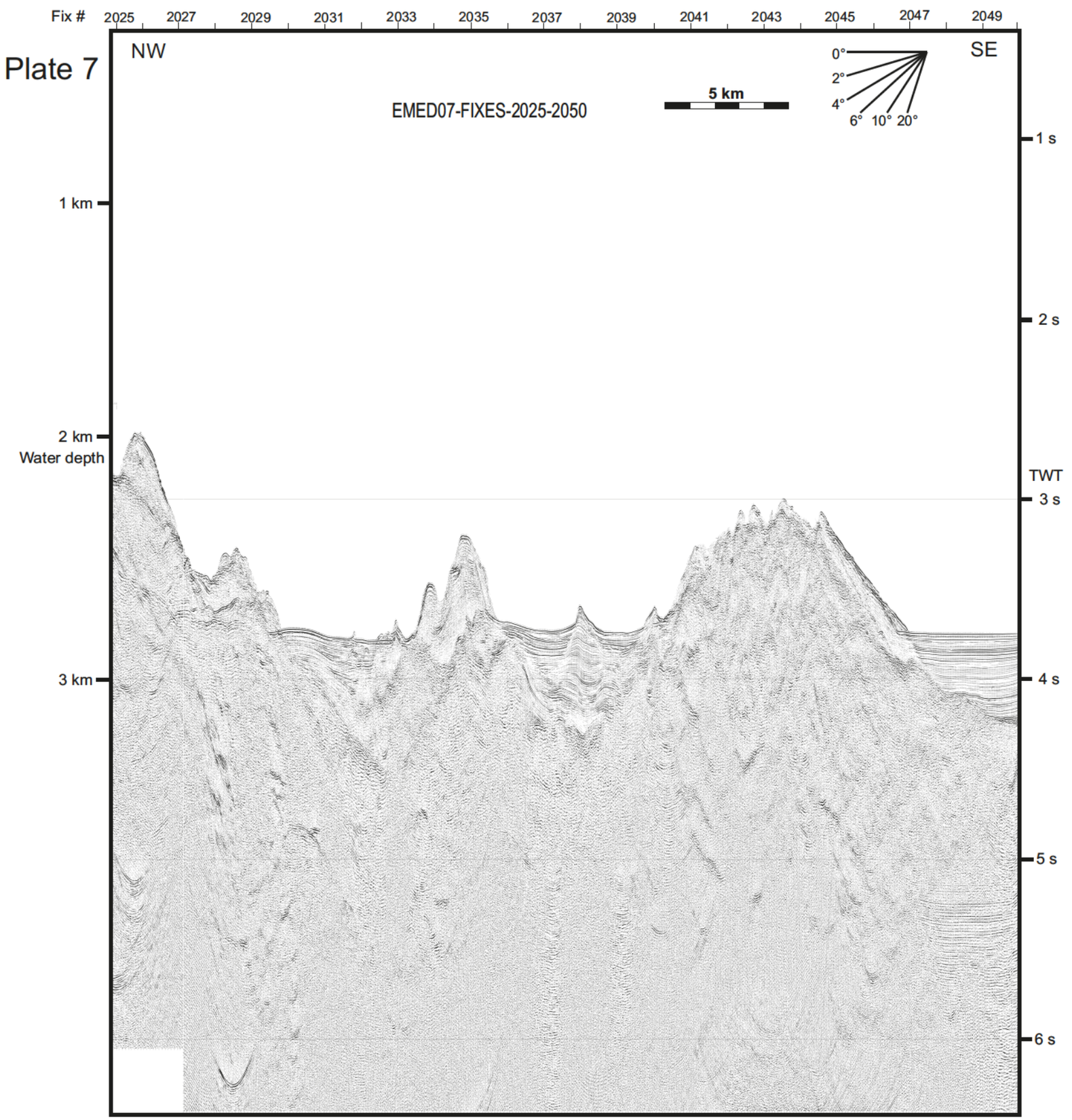
Plate 7
Fix #
2025
2027
2029
2031
2033
2035
2037
2039
2041
2043
2045
2047
2049
NW
SE
EMED07-FIXES-2025-2050
5 km
0°
2°
4°
6°
10°
20°
1 s
1 km
2 s
2 km
Water depth
TWT
3 s
3 km
4 s
5 s
6 s

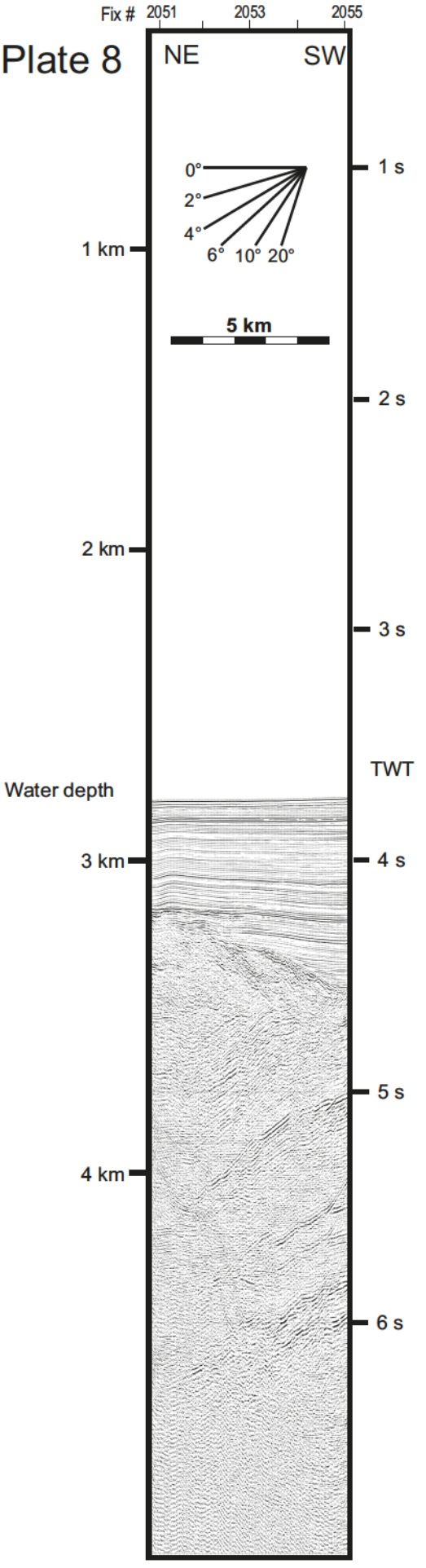

EMED07-FIXES-2051-2055

Plate 9

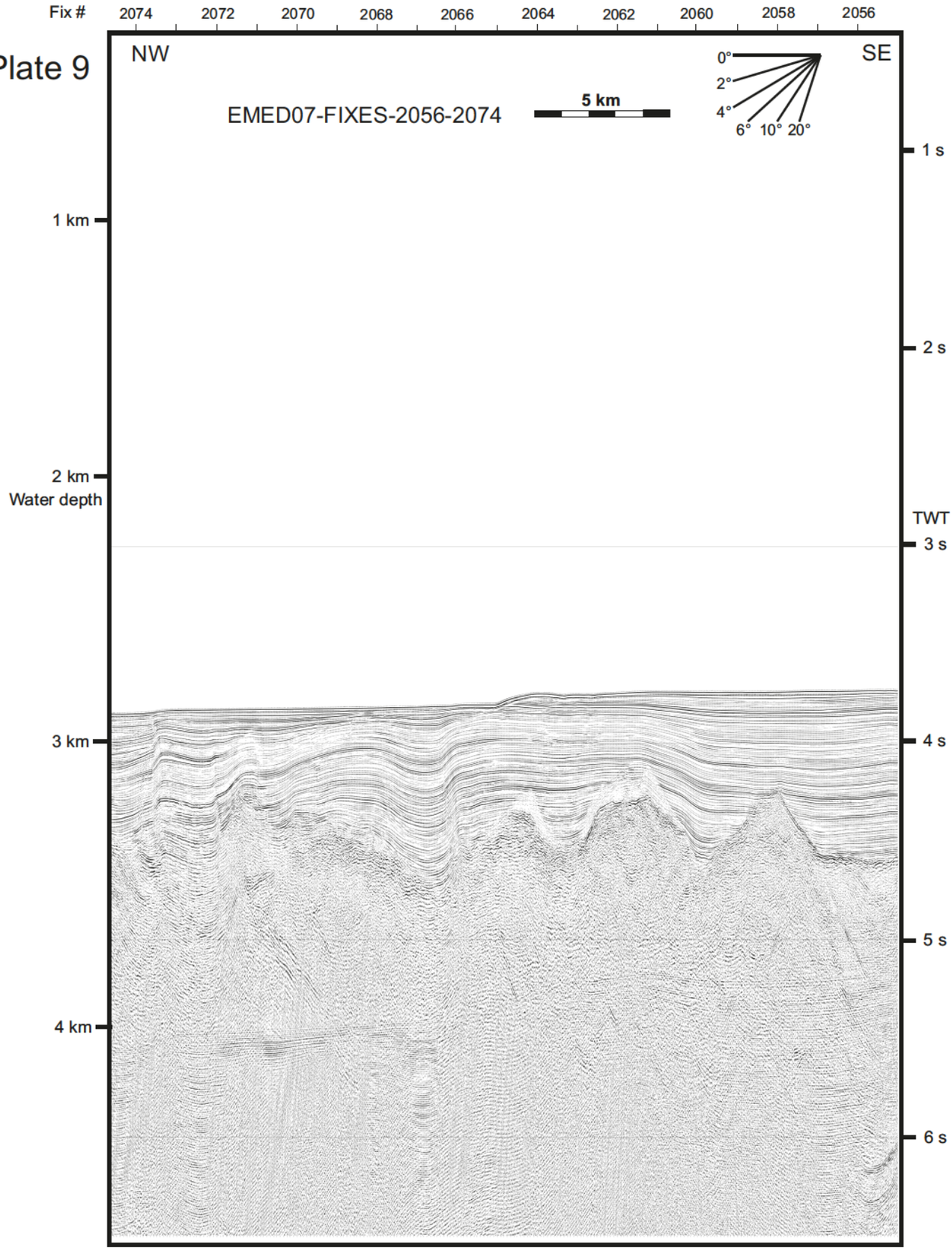
Fix #
2074
2072
2070
2068
2066
2064
2062
2060
2058
2056
NW
SE
EMED07-FIXES-2056-2074
5 km
0°
2°
4°
6°
10°
20°
1 km
2 km
Water depth
3 km
4 km
1 s
2 s
TWT
3 s
4 s
5 s
6 s

Plate 10

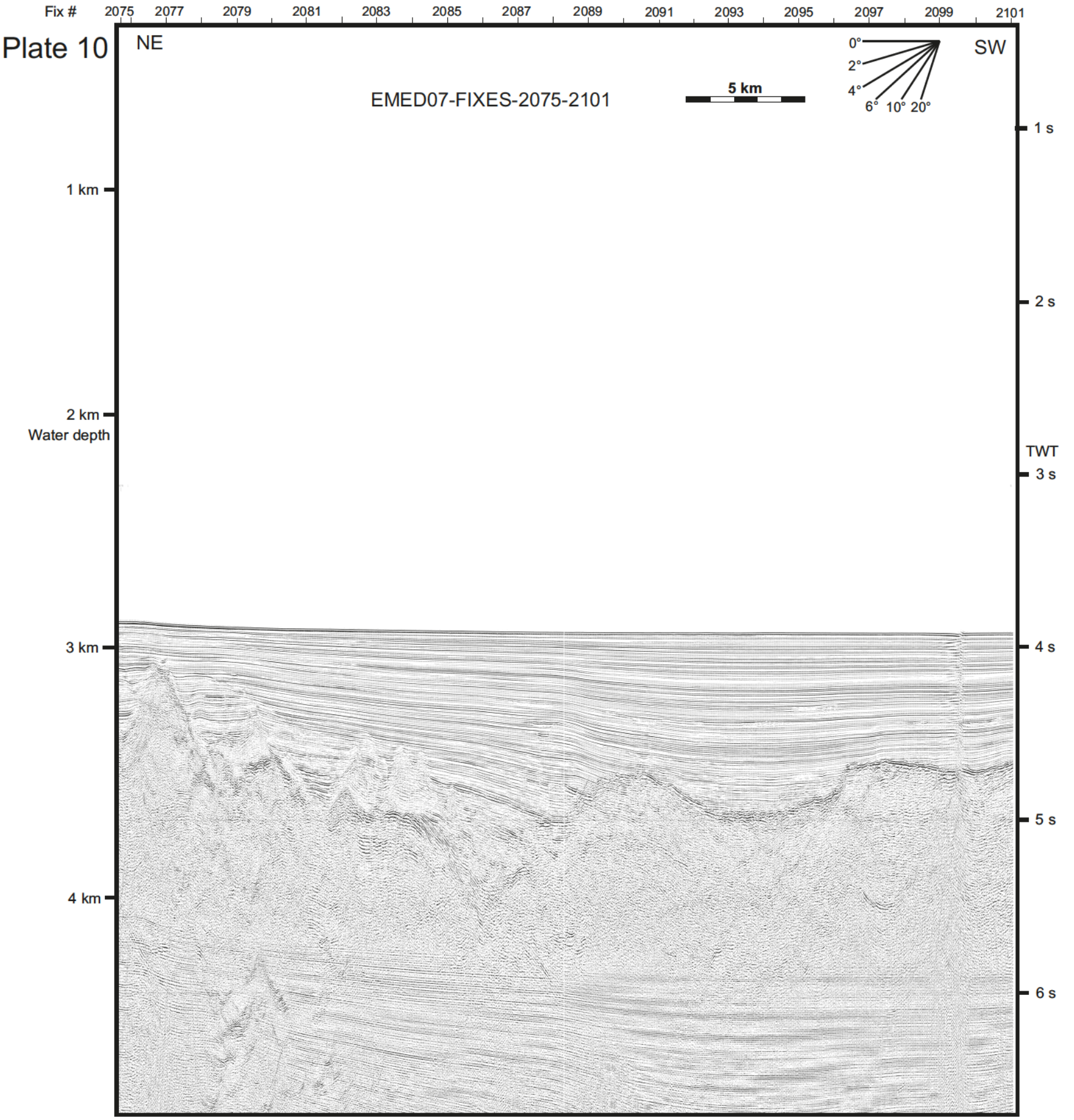
Fix #
2075
2077
2079
2081
2083
2085
2087
2089
2091
2093
2095
2097
2099
2101
NE
SW
EMED07-FIXES-2075-2101
5 km
0°
2°
4°
6°
10°
20°
1 s
1 km
2 s
2 km
Water depth
TWT
3 s
3 km
4 s
5 s
4 km
6 s

Plate 11

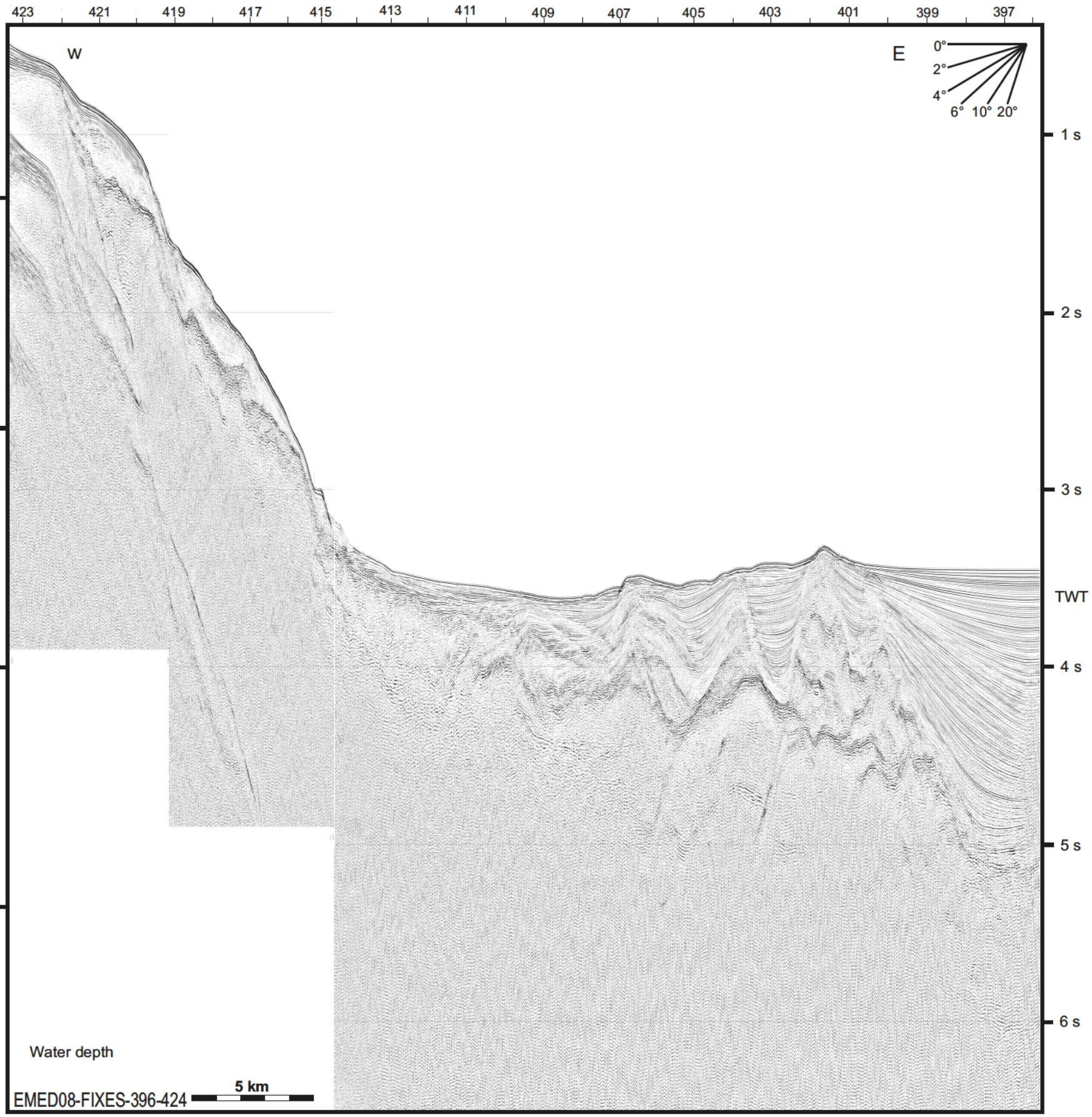
Fix #
423
421
419
417
415
413
411
409
407
405
403
401
399
397
W
E
0°
2°
4°
6°
10°
20°
1 km
2 km
3 km
4 km
1 s
2 s
3 s
TWT
4 s
5 s
6 s
Water depth
5 km
EMED08-FIXES-396-424

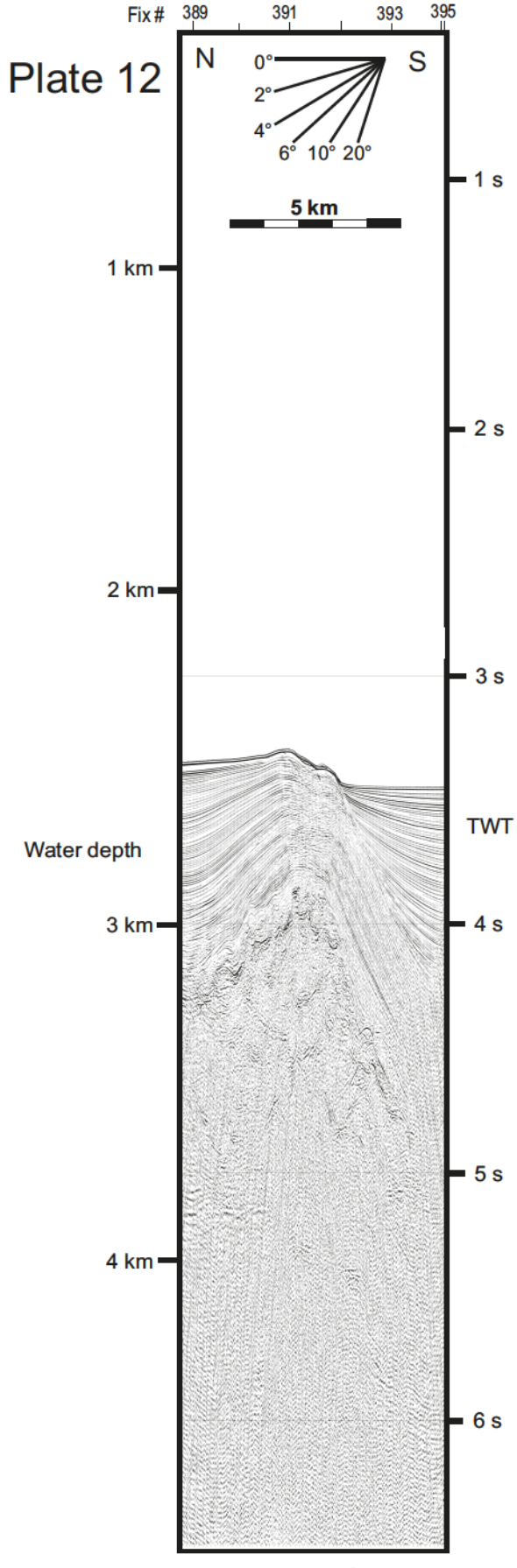

EMED08-FIXES-389-395

Plate 13

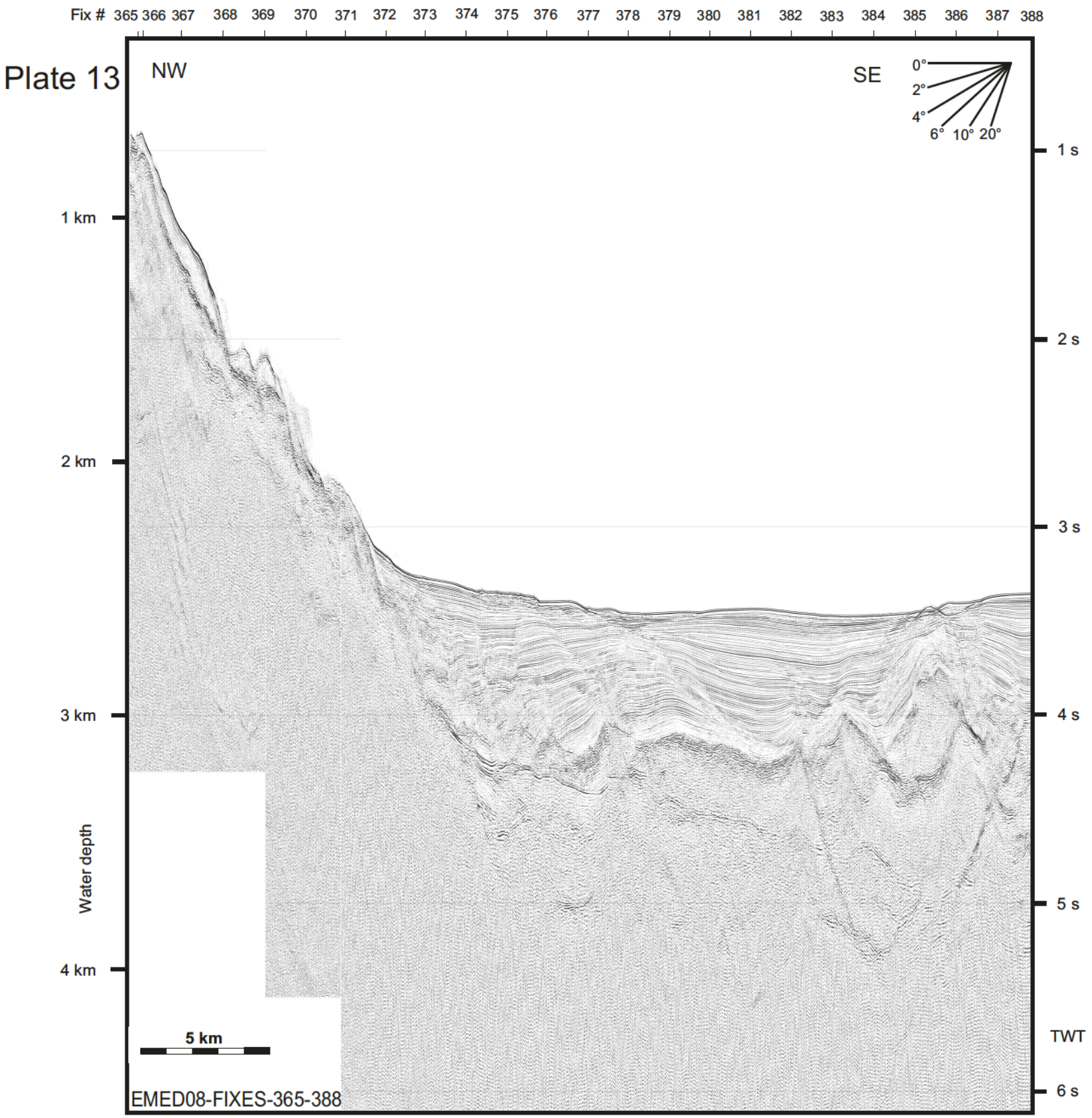
Fix # 365 366 367 368 369 370 371 372 373 374 375 376 377 378 379 380 381 382 383 384 385 386 387 388
NW
SE
0°
2°
4°
6° 10° 20°
1 km
2 km
3 km
4 km
Water depth
1 s
2 s
3 s
4 s
5 s
6 s
TWT
5 km
EMED08-FIXES-365-388

Plate 14

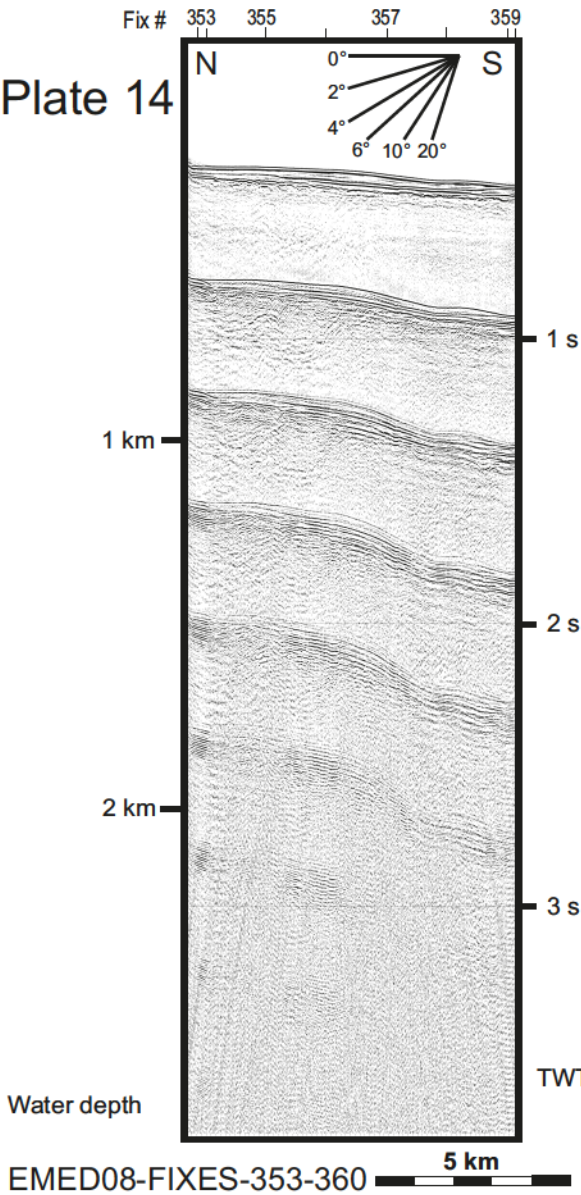

EMED08-FIXES-353-360

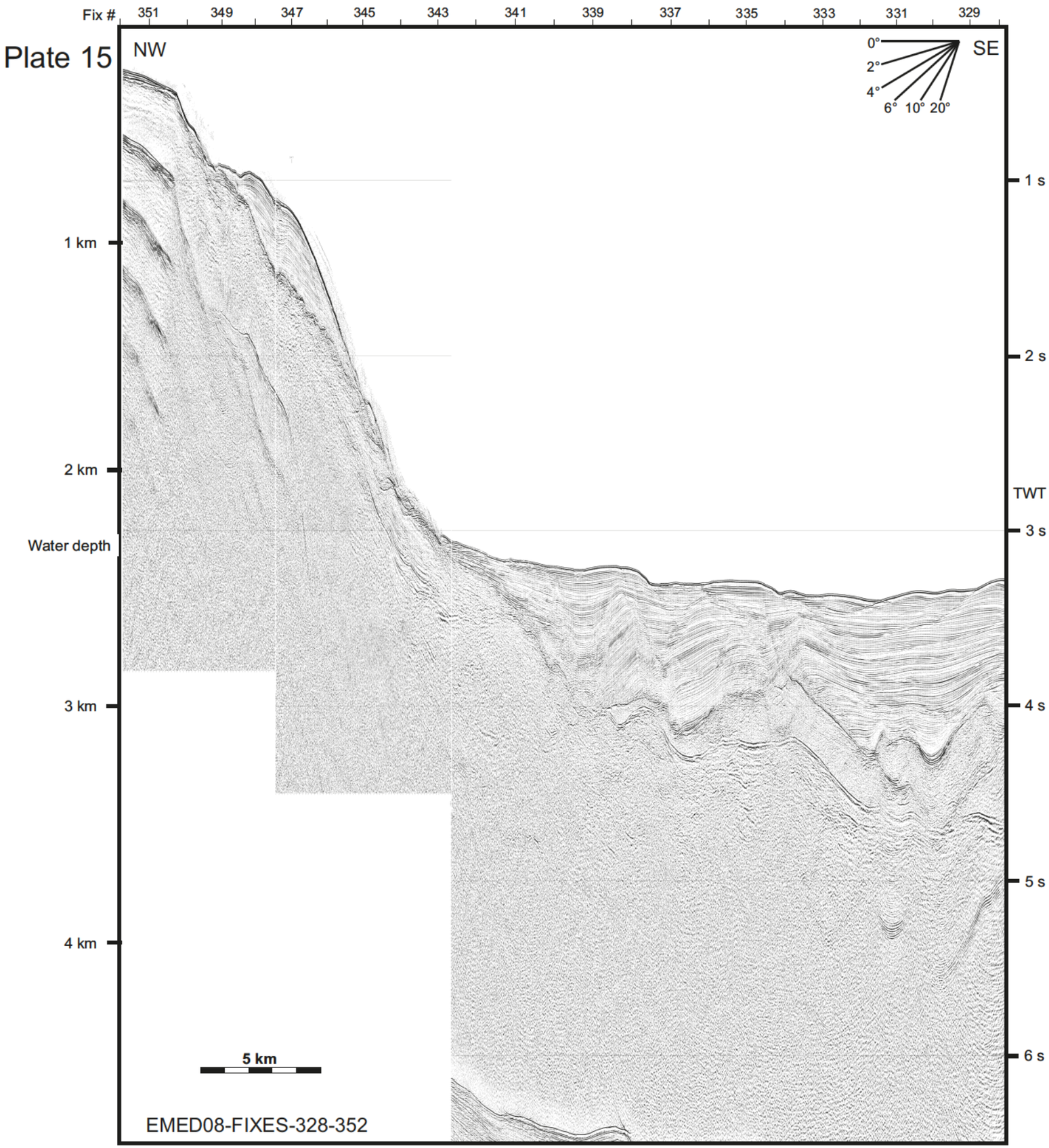
Plate 15
Fix #
351
349
347
345
343
341
339
337
335
333
331
329
NW
SE
0°
2°
4°
6°
10°
20°
1 km
2 km
Water depth
3 km
4 km
1 s
2 s
TWT
3 s
4 s
5 s
6 s
5 km
EMED08-FIXES-328-352

Plate 16

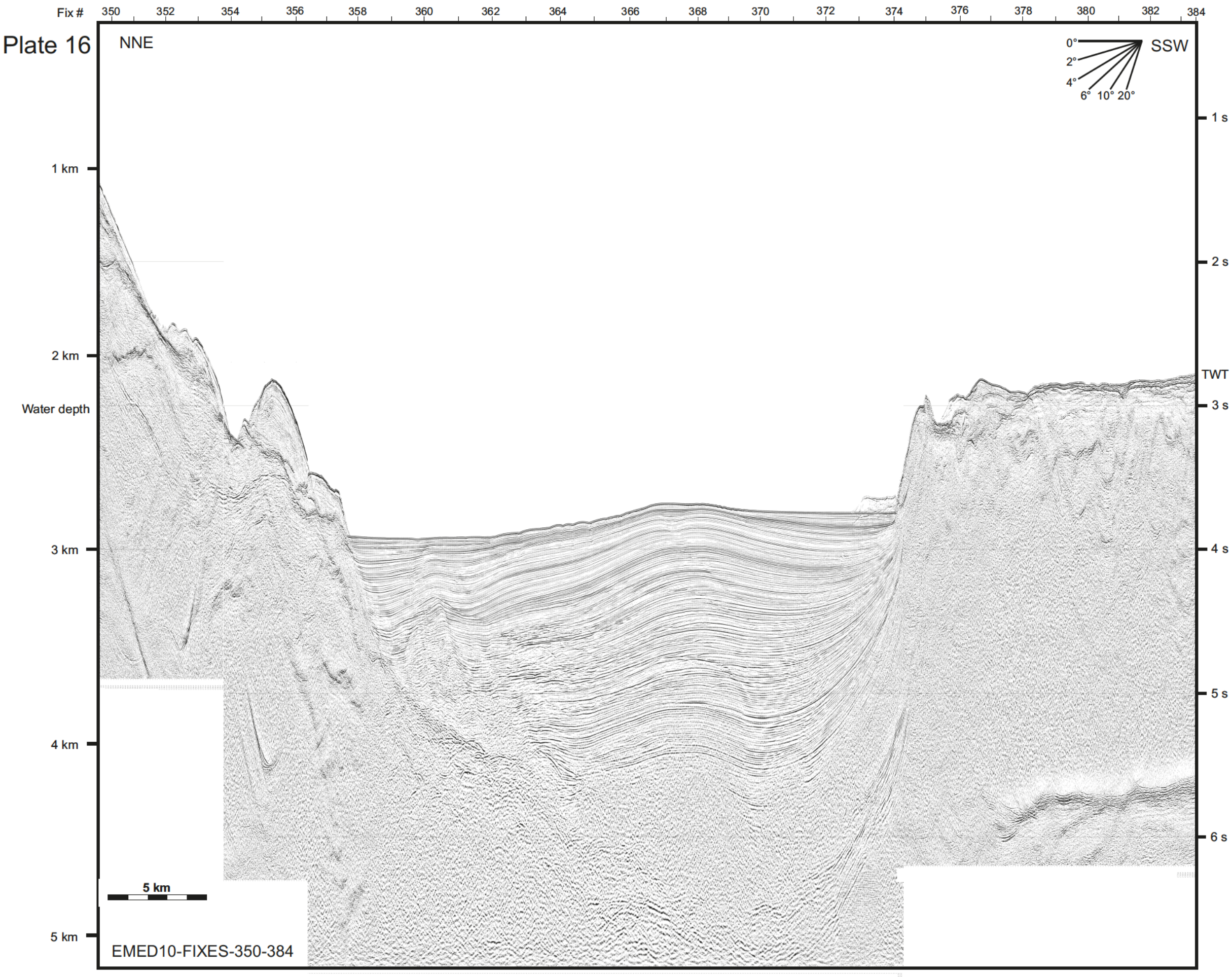
Fix #
350
352
354
356
358
360
362
364
366
368
370
372
374
376
378
380
382
384
NNE
SSW
0°
2°
4°
6°
10°
20°
1 km
2 km
Water depth
3 km
4 km
5 km
1 s
2 s
TWT
3 s
4 s
5 s
6 s
5 km
EMED10-FIXES-350-384

Plate 17

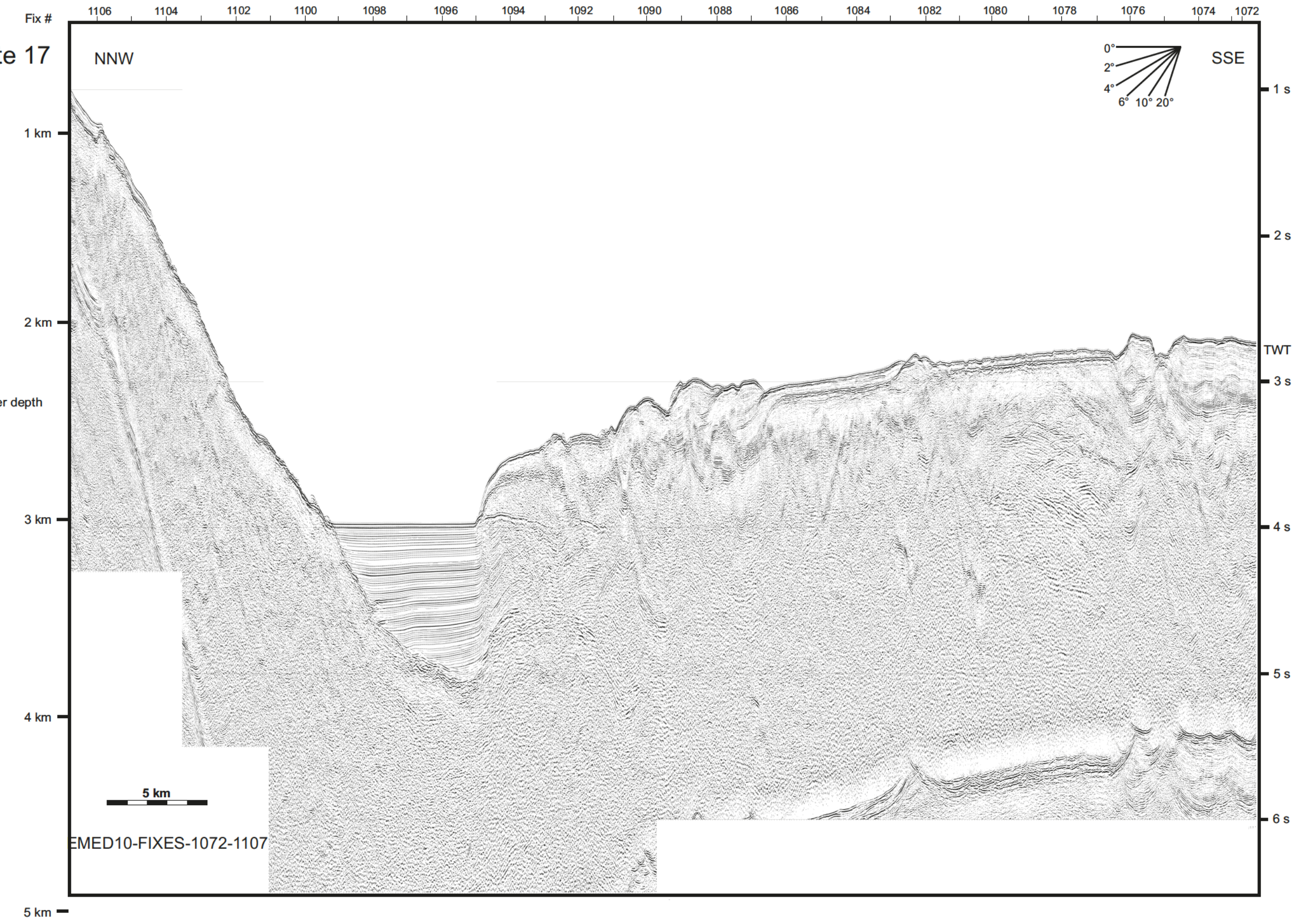
Fix #
1106
1104
1102
1100
1098
1096
1094
1092
1090
1088
1086
1084
1082
1080
1078
1076
1074
1072
NNW
SSE
0°
2°
4°
6°
10°
20°
1 km
2 km
Water depth
3 km
4 km
5 km
1 s
2 s
TWT
3 s
4 s
5 s
6 s
5 km
EMED10-FIXES-1072-1107

Plate 18

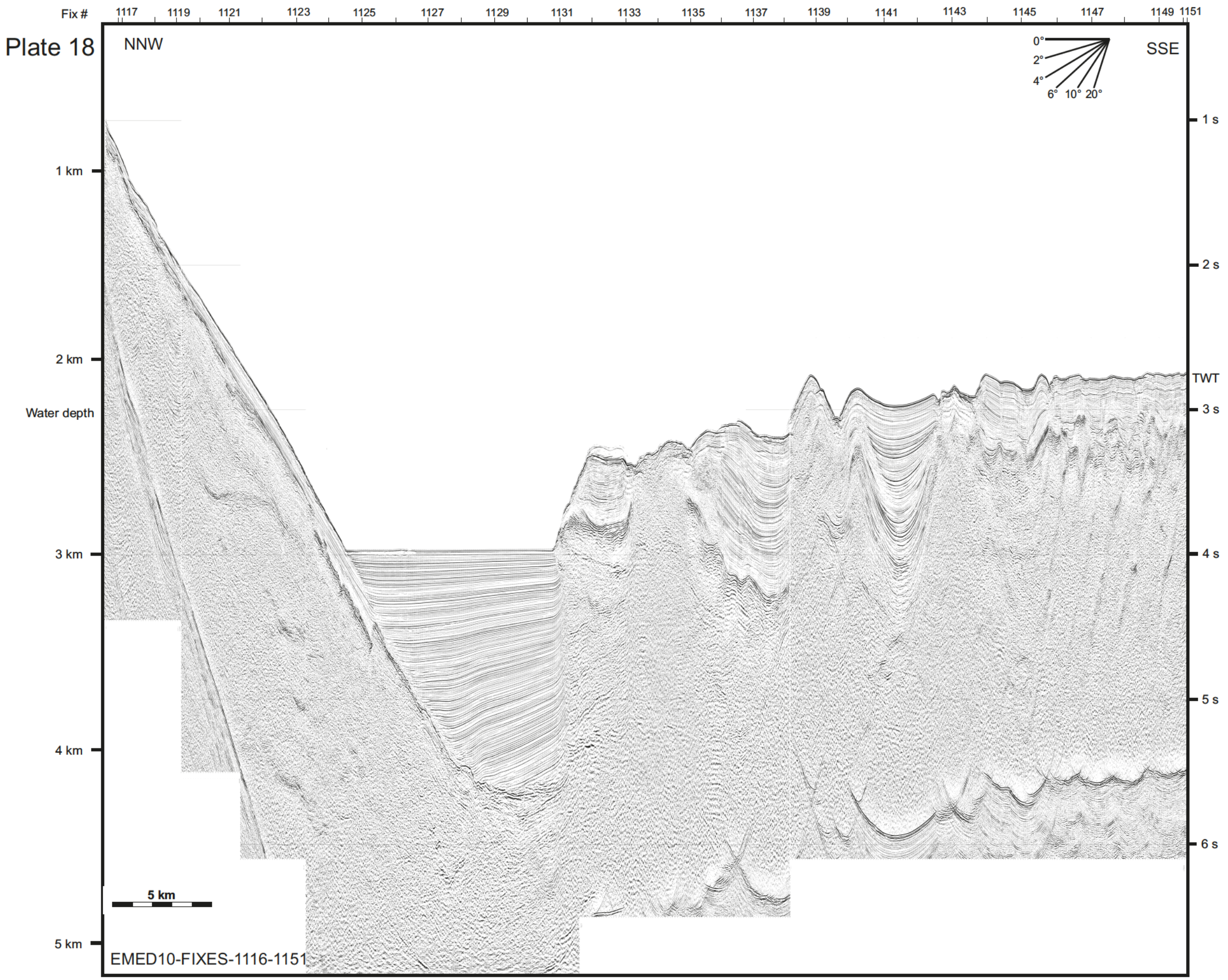
Fix #
1117
1119
1121
1123
1125
1127
1129
1131
1133
1135
1137
1139
1141
1143
1145
1147
1149
1151
NNW
SSE
0°
2°
4°
6°
10°
20°
1 km
2 km
Water depth
3 km
4 km
5 km
1 s
2 s
TWT
3 s
4 s
5 s
6 s
5 km
EMED10-FIXES-1116-1151

Plate 19a

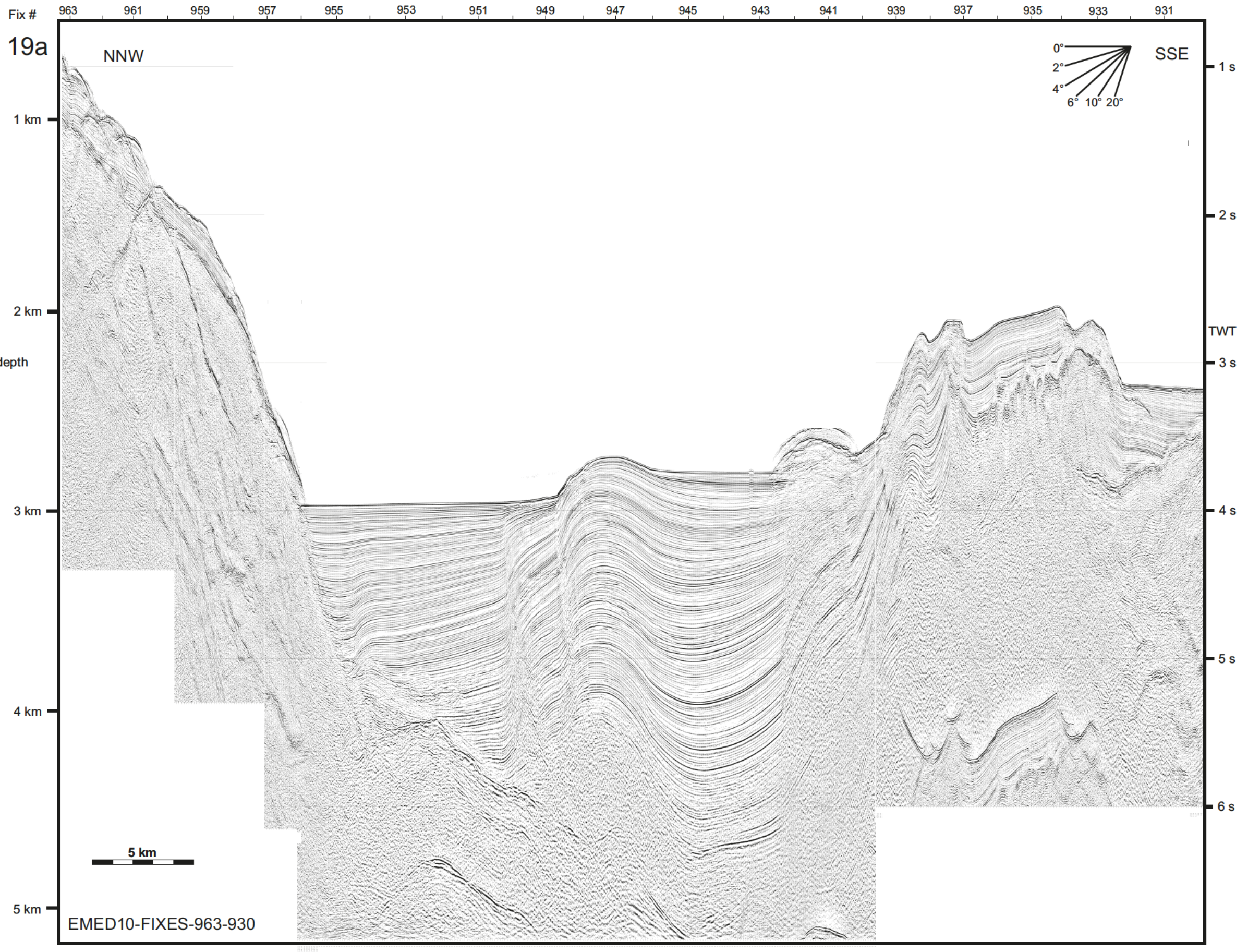
Fix #
963
961
959
957
955
953
951
949
947
945
943
941
939
937
935
933
931
NNW
SSE
0°
2°
4°
6°
10°
20°
1 km
2 km
3 km
4 km
5 km
Water depth
1 s
2 s
3 s
4 s
5 s
6 s
TWT
5 km
EMED10-FIXES-963-930

Plate 19b

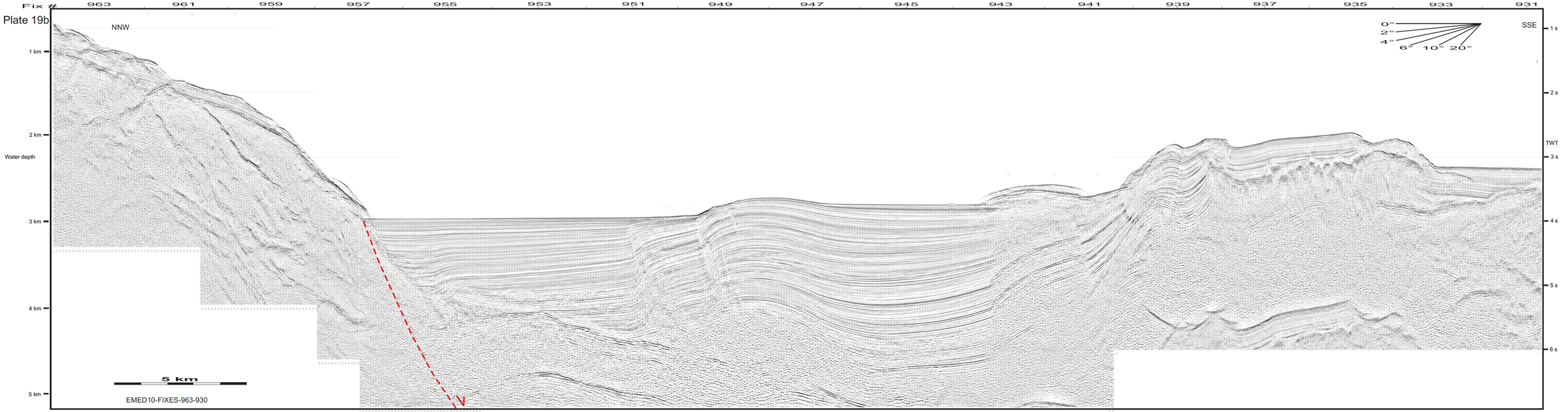
Fix #
963
961
959
957
955
953
951
949
947
945
943
941
939
937
935
933
931
NNW
SSE
0°
2°
4°
6°
10°
20°
1 km
2 km
Water depth
3 km
4 km
5 km
1 s
2 s
TWT
3 s
4 s
5 s
6 s
5 km
EMED10-FIXES-963-930

PLATE 20

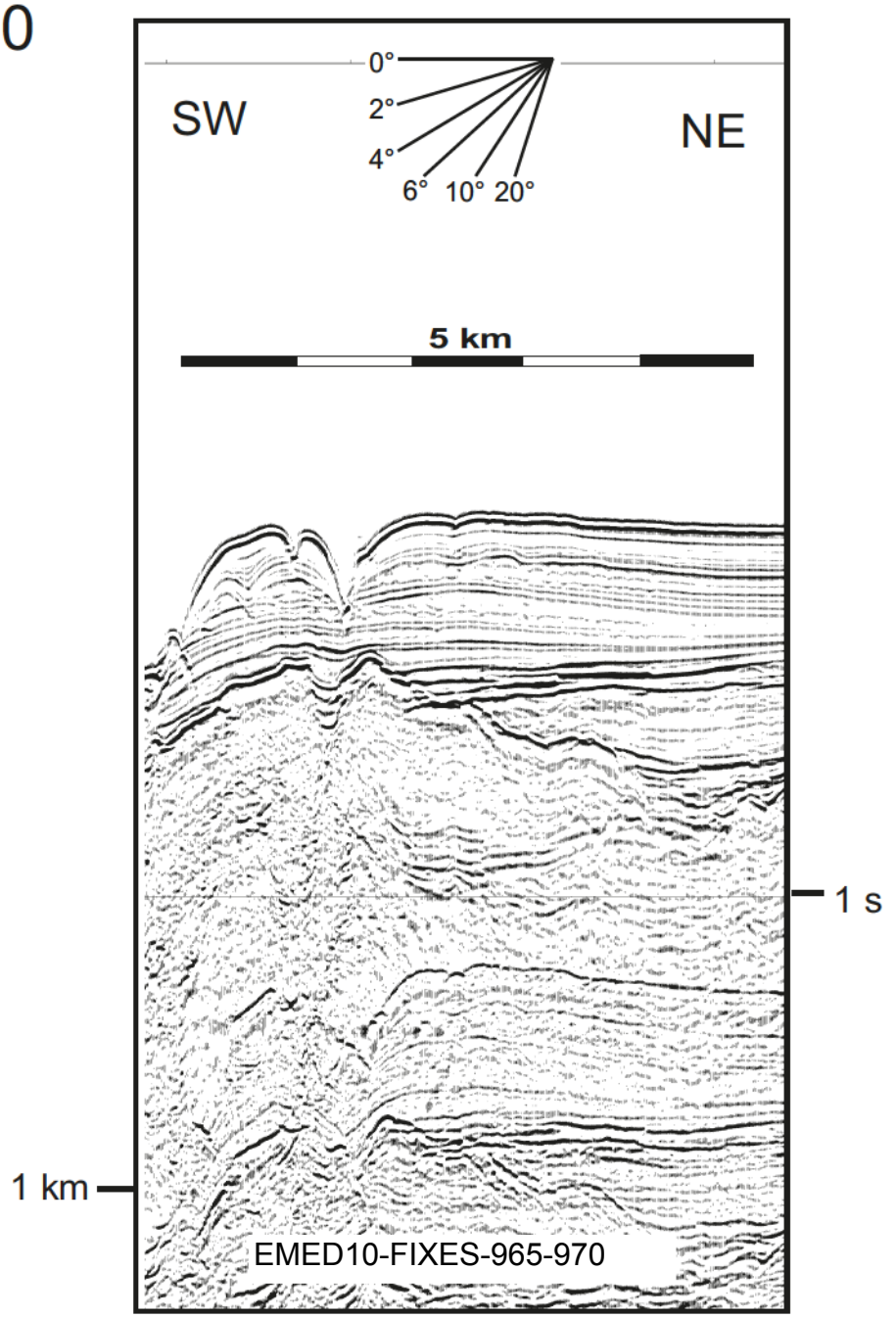

Plate 21a

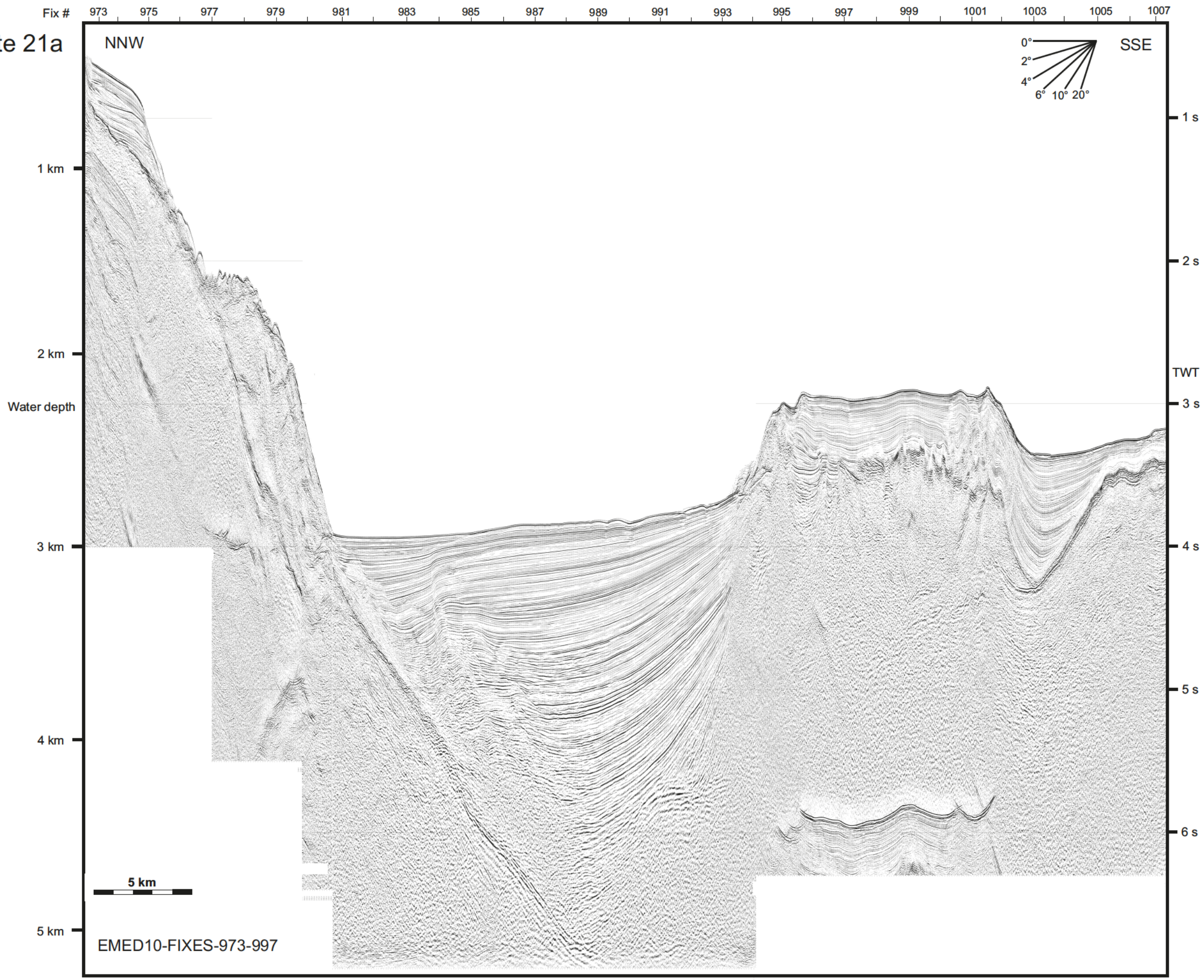
Fix #
973
975
977
979
981
983
985
987
989
991
993
995
997
999
1001
1003
1005
1007
NNW
SSE
0°
2°
4°
6°
10°
20°
1 km
2 km
Water depth
3 km
4 km
5 km
1 s
2 s
TWT
3 s
4 s
5 s
6 s
5 km
EMED10-FIXES-973-997

Plate 21b

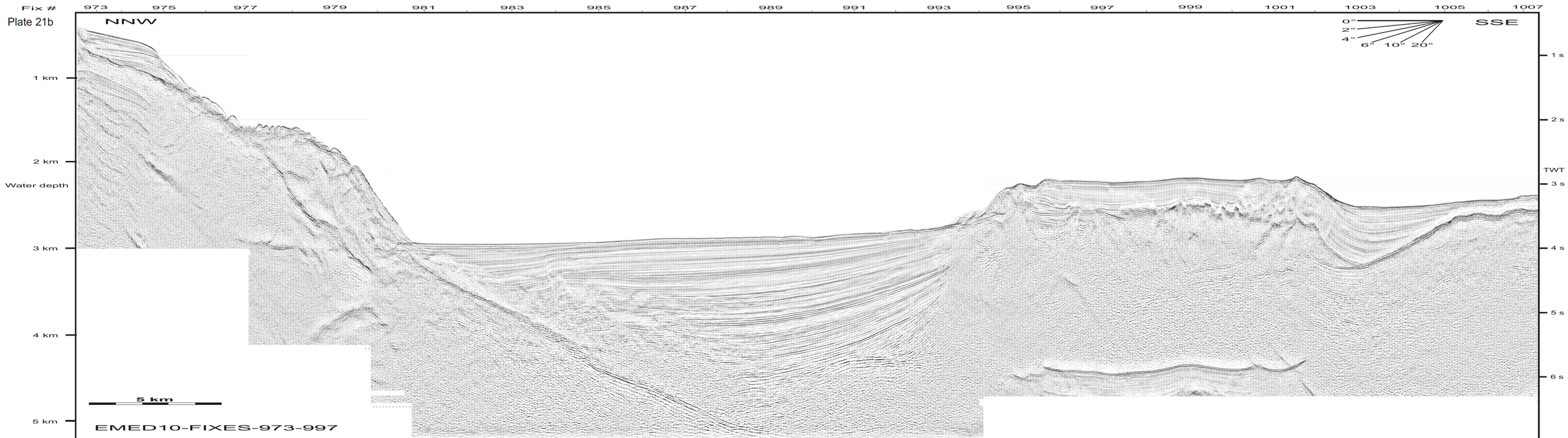
Fix #
973
975
977
979
981
983
985
987
989
991
993
995
997
999
1001
1003
1005
1007
NNW
SSE
0°
2°
4°
6°
10°
20°
1 km
2 km
Water depth
3 km
4 km
5 km
1 s
2 s
TWT
3 s
4 s
5 s
6 s
5 km
EMED10-FIXES-973-997

Plate 22

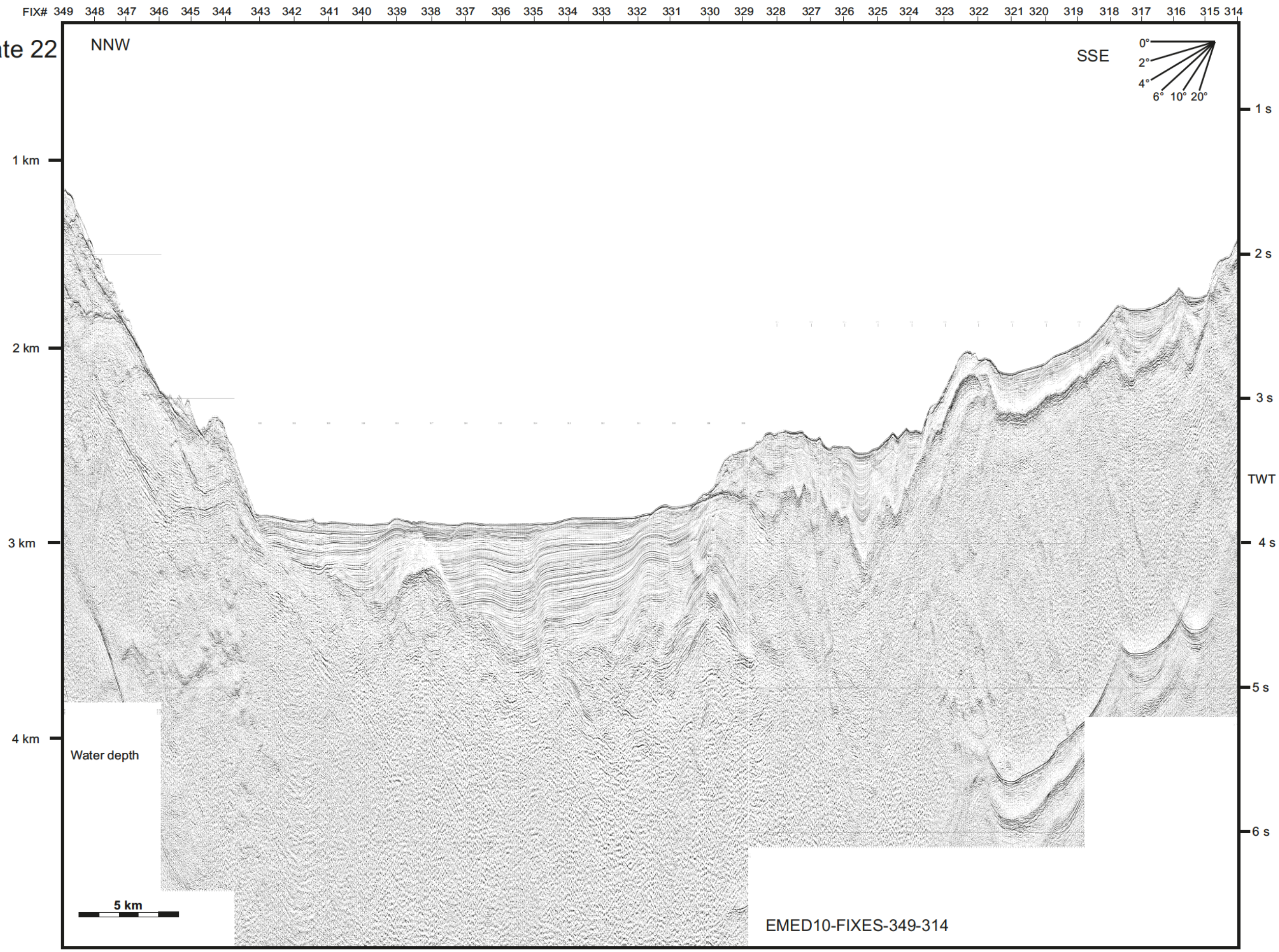
FIX# 349 348 347 346 345 344 343 342 341 340 339 338 337 336 335 334 333 332 331 330 329 328 327 326 325 324 323 322 321 320 319 318 317 316 315 314
NNW
SSE
0°
2°
4°
6°
10°
20°
1 km
2 km
3 km
4 km
1 s
2 s
3 s
TWT
4 s
5 s
6 s
Water depth
5 km
EMED10-FIXES-349-314

Plate 23

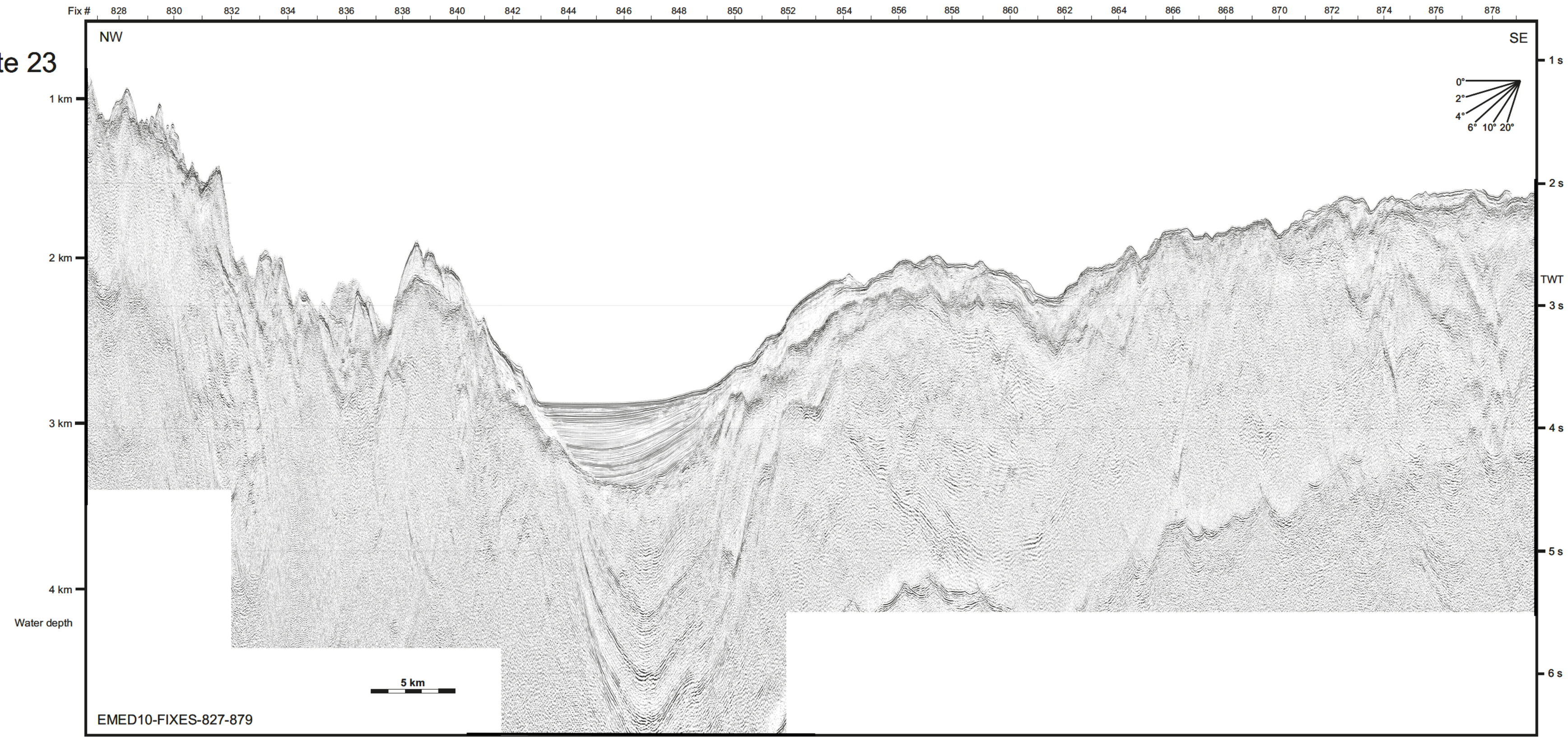
Fix #
828
830
832
834
836
838
840
842
844
846
848
850
852
854
856
858
860
862
864
866
868
870
872
874
876
878
NW
SE
0°
2°
4°
6°
10°
20°
1 km
2 km
3 km
4 km
Water depth
1 s
2 s
TWT
3 s
4 s
5 s
6 s
5 km
EMED10-FIXES-827-879

Plate 24

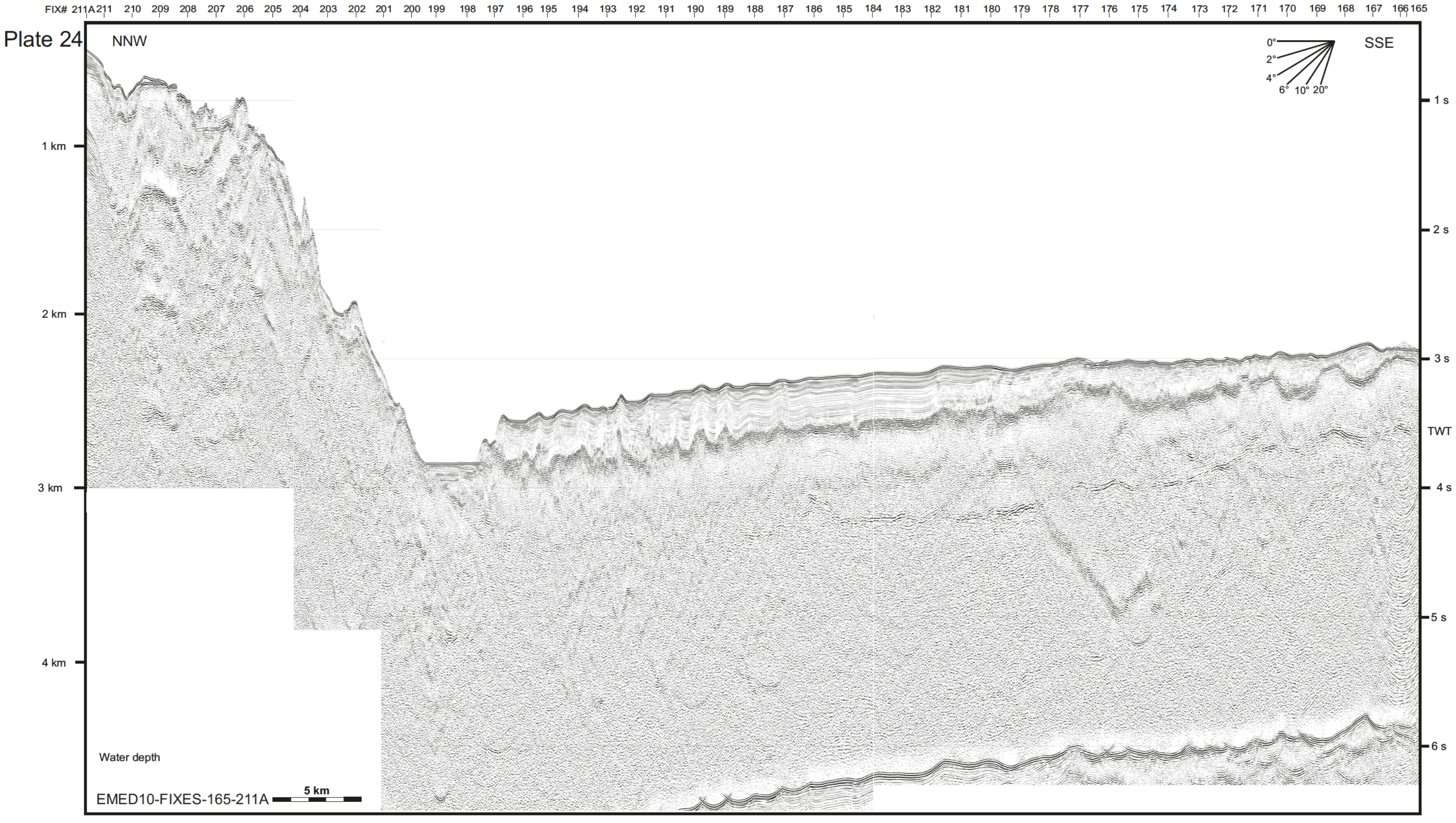
FIX# 211A 211 210 209 208 207 206 205 204 203 202 201 200 199 198 197 196 195 194 193 192 191 190 189 188 187 186 185 184 183 182 181 180 179 178 177 176 175 174 173 172 171 170 169 168 167 166 165
NNW
SSE
0°
2°
4°
6°
10°
20°
1 km
2 km
3 km
4 km
1 s
2 s
3 s
TWT
4 s
5 s
6 s
Water depth
5 km
EMED10-FIXES-165-211A

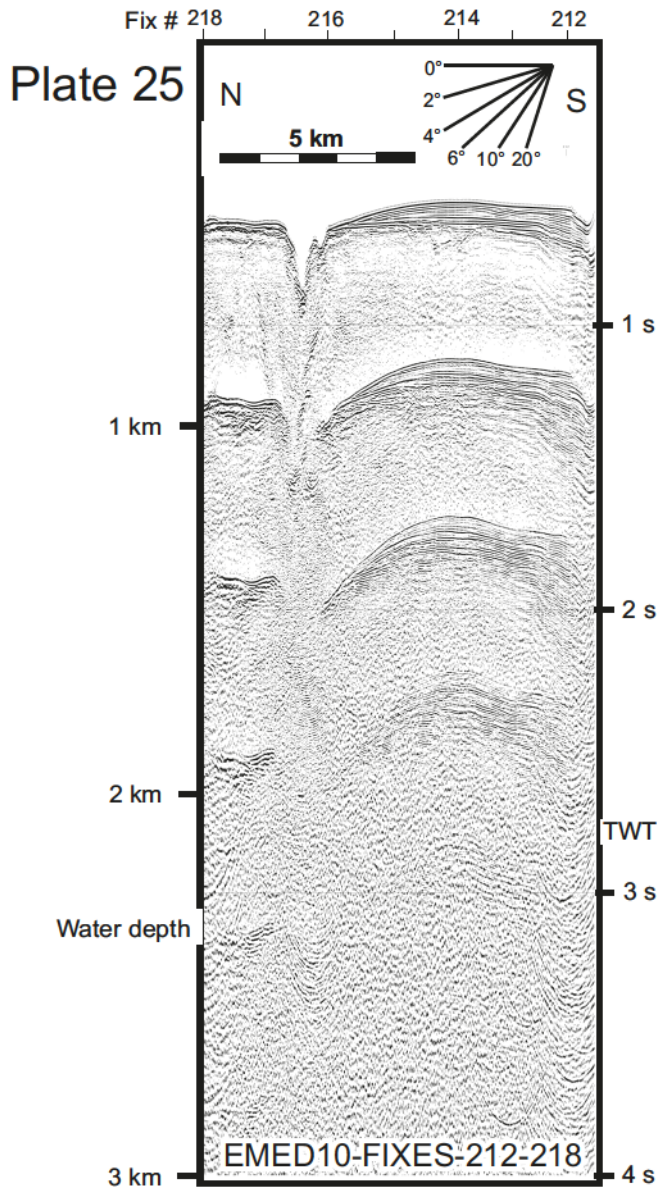
Plate 25
Fix # 218
216
214
212
N
S
0°
2°
4°
6°
10°
20°
5 km
1 s
1 km
2 s
2 km
TWT
3 s
Water depth
EMED10-FIXES-212-218
3 km
4 s

Plate 26

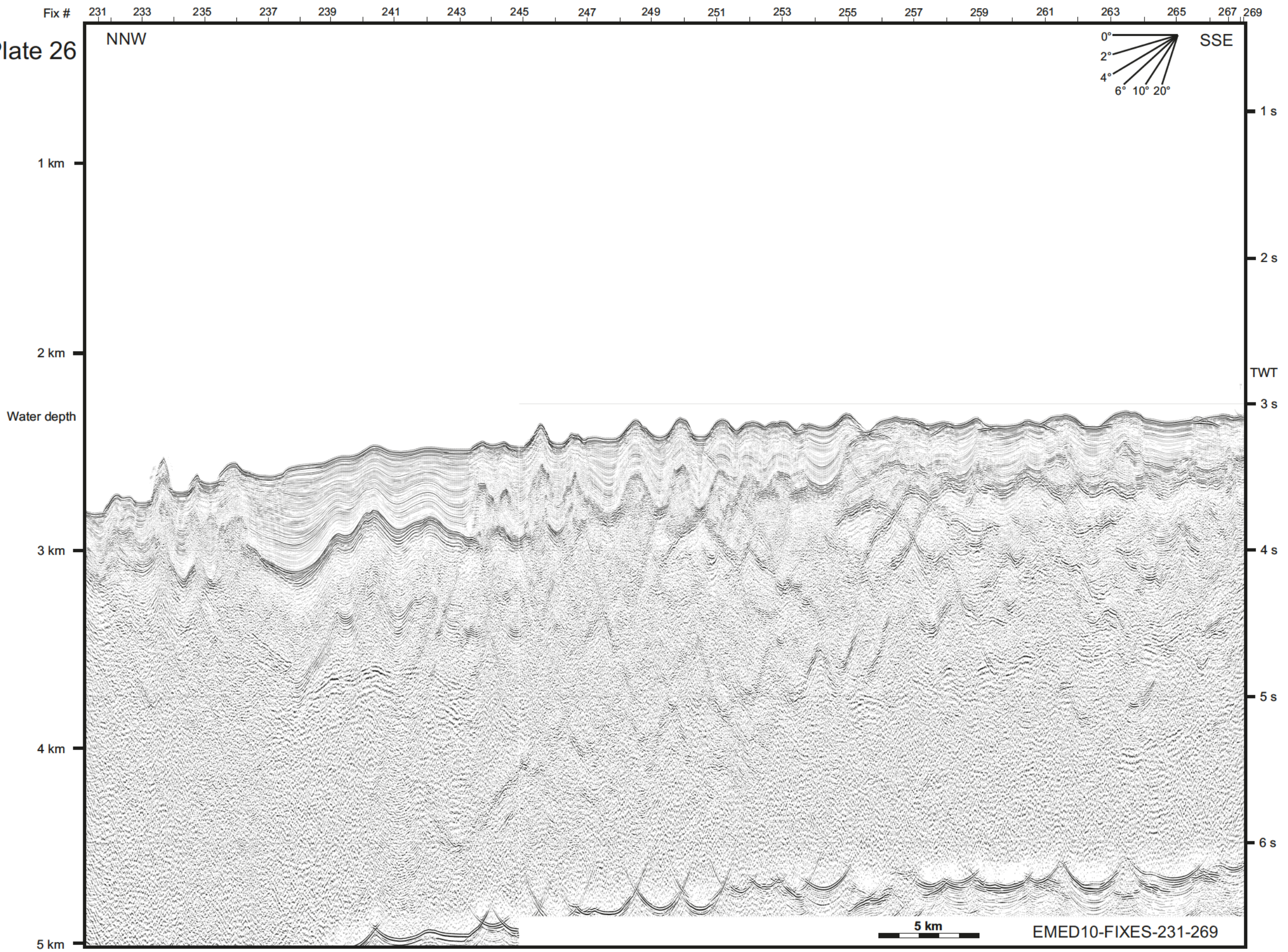
Fix #
231
233
235
237
239
241
243
245
247
249
251
253
255
257
259
261
263
265
267
269
NNW
SSE
0°
2°
4°
6°
10°
20°
1 km
2 km
Water depth
3 km
4 km
5 km
1 s
2 s
TWT
3 s
4 s
5 s
6 s
5 km
EMED10-FIXES-231-269

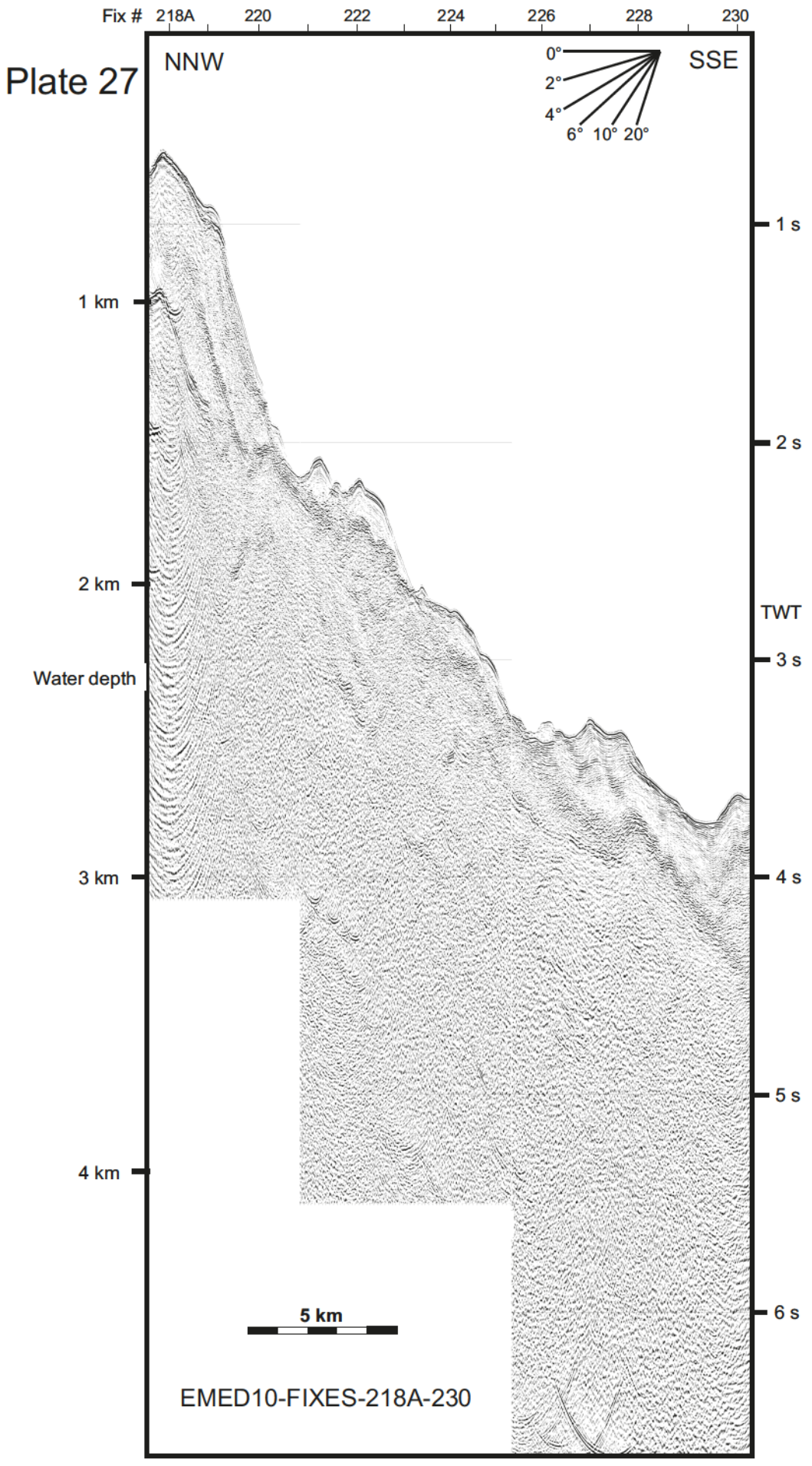
Plate 27
Fix # 218A 220 222 224 226 228 230
NNW
SSE
0°
2°
4°
6° 10° 20°
1 km
2 km
Water depth
3 km
4 km
1 s
2 s
TWT
3 s
4 s
5 s
6 s
5 km
EMED10-FIXES-218A-230

Plate 28

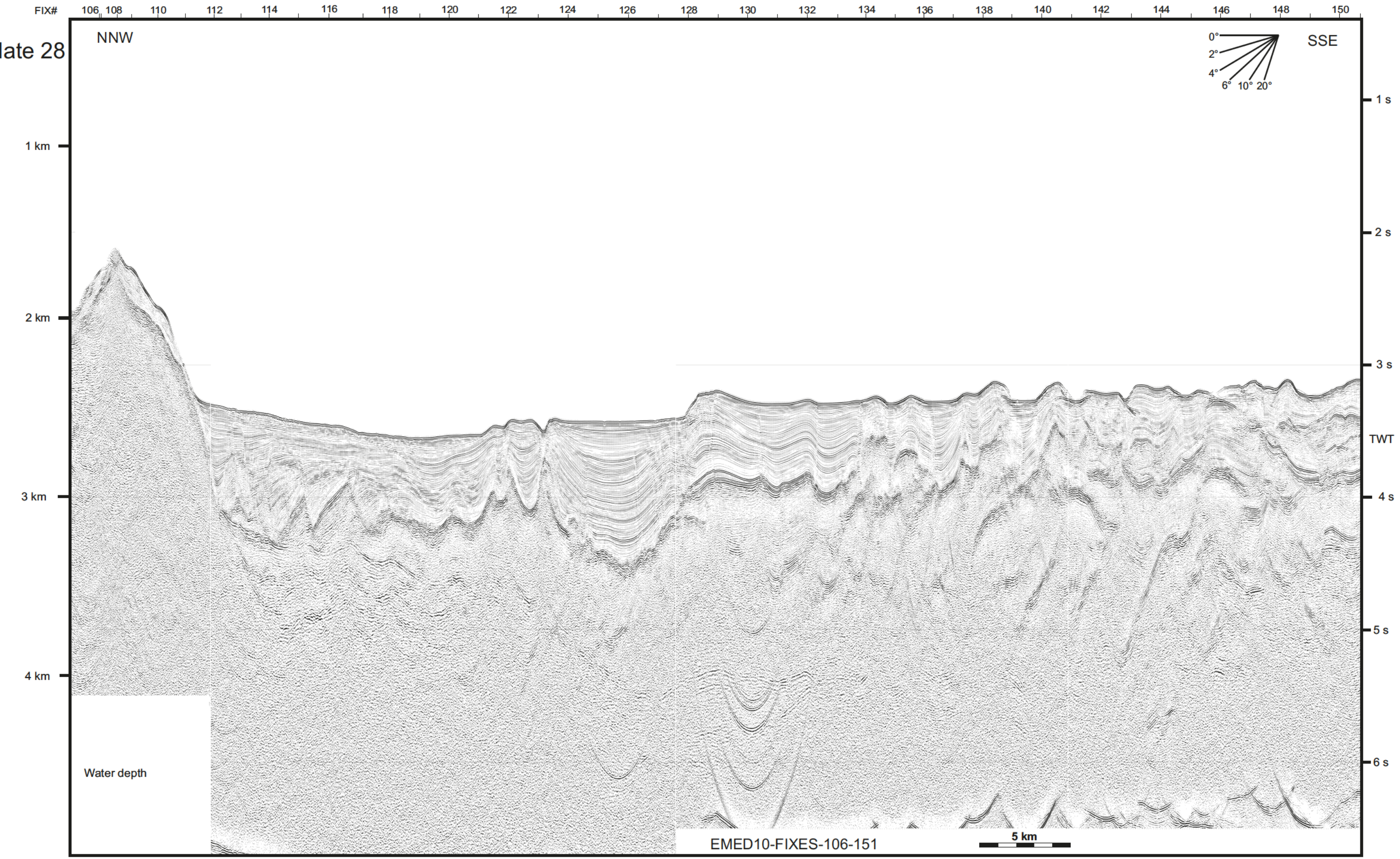
FIX#
106 108 110 112 114 116 118 120 122 124 126 128 130 132 134 136 138 140 142 144 146 148 150
NNW
SSE
0°
2°
4°
6° 10° 20°
1 km
2 km
3 km
4 km
1 s
2 s
3 s
TWT
4 s
5 s
6 s
Water depth
EMED10-FIXES-106-151
5 km

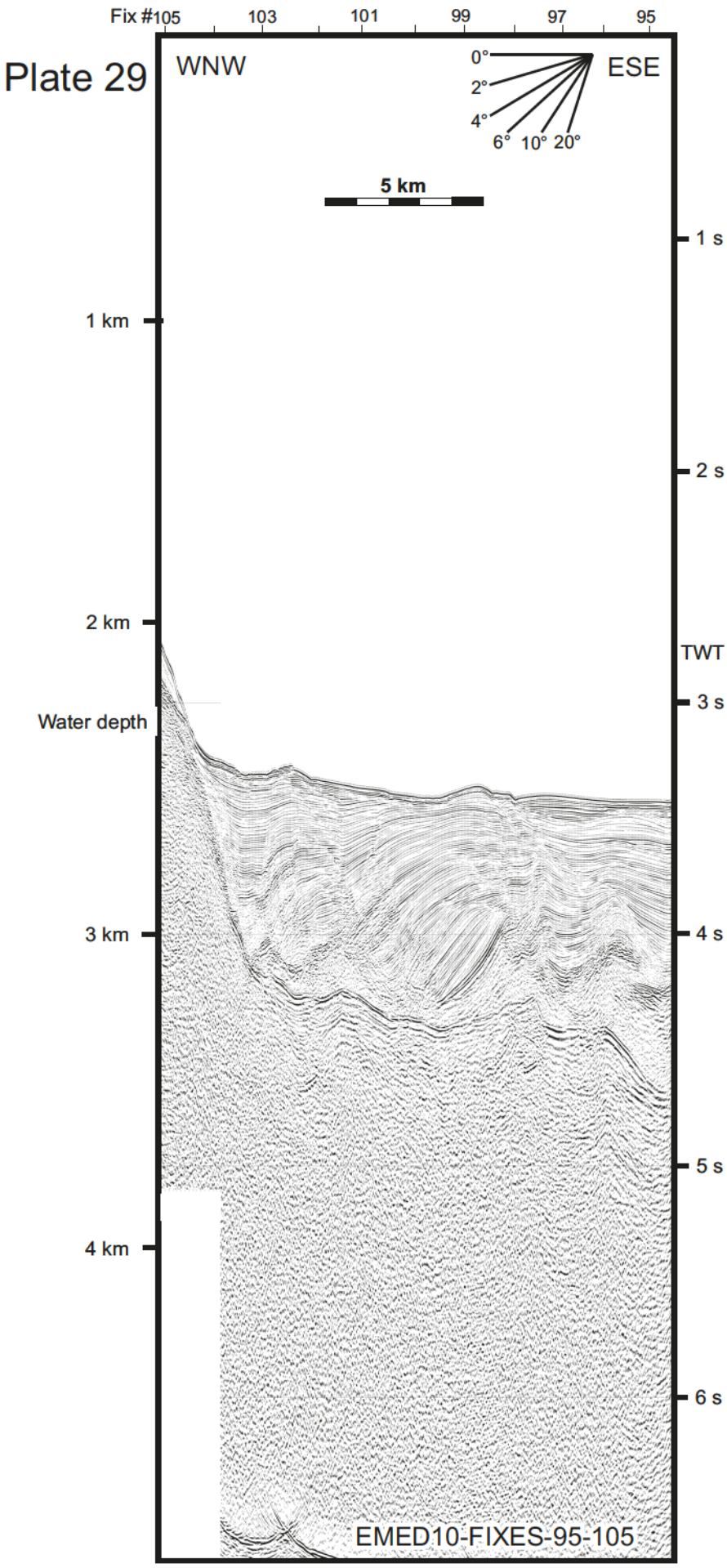
Plate 29
Fix #105
103
101
99
97
95
WNW
ESE
0°
2°
4°
6°
10°
20°
5 km
1 km
2 km
3 km
4 km
Water depth
1 s
2 s
TWT
3 s
4 s
5 s
6 s
EMED10-FIXES-95-105

Plate 30

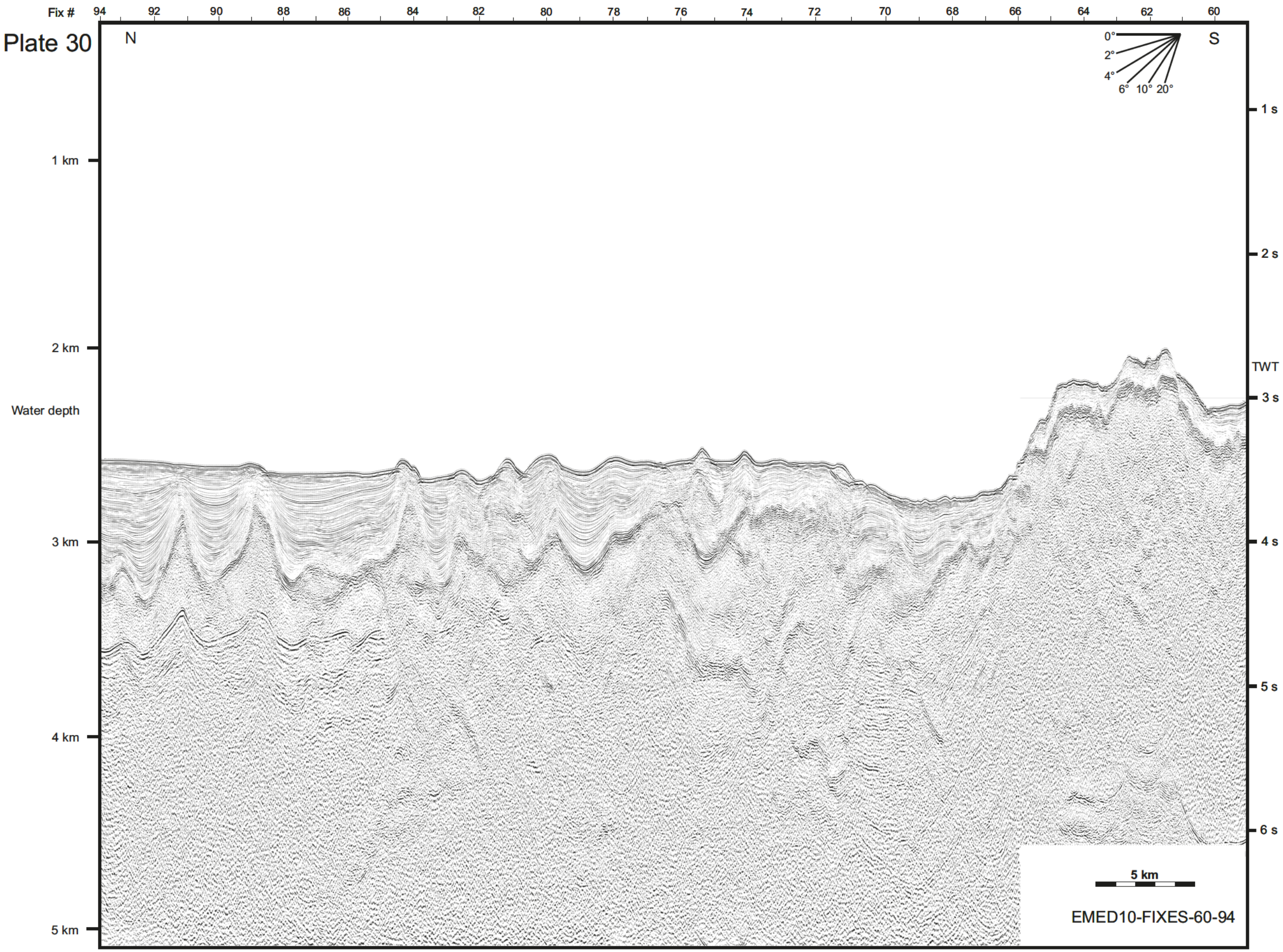
Fix #
94 92 90 88 86 84 82 80 78 76 74 72 70 68 66 64 62 60
N
S
0°
2°
4°
6°
10°
20°
1 km
2 km
Water depth
3 km
4 km
5 km
1 s
2 s
TWT
3 s
4 s
5 s
6 s
5 km
EMED10-FIXES-60-94